

**Dissecting the molecular mechanism of chromosome axis  
remodeling during meiosis in *Arabidopsis thaliana*  
and towards live cell imaging of meiosis in *Zea mays***

Dissertation with the aim of achieving a doctoral degree  
at the faculty of Mathematics, Informatics and Natural Sciences

Department of Biology

Universität Hamburg

Submitted by

Martina Balboni

2021 in Hamburg, Germany



Supervisor: Prof. Dr. Arp Schnittger

First Examiner: Prof. Dr. Arp Schnittger

Second Examiner: Prof. Dr. Sigrun Reumann

Date of oral defence: 22.04.2021





# Index

Abstract.....	6
Zusammenfassung.....	8
1. Introduction .....	11
1.1 Meiosis, a special kind of division.....	11
1.2 Overview of meiosis .....	12
1.3 The chromosome axis .....	15
1.3.1 The axis core proteins.....	16
1.3.2 The meiotic HORMADs .....	17
1.4 The Synaptonemal Complex.....	17
1.5 Meiotic recombination .....	19
1.6 Sister chromatid cohesion.....	23
1.7 Cell cycle regulation .....	25
References .....	29
Research aim.....	40
Chapter 1.....	42
Dissecting the molecular mechanism of chromosome axis remodeling during meiosis in <i>Arabidopsis thaliana</i> .....	42
1 Introduction .....	43
1.1 The HORMA domain proteins.....	43
1.1.1 Mad2 .....	43
1.1.2 The meiotic HORMADs .....	45
1.1.3 P31comet .....	46

2	Results .....	48
2.1	Generation of a comet mutant in Arabidopsis.....	48
2.2	Loss of COMET leads to defective synapsis and reduced CO number .....	57
2.3	Chromosome axis remodeling is affected in comet.....	62
2.4	COMET functions as a cofactor for the action of PCH2.....	68
3	Discussion.....	72
3.1	Multiple roles of COMET-PCH2 .....	72
3.2	COMET in meiosis outside of Arabidopsis.....	76
4	Material and methods .....	78
4.1	Plant material.....	78
4.2	Plant growth conditions.....	78
4.3	Plasmid construction.....	78
4.4	Plant transformation.....	79
4.5	CRISPR/Cas9 genome editing.....	79
4.6	Genotyping .....	80
4.7	Phenotype evaluation.....	80
4.8	Root growth assay and oryzalin treatment.....	80
4.9	Chromosome spread analysis .....	81
4.10	Confocal microscopy.....	81
4.11	Yeast two-hybrid assay.....	81
4.12	Protein expression and purification .....	82
4.13	Pull down assay.....	82
4.14	Immunolocalization .....	83
4.15	Quantification and statistical analysis .....	83
	References .....	90
	Chapter 2.....	96
	Towards live cell imaging of meiosis in Zea mays.....	96

1	Introduction .....	97
1.1	Maize as a crop model system.....	97
1.2	Meiosis in maize.....	98
1.3	Studying meiosis: a live cell imaging approach.....	101
1.3.1	Previous experimental set-ups for live cell imaging of meiosis .....	102
2	Results .....	105
2.1	Determination of the developmental stage for sample harvesting .....	105
2.2	Identification of candidate genes .....	107
2.3	Generation of reporter lines .....	109
2.3.1	Fluorescent proteins .....	111
2.3.2	Chromosome markers.....	112
2.3.3	Marker for synapsis .....	121
2.3.4	Meiosis initiation and progression.....	127
2.3.5	Marker for meiotic recombination.....	132
2.3.6	Cytoskeleton marker .....	136
2.4	Overview of the generated and analysed reporter lines.....	139
2.5	Experimental set-up for maize live cell imaging.....	140
2.5.1	Sample isolation and mounting.....	140
2.5.2	Microscope set-up .....	141
2.6	Live cell imaging of DSY2 in maize anthers.....	141
3	Discussion.....	145
3.1	Live cell imaging: technique development .....	145
3.1.1	How to visualize meiotic players in living cells.....	145
3.1.2	Sample mounting and imaging .....	147
3.2	Future experiments .....	149
4	Material and methods .....	153
4.1	Plant material and growth conditions.....	153
4.2	Generation of reporter lines .....	153

4.3 Plant transformation .....	154
4.4 Chromosome spreads (acetocarmine staining) .....	155
4.5 Confocal microscopy .....	155
4.5.1 Localization analysis .....	155
4.5.2 Live cell imaging .....	155
4.5.3 Live cell imaging data processing .....	156
References .....	163
Publications and presentations.....	170
Eidesstattliche Vesricherung/Declaration On Oath .....	171
Declaration of contributions.....	172
Confirmation of correct English .....	173
Acknowledgments.....	174



## Abstract

Meiosis is a specialized cell division with a central role in the life cycle of all sexually reproducing organisms. It relies on a coordinated series of events, which results in recombination of homologous chromosomes and ensures the formation of gametes with half of the DNA content of the progenitor cell. In plants, aberration of meiosis can result in the production of aneuploid progeny, reduced fertility and thus, decreased yield. Therefore, understanding the mechanisms that regulate meiosis is of crucial importance for plant breeding and for meeting the increasing food demand.

In this dissertation, I investigated the molecular mechanisms which control chromosome axis remodeling during meiosis in *Arabidopsis thaliana* and I established the basis of a live cell imaging technique to investigate meiotic chromosome dynamics in maize (*Zea mays*).

The chromosome axis is a meiosis-specific protein assembly, built along the entire length of each homolog. HORMA domain proteins (HORMADs) are key components of the chromosome axis and their chromosomal association is dynamic, e.g., ASY1 in *Arabidopsis* is recruited to the axis at early prophase and later largely removed when homologous chromosomes synapse. However, how the dynamics of meiotic HORMADs are brought about is poorly understood. In this study, I identified COMET, the *Arabidopsis* homolog of human p31<sup>comet</sup>, which is known for its function in the Spindle Assembly Checkpoint (SAC), to be a central regulator of ASY1 dynamics in meiosis. I showed that COMET mediates the nuclear targeting of ASY1 in early prophase and later also promotes the release of ASY1 from the chromosome axes to allow full synapsis. Additionally, evidence is provided that COMET regulates ASY1 by serving as an adaptor for the AAA+ ATPase PCH2.

In the second part of my thesis, I focused on developing a live cell imaging approach for studying meiosis in the crop model organism maize. So far, most studies on meiosis have relied on the analysis of fixed material, which, despite informative, can capture the underlying cellular dynamics only to a small degree. Conversely, live cell imaging represents a unique tool to investigate the temporal and spatial aspects and allows the observation of individual cells over time. For this purpose, I generated stable reporter lines for different genes of interest, which

highlight hallmarks of meiosis, e.g., for DSY2, a component of the chromosome axis and for ZYP1, marking the central element of the synaptonemal complex. In total, 21 genomic constructs were cloned and have been transformed into maize. In addition, a live cell imaging protocol from Arabidopsis was adapted to maize, i.e., living anthers of maize were isolated, cultured on a suitable medium and imaged by confocal microscopy. The first live cell imaging data are based on the observation of DSY2 in living maize anthers, which could be kept alive for a period of 50 hours and allowed gaining insights into chromosome dynamics during prophase I. In combination with the other reporters, it will now be possible to investigate the dynamics of key meiotic events, such as pairing and synapsis, which numerous studies have demonstrated to be dependent on intense chromosome movements. Thus, this approach will allow studying maize meiosis from a spatio-temporal perspective, allowing new insights into this fundamental process in a monocotyledonous crop.

# Zusammenfassung

Meiose ist eine spezielle Form der Zellteilung mit einer zentralen Rolle im Lebenszyklus aller sich sexuell reproduzierenden Organismen. Es beruht auf einer koordinierten Abfolge von Ereignissen, die zur Rekombination homologer Chromosomen führen und die die Bildung von Gameten mit der Hälfte des DNA-Gehalts der Vorläuferzelle sicherstellen. In Pflanzen kann eine Aberration der Meiose zur Produktion aneuploider Nachkommen, einer verringerten Fruchtbarkeit und damit zu einem verringerten Ertrag führen. Daher ist das Verständnis der Mechanismen, die die Meiose regulieren, für die Pflanzenzüchtung und somit auch für die Deckung des steigenden Nahrungsbedarfs von entscheidender Bedeutung.

In dieser Dissertation wurden die molekularen Mechanismen untersucht, die den Umbau der Chromosomenachse während der Meiose in *Arabidopsis thaliana* steuern. Darüber hinaus wurde die Grundlage zur Untersuchung der Dynamik meiotischer Chromosomen in Mais (*Zea mays*) mit Hilfe der Lebendzellbeobachtung („Live Cell Imaging“) gelegt.

Die Chromosomenachse besteht aus einer Meiose-spezifischen Proteinanordnung, die sich über die gesamte Länge jedes homologen Chromosoms erstreckt. HORMA-Domänenproteine (HORMADs) sind Schlüsselkomponenten der Chromosomenachse und ihre chromosomale Assoziation ist dynamisch. So wird z.B. ASY1 in *Arabidopsis* in der frühen Prophase auf der Achse rekrutiert und später, wenn homologe Chromosomen den synaptomenalen Komplex ausbilden, weitestgehend entfernt. Wie die Dynamik meiotischer HORMAD Proteine reguliert wird, ist jedoch kaum bekannt. In dieser Studie wurde COMET, das *Arabidopsis*-Homolog des menschlichen p31<sup>comet</sup>, das für seine Funktion im Spindle Assembly Checkpoint (SAC) bekannt ist, als zentraler Regulator der ASY1-Dynamik während der Meiose identifiziert. Es konnte gezeigt werden, dass COMET das nukleare Targeting von ASY1 in der frühen Prophase vermittelt und später auch die Freisetzung von ASY1 aus den Chromosomenachsen fördert, um eine vollständige Synapse zu ermöglichen. Zusätzlich wurde der Nachweis erbracht, dass COMET ASY1 reguliert, indem es als Adapter für die AAA + ATPase PCH2 dient.

Im zweiten Teil meines Projekts konzentrierte ich mich auf die Entwicklung eines „Live cell imaging“ Ansatzes zur Untersuchung der Meiose im Mais als weiteren Pflanzenmodellorganismus. Bisher stützten sich die meisten Studien zur



Meiose auf die Analyse von fixiertem Material. Trotz vieler dabei gewonnener Informationen kann dabei die zugrunde liegende Zelldynamik nur in geringem Maße erfassen werden. Im Gegensatz dazu stellt das „Live Cell Imaging“ ein einzigartiges Werkzeug dar, um zeitliche und räumliche Aspekte zu untersuchen und die Beobachtung einzelner Zellen zu ermöglichen. Zu diesem Zweck wurden Reporterlinien für verschiedene Gene hergestellt, die unterschiedliche Komponenten der Meiose hervorheben, z.B. für DSY2, eine Komponente der Chromosomenachse, und für ZYP1, das das zentrale Element des synaptonemalen Komplexes markiert. Zusätzlich wurde ein „Live Cell Imaging“ Protokoll für lebende Zellen von Arabidopsis an Mais angepasst. Dazu wurden lebende Antheren von Mais isoliert, auf einem geeigneten Medium kultiviert und durch konfokale Lasermikroskopie analysiert. Die ersten „Live Cell Imaging“ Daten basieren auf der Beobachtung von DSY2 in Mais-Antheren, die über einen Zeitraum von 50 Stunden am Leben gehalten werden konnten und Einblicke in die Chromosomendynamik während der Prophase I ermöglichten. In Kombination mit den anderen Reportern wird es nun möglich sein, die Dynamik wichtiger meiotischer Prozesse wie Paarung und Synapsis zu untersuchen, von denen zahlreiche Studien gezeigt haben, dass sie von intensiven Chromosomenbewegungen abhängen. Dieser Ansatz ermöglicht es daher, die Meiose von Mais aus einer räumlich-zeitlichen Perspektive zu untersuchen und neue Einblicke in diesen grundlegenden Prozess in einer Monokotylen Pflanzenspezies zu erhalten.



# 1. Introduction

## 1.1 Meiosis, a special kind of division

Meiosis is a specialized cell division characteristic for eukaryotes and essential for sexual reproduction. The function of meiosis is to generate cells that contain half of the genetic material of the parental cells and which develop into germ cells. Subsequently, the fusion of germ cells (fertilization) can restore the original ploidy level in the offspring. Thus, meiosis allows the formation of haploid gametes from a diploid organism. Moreover, meiosis drives genetic diversity as homologous chromosomes of different parental origin recombine, giving rise to a new assortment of genetic alleles [1].

In Angiosperms, such as the model organism *Arabidopsis thaliana*, meiosis occurs within reproductive tissues of the flower, the anther and the ovule, while they are still enclosed in the immature, developing flower bud. Compared to animals, the establishment of a germline occurs at late stages of development, after the transition from a vegetative to a floral meristem, and it relies on an intricate regulation at transcriptional, translational and post-translational level [2].

In meiosis, a single round of DNA replication is followed by two rounds of chromosome segregation: meiosis I, in which the pairs of homologous chromosomes segregate (reductional cell division) and meiosis II, where the sister chromatids are separated (equational cell division). Failure in the proper execution of chromosome and/or chromatid segregation leads to the formation of unbalanced gametes and aneuploid or polyploid progeny. To ensure the correct completion of the meiotic division program, several coordinated events must take place.

First, the success of the reductional division depends on correct pairing and synapsis, i.e., homolog juxtaposition and interaction, and on crossover (CO) formation between the homologs, which creates a physical link. The presence of at least one CO per bivalent (a pair of homologous chromosomes) is known as CO-insurance and is an absolute requirement for proper segregation.

Second, an accurate deposition and removal of cohesin, the protein complex responsible for establishing cohesion between sister chromatids, which also influences synapsis and recombination [3].

Third, there is a requirement for co-orientation of sister chromatids during meiosis I, so that sister kinetochores (proteinaceous complexes that assemble on each chromosome and mediate their interaction with microtubules) are captured by microtubules emanating from the same pole, and bi-orientation of sister chromatids in the following meiosis II, when sister chromatids separate and move to opposite poles [4].

Last, the mitotic rules of the cell cycle, where each DNA replication is followed by nuclear division, need to be modified to prevent an intervening replication step between the two meiotic divisions [5].

## **1.2 Overview of meiosis**

The meiotic cell cycle consists of a series of consecutive phases, i.e., meiotic interphase, which comprises the G1, S and G2 sub-phases, followed by meiosis I and meiosis II (**Figure 1**). During S-phase the DNA is duplicated and several important events occur, e.g., chromatin modifications and the expression of many meiotic genes, to ensure a successful entry, progression and completion of meiosis [6-8]. Thus, the S-phase separates the G1 phase with unreplicated chromosomes from the G2 phase in which all chromosomes consist of two chromatids [6]. Both meiosis I and meiosis II are divided into four substages: prophase, metaphase, anaphase and telophase.

Meiotic prophase I is a long and complex process and has been further subdivided into five sub-stages according to cytological features of the chromosomes: leptotene, zygotene, pachytene, diplotene, and diakinesis [9].

Early in prophase I chromosomes start to condense and become visible as thin and unsynapsed threads, organized by the formation of the chromosome axis (leptotene stage). Concomitantly, meiotic recombination is initiated by the occurrence of double-strand breaks (DSBs) on the chromosomes.

In order to achieve the ploidy reduction in meiosis I, homologs must recognize each other and pair, preparing for separation afterwards. The term "pairing" describes the transient interaction at localized regions of homologs and in most organisms, it depends on DNA homology to verify that the interacting chromosomes are indeed homologous, however, the exact mechanism remains poorly understood [10]. Chromosome movements and temporary chromosome arrangements, like the telomere bouquet, are thought to contribute to the search of homologs [11-14]. Local pairing progresses to homolog juxtaposition, which is

also homology-dependent and refers to the coming together of homologs after the initial transient interactions [10], and eventually evolves into synapsis.

Synapsis is initiated at zygotene and consists of an extensive and stable interaction between the homologs, which involves the formation of a complex proteinaceous structure called the synaptonemal complex (SC). During this stage parts of homologs can be detected as "fused" together (synaptic region) by microscopic analysis. When the homologs are fully synapsed (pachytene), the SC mediates the intimate connection along their length and each pair of synapsed homologs appears as a thick thread-like structure. A large proportion of the DSBs has by now been repaired by the recombination machinery and this results in the formation of crossovers (COs) and non-crossovers (NCOs).

After pachytene, the SC is disassembled and homologs partially separate, except at the chiasmata, the cytological manifestation of a CO. This substage is recognized as diplotene. Subsequent chromosome condensation results in highly compacted bivalents (attached pairs of homologs), reaching diakinesis at the end of prophase I.

The bivalents move to the center of the cell and align at the equatorial plane at metaphase I, with each bivalent displaying one to three chiasmata [6]. The spindle, a microtubule-based structure, is formed and the homologs are captured by microtubules that emanate from opposite poles, whereas sister kinetochores by microtubules emanating from the same pole (co-orientation).

Homologs are pulled towards the two opposite poles of the cells (anaphase I) and cohesion is cleaved from the chromosome arms, but not at centromeres in order to avoid premature separation of sister chromatids. At telophase I, meiocytes present two distinct clusters of decondensed chromosomes at each pole; the nuclear envelope (NE) is reformed. Interkinesis is a short stage between meiosis I and meiosis II, in which chromosomes decondense.

The second meiotic division (meiosis II) begins with prophase II, when chromosomes re-condense. The two groups of chromosomes are aligned separately at two division planes in metaphase II and two spindles are formed. At the onset of anaphase II, all cohesion associated with chromatin is cleaved and sister kinetochores are captured by microtubules emanating from opposite poles (bi-orientation), thereby promoting sister chromatids segregation to opposite poles and the formation of four clusters of chromosomes.

Chromosomes decondense, the nuclear envelope reforms at telophase II and cytokinesis concludes the formation of four haploid daughter cells. Notably, in *Arabidopsis* a simultaneous cytokinesis takes place at the end of meiosis II in male meiosis [15], whereas cytokinesis in female meiocytes is executed twice, at the end of meiosis I and II (successive cytokinesis), similarly to other plants such as maize and rice [16].

In *Arabidopsis*, meiosis takes approximately 33 hours, most of which (at least 26 hours) is dedicated to prophase I [7, 17]. Then, the time-span from metaphase I to the onset of meiosis II is only 2 hours, while meiosis II takes another 4 hours to complete [17].

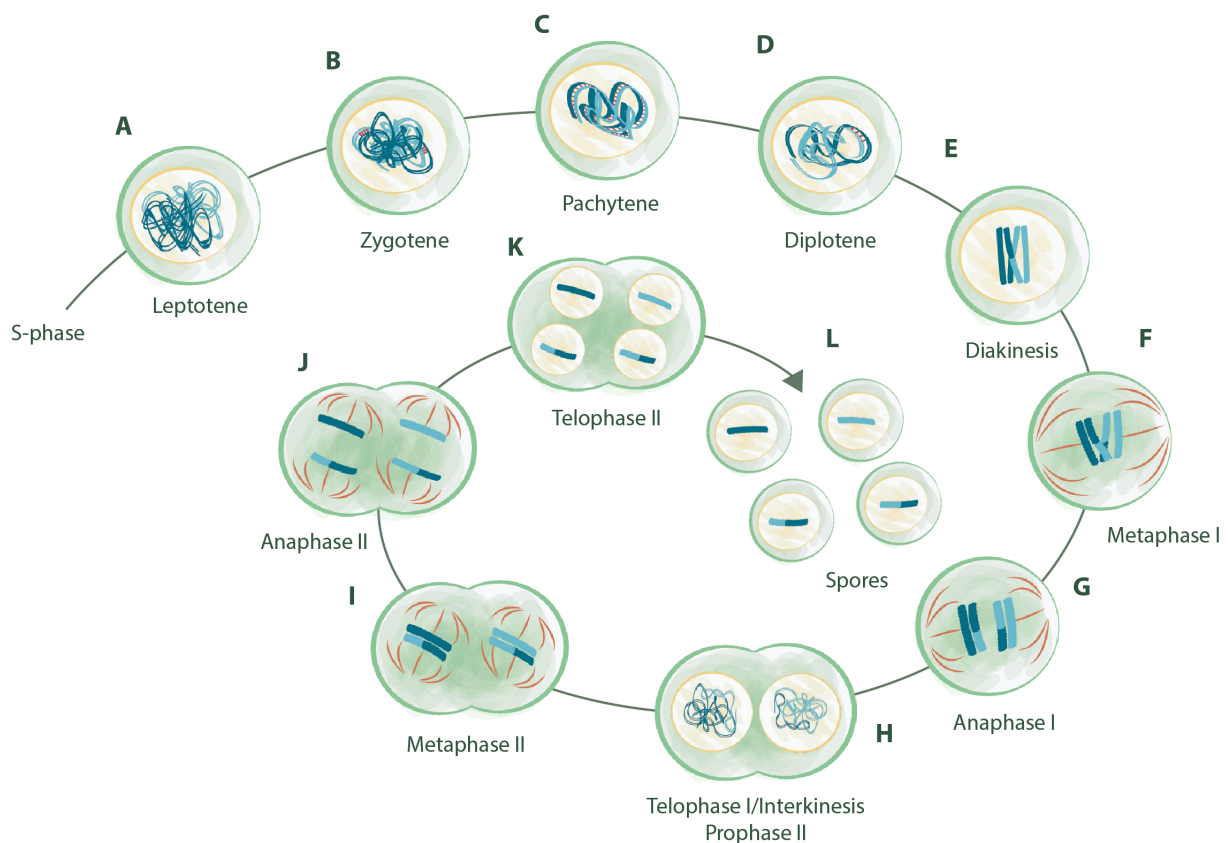


**Figure 1: Schematic overview of meiosis in *Arabidopsis thaliana***

Cytoplasm is depicted in green, nucleus in yellow, homologous chromosomes in blue and light blue, cytoskeleton in red.

At leptotene, the chromosome axes are formed and recombination initiates (A). During zygotene, homologous chromosomes start pairing and eventually synapsis takes place through the polymerization of the synaptonemal complex and recombination progresses (B). At pachytene, synapsis is completed and recombination further progresses (C). At

diplotene, the synaptonemal complex disassembles and homologs partially separate, except at the chiasmata (D). At diakinesis, chromosome condense and bivalents are visible I. At metaphase I the spindle forms and aligns the bivalents at the metaphase plate (F). The release of arm sister chromatid cohesion allows the migration of chromosomes to the two poles at anaphase I, while pericentromeric cohesion is specifically protected (G). At interkinesis, two nuclei are formed, chromosomes experience a significant decondensation and meiosis II is prepared (this stage encompasses telophase I and prophase II) (H). At metaphase II, two spindles form and align chromosomes on two metaphase plates (I). At anaphase II, sister chromatids separate following centromeric cohesion release (J). At telophase II, four nuclei are formed and cytokinesis initiate (K). At the end of meiosis, four haploid spores are released after cytokinesis (L).

### **1.3 The chromosome axis**

The emergence of meiosis during evolution required major innovations in chromosome organization. A hallmark feature of meiosis is the formation of the chromosome axis.

The chromosome axis assembles in early meiotic prophase and fulfills important functions in meiosis. First, it provides a scaffold for the organization of the replicated chromosomes into linear arrays of DNA loops, with one axis per chromosome, i.e., sister chromatids are anchored to the same proteinaceous core [10, 18]. Second, it orchestrates the formation of DSBs and their repair as inter-homolog crossovers [1, 19-27] and third it serves as a structural element of the synaptonemal complex (SC), as the chromosome axes of each homolog pair become integrated into the SC as lateral elements and linked by coiled-coil transverse filaments along their entire length [10, 28].

Upon early axis assembly chromosomes become microscopically visible as “thin threads”, a feature after which the leptotene stage is named. As cells progress through zygotene and pachytene, chromosomes undergo significant linear compaction without disruption of the chromosome axes. The composition of the chromosome axis is highly conserved in eukaryotes and its components include DNA-binding and organizing cohesin complexes, axis core proteins and HORMA domain proteins (HORMADs) (**Figure 2**).

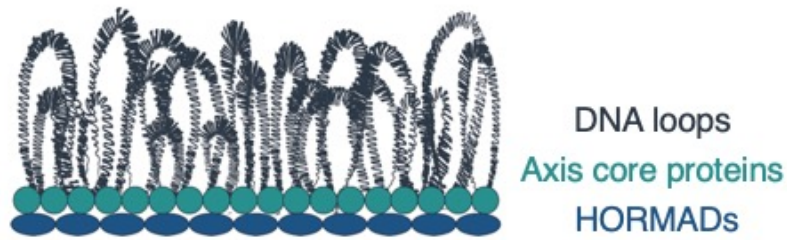


**Figure 2: The chromosome axis**

Schematic representation of the architecture of the meiotic chromosome axis. Chromosomes are organized in linear array of DNA loops (depicted in black), which emanate outward from the axis. Components of the chromosome axis include DNA-binding cohesin complexes, axis core proteins (in green) and HORMA domain proteins (in blue).

### 1.3.1 The axis core proteins

The axis core proteins associate with cohesin complexes – protein complexes which mediate sister chromatid cohesion (see paragraph 1.6) – and then form bundles to assemble a flexible scaffold on which meiotic recombination takes place [29]. The first identified axis core protein was the coiled-coil protein Red1 in budding yeast [30] and orthologs have been identified in mammals such as SYCP2 and SYCP3 [31, 32]. In *Arabidopsis thaliana*, despite low sequence similarity, ASY3 has been proposed to be the functional homolog of Red1 [33], based on phenotypic similarities of the respective mutants and the presence of a conserved C-terminus with predicted coiled-coil character [33]. In addition, ASY4, a short protein with high homology to the ASY3 coiled-coil domain and able to interact with ASY3, was recently described to be part of the chromosome axis as well [34, 35]. Also in other plants, Red1 orthologs have been identified, e.g., PAIR3 in rice [36] and DSY2 in maize [37].

A key conserved function of the axis core proteins is to recruit another important class of proteins to the chromosomal axes, the meiotic HORMADs. Thus, loss of ASY3 in *Arabidopsis* disrupts the axial assembly of the *Arabidopsis* HORMAD protein ASY1 and the subsequent formation of the synaptonemal complex (SC) [33], resulting in a reduced number of COs.



### 1.3.2 The meiotic **HORMADs**

Meiotic **HORMADs** include Hop1 in yeast [38], Hormad1 and Hormad2 in mammals [39], HIM-3, HTP-1, HTP-2, and HTP-3 in *C. elegans* [40-42], PAIR2 in rice [43] and, as mentioned above, ASY1 in Arabidopsis [44].

In early meiotic prophase the meiosis-specific **HORMA** domain proteins localize to the chromosome axis and play a crucial role in cross-over (CO) formation and in directing recombination towards the homolog, i.e., away from the sister chromatid. **HORMADs** have been shown to mediate homolog pairing and SC assembly [25, 45], where the assembly of the SC along each pair of homologs is coordinated with the removal of the meiotic **HORMADs** from chromosomes [39, 46-48]. This meiotic **HORMAD** removal is also thought to constitute a feedback mechanism suppressing further recombination on chromosomes/regions that have already obtained COs [46, 49].

The chromosome association of ASY1 was found to be dependent on ASY3 in a non-reciprocal way, a relationship that seems conserved across the sexually reproducing organisms, including yeast, plants and animals [33, 36, 37, 50], while ASY3 localization is reliant on the cohesin complex, suggesting a hierarchical axis assembly: cohesion -> ASY3 -> ASY1 [33].

Mutants deficient in any of these axial proteins show severe meiotic defects in recombination such as DSBs formation and repair, interhomolog biased recombination and CO formation as well as in chromosome synapsis, highlighting the indispensable functions of the chromosome axis for those meiotic events [33, 36, 37, 51, 52].

### 1.4 The **Synaptonemal Complex**

The synaptonemal complex (SC) was first discovered by Moses [53] and Fawcett [54]. This prominent and evolutionarily well-conserved, yet functionally enigmatic, structure is strictly meiotic.

Establishment of the SC follows the initial alignment and loose pairing of the homologous chromosomes, and is characterized by the appearance of transverse filaments (TFs) which span the gap between the chromosome axes (AE, axial elements), now referred to as lateral elements [10, 55] (**Figure 3**). The zone where the TFs meet and interdigitate constitutes the central element that runs

parallel to and between the lateral elements [55]. Thus, using electron microscopy, the SC can be seen as a tripartite proteinaceous structure [10].

The establishment of the SC is initiated in zygotene and completed by pachytene. As meiosis progresses through diplotene and diakinesis the SC disassembles, so that the homologous chromosomes remain associated only by chiasmata, the cytologically manifestation of crossover events.

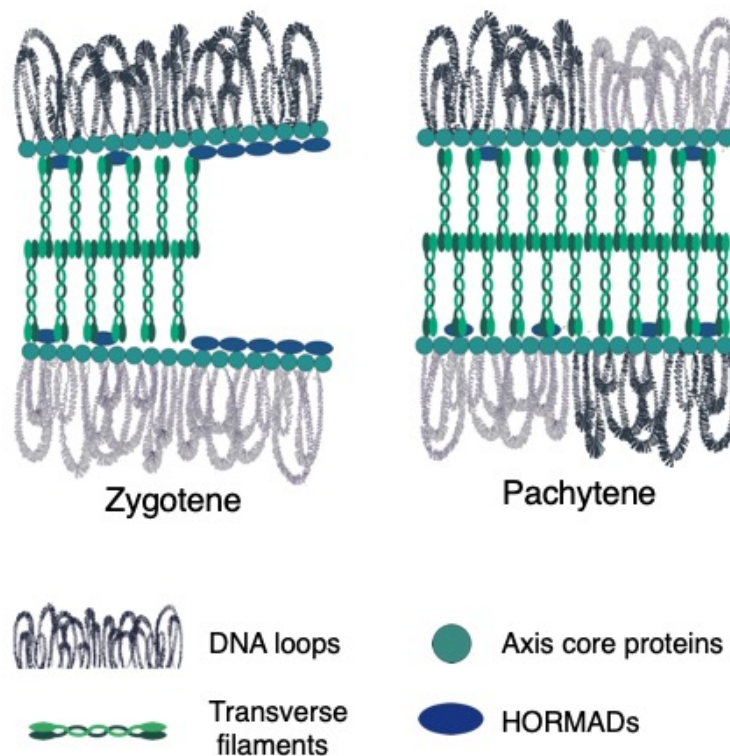


### Figure 3: The synaptonemal complex

Schematic representation of the synaptonemal complex. The establishment of the synaptonemal complex starts at zygotene and is completed by pachytene, when the transverse filaments entirely span the gap between the chromosome axes.

TF proteins have been identified in different eukaryotic organisms such as Zip1 in budding yeast [56], SYP1 in *C. elegans* [57], SCP1 in mammals [58], and within the plant kingdom ZEP1 in rice [59], ZYP1 in barley [60] and the functionally indistinguishable ZYP1a and ZYP1b in Arabidopsis [55].

Central-element proteins are poorly conserved at the primary sequence level, but they share similar structural properties which account for the conservation of SC ultrastructure among eukaryotes. These proteins possess a central coiled-coil

domain, flanked by globular domains at the N and C termini [61]. Studies in yeast and in mouse indicate that the TFs form parallel homodimers that are oriented such that their C termini align along the lateral elements and the N termini of the proteins in a dimer overlap in the central region of the SC, giving rise to the central element.

The interplay between SC and recombination varies among eukaryotes. In *Arabidopsis*, the initial localization of ZYP1 proteins is dependent upon DSB formation and occurs when recombination is at an early stage, prior to extensive strand invasion [55]. Loss of ZYP1a/ZYP1b results in aberrant associations and recombination between nonhomologous chromosomes [55], suggesting that in *Arabidopsis* ZYP1 prevents recombination between nonhomologous chromosomes, rather than limiting homologous CO formation as in the case of rice, where *zep1* mutants show an increase in chiasmata formation [59]. This contrasts with the function of ZYP1 in promoting CO in barley [60], similar to the role of Zip1 in *S. cerevisiae* [62].

## 1.5 Meiotic recombination

Recombination is a prominent feature of meiosis. Meiotic recombination is responsible for allelic shuffling over generation; thus, it increases genetic diversity in the offspring. New, possibly advantageous allele combinations can be obtained, hence forming the basis for plant adaptation to changing environment and for the breeding of new varieties. This genetic mechanism has also likely contributed to the success of eukaryotes during evolution.

Homologous recombination occurs during prophase I, starting at leptotene and is completed by pachytene stage. It is initiated by the formation of programmed DNA double-strand breaks (DSBs) by Spo11 [63] (**Figure 4**); Spo11 appears to be universally conserved among eukaryotes that undergo meiosis [64] and it shares sequence similarity with the A subunit of the archaeal topoisomerase VI (TopVIA) [63]. *Arabidopsis* contains three Spo11 paralogues, two of which, AtSPO11-1 and AtSPO11-2, are required for meiosis [65]. The catalytically active tyrosine residues of both proteins are necessary for DSB formation and the paralogues probably function as a heterodimer [66]. By contrast, AtSPO11-3 is involved in somatic endoreduplication and does not play a role in meiosis [5].

In addition to Spo11, DSB formation requires the presence of accessory proteins such as PRD1, PRD2, PRD3 and DFO in *Arabidopsis* as well as PAIR1, CRC1, SDS

and P31<sup>comet</sup> in rice [67, 68]. In plants, the responsible genes have been identified in fertility screens having a similar mutant phenotype, namely an absence of early recombination markers, like DMC1 foci, no synapsis and no CO formation, leading to random chromosome segregation at anaphase I [69]. Additionally, these mutants can suppress the DSB repair defects of meiotic mutants, such as *rad51*, indicating that they are required for DSB formation itself, rather than DSB repair. Rice CRC1, the ortholog of *S. cerevisiae* PCH2, is a central element component of the synaptonemal complex (SC) and it is also required for DSB formation [70]. Also P31<sup>comet</sup>, recently identified as interacting partner of CRC1, was shown to be a component of the SC and involved in DSB formation [71]. However, the situation is not alike in all plant species. For example rice CRC1 [70] and SDS [72] are required for DSB formation, whereas the corresponding orthologs in Arabidopsis, i.e., PCH2 [47] and SDS, [73] are necessary for meiosis, but dispensable for DSB formation. This suggests a diverse regulation among different species. The majority of meiotic DSBs is repaired without an exchange of DNA between homologous chromosomes. These events are called non-crossovers (NCO). In Arabidopsis, meiotic recombination is initiated by approximately 150-250 DSBs, as estimated by immunostaining of DSB markers, such as  $\gamma$ H2A.X, RAD51, and DMC1 [68], while the number of cross-overs per nucleus falls in the range between 8 and 12 [45, 74].

Following DSB formation, Spo11 remains covalently attached to the 5' -ends of the DNA, until the MRX-N complex [Mre11-Rad50-Xrs2 (Nbs1)] and Com1 (Sae2) promote its endonucleolytic cleavage and eventually DSB processing [68]. The 5' DNA ends are resected to generate 3' single-stranded DNA (ssDNA) tails. The 3' single-strand DNA ends interact with the recombinases DMC1 and RAD51, the homologues of the bacterial RecA, to form a nucleoprotein filament. In vertebrate animals and plants, the *RAD51* gene family is highly conserved and is involved in both mitotic and meiotic recombination; mutations in any of the RAD51 genes required for meiotic recombination results in meiotic chromosome fragmentation, indicating a defect in meiotic DSB repair [67, 68]. Conversely, DMC1 is exclusively active in meiosis. In Arabidopsis, *dmc1* mutants exhibit 10 unfragmented univalents instead of 5 bivalents. The lack of chromosome fragmentation in *dmc1* suggests that cells lacking DMC1 can repair meiotic DSBs using sister chromatids as templates [75]. Thus, in wildtype meiocytes, DMC1 has a role in promoting inter-homologue recombination and RAD51 functions as a

DMC1 accessory factor. The recombinases DMC1 and RAD51 mediate the 3' single strand invasion into the double helix of one of the two non-sister chromatids of the paired homologous chromosome to form a recombination intermediate, called a D loop. The invading 3' end is a target for recombination-associated DNA synthesis, which extends the D loop to expose sequences that can anneal to the second 3' end on the opposite side of the original break in a process called second-end capture [68]. Additional DNA synthesis using the second 3' end, followed by ligation, yields an intermediate called a double Holliday junction (dHJ), which link the four DNA strands of two homologous chromosomes.

Primarily the resolution of dHJ leads to the formation of COs [76]. Two types of COs exist, generally referred to as class I and class II COs. The two CO pathways differ not only in their molecular machinery, but also in the distribution of the resulting COs. Whereas class I COs are further apart than expected by chance (CO interference), class II COs are distributed independently of one another [5]. Type I CO constitute the majority of COs (70-85%) and depend on the ZMM group proteins (MSH4, MSH5, MER3, HEI10, ZIP4, SHOC1, PTD), as well as in Arabidopsis on MLH1 and MLH3. Regarding the high degree of protein conservation, this mechanism of type I CO formation seems to be conserved among plant species [68]. Much less is known about the molecular players of the non-ZMM CO pathways in plants, with MUS81 being the only player characterized up to now [77]. In addition to class I and II CO pathways, an alternative CO pathway may exist, since double mutants of factors in both classes, such as *msh4 mus81*, have a residual 5–10% of COs [77]. However, the nature of this pathway remains unclear and it may be active only when the primary pathways are affected [5].

CO control in Arabidopsis is tightly regulated: each of the five chromosome pairs gets at least one, a phenomenon called CO assurance, in order to ensure proper chromosome segregation by creating a physical link between homologs. Moreover, the fact that only few DSBs are repaired as COs suggests the presence of inhibitory mechanisms (anticrossover factors) that prevent CO formation. Recently, molecular genetic studies have identified three types of anticrossover factors in Arabidopsis: the BTR complex consisting of RECQ4A, RECQ4B DNA helicases, TOPOISOMERASE3 $\alpha$ , and RMI1; the FANCM DNA helicase including the MHF1 and MHF2 cofactors and the AAA-ATPase FIDGETIN-LIKE1 (FIGL1) in combination with its FIDGETIN-LIKE-1 INTERACTING PROTEIN (FLIP) [68].

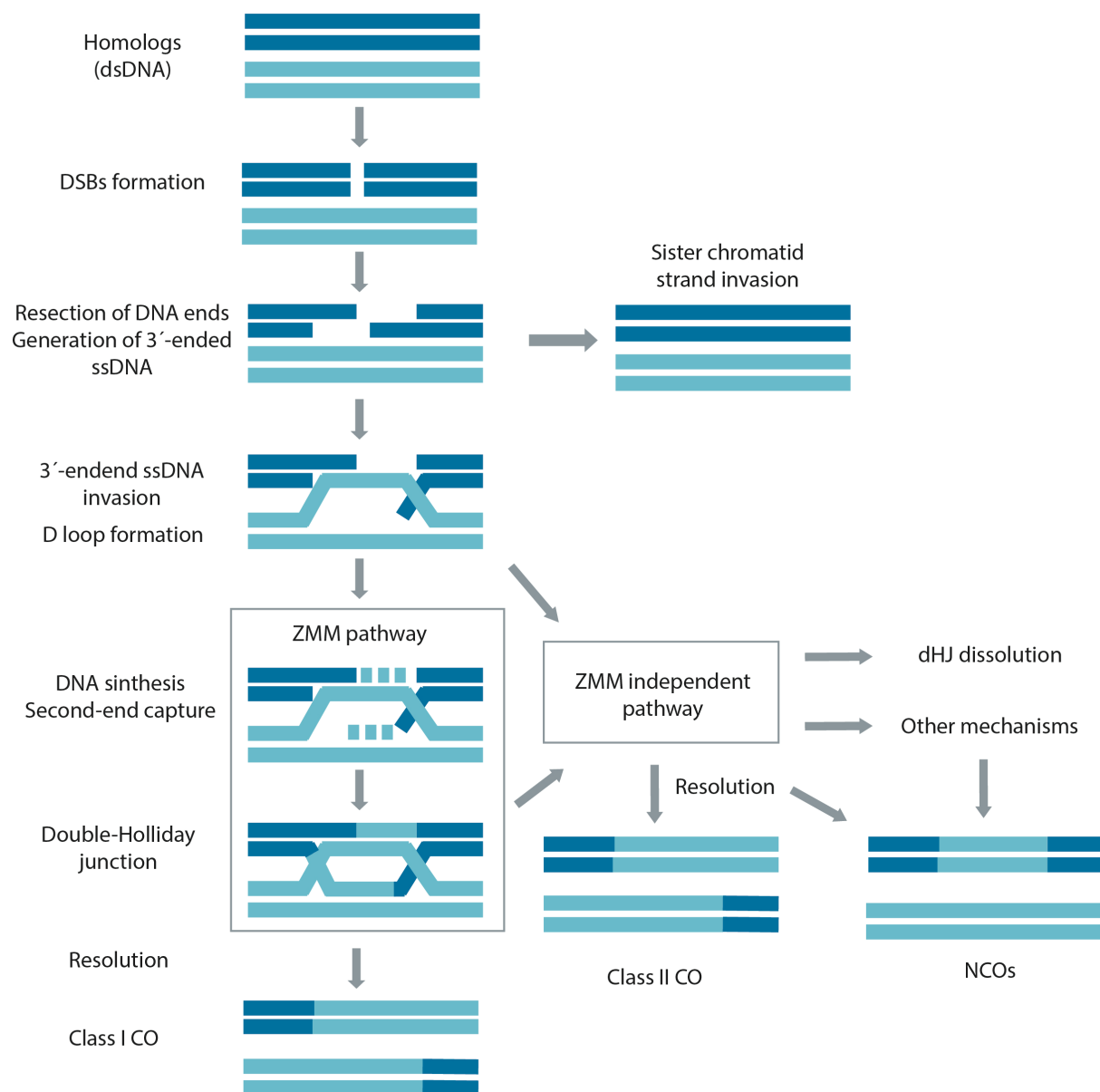


**Figure 4: Model of meiotic recombination mechanisms in *Arabidopsis thaliana***

Meiotic recombination is initiated by the formation of a large number of double-strand breaks (DSBs). DSB ends are resected to yield 3' single-strand tails, which can invade either the sister chromatid or one of the non-sister chromatids of the homologous chromosome to form a D loop. DNA synthesis (dashed lines), second-end capture and ligation lead to the formation of double Holliday junctions (dHJ). Primarily the resolution of dHJ leads to the formation of crossovers (COs), although a small number of non-crossovers (NCOs) might originate from this pathway. The intermediates can be resolved as class I COs by the ZMM pathway. A portion of intermediates is resolved into class II COs by a ZMM-independent pathway. Alternatively, the intermediates can be matured into noncrossovers (NCOs) through dHJ dissolution and other mechanisms.

## 1.6 Sister chromatid cohesion

In eukaryotes, DNA faithfully duplicates during the S phase of the cell cycle. The two products of replication of a chromosome are called sister chromatids. The correct transmission of chromosomes during meiosis requires the establishment of cohesion between sister chromatids at the time of their synthesis [78] and the subsequent release in a stepwise manner [3]. At the end of prophase I, cohesion is released along the chromosome arms to facilitate the resolution of chiasmata (which hold homologs together), but is maintained at centromeres preventing precocious sister chromatid segregation [79]. At anaphase II, destruction of centromeric cohesion allows the separation of sister chromatids.

Moreover, sister chromatid cohesion is required for proper attachment of chromosomes to the spindle with the same polarity (monopolar attachment) during the first meiotic division and subsequently, during meiosis II, in a bi-polar way. Maintenance and regulation of the sister chromatid cohesion (SCC) is performed by the cohesin protein complex. SCC plays a crucial role not only in chromosome segregation, but also in DNA recombination repair, chromosome structure organization and gene expression in eukaryotes [80, 81].

The cohesin complex contains four core subunits: two members of the structural maintenance of chromosomes (SMC) protein family, named SMC1 and SMC3; the  $\alpha$ -kleisin sister chromatid cohesion protein 1 (SCC1) and the SCC3 subunit [80]. The four core subunits are organized in a ring-like structure which holds the two sister chromatids together [82] (**Figure 5**).

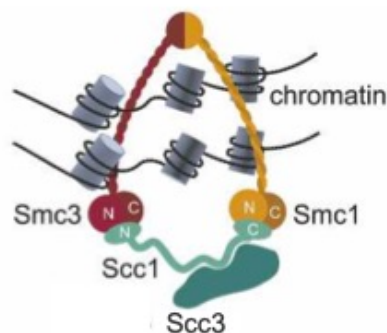


**Figure 5: The cohesin complex**

Model for the architecture of the cohesin complex on chromatin (adapted from [83]). The cohesin complex contains four core subunits: SMC1, SMC3, SCC1 and SCC3. According to the "ring" model, cohesin mediates sister chromatid cohesion by topological embrace, i.e., a single cohesin ring encircles the replicated sister chromatids.

The Arabidopsis genome encodes for single-copy genes of *SMC1*, *SMC3* and *SCC3*, which were identified in somatic and meiotic tissue [84, 85] and for four kleisins genes: *SYN1*, *SYN2*, *SYN3* and *SYN4* also known as *REC8*, *RAD21.1*, *RAD21.2*, and *RAD21.3* [86]. Even though a certain level of redundancy has been observed, the four complexes, which differ by the kleisin subunit, exert different functions [86]. *REC8* mediates cohesion exclusively during meiosis [79, 87, 88], *RAD21.1* and *RAD21.3* are mainly expressed in meristematic tissues and are predicted to represent mitotic cohesins [89], *RAD21.2* is expressed in both somatic and meiotic cells and has been described as enriched in the nucleolus, which suggests an additional involvement in controlling rDNA structure and transcription or in rRNA processing [90]. *RAD21.2* seems especially relevant for reproduction, since knockdown of *RAD21.2* results in defects in chromosome synapsis and early recombination [90, 91]. Four kleisin genes showing different functions in somatic cells and during meiosis, were also reported for *C. elegans* [92, 93] and rice [94-96], while in maize *AFD1* was found to be the meiosis specific kleisin [97, 98]. In addition to the core components, three other proteins have been identified that are associated with cohesin. Precocious dissociation of sisters protein 5 (*Pds5*), which assists an acetylation of the *SMC3* subunit and is needed to close the cohesin ring [99], *Wings apart-like protein* (*Wapl*), a cohesin dissociation factor [100], and a *WAPL* inhibitor, *Sororin* in vertebrates [101, 102] and *SWITCH1/DYAD* in Arabidopsis [103].

Sister chromatid cohesion is released in a stepwise manner [3] (**Figure 6**). To prevent a premature release of sister chromatid cohesion, at early meiosis *SWI1* is recruited to chromosomes by interacting with *PDS5* proteins. The maintenance of cohesion is ensured by the binding of *SWI1* to *PDS5*, thus preventing a *WAPL*-*PDS5* interaction. Later, *SWI1* is released from chromatin by *CDKA;1*-dependent phosphorylation and degraded, hence allowing the interaction between *WAPL* and *PDS5* and activating a removal pathway of cohesion. Cohesion is removed on the one hand by the non-proteolytic action of *WAPL* but also released by a separase-dependent proteolytic cleavage of the kleisin subunit *REC8*. The endopeptidase separase recognizes phosphorylated *REC8* as a target [104]. However, at anaphase I centromeric cohesin is largely protected by the Shugoshin-*PP2A* complex, which binds and dephosphorylates cohesin, preventing its removal [105, 106]. Additionally, another important protector of *REC8*, *PATRONUS*



(PANS1) has been identified in plants, having a prominent role in guarding centromere cohesion during interkinesis [107].

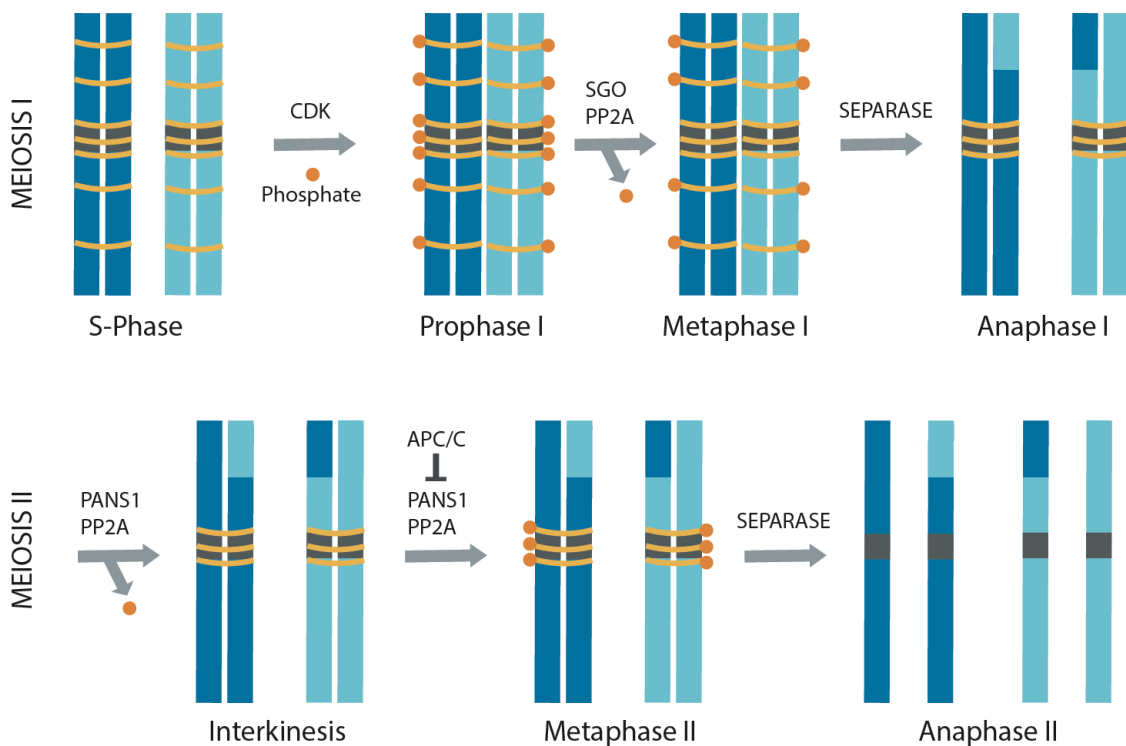


**Figure 6: Cohesion dynamics during meiosis**

During interphase, cohesin rings are loaded and closed on chromosomes hence establishing sister chromatid cohesion (SCC). During late prophase I, SCC is largely removed from the chromosome arms by a WAPL-mediated non-proteolytic prophase pathway. At anaphase I onset, the cohesin on chromosome arms is cleaved completely by Separase, which recognizes phosphorylated REC8 as a target, while the centromeric cohesin is protected by the Shugoshin-PP2A (Sgo-PP2A) complex. Patronus-PP2A (PANS1-PP2A) protect centromeric cohesion in interkinesis; at anaphase II onset, the remaining cohesin at centromeres is released by the cleavage of Separase, thus allowing the separation of sister chromatids.

## 1.7 Cell cycle regulation

The meiotic sequence of two nuclear divisions without an intervening DNA replication is a unique bending of the cell cycle rules, which usually ensure the strict alternation of one replication and one division in mitotic cells. Other exceptions to this typical cell cycle control are endomitosis and endoreplication,

where several replications occur without chromosome segregation, leading to cellular ploidy increase [108].

Hence, special events must exist to specify meiotic cells and to precisely control the entry, the progression and the exit from the meiotic division program. How the core cell cycle machinery is modified for the purpose of meiosis is not yet fully understood. Interestingly, in spite of the differences in the kind of cell division, mitosis and meiosis are mainly controlled by the same regulators, i.e., cyclins, cyclin-dependent kinases (CDKs) and the anaphase-promoting complex/cyclosome (APC/C), a conserved multi-subunit E3 ubiquitin ligase that triggers the degradation of multiple substrates, including cyclins [109]. This suggests a difference in the regulation of these control factors between mitosis and meiosis [110].

In flowering plants meiotic cells are formed late during development. It has been found that post-transcriptional regulation, i.e., at the RNA level, is important for germ cell specification in Arabidopsis, maize and rice where small RNAs are implicated in the repression of a germ cell fate in somatic tissues [111-113]; another example comes from rice, where the loss of *MEIOSIS ARRESTED AT LEPTOTENE 2 (MEL2)*, which encodes for a protein with a RNA recognition motif, results in failure of most meiocytes to enter the meiotic S phase [114]. However, it is not yet understood how developmental regulators of meiotic cell fate initiate the meiotic cell division program. Programming of meiosis already starts before or during the meiotic S phase, as suggested by the observation that meiotic S phase is much longer than an S phase preceding mitosis [115, 116].

Progression through the cell cycle has been found to rely on quantitative and qualitative aspects of CDK-cyclin complexes [110, 117] (**Figure 7**). During mitosis (**Figure 7A**), medium levels of CDK activity are required for the induction of S phase and high levels are necessary to promote onset of M phase. The oscillations in the activity of CDK-cyclin complexes not only define the different phases, but also ensure a unidirectional progression in the cell cycle.

In plant meiosis (**Figure 7B**), during the extended meiotic prophase I, the activity of CDK-cyclin complexes increases slowly until peaking at the onset of the first division [110]. This activity drops when cyclins are degraded by the APC/C to allow the segregation of homologous chromosomes at anaphase I [109]. The transition from meiosis I to meiosis II through interkinesis requires a fine-tuning of cyclin-CDK activity. The drop in activity is not complete, however, it must be

low enough to allow spindle disassembly and exit from meiosis I, but high enough to avoid complete exit from meiosis, allowing entry into the second division without another round of DNA replication [110]. CDK-cyclin activity increases again at meiosis II, followed by a complete abolishment of this activity by the APC/C that allows sister chromatids to segregate to opposite poles [110]. The mechanisms that ensure the entry into a second division must be turned off to avoid the entry into a third division and ensure meiotic exit.

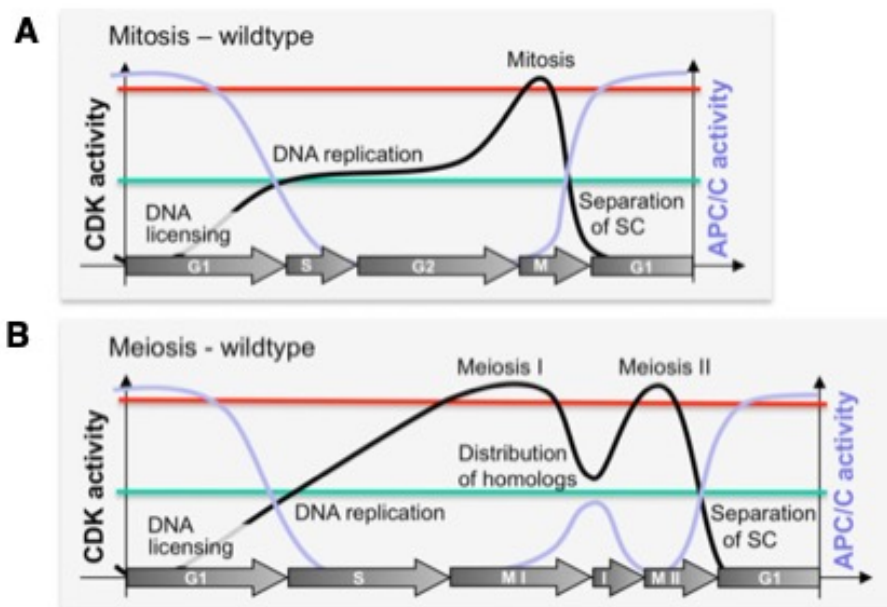


**Figure 7: Cell cycle regulation in mitosis and meiosis**

Hypothetical activity levels of CDK and APC/C complexes during mitosis and meiosis (adapted from [110]). Levels of CDK activity are depicted in black and putative threshold for S phase in green and for M phase in red; levels of APC/C are depicted in violet.

Progression through mitosis is thought to rely on increasing levels of CDK activity. Medium levels of CDK activity are required for the induction of S phase, and high levels are necessary to promote M phase. In order to license the origins of replication for S phase, CDK activity has to be low; this is largely accomplished by the activity of the APC/C that mediates the degradation of cyclins at the end of mitosis and thus sets back CDK activity. The APC/C is kept largely inactive until anaphase; this inhibition is released only if all chromosomes are attached to the mitotic spindle (A). During meiotic prophase I, the activity of CDK-cyclin complexes increases slowly until peaking at the onset of the first division. The activity drops with the degradation of cyclins by the APC/C allowing the segregation of homologous chromosomes at anaphase I. The transition from meiosis I to meiosis II requires a fine-tuning of cyclin-CDK activity, with a partial reduction that has to be low enough to allow spindle disassembly and exit from meiosis I, but high enough to avoid complete exit from meiosis and entry into the second division without DNA

replication. CDK-cyclin activity increases again at meiosis II, followed by a complete abolishment of this activity by the APC/C that allow sister chromatids to segregate to opposite poles (B).

Arabidopsis has at least five cell cycle controlling CDKs (CDKA;1, CDKB;1, CDKB1;2, CDKB2;1 and CDKB2;2) and more than 50 cyclins [118, 119]. For full activity CDKs require the binding of cyclin partners. CDKA;1 has been characterized as the major cyclin-dependent kinase that drives mitotic and meiotic progression in plants [48, 120]. Whereas several cyclins have been shown to play a role during meiosis, the core cyclins that directly regulate meiotic progression still remain to be fully identified.

According to their sequence similarity to animal cyclins, cyclins have been classified as A-, B-, C-, D-, H-, and L-type cyclins. In Arabidopsis we find 41 A-type, nine B-type and four D-type cyclins as well as SDS, an atypical meiosis-specific cyclin that displays similarities with A- and B-type cyclins [118, 119, 121]. Cyclins contain a conserved 250-amino acid region called "cyclin core" [122], which comprises the CDK-binding site. In addition, some cyclins contain a Destruction box (D-box), which is involved in cyclin proteolysis by the ubiquitin-dependent proteasome pathway [119, 123-125], or another motif called PEST region, which is rich in Proline (P), Glutamic acid (E), Serine (S) and Threonine (T) residues, and is a marker for unstable proteins [126]. The presence of these motifs is consistent with cyclin function, which requires rapid degradation to terminate CDK activity at a specific point during the cell cycle.

The first cyclins in Arabidopsis that were shown to have a meiotic function are the A-type cyclin TAM, also called CYCA1;2, essential for the transition from meiosis I to meiosis II [121, 127], SOLO DANCERS (SDS), whose mutation affects pairing and recombination level [69, 73] and CYCB3;1, the only B-type cyclin that was found to be expressed in meiosis, and specifically accumulated in metaphase I and metaphase II localizing to the spindle [128]. Additionally, TDM1/MS5 (THREE DIVISION MUTANT1/MALE STERILE 5) which is required for meiotic exit – *tdm1* mutant fails to terminate meiosis after meiosis II and go through an aberrant third division [129-131]. The turnover of cyclins is regulated by the APC/C and mutants in an APC/C inhibitor protein called OMISSION OF SECOND DIVISION 1 (OSD1)/GIGAS CELL (GIG) exit meiosis after the first division [132, 133].

## References

1. Zickler, D., and Kleckner, N. (2015). Recombination, pairing, and synapsis of homologs during meiosis. *Cold Spring Harbor perspectives in biology* 7, a016626.
2. Schmidt, A., Schmid, M. W., and Grossniklaus, U. (2015). Plant germline formation: common concepts and developmental flexibility in sexual and asexual reproduction. *Development* 142, 229-241.
3. Revenkova, E., and Jessberger, R. (2005). Keeping sister chromatids together: cohesins in meiosis. *Reproduction* 130, 783-790.
4. Watanabe, Y. (2012). Geometry and force behind kinetochore orientation: lessons from meiosis. *Nature reviews Molecular cell biology* 13, 370-382.
5. Mercier, R., Mézard, C., Jenczewski, E., Macaisne, N., and Grelon, M. (2015). The molecular biology of meiosis in plants. *Annual review of plant biology* 66, 297-327.
6. Armstrong, S. J., and Jones, G. H. (2003). Meiotic cytology and chromosome behaviour in wild-type *Arabidopsis thaliana*. *Journal of experimental botany* 54, 1-10.
7. Armstrong, S., Franklin, F., and Jones, G. (2003). A meiotic time-course for *Arabidopsis thaliana*. *Sexual Plant Reproduction* 16, 141-149.
8. Tiang, C.-L., He, Y., and Pawlowski, W. P. (2012). Chromosome organization and dynamics during interphase, mitosis, and meiosis in plants. *Plant Physiol* 158, 26-34.
9. Ma, H. (2006). *A Molecular Portrait of Arabidopsis Meiosis*.
10. Zickler, D., and Kleckner, N. (1999). Meiotic Chromosomes: Integrating Structure and Function. *Annual Review of Genetics* 33, 603-754.
11. Bass, H. W., Riera-Lizarazu, O., Ananiev, E. V., Bordoli, S. J., Rines, H. W., Phillips, R. L., Sedat, J. W., Agard, D. A., and Cande, W. Z. (2000). Evidence for the coincident initiation of homolog pairing and synapsis during the telomere-clustering (bouquet) stage of meiotic prophase. *Journal of Cell Science* 113, 1033-1042.
12. Golubovskaya, I. N., Harper, L. C., Pawlowski, W. P., Schichnes, D., and Cande, W. Z. (2002). The *pam1* gene is required for meiotic bouquet formation and efficient homologous synapsis in maize (*Zea mays* L.). *Genetics* 162, 1979-1993.
13. Cowan, C. R., and Cande, W. Z. (2002). Meiotic telomere clustering is inhibited by colchicine but does not require cytoplasmic microtubules. *Journal of Cell Science* 115, 3747-3756.
14. Harper, L., Golubovskaya, I., and Cande, W. Z. (2004). A bouquet of chromosomes. *Journal of Cell Science* 117, 4025-4032.
15. Otegui, M., and Staehelin, L. A. (2000). Cytokinesis in flowering plants: more than one way to divide a cell. *Current opinion in plant biology* 3, 493-502.
16. Zhang, C., Shen, Y., Tang, D., Shi, W., Zhang, D., Du, G., Zhou, Y., Liang, G., Li, Y., and Cheng, Z. (2018). The zinc finger protein DCM1 is required for male meiotic cytokinesis by preserving callose in rice. *PLoS genetics* 14, e1007769.

17. Prusicki, M. A., Keizer, E. M., van Rosmalen, R. P., Komaki, S., Seifert, F., Muller, K., Wijnker, E., Fleck, C., and Schnittger, A. (2019). Live cell imaging of meiosis in *Arabidopsis thaliana*. *Elife* 8.
18. van Heemst, D., and Heyting, C. (2000). Sister chromatid cohesion and recombination in meiosis. *Chromosoma* 109, 10-26.
19. Panizza, S., Mendoza, M. A., Berlinger, M., Huang, L., Nicolas, A., Shirahige, K., and Klein, F. (2011). Spo11-accessory proteins link double-strand break sites to the chromosome axis in early meiotic recombination. *Cell* 146, 372-383.
20. Kim, K. P., Weiner, B. M., Zhang, L., Jordan, A., Dekker, J., and Kleckner, N. (2010). Sister cohesion and structural axis components mediate homolog bias of meiotic recombination. *Cell* 143, 924-937.
21. Subramanian, V. V., and Hochwagen, A. (2014). The meiotic checkpoint network: step-by-step through meiotic prophase. *Cold Spring Harbor perspectives in biology* 6, a016675.
22. Blat, Y., Protacio, R. U., Hunter, N., and Kleckner, N. (2002). Physical and functional interactions among basic chromosome organizational features govern early steps of meiotic chiasma formation. *Cell* 111, 791-802.
23. Hollingsworth, N. M. (2010). Phosphorylation and the creation of interhomolog bias during meiosis in yeast. (Taylor & Francis).
24. Humphries, N., and Hochwagen, A. (2014). A non-sister act: Recombination template choice during meiosis. *Exp Cell Res* 329, 53-60.
25. Carballo, J. A., Johnson, A. L., Sedgwick, S. G., and Cha, R. S. (2008). Phosphorylation of the axial element protein Hop1 by Mec1/Tel1 ensures meiotic interhomolog recombination. *Cell* 132, 758-770.
26. Niu, H., Li, X., Job, E., Park, C., Moazed, D., Gygi, S. P., and Hollingsworth, N. M. (2007). Mek1 kinase is regulated to suppress double-strand break repair between sister chromatids during budding yeast meiosis. *Molecular and cellular biology* 27, 5456-5467.
27. Lao, J. P., Cloud, V., Huang, C.-C., Grubb, J., Thacker, D., Lee, C.-Y., Dresser, M. E., Hunter, N., and Bishop, D. K. (2013). Meiotic crossover control by concerted action of Rad51-Dmc1 in homolog template bias and robust homeostatic regulation. *PLoS genetics* 9.
28. Kleckner, N. (2006). Chiasma formation: chromatin/axis interplay and the role (s) of the synaptonemal complex. *Chromosoma* 115, 175.
29. West, A. M. V., Rosenberg, S. C., Ur, S. N., Lehmer, M. K., Ye, Q., Hagemann, G., Caballero, I., Usón, I., MacQueen, A. J., Herzog, F., et al. (2019). A conserved filamentous assembly underlies the structure of the meiotic chromosome axis. *eLife* 8.
30. Smith, A. V., and Roeder, G. S. (1997). The Yeast Red1 Protein Localizes to the Cores of Meiotic Chromosomes. *Journal of Cell Biology* 136, 957-967.
31. Li, X. C., Bolcun-Filas, E., and Schimenti, J. C. (2011). Genetic evidence that synaptonemal complex axial elements govern recombination pathway choice in mice. *Genetics* 189, 71-82.

32. Winkel, K., Alsheimer, M., Öllinger, R., and Benavente, R. (2009). Protein SYCP2 provides a link between transverse filaments and lateral elements of mammalian synaptonemal complexes. *Chromosoma* *118*, 259-267.
33. Ferdous, M., Higgins, J. D., Osman, K., Lambing, C., Roitinger, E., Mechtler, K., Armstrong, S. J., Perry, R., Pradillo, M., Cuñado, N., et al. (2012). Inter-Homolog Crossing-Over and Synapsis in Arabidopsis Meiosis Are Dependent on the Chromosome Axis Protein AtASY3. *PLoS Genetics* *8*.
34. Chambon, A., West, A., Vezon, D., Horlow, C., De Muyt, A., Chelysheva, L., Ronceret, A., Darbyshire, A., Osman, K., and Heckmann, S. (2018). Identification of ASYNAPTIC4, a component of the meiotic chromosome axis. *Plant Physiol* *178*, 233-246.
35. Osman, K., Yang, J., Roitinger, E., Lambing, C., Heckmann, S., Howell, E., Cuacos, M., Imre, R., Dürnberger, G., and Mechtler, K. (2018). Affinity proteomics reveals extensive phosphorylation of the Brassica chromosome axis protein ASY 1 and a network of associated proteins at prophase I of meiosis. *The Plant Journal* *93*, 17-33.
36. Wang, K., Wang, M., Tang, D., Shen, Y., Qin, B., Li, M., and Cheng, Z. (2011). PAIR3, an axis-associated protein, is essential for the recruitment of recombination elements onto meiotic chromosomes in rice. *Mol Biol Cell* *22*, 12-19.
37. Lee, D. H., Kao, Y.-H., Ku, J.-C., Lin, C.-Y., Meeley, R., Jan, Y.-S., and Wang, C.-J. R. (2015). The axial element protein DESYNAPTIC2 mediates meiotic double-strand break formation and synaptonemal complex assembly in maize. *The Plant Cell* *27*, 2516-2529.
38. Hollingsworth, N. M., Goetsch, L., and Byers, B. (1990). The HOP1 gene encodes a meiosis-specific component of yeast chromosomes. *Cell* *61*, 73-84.
39. Wojtasz, L., Daniel, K., Roig, I., Bolcun-Filas, E., Xu, H., Boonsanay, V., Eckmann, C. R., Cooke, H. J., Jasin, M., and Keeney, S. (2009). Mouse HORMAD1 and HORMAD2, two conserved meiotic chromosomal proteins, are depleted from synapsed chromosome axes with the help of TRIP13 AAA-ATPase. *PLoS genetics* *5*.
40. Couteau, F., and Zetka, M. (2005). HTP-1 coordinates synaptonemal complex assembly with homolog alignment during meiosis in *C. elegans*. *Genes Dev* *19*, 2744-2756.
41. Goodyer, W., Kaitna, S., Couteau, F., Ward, J. D., Boulton, S. J., and Zetka, M. (2008). HTP-3 links DSB formation with homolog pairing and crossing over during *C. elegans* meiosis. *Developmental cell* *14*, 263-274.
42. Hodgkin, J., Horvitz, H. R., and Brenner, S. (1979). Nondisjunction mutants of the nematode *Caenorhabditis elegans*. *Genetics* *91*, 67-94.
43. Nonomura, K.-I., Nakano, M., Murata, K., Miyoshi, K., Eiguchi, M., Miyao, A., Hirochika, H., and Kurata, N. (2004). An insertional mutation in the rice PAIR2 gene, the ortholog of Arabidopsis ASY1, results in a defect in homologous chromosome pairing during meiosis. *Mol Genet Genomics* *271*, 121-129.
44. Caryl, A. P., Armstrong, S. J., Jones, G. H., and Franklin, F. C. H. (2000). A homologue of the yeast HOP1 gene is inactivated in the Arabidopsis meiotic mutant *asy1*. *Chromosoma* *109*, 62-71.

45. Sanchez-Moran, E., Santos, J.-L., Jones, G. H., and Franklin, F. C. H. (2007). ASY1 mediates AtDMC1-dependent interhomolog recombination during meiosis in Arabidopsis. *Genes Dev* 21, 2220-2233.
46. Börner, G. V., Barot, A., and Kleckner, N. (2008). Yeast Pch2 promotes domainal axis organization, timely recombination progression, and arrest of defective recombinosomes during meiosis. *Proceedings of the National Academy of Sciences* 105, 3327-3332.
47. Lambing, C., Osman, K., Nuntasontorn, K., West, A., Higgins, J. D., Copenhaver, G. P., Yang, J., Armstrong, S. J., Mechtler, K., Roitinger, E., et al. (2015). Arabidopsis PCH2 Mediates Meiotic Chromosome Remodeling and Maturation of Crossovers. *PLOS Genetics* 11, e1005372.
48. Yang, C., Sofroni, K., Wijnker, E., Hamamura, Y., Carstens, L., Harashima, H., Stolze, S. C., Vezon, D., Chelysheva, L., Orban-Nemeth, Z., et al. (2020). The Arabidopsis Cdk1/Cdk2 homolog CDKA;1 controls chromosome axis assembly during plant meiosis. *The EMBO journal* 39, e101625.
49. Zanders, S., and Alani, E. (2009). The pch2 $\Delta$  mutation in baker's yeast alters meiotic crossover levels and confers a defect in crossover interference. *PLoS genetics* 5.
50. de los Santos, T., and Hollingsworth, N. M. (1999). Red1p, a MEK1-dependent phosphoprotein that physically interacts with Hop1p during meiosis in yeast. *Journal of Biological Chemistry* 274, 1783-1790.
51. Armstrong, S. J., Caryl, A. P., Jones, G. H., and Franklin, F. C. H. (2002). Asy1, a protein required for meiotic chromosome synapsis, localizes to axis-associated chromatin in Arabidopsis and Brassica. *Journal of cell science* 115, 3645-3655.
52. Sanchez-Moran, E., Osman, K., Higgins, J., Pradillo, M., Cunado, N., Jones, G., and Franklin, F. (2008). ASY1 coordinates early events in the plant meiotic recombination pathway. *Cytogenetic and genome research* 120, 302-312.
53. Moses, M. J. (1956). Chromosomal structures in crayfish spermatocytes. *The Journal of biophysical and biochemical cytology* 2, 215.
54. Fawcett, D. W. (1956). The fine structure of chromosomes in the meiotic prophase of vertebrate spermatocytes. *The Journal of Cell Biology* 2, 403-406.
55. Higgins, J. D., Sanchez-Moran, E., Armstrong, S. J., Jones, G. H., and Franklin, F. C. H. (2005). The Arabidopsis synaptonemal complex protein ZYP1 is required for chromosome synapsis and normal fidelity of crossing over. *Genes Dev* 19, 2488-2500.
56. Sym, M., Engebrecht, J., and Roeder, G. S. (1993). ZIP1 is a synaptonemal complex protein required for meiotic chromosome synapsis. *Cell* 72, 365-378.
57. MacQueen, A. J., Colaiácovo, M. P., McDonald, K., and Villeneuve, A. M. (2002). Synapsis-dependent and-independent mechanisms stabilize homolog pairing during meiotic prophase in *C. elegans*. *Genes Dev* 16, 2428-2442.
58. Meuwissen, R., Offenberg, H. H., Dietrich, A., Riesewijk, A., van Iersel, M., and Heyting, C. (1992). A coiled-coil related protein specific for synapsed regions of meiotic prophase chromosomes. *The EMBO journal* 11, 5091-5100.



59. Wang, M., Wang, K., Tang, D., Wei, C., Li, M., Shen, Y., Chi, Z., Gu, M., and Cheng, Z. (2010). The central element protein ZEP1 of the synaptonemal complex regulates the number of crossovers during meiosis in rice. *The Plant Cell* 22, 417-430.
60. Barakate, A., Higgins, J. D., Vivera, S., Stephens, J., Perry, R. M., Ramsay, L., Colas, I., Oakey, H., Waugh, R., and Franklin, F. C. H. (2014). The synaptonemal complex protein ZYP1 is required for imposition of meiotic crossovers in barley. *The Plant Cell* 26, 729-740.
61. Heyting, C. (1996). Synaptonemal complexes: structure and function. *Curr Opin Cell Biol* 8, 389-396.
62. Börner, G. V., Kleckner, N., and Hunter, N. (2004). Crossover/noncrossover differentiation, synaptonemal complex formation, and regulatory surveillance at the leptotene/zygotene transition of meiosis. *Cell* 117, 29-45.
63. Keeney, S., Giroux, C. N., and Kleckner, N. (1997). Meiosis-specific DNA double-strand breaks are catalyzed by Spo11, a member of a widely conserved protein family. *Cell* 88, 375-384.
64. Keeney, S. (2007). Spo11 and the formation of DNA double-strand breaks in meiosis. In *Recombination and meiosis*. (Springer), pp. 81-123.
65. Stacey, N. J., Kuromori, T., Azumi, Y., Roberts, G., Breuer, C., Wada, T., Maxwell, A., Roberts, K., and Sugimoto-Shirasu, K. (2006). Arabidopsis SPO11-2 functions with SPO11-1 in meiotic recombination. *The Plant Journal* 48, 206-216.
66. Hartung, F., Wurz-Wildersinn, R., Fuchs, J., Schubert, I., Suer, S., and Puchta, H. (2007). The catalytically active tyrosine residues of both SPO11-1 and SPO11-2 are required for meiotic double-strand break induction in Arabidopsis. *The Plant Cell* 19, 3090-3099.
67. Osman, K., Higgins, J. D., Sanchez-Moran, E., Armstrong, S. J., and Franklin, F. C. H. (2011). Pathways to meiotic recombination in Arabidopsis thaliana. *New Phytologist* 190, 523-544.
68. Wang, Y., and Copenhaver, G. P. (2018). Meiotic recombination: mixing it up in plants. *Annual review of plant biology* 69, 577-609.
69. De Muyt, A., Pereira, L., Vezon, D., Chelysheva, L., Gendrot, G., Chambon, A., Laine-Choinard, S., Pelletier, G., Mercier, R., and Nogue, F. (2009). A high throughput genetic screen identifies new early meiotic recombination functions in Arabidopsis thaliana. *PLoS genetics* 5.
70. Miao, C., Tang, D., Zhang, H., Wang, M., Li, Y., Tang, S., Yu, H., Gu, M., and Cheng, Z. (2013). CENTRAL REGION COMPONENT1, a Novel Synaptonemal Complex Component, Is Essential for Meiotic Recombination Initiation in Rice. *The Plant Cell* 25, 2998-3009.
71. Ji, J., Tang, D., Shen, Y., Xue, Z., Wang, H., Shi, W., Zhang, C., Du, G., Li, Y., and Cheng, Z. (2016). P31comet, a member of the synaptonemal complex, participates in meiotic DSB formation in rice. *Proceedings of the National Academy of Sciences of the United States of America* 113, 10577-10582.
72. Wu, Z., Ji, J., Tang, D., Wang, H., Shen, Y., Shi, W., Li, Y., Tan, X., Cheng, Z., and Luo, Q. (2015). OsSDS is essential for DSB formation in rice meiosis. *Frontiers in plant science* 6, 21.

73. Azumi, Y., Liu, D., Zhao, D., Li, W., Wang, G., Hu, Y., and Ma, H. (2002). Homolog interaction during meiotic prophase I in *Arabidopsis* requires the SOLO DANCERS gene encoding a novel cyclin-like protein. *The EMBO journal* *21*, 3081-3095.
74. Higgins, J. D., Armstrong, S. J., Franklin, F. C. H., and Jones, G. H. (2004). The *Arabidopsis* MutS homolog AtMSH4 functions at an early step in recombination: evidence for two classes of recombination in *Arabidopsis*. *Genes Dev* *18*, 2557-2570.
75. Couteau, F., Belzile, F., Horlow, C., Grandjean, O., Vezon, D., and Doutriaux, M.-P. (1999). Random chromosome segregation without meiotic arrest in both male and female meiocytes of a *dmc1* mutant of *Arabidopsis*. *The Plant Cell* *11*, 1623-1634.
76. Wyatt, H. D., and West, S. C. (2014). Holliday junction resolvases. *Cold Spring Harbor perspectives in biology* *6*, a023192.
77. Higgins, J. D., Buckling, E. F., Franklin, F. C. H., and Jones, G. H. (2008). Expression and functional analysis of AtMUS81 in *Arabidopsis* meiosis reveals a role in the second pathway of crossing-over. *The Plant Journal* *54*, 152-162.
78. Uhlmann, F., and Nasmyth, K. (1998). Cohesion between sister chromatids must be established during DNA replication. *Current Biology* *8*, 1095-1102.
79. Cai, X., Dong, F., Edelman, R. E., and Makaroff, C. A. (2003). The *Arabidopsis* SYN1 cohesin protein is required for sister chromatid arm cohesion and homologous chromosome pairing. *Journal of Cell Science* *116*, 2999-3007.
80. Bolaños-Villegas, P., De, K., Pradillo, M., Liu, D., and Makaroff, C. A. (2017). In favor of establishment: regulation of chromatid cohesion in plants. *Frontiers in plant science* *8*, 846.
81. Makrantonis, V., and Marston, A. L. (2018). Cohesin and chromosome segregation. *Current Biology* *28*, R688-R693.
82. Haering, C. H., Löwe, J., Hochwagen, A., and Nasmyth, K. (2002). Molecular architecture of SMC proteins and the yeast cohesin complex. *Mol Cell* *9*, 773-788.
83. Peters, J.-M., Tedeschi, A., and Schmitz, J. (2008). The cohesin complex and its roles in chromosome biology. *Genes Dev* *22*, 3089-3114.
84. Chelysheva, L., Diallo, S., Vezon, D., Gendrot, G., Vrielynck, N., Belcram, K., Rocques, N., Márquez-Lema, A., Bhatt, A. M., and Horlow, C. (2005). AtREC8 and AtSCC3 are essential to the monopolar orientation of the kinetochores during meiosis. *Journal of cell science* *118*, 4621-4632.
85. Lam, W. S., Yang, X., and Makaroff, C. A. (2005). Characterization of *Arabidopsis thaliana* SMC1 and SMC3: evidence that AtSMC3 may function beyond chromosome cohesion. *Journal of cell science* *118*, 3037-3048.
86. Schubert, V., Weißleder, A., Ali, H., Fuchs, J., Lermontova, I., Meister, A., and Schubert, I. (2009). Cohesin gene defects may impair sister chromatid alignment and genome stability in *Arabidopsis thaliana*. *Chromosoma* *118*, 591-605.
87. Bai, X., Peirson, B. N., Dong, F., Xue, C., and Makaroff, C. A. (1999). Isolation and characterization of SYN1, a RAD21-like gene essential for meiosis in *Arabidopsis*. *The Plant Cell* *11*, 417-430.

88. Bhatt, A. M., Lister, C., Page, T., Fransz, P., Findlay, K., Jones, G. H., Dickinson, H. G., and Dean, C. (1999). The DIF1 gene of Arabidopsis is required for meiotic chromosome segregation and belongs to the REC8/RAD21 cohesin gene family. *The Plant Journal* *19*, 463-472.
89. Dong, F., Cai, X., and Makaroff, C. (2001). Cloning and characterization of two Arabidopsis genes that belong to the RAD21/REC8 family of chromosome cohesin proteins. *Gene* *271*, 99-108.
90. Jiang, L., Xia, M., Strittmatter, L. I., and Makaroff, C. A. (2007). The Arabidopsis cohesin protein SYN3 localizes to the nucleolus and is essential for gametogenesis. *The Plant Journal* *50*, 1020-1034.
91. Yuan, L., Yang, X., Ellis, J. L., Fisher, N. M., and Makaroff, C. A. (2012). The Arabidopsis SYN3 cohesin protein is important for early meiotic events. *The Plant Journal* *71*, 147-160.
92. Mito, Y., Sugimoto, A., and Yamamoto, M. (2003). Distinct developmental function of two *Caenorhabditis elegans* homologs of the cohesin subunit Scc1/Rad21. *Mol Biol Cell* *14*, 2399-2409.
93. Pasierbek, P., Jantsch, M., Melcher, M., Schleiffer, A., Schweizer, D., and Loidl, J. (2001). A *Caenorhabditis elegans* cohesion protein with functions in meiotic chromosome pairing and disjunction. *Genes Dev* *15*, 1349-1360.
94. Tao, J., Zhang, L., Chong, K., and Wang, T. (2007). OsRAD21-3, an orthologue of yeast RAD21, is required for pollen development in *Oryza sativa*. *The Plant Journal* *51*, 919-930.
95. Zhang, L. R., Tao, J. Y., and Wang, T. (2004). Molecular characterization of OsRAD21-1, a rice homologue of yeast RAD21 essential for mitotic chromosome cohesion. *Journal of experimental botany* *55*, 1149-1152.
96. Zhang, L., Tao, J., Wang, S., Chong, K., and Wang, T. (2006). The rice OsRad21-4, an orthologue of yeast Rec8 protein, is required for efficient meiosis. *Plant molecular biology* *60*, 533-554.
97. Yu, H.-G., and Dawe, R. K. (2000). Functional redundancy in the maize meiotic kinetochore. *The Journal of cell biology* *151*, 131-142.
98. Golubovskaya, I. N., Hamant, O., Timofejeva, L., Wang, C.-J. R., Braun, D., Meeley, R., and Cande, W. Z. (2006). Alleles of *afd1* dissect REC8 functions during meiotic prophase I. *Journal of cell science* *119*, 3306-3315.
99. Vaur, S., Feytout, A., Vazquez, S., and Javerzat, J. P. (2012). Pds5 promotes cohesin acetylation and stable cohesin-chromosome interaction. *EMBO reports* *13*, 645-652.
100. De, K., Sterle, L., Krueger, L., Yang, X., and Makaroff, C. A. (2014). Arabidopsis thaliana WAPL is essential for the prophase removal of cohesin during meiosis. *PLoS genetics* *10*.
101. Ladurner, R., Kreidl, E., Ivanov, M. P., Ekker, H., Idarraga-Amado, M. H., Busslinger, G. A., Wutz, G., Cisneros, D. A., and Peters, J. M. (2016). Sororin actively maintains sister chromatid cohesion. *The EMBO journal* *35*, 635-653.

102. Nishiyama, T., Ladurner, R., Schmitz, J., Kreidl, E., Schleiffer, A., Bhaskara, V., Bando, M., Shirahige, K., Hyman, A. A., and Mechtler, K. (2010). Sororin mediates sister chromatid cohesion by antagonizing Wapl. *Cell* *143*, 737-749.
103. Yang, C., Hamamura, Y., Sofroni, K., Böwer, F., Stolze, S. C., Nakagami, H., and Schnittger, A. (2019). SWITCH 1/DYAD is a WINGS APART-LIKE antagonist that maintains sister chromatid cohesion in meiosis. *Nature Communications* *10*, 1755.
104. Katis, V. L., Lipp, J. J., Imre, R., Bogdanova, A., Okaz, E., Habermann, B., Mechtler, K., Nasmyth, K., and Zachariae, W. (2010). Rec8 phosphorylation by casein kinase 1 and Cdc7-Dbf4 kinase regulates cohesin cleavage by separase during meiosis. *Developmental cell* *18*, 397-409.
105. Kitajima, T. S., Kawashima, S. A., and Watanabe, Y. (2004). The conserved kinetochore protein shugoshin protects centromeric cohesion during meiosis. *Nature* *427*, 510-517.
106. Riedel, C. G., Katis, V. L., Katou, Y., Mori, S., Itoh, T., Helmhart, W., Gálová, M., Petronczki, M., Gregan, J., and Cetin, B. (2006). Protein phosphatase 2A protects centromeric sister chromatid cohesion during meiosis I. *Nature* *441*, 53-61.
107. Cromer, L., Jolivet, S., Horlow, C., Chelysheva, L., Heyman, J., De Jaeger, G., Koncz, C., De Veylder, L., and Mercier, R. (2013). Centromeric cohesion is protected twice at meiosis, by SHUGOSHINS at anaphase I and by PATRONUS at interkinesis. *Current Biology* *23*, 2090-2099.
108. De Veylder, L., Larkin, J. C., and Schnittger, A. (2011). Molecular control and function of endoreplication in development and physiology. *Trends Plant Sci* *16*, 624-634.
109. Pesin, J. A., and Orr-Weaver, T. L. (2008). Regulation of APC/C activators in mitosis and meiosis. *Annual review of cell and developmental biology* *24*, 475-499.
110. Wijnker, E., and Schnittger, A. (2013). Control of the meiotic cell division program in plants. *Plant reproduction* *26*, 143-158.
111. Nonomura, K.-I., Morohoshi, A., Nakano, M., Eiguchi, M., Miyao, A., Hirochika, H., and Kurata, N. (2007). A germ cell-specific gene of the ARGONAUTE family is essential for the progression of premeiotic mitosis and meiosis during sporogenesis in rice. *The Plant Cell* *19*, 2583-2594.
112. Olmedo-Monfil, V., Durán-Figueroa, N., Arteaga-Vázquez, M., Demesa-Arévalo, E., Autran, D., Grimanelli, D., Slotkin, R. K., Martienssen, R. A., and Vielle-Calzada, J.-P. (2010). Control of female gamete formation by a small RNA pathway in Arabidopsis. *Nature* *464*, 628.
113. Singh, M., Goel, S., Meeley, R. B., Dantec, C., Parrinello, H., Michaud, C., Leblanc, O., and Grimanelli, D. (2011). Production of viable gametes without meiosis in maize deficient for an ARGONAUTE protein. *The Plant Cell* *23*, 443-458.
114. Nonomura, K.-I., Eiguchi, M., Nakano, M., Takashima, K., Komeda, N., Fukuchi, S., Miyazaki, S., Miyao, A., Hirochika, H., and Kurata, N. (2011). A novel RNA-recognition-motif protein is required for premeiotic G 1/S-phase transition in rice (*Oryza sativa* L.). *PLoS Genet* *7*, e1001265.

115. Bennett, M. D., and Smith, J. (1972). The effects of polyploidy on meiotic duration and pollen development in cereal anthers. *Proceedings of the Royal Society of London. Series B. Biological Sciences* 181, 81-107.
116. Holm, P. B. (1977). The premeiotic DNA replication of euchromatin and heterochromatin in *Lilium longiflorum* (Thunb.). *Carlsberg Res Commun* 42, 249-281.
117. Marston, A. L., and Amon, A. (2004). Meiosis: cell-cycle controls shuffle and deal. *Nature Reviews Molecular Cell Biology* 5, 983-997.
118. Wang, G., Kong, H., Sun, Y., Zhang, X., Zhang, W., Altman, N., dePamphilis, C. W., and Ma, H. (2004). Genome-wide analysis of the cyclin family in *Arabidopsis* and comparative phylogenetic analysis of plant cyclin-like proteins. *Plant Physiol* 135, 1084-1099.
119. Vandepoele, K., Raes, J., De Veylder, L., Rouzé, P., Rombauts, S., and Inzé, D. (2002). Genome-wide analysis of core cell cycle genes in *Arabidopsis*. *The Plant Cell* 14, 903-916.
120. Dissmeyer, N., Nowack, M. K., Pusch, S., Stals, H., Inzé, D., Grini, P. E., and Schnittger, A. (2007). T-Loop Phosphorylation of *Arabidopsis* CDKA1 Is Required for Its Function and Can Be Partially Substituted by an Aspartate Residue. *The Plant Cell* 19, 972-985.
121. Bulankova, P., Riehs-Kearnan, N., Nowack, M. K., Schnittger, A., and Riha, K. (2010). Meiotic progression in *Arabidopsis* is governed by complex regulatory interactions between SMG7, TDM1, and the meiosis I-specific cyclin TAM. *The Plant Cell* 22, 3791-3803.
122. Nugent, J., Alfa, C. E., Young, T., and Hyams, J. S. (1991). Conserved structural motifs in cyclins identified by sequence analysis. *Journal of cell science* 99, 669-674.
123. Peters, J.-M. (1998). SCF and APC: the Yin and Yang of cell cycle regulated proteolysis. *Curr Opin Cell Biol* 10, 759-768.
124. Renaudin, J.-P., Doonan, J. H., Freeman, D., Hashimoto, J., Hirt, H., Inzé, D., Jacobs, T., Kouchi, H., Rouzé, P., and Sauter, M. (1996). Plant cyclins: a unified nomenclature for plant A-, B- and D-type cyclins based on sequence organization. *Plant molecular biology* 32, 1003-1018.
125. Glotzer, M., Murray, A. W., and Kirschner, M. W. (1991). Cyclin is degraded by the ubiquitin pathway. *Nature* 349, 132-138.
126. Rogers, S., Wells, R., and Rechsteiner, M. (1986). Amino acid sequences common to rapidly degraded proteins: the PEST hypothesis. *Science* 234, 364-368.
127. d'Erfurth, I., Cromer, L., Jolivet, S., Girard, C., Horlow, C., Sun, Y., To, J. P., Berchowitz, L. E., Copenhaver, G. P., and Mercier, R. (2010). The cyclin-A CYCA1; 2/TAM is required for the meiosis I to meiosis II transition and cooperates with OSD1 for the prophase to first meiotic division transition. *PLoS genetics* 6.
128. Bulankova, P., Akimcheva, S., Fellner, N., and Riha, K. (2013). Identification of *Arabidopsis* meiotic cyclins reveals functional diversification among plant cyclin genes. *PLoS genetics* 9.

129. Ross, K., Fransz, P., Armstrong, S., Vizir, I., Mulligan, B., Franklin, F., and Jones, G. (1997). Cytological characterization of four meiotic mutants of *Arabidopsis* isolated from T-DNA-transformed lines. *Chromosome Research* 5, 551-559.
130. Glover, J., Grelon, M., Craig, S., Chaudhury, A., and Dennis, E. (1998). Cloning and characterization of MS5 from *Arabidopsis* : a gene critical in male meiosis. *The Plant Journal* 15, 345-356.
131. Cifuentes, M., Jolivet, S., Cromer, L., Harashima, H., Bulankova, P., Renne, C., Crismani, W., Nomura, Y., Nakagami, H., and Sugimoto, K. (2016). TDM1 regulation determines the number of meiotic divisions. *PLoS genetics* 12.
132. Cromer, L., Heyman, J., Touati, S., Harashima, H., Araou, E., Girard, C., Horlow, C., Wassmann, K., Schnittger, A., and De Veylder, L. (2012). OSD1 promotes meiotic progression via APC/C inhibition and forms a regulatory network with TDM and CYCA1; 2/TAM. *PLoS genetics* 8.
133. d'Erfurth, I., Jolivet, S., Froger, N., Catrice, O., Novatchkova, M., and Mercier, R. (2009). Turning meiosis into mitosis. *PLoS Biol* 7.



## Research aim

Meiosis is a specialized cell division, essential for most reproducing organisms to reduce the genome by half through two consecutive chromosome separation events, thereby enabling the restoration of ploidy levels during fertilization. However, despite of its importance, many crucial steps in meiosis are not well understood yet.

In the first chapter of this dissertation, I investigated the regulation of the chromosome axis in meiosis. The chromosome axis is a ubiquitous feature of meiosis, important for homologous pairing, synapsis and recombination, hence it is fundamental to meiosis. HORMA domain proteins are key components of the chromosome axis, however, little is known about the mechanisms regulating their ordered chromosomal assembly and disassembly during meiosis. Proteins from the AAA+ ATPase family, such as PCH2, are well-known regulators of HORMADs in many organisms, however, so far, no direct interaction has been found between PCH2 and the respective HORMAD substrates in any organism outside of budding yeast. In this study, the identification and characterisation of COMET as an adaptor protein for PCH2 revealed a new regulatory mechanism for the meiotic HORMAD ASY1 in Arabidopsis, providing new insight into a fundamental mechanism of meiosis.

The aim of the study presented in the second chapter of this dissertation, was the establishment of a live cell imaging technique to follow meiosis in living maize meiocytes. Live cell imaging is a powerful approach to study the spatio-temporal dynamics of cellular processes and events, such as meiosis. With respect to plant meiosis, only few attempts have been conducted to date as meiosis has been traditionally investigated by the analysis of fixed material, which, although informative, can capture the cellular dynamics only to a small degree. My work towards the establishment of a robust live cell imaging technique included the generation of reporter lines highlighting hallmarks of meiosis and the identification of suitable culturing and imaging condition for maize anthers. This sets the base for investigating the dynamics of meiotic processes in maize and could ultimately lead to crop improvement, e.g., through a better understanding of how to control and modify recombination patterns.





# Chapter 1

## **Dissecting the molecular mechanism of chromosome axis remodeling during meiosis in *Arabidopsis thaliana***

Based on the published paper “**COMET functions as a PCH2 cofactor in regulating the HORMA domain protein ASY1**”

Authors: **Martina Balboni**,<sup>1</sup> Chao Yang,<sup>1</sup> Shinichiro Komaki,<sup>1,2</sup> Jordan Brun,<sup>1</sup> and Arp Schnittger<sup>1,3</sup>

<sup>1</sup>Department of Developmental Biology, University of Hamburg, Ohnhorststraße 18, Hamburg 22609, Germany

<sup>2</sup>Graduate School of Biological Sciences, Nara Institute of Science and Technology, 8916-5 Takayama, Ikoma, Nara 630-0192, Japan

Published on **Current Biology** 30, 1–15, November 2, 2020

# 1 Introduction

## 1.1 The HORMA domain proteins

The HORMA domain was first identified through sequence similarity among three functionally unrelated proteins in budding yeast: Hop1, the meiotic chromosome axis protein; Rev7, an accessory subunit of the translesion DNA polymerase  $\xi$  and the spindle assembly checkpoint (SAC) protein Mad2 (HORMA: Hop1/Rev7/Mad2) [1]. More recently, three additional HORMA domain proteins (HORMADs) have been characterized: p31<sup>comet</sup> as a Mad2 regulator [2-7] and the autophagy factors Atg13 and Atg101 [8-10]. Despite the radically diverse tasks performed by the different HORMADs, the core function of the HORMA domain remains remarkably constant, occupying key regulatory roles through the controlled assembly and disassembly of protein complexes.

### 1.1.1 Mad2

Mad2 is conserved in all eukaryotes studied so far and is the best-characterized HORMA domain protein [11]. Through its HORMA domain, Mad2 plays a key role in the SAC, a conserved surveillance system which monitors whether all chromosomes are correctly attached via their kinetochore to the spindle to ensure equal segregation of chromosomes in anaphase [12]. Mad2 contains a HORMA domain that can adopt two different conformations: an inactive “open” conformation (O-Mad2), and a “closed” conformation (C-Mad2) that binds short peptide motifs, called closure motifs, in a binding partner [13].

At unattached kinetochore O-Mad2 is converted into the active C-Mad2 which can be incorporated into the mitotic checkpoint complex MCC [14], along with BubR1, Bub3 and Cdc20 (**Figure 1A**). The MCC inhibits the Anaphase-Promoting Complex/Cyclosome (APC/C), thus delays anaphase onset [11, 15-18].

Once all kinetochores are connected to microtubules and under tension, the MCC is not assembled anymore, and in addition, the existing complexes are disassembled, with Mad2 experiencing a conversion from the closed to the inactive open state (**Figure 1B**).

These conformational changes in Mad2 are promoted by TRIP13/PCH2, a member of the AAA+ ATPase protein family. Proteins of this family share a common architecture with a N-terminal domain responsible for substrate

recognition and an AAA+ ATPase module that typically assembles into a hexameric ring. AAA+-ATPase proteins are involved in a wide range of cellular processes and known to couple ATP binding and/or ATP hydrolysis to induce conformational changes on target proteins [19-23]. In the SAC, this process requires the presence of another protein, p31<sup>comet</sup>, which directly binds to both Mad2 and TRIP13/PCH2 and acts as an adaptor to recruit TRIP13/PCH2 to Mad2 to promote its conformational changes [4, 5, 7, 24-26].

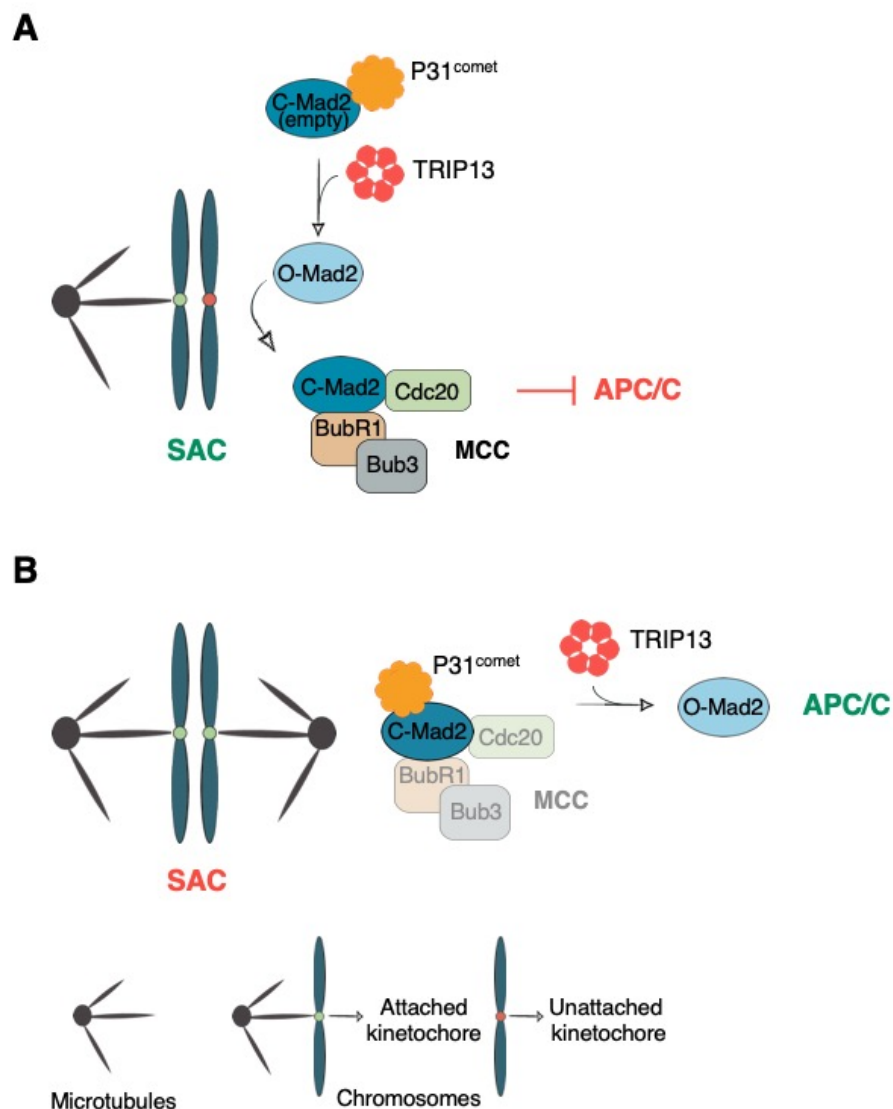


**Figure 1: P31<sup>comet</sup>-TRIP13 mediated changes of HORMAD Mad2 affect MCC assembly and disassembly**

The joint action of p31<sup>comet</sup> and TRIP13 ensures a sufficient supply of O-Mad2, which at unattached kinetochore is converted into the active C-Mad2 and incorporated into the mitotic checkpoint complex (MCC), which inhibits the

anaphase promoting complex/cyclosome (APC/C) (A). When all the kinetochores are attached to microtubules, p31<sup>comet</sup> binds C-Mad2 and serves as an adaptor for TRIP13 to convert it into the inactive O-Mad2, which destabilizes the MCC, allows SAC silencing and promotes APC/C activation (B).

### **1.1.2 The meiotic HORMADs**

Meiotic HORMADs have been identified in yeast (Hop1) [27], mammals (Hormad1 and Hormad2) [19], *C. elegans* (HIM-3, HTP-1, HTP-2, and HTP-3) [28-30], rice (PAIR2) [31] and in Arabidopsis (ASY1) [32] and shown to play an important role in the tight regulation of chromosome axis assembly and disassembly. However, despite their wide conservation and fundamental role, it is still largely unknown how the HORMA domain proteins interact with each other to establish the meiotic chromosome axis and to govern chromosome dynamics.

In *C. elegans*, HTP-3 is required for axis localization of the other meiotic HORMADs [29, 33] which then associate with one another through binding of the HORMA domain of one HORMAD to the closure motif in the C-terminal tail of another HORMAD [34]. This results in a hierarchical assembly of HORMA domain proteins, which are critical for the correct assembly of the chromosome axis, formation of the SC, proper regulation of CO formation and the faithful segregation of chromosomes in meiosis [34].

Like the four *C. elegans* proteins, the mammalian HORMADs harbor in their C-terminal tail a sequence that can act as a closure motif, suggesting that the HORMA domain-tail interactions are also conserved in mammals [34].

In *S. cerevisiae*, the meiotic HORMA domain protein Hop1 also possesses a short, highly-conserved C-terminal region, whose disruption or mutation affects its localization and spore viability [35, 36]. Moreover, the initial recruitment of Hop1 to the meiotic chromosome axis requires its binding partner Red1, which also contains a closure motif, thus it is mediated by HORMA domain-closure motif interaction of Hop1 and Red1 [37]. Additional Hop1 recruitment to the axis is then mediated by head-to-tail oligomerization of Hop1 [37].

Thus, the current model for meiotic HORMAD localization is that their HORMA domains bind closure motif sequences within cohesin or cohesin-binding axis proteins, like Red1, to mediate initial recruitment, followed by head-to-tail assembly of larger complexes on chromosomes.

With respect to plants, the meiotic HORMAD ASY1 in Arabidopsis also possesses a closure motif at its C terminus. ASY1 tends to spontaneously fold in a self-closed state, with the HORMA domain bound by its own closure motif [21, 38]. The chromosomal assembly is subsequent to an active conversion of ASY1 from the self-closed state to a transient unlocked state at early prophase, which allows the binding of the HORMA domain of ASY1 to the closure motif of ASY3. This gives rise to a closed and stably axis-bound form of ASY1, which, differently from other organisms, does not require a head-to-tail oligomerization for localization along the axes [38].

During meiosis, the chromosomal localization of meiotic HORMADs is dynamic: at early prophase they are recruited to and assembled on the axes, where they localize along their entire length, and later they are largely removed from the axes upon the formation of the SC. The removal of meiotic HORMADs from chromosome axes at late prophase is catalyzed by PCH2/TRIP13 and has been studied in different organisms [19-21, 38], however, the molecular mechanism is poorly understood as no direct interaction was found between PCH2/TRIP13 and the presumptive HORMAD substrates in any organisms studied other than in *S. cerevisiae* [22]. In fact, only in yeast, Pch2 directly binds Hop1 and thereby displaces it from the DNA restricting Hop1 localization to specific chromosomal regions and thus setting up a chromosomal organization that promotes interhomolog repair at CO designation sites [22].

### **1.1.3 P31<sup>comet</sup>**

P31<sup>comet</sup> was initially identified in HeLa cells as a Mad2-interacting protein and named Caught by MAD two (CMT2) [6]. CMT2 was renamed p31<sup>comet</sup> because of its comet tail-like localization pattern during mitosis.

In humans, p31<sup>comet</sup> acts to monitor the spindle checkpoint as an interacting partner of Mad2 and mediates the interaction between this HORMA domain protein and the remodeler TRIP13 [2-5, 7, 24, 39, 40]. In fact, the joint action of p31<sup>comet</sup> and TRIP13 in the SAC ensures, first, a sufficient supply of O-Mad2 by counteracting the spontaneous O-Mad2 to C-Mad2 conversion – which would result in an “empty” C-Mad2 which cannot bind Cdc20 by itself [41] –, thus promoting MCC assembly and maintaining the SAC active [7, 39]. Second, when the SAC is satisfied and the MCC needs to be disassembled, p31<sup>comet</sup> recognizes C-Mad2 and serves as an adaptor for TRIP13 to convert Mad2 into the inactive open

conformation, which destabilizes the MCC, unleashes Cdc20 and allows SAC silencing, thus APC/C activation and anaphase onset (**Figure 1**) [4, 5, 7, 24, 39, 40].

Interestingly, the meiotic HORMADs seem to recapitulate Mad2 dynamics as their dynamic chromosomal localization was recently found to be dependent on conformational changes in different organisms [34, 37, 38]. In particular, in Arabidopsis, ASY1 loading onto chromosomes and subsequent removal rely on the conversion from a closed state into an, albeit transient, open state [38]. Remarkably, these conformational changes are mediated by PCH2, but the mechanism remains elusive.

Recently, the ortholog of p31<sup>comet</sup> was identified in rice: *P31<sup>comet</sup>* mutant plants were sterile, thus suggesting for a meiotic function of p31<sup>comet</sup> as well [42].

These observations led to the hypothesis whether p31<sup>comet</sup> could possibly mediate the interaction between PCH2 and the meiotic HORMADs. Hence, in this study, I investigated the presence of a p31<sup>comet</sup>-like adaptor protein in Arabidopsis and characterized its function at a molecular level.

## 2 Results

### 2.1 Generation of a *comet* mutant in *Arabidopsis*

To identify a p31<sup>comet</sup> homolog in *Arabidopsis*, we performed reciprocal BLAST searches with NCBI's BLASTp tool using the human and rice p31<sup>comet</sup> protein sequences as initial queries. This search delivered a candidate protein (At1g03180) of 265 amino acids that shares 22%/39% and 44%/63% identity/similarity with the human and rice p31<sup>comet</sup> proteins, respectively (**Figure 2A**).

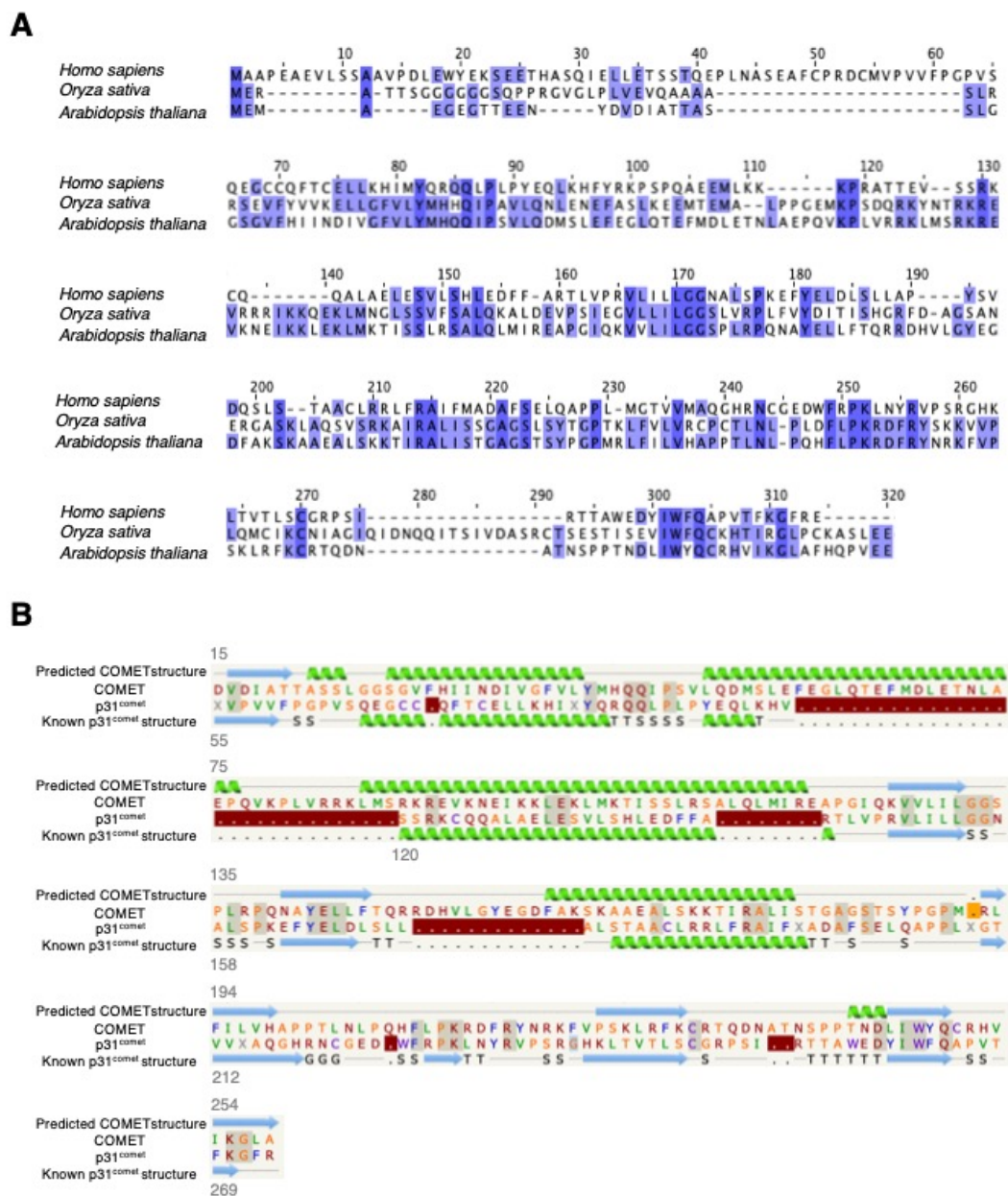


**Figure 2: Identification of *COMET* in *Arabidopsis thaliana***

Alignment of full-length protein sequence of p31<sup>comet</sup> (*Homo sapiens*), P31<sup>comet</sup> (*Oryza sativa*) and *COMET* (*Arabidopsis thaliana*). The alignment was done with Clustal Omega



[43]; conserved residues are highlighted (A). Secondary structure prediction of the COMET HORMA domain based on the known structure of the human p31<sup>comet</sup> using the Phyre2 protein structure prediction server (B).

The Phyre2 algorithm [44] predicted for At1g03180 a structure similar to the human p31<sup>comet</sup> (PDB code: c2qyfD, 100% confidence and 71% coverage), indicating that At1g03180 adopts a HORMA domain-like fold, which occupies the largest part of the protein (**Figure 2B**) [3, 14]. Thus, we named At1g03180 COMET.

To investigate the function of COMET in Arabidopsis, we generated a mutant using the CRISPR/Cas9 system. Cas9 was targeted to the fourth exon of the *COMET* gene by a single guide-RNA of 20 bases (**Figure 3A**). A T2 plant devoid of Cas9 was recovered that had one nucleotide (Thymine) insertion in the fourth exon at 544bp of the coding sequence of *COMET* (**Figure 3B and 3C**). This insertion leads to a frame shift and a premature stop codon (TAA) at 634bp of the coding sequence disrupting the translation of the HORMA domain after amino acid 211 and thus leading very likely to the complete loss of *COMET* function (**Figure 3D**).

First, we performed a root growth assay and tested the behavior of homozygous *comet-1* seedlings on media containing the microtubule-destabilizing drug oryzalin to address a possible function of COMET in the mitotic SAC, considering that the SAC is especially important for plant growth under microtubule-destabilizing conditions [45], and consistent with the expression atlas on The Arabidopsis Information Resource (TAIR) website for COMET. The *mad2* mutants were used as a positive control. Our assay revealed that while *mad2* mutants (n=39 seedlings analyzed) showed hypersensitivity to the oryzalin treatment, the root growth of *comet-1* (n=39 seedlings analyzed) on oryzalin-containing media was indistinguishable from the wildtype (n=39 seedlings analyzed), suggesting that COMET does not play a crucial role in the SAC in Arabidopsis (**Figure 3E and 3F**).

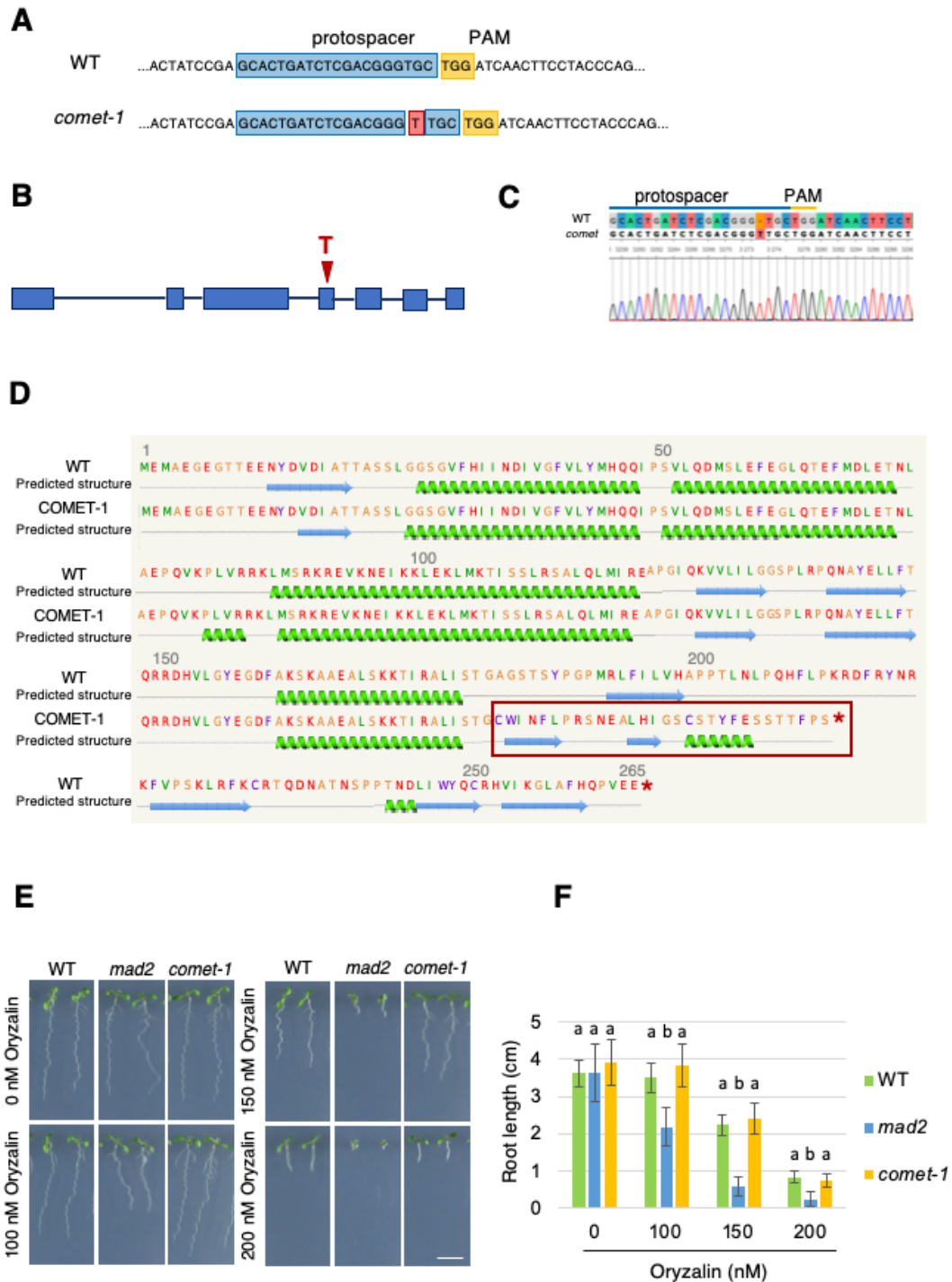


**Figure 3: Generation of *comet-1* mutants by CRISPR/Cas9 and root growth assay**  
*COMET* sequence of the fourth exon, the 20 nt target sequence (protospacer) used as the guide RNA (highlighted in blue) and the 3 nt protospacer-adjacent motif (PAM; highlighted in yellow) are indicated. The *comet-1* mutation harbors one nucleotide (T) insertion (highlighted in red) at the position of three base pairs upstream of the PAM (A). Schematic representation of the *COMET* gene. Boxes correspond to exons, bars to introns; the red arrowhead indicates the position of the T insertion (B). The presence of the targeted CRISPR edit (T insertion) was confirmed by DNA sequencing (C). Prediction of the

secondary structure of wild-type and mutant COMET protein using the Phyre2 protein structure prediction server. The T-insertion leads to a frameshift and thus a premature stop codon (D). Five-day-old seedlings of wildtype, *mad2* and *comet-1* grown on plates without and with 100, 150 and 200 nM oryzalin; *mad2* is used as positive control. Bar 1 cm (A). Quantification of the root growth assay shown in (E) (F); data are represented as the mean value  $\pm$  standard deviation (SD) of wild-type (n=39), *mad2* (n=39) and *comet-1* (n=39) seedlings. Level of significance is indicated by different letters and it was determined by one-way ANOVA followed by Tukey-Kramer test for each growth condition. The figures 3E and 3F are made with the data kindly provided by Dr. Shinichiro Komaki.

Moreover, the vegetative growth of *comet-1* plants was indistinguishable from the wildtype (**Figure 4A**). However, the mutants displayed reduced fertility. While we only found on average 0.2 aborted seeds per silique in the wildtype (n=15 siliques analyzed), homozygous *comet-1* mutants showed with 24.5 a significantly larger number of aborted seeds per silique (n=50 siliques analyzed;  $p < 0.001$ ) (**Figure 4B and 4E**). Additionally, in *comet-1* mutants, 9.7% of pollen grains (from n=9 flowers; 2675 pollen grains analyzed) were dead compared to 1.1% in the wildtype (from n=9 flowers; 4058 pollen grains analyzed) as revealed by Peterson staining ( $p < 0.001$ ) (**Figure 4C and 4F**). Since heterozygous *comet-1* mutant plants (referred to as *comet-1* (+/-)) did not show any reduction in fertility compared to wild-type plants, neither in the seed set (n=25 siliques analyzed) (**Figure 4H and 4J**) nor in pollen viability (from n=9 flowers) (**Figure 4I and 4K**), we conclude that these defects have a sporophytic, e.g., meiotic, and not a gametophytic origin.

Further examination of the fertility defects was conducted by performing reciprocal crosses between wild-type and homozygous *comet-1* plants. We used pollen from homozygous *comet-1* mutant plants to pollinate wild-type pistils and we found a slightly reduced seed set (n=24 siliques analyzed;  $p < 0.05$ ) from this cross, compared to the pollination of wild-type plants with wild-type pollen (n=24 siliques analyzed) (**Figure 4D and 4G**). This suggests that some mutant pollen is able to reach the female reproductive organs and causes post-fertilization defects leading to seed abortion.

In the cross between *comet-1* and wild-type plants, where wild-type pollen was used to pollinate homozygous *comet-1* pistils, we found a significantly larger reduction in the number of seeds per silique (n=25 siliques analyzed;  $p < 0.001$ ) compared to the wild-type control crosses. Notably, the abortion rate in this cross

is similar to what we observed when homozygous *comet-1* plants were pollinated with pollen from homozygous *comet-1* mutants (n=24 silique analyzed) consistent with the relatively low reduction in fertility through pollen from *comet-1* mutants (**Figure 4D and 4G**). Taken together, these results suggest that in *comet-1* mutants both male and female fertility is affected.

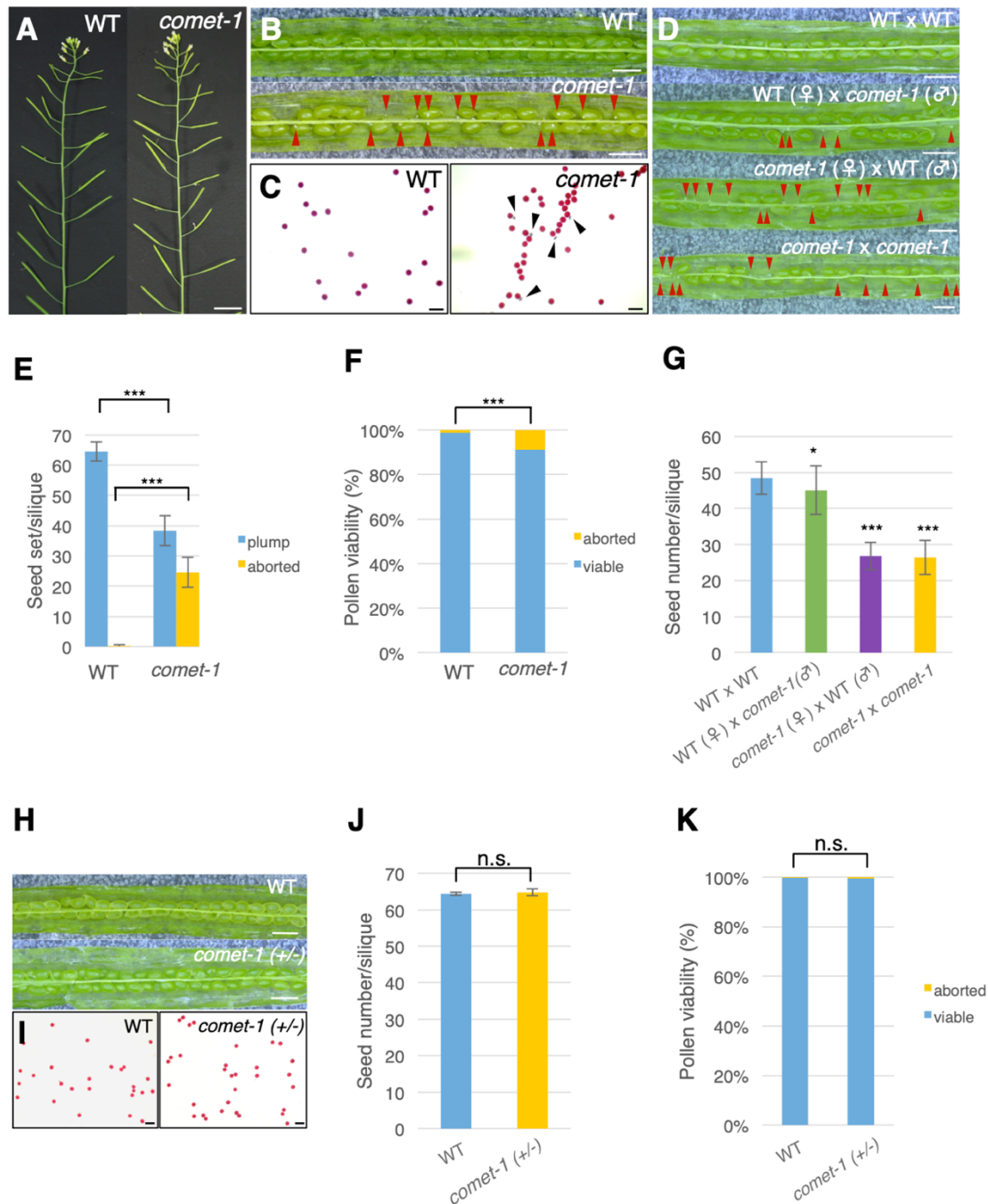


**Figure 4: Mutants in *COMET-1* have fertility defects**

Main inflorescence of wild-type and *comet-1* mutant plants. Bars 1 cm (A). Open siliques of wild-type and *comet-1* plants, red arrowheads indicate aborted seeds. Bars 1 mm (B).

Peterson staining of pollen of wild-type and *comet-1* plants, black arrowheads indicate aborted pollen. Bars 50  $\mu$ m (C). Open siliques of reciprocal crosses between wild-type and *comet-1* plants, red arrowheads indicate aborted seeds. Bars 1 mm (D). Quantification of seed set per silique (E); data are represented as the mean value  $\pm$  standard deviation (SD) of plump and aborted seeds in the wildtype (n=15 siliques analyzed) and in *comet-1* (n=50 siliques analyzed). Quantification of pollen viability (F); data are represented as the percentage values of viable and aborted pollen grains counted for wild-type (from n=9 flowers) and *comet-1* plants (from n=9 flowers). Quantification of seed set per silique (G); data are represented as the mean value  $\pm$  standard deviation (SD) of plump seeds in the siliques resulting from the pollination of wild-type plants with wild-type pollen (n=24 siliques analyzed), wild-type plants with *comet-1* pollen (n=24 siliques analyzed), *comet-1* plants with wild-type pollen (n=25 siliques analyzed) and *comet-1* plants with *comet-1* pollen (n=24 siliques analyzed). Open siliques of wild-type and heterozygous *comet-1* plants (referred to as *comet-1(+/-)*). Bars 1 mm (H). Peterson staining of pollen of wild-type and heterozygous *comet-1* plants (referred to as *comet-1(+/-)*). Bars 50  $\mu$ m (I). Quantification of seed set per silique (J); data are represented as the mean value  $\pm$  standard deviation (SD) of plump seeds in the wildtype (n=25 siliques analyzed) and in *comet-1(+/-)* (n=25 siliques analyzed). Quantification of pollen viability (K); data are represented as the percentage values of viable and aborted pollen grains counted for wild-type (from n=9 flowers) and *comet-1(+/-)* plants (from n=9 flowers). Level of significance is determined by Student's t-test (\*p< 0.05; \*\*\* p<0.001; n.s. depicts no significant difference).

To verify whether these fertility defects resulted from the mutation in *COMET*, four additional CRISPR/Cas9 alleles were generated (referred to as *comet-2*, *comet-3*, *comet-4*, and *comet-5*). Cas9 was targeted to the first exon of the *COMET* gene by a single guide-RNA of 20 bases (**Figure 5A**). These CRISPR edits lead to premature stop codons at the end of the first exon preventing the translation of the entire HORMA domain (**Figure 5B and 5C**). As on the TAIR website several putative splice variants are annotated for *COMET*, we made sure in the generation of the 5 different mutant alleles to target a genomic region which is transcribed in all splice variants. All mutant lines resembled the phenotype of the *comet-1* plants, i.e., reduced fertility with a significantly larger number of aborted seeds and aborted pollen grains than the wildtype (**Figure 5D, 5E and 5F**).

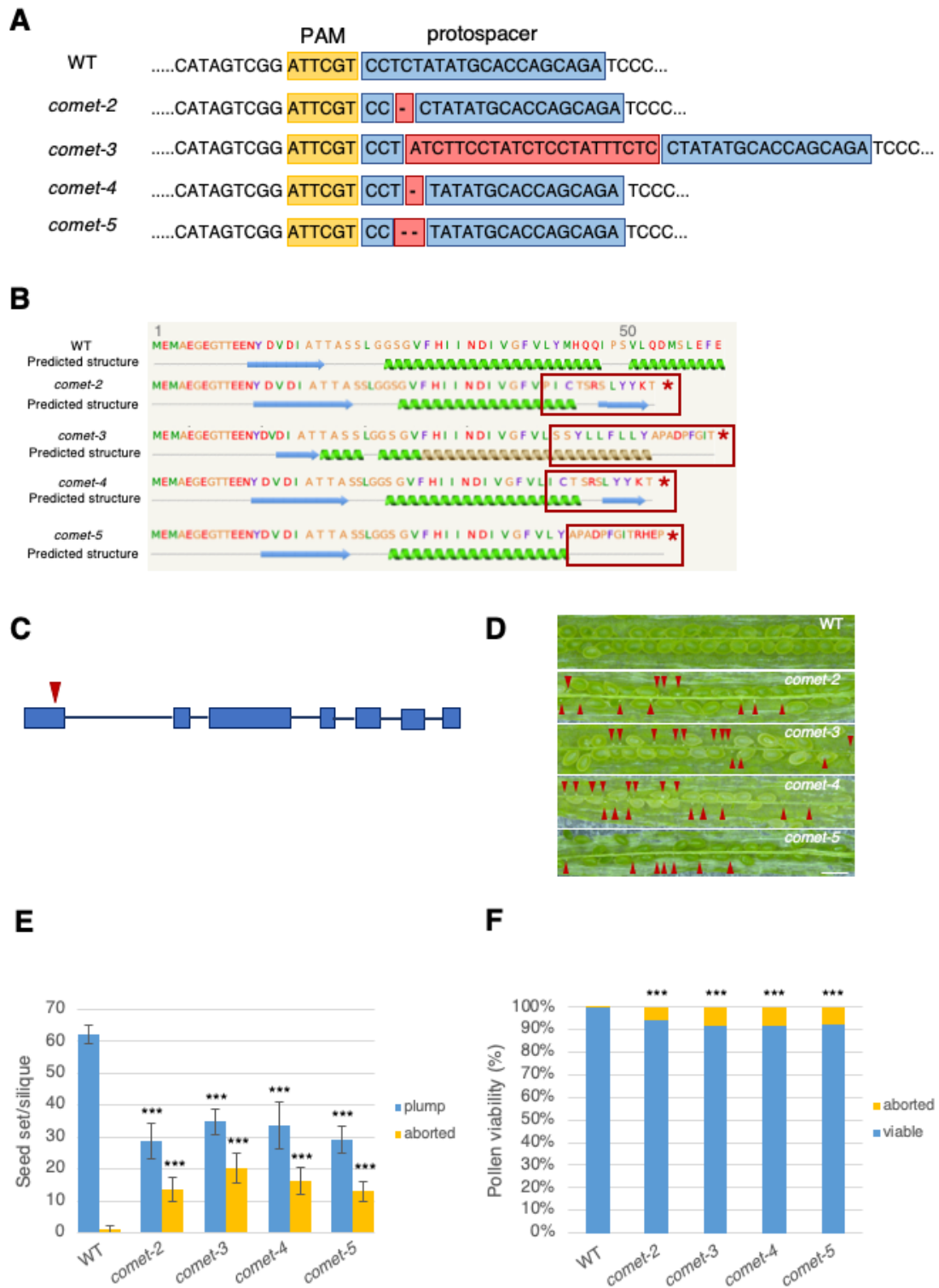


**Figure 5: Four additional *comet* CRISPR/Cas9 alleles show reduced fertility**

*COMET* sequence of the first exon, the 20 nt target sequence (protospacer) used as the guide RNA (highlighted in blue) and the 3 nt protospacer-adjacent motif (PAM; highlighted in yellow) are indicated. The CRISPR edit is highlighted in red for each allele (*comet-2*, *comet-3*, *comet-4* and *comet-5*). Prediction of the secondary structure of *COMET* in wildtype and in the four different *comet* mutants using the Phyre2 protein structure

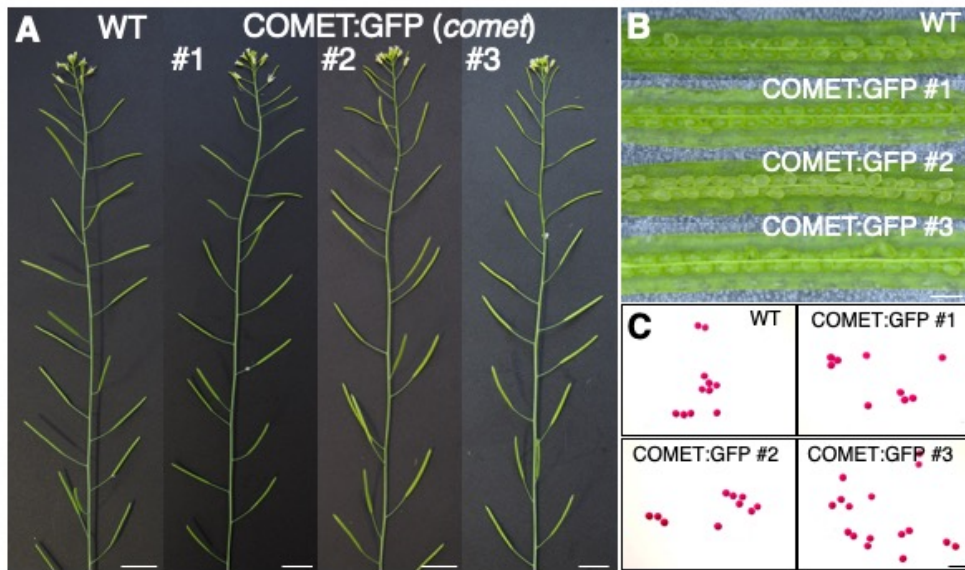
prediction server (B). These mutations change the protein sequences (red frame) and lead to premature stop codons (B). Schematic representation of *COMET* gene. Boxes correspond to exons, bars to introns; the red arrowhead indicates the position of the CRISPR edits (C). Open siliques of wild-type and *comet-2*, *comet-3*, *comet-4* and *comet-5* plants, red arrowheads indicate aborted seeds. Bar 1 mm (D). Quantification of seed set per silique (E); data are represented as the mean value  $\pm$  standard deviation (SD) of plump and aborted seeds in the wildtype (n=15 siliques analyzed), *comet-2*, *comet-3*, *comet-4* and *comet-5 mutants* (n=25 siliques analyzed per each line). Quantification of pollen viability (F); data are represented as the percentage values of viable and aborted pollen grains counted for wildtype (from n=9 flowers), *comet-2*, *comet-3*, *comet-4* and *comet-5 mutants* (from n=9 flowers per each line). Level of significance between the wildtype and each *comet* mutant is determined by Student's t-test ( $p < 0.001$  \*\*\*). The figures 5D, 5E and 5F are made with the data kindly provided by Jordan Brun.

In addition, homozygous *comet-1* plants were transformed with a 5.2 kb fragment spanning the *COMET* genomic region in which the ORF of *GFP* was introduced at the N- or C-terminus of *COMET*. However, the N-terminal fusion did not produce a GFP signal *in planta* and the C-terminal fusion did not rescue the *comet-1* mutant phenotype (data not shown). Hence, we introduced GFP at two internal positions, which were predicted to have no ordered secondary structures (**Figure 3D**), i.e., after amino acid 73 and 154 with respect to the *COMET* protein. The expression of the *COMET* version with the insertion at amino acid 73 also did not complement the *comet-1* mutant phenotype.

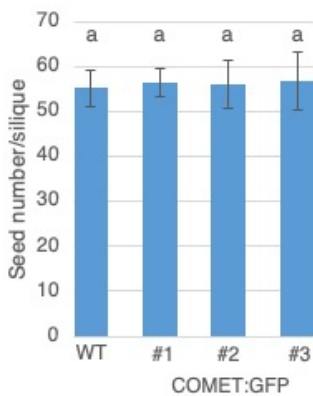
Only the insertion at amino acid 154 (called *COMET:GFP*) turned out to be fully functional, suggesting that *COMET* is a single-domain protein sensible to structural perturbation; the resulting transgenic plants harboring this construct were fully fertile corroborating that the mutant phenotype was due to a defective *COMET* gene (**Figure 6**).

All further experiments were performed using *comet-1* as the representative mutant allele, which we refer to in following as *comet*.





**D**



**E**

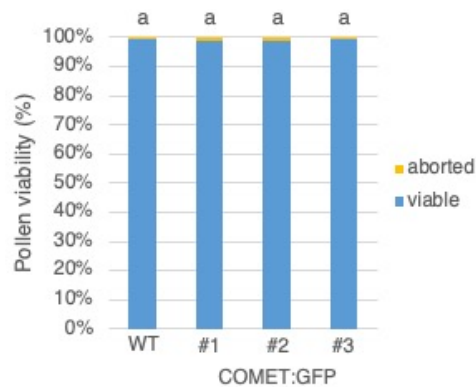


### Figure 6: COMET:GFP is fully functional

Main inflorescence of wildtype and three independent COMET:GFP reporter lines in homozygous *comet* background. Bars 1 cm (A). Open siliques of wildtype and three independent COMET:GFP reporter lines. Bar 1 mm (B). Peterson staining of pollen from wildtype and three independent COMET:GFP lines. Bar 50  $\mu$ m (C). Quantification of plump seed in the wildtype (n=15 siliques analyzed) and the three independent COMET:GFP reporter lines (n=25 siliques analyzed per line) (D); data are represented as the mean value  $\pm$  standard deviation (SD). Quantification of pollen viability (n=9 flowers per line) (E); data are represented as the percentage values of viable and aborted pollen grains counted for wildtype (from n=9 flowers) and the three independent COMET:GFP reporter lines (from n=9 flowers per line). Level of significance ( $p < 0.05$  \*;  $p < 0.01$  \*\*;  $p < 0.001$  \*\*\*) is determined by the one-way ANOVA followed by Tukey's test.



## 2.2 Loss of COMET leads to defective synapsis and reduced CO number

The reduced fertility of *comet* plants together with a previously reported role in meiosis of the COMET homolog in rice [42], prompted us to analyze male meiosis in *comet* mutants by chromosome spreading of pollen mother cells (PMCs). During the first meiotic division in the wildtype (**Figure 7A**), chromosomes start to condense during early prophase I, the formation of the SC is initiated at zygotene, and at pachytene, homologous chromosomes appear as a thick thread-like structure indicative of full synapsis. The SC is then disassembled during diplotene and homologs separate, remaining connected through chiasmata. Subsequently, chromosomes fully condense and compacted bivalents become visible at diakinesis before they align in the metaphase plate prior to segregation.

In contrast, although synapsis was initiated at zygotene, pachytene stages were not observed in male meiocytes of *comet* mutants (n=30). Instead, *comet* meiocytes at pachytene-like stages showed only partial synapsis and non-synapsed regions, where the chromosome axes were juxtaposed (**Figure 7B and 7C**).

To verify this, we introduced a previously generated functional reporter construct *PRO<sub>ZYP1B</sub>: ZYP1B:GFP*, a component of the central region of the SC, in *comet* mutants and combined it with a functional reporter *PRO<sub>ASY3</sub>:ASY3:RFP*, an axis core protein [46]. In wild-type meiocytes, the ZYP1B signal is detectable at zygotene when it starts to appear in several small nucleation sites and becomes linear with the progression of synapsis, labeling the entire chromosome axis in pachytene (**Figure 8A**). In *comet* meiocytes, the ZYP1B signal is first detectable at zygotene similarly as in the wildtype as small foci, however, pachytene-like meiocytes never show a linear ZYP1B signal labeling whole chromosomes (**Figure 8B**), suggesting that synapsis is hindered in *comet* mutants. Compromised synapsis was further confirmed by immunolocalization of ZYP1 (**Figure 8C and 8D**).

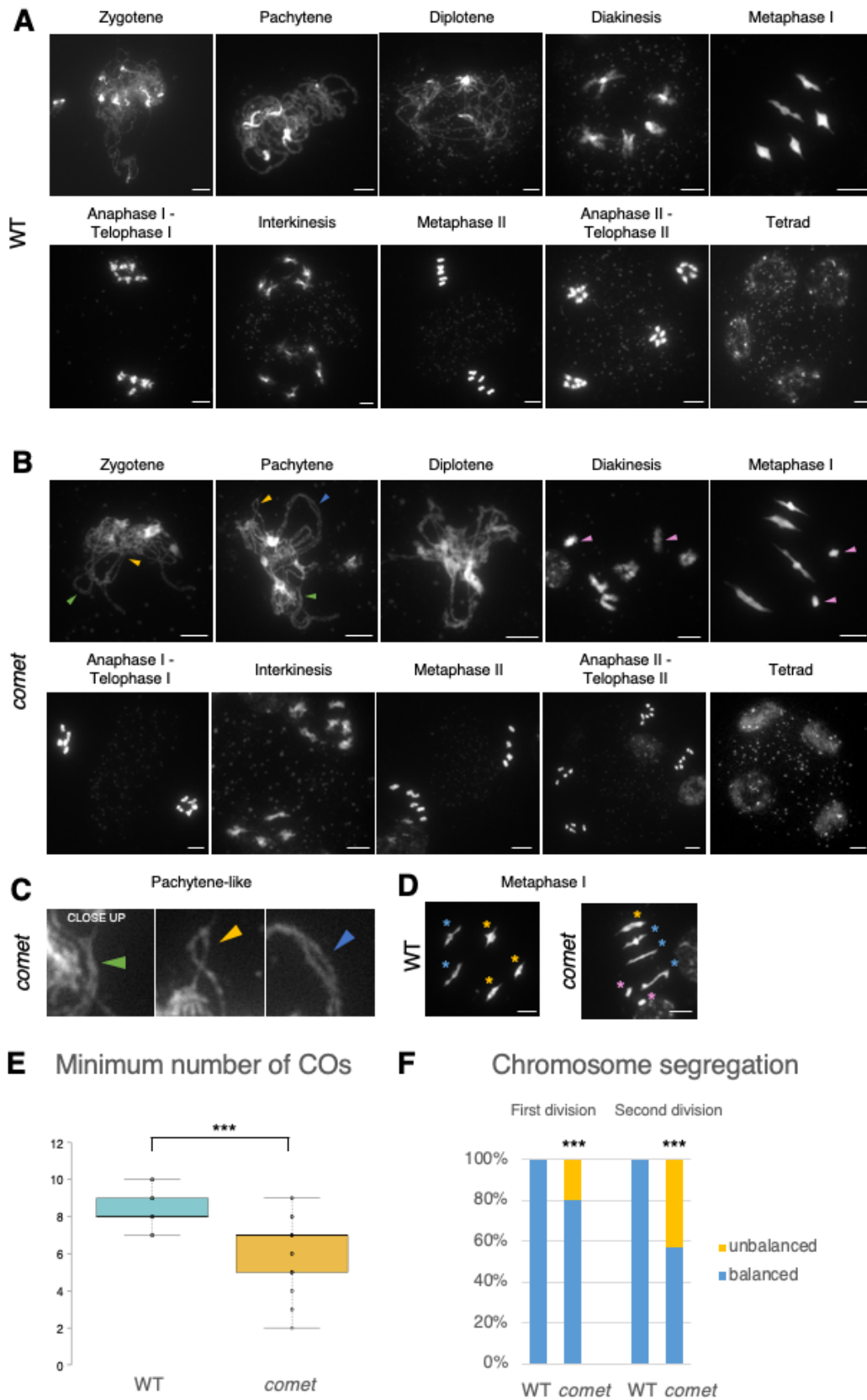


**Figure 7: Mutants in *COMET* show defective chromosome behavior in meiosis**

Chromosome behavior of pollen mother cells (PMCs) in wildtype (A) and *comet* (B). Green arrowheads indicate synapsed chromosomes at zygotene and pachytene-like stages,

yellow arrowheads point at unsynapsed chromosomes and blue arrowheads at pairing defects in *comet*. Magenta arrowheads indicate univalents (B). Close-up of pachytene-like meiocytes in *comet* (C). Representative picture of chromosomes at metaphase I in wild-type and *comet* meiocytes (D). Blue asterisks depict bivalents bound by a chiasma in one arm only (rod-like shape) and yellow asterisks depict bivalents with both arms bound by chiasmata (ring-like shape), in both wild-type and *comet* meiocytes; pink asterisks depict univalents in *comet* meiocytes (D). Quantification of the minimum number of COs in wild-type (n=78 cells) and *comet* meiocytes (n=71 cells) (E). Quantification of defects in chromosome segregation during first and second meiotic division; data are represented as the percentage of occurrence of balanced and unbalanced pool of chromosomes during both the first meiotic division in the wildtype (n=71 cells) and *comet* (n=135 cells) and the second meiotic division in the wildtype (n=34 cells) and *comet* (n=54 cells) (F). Bars: 5  $\mu$ m. Level of significance is determined by Student's t-test (\*\*\*) p<0.001).

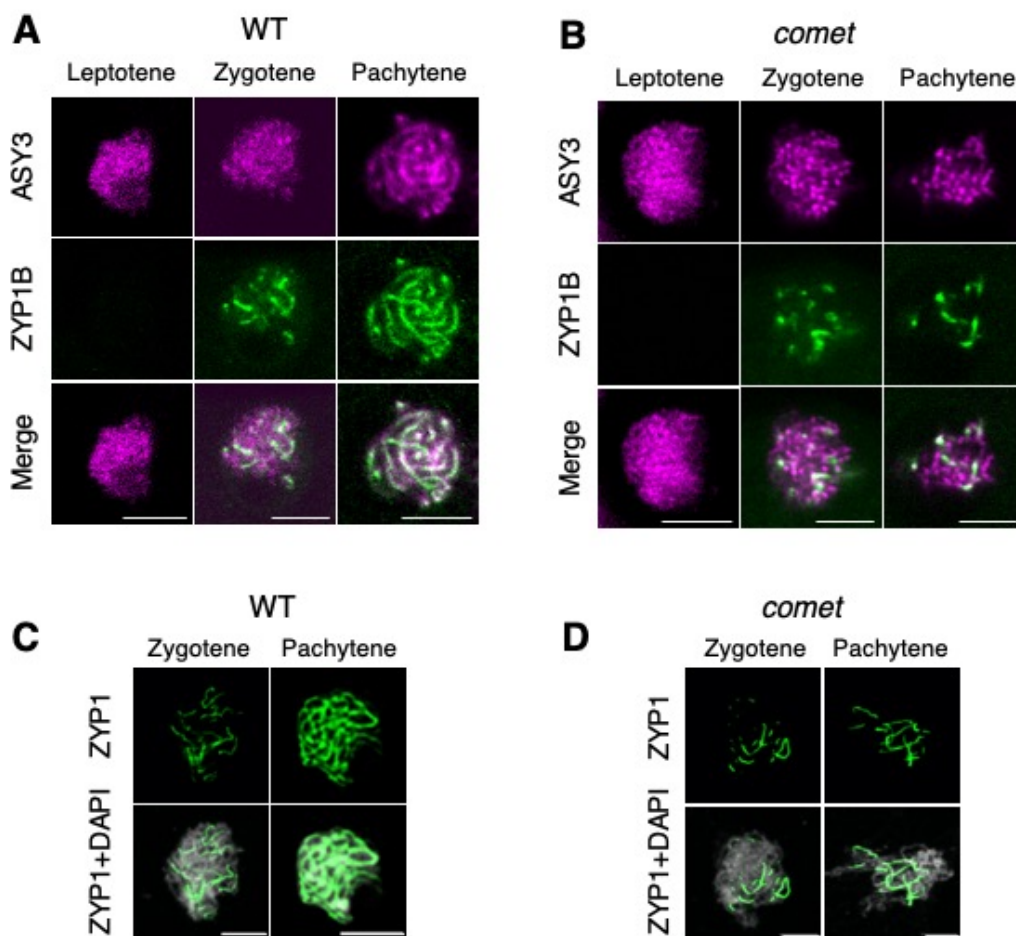


**Figure 8: Mutants in *COMET* have defective synapsis**

Confocal laser scanning micrographs of co-localization of ASY3 and ZYP1B in wild-type (A) and *comet* (B) meiocytes at leptotene, zygotene and pachytene stages.

Immunolocalization of ZYP1 in wild-type (C) and *comet* (D) meiocytes at zygotene and pachytene stages. Bars: 5  $\mu$ m. The figures 8C and 8D are made with the data kindly provided by Dr. Chao Yang.

Next, we estimated the minimum number of COs in wild-type (n=78) and *comet* meiocytes (n=71). We analyzed cells at metaphase I of spread chromosomes and recorded the number of chiasmata, the cytological manifestation of COs. At this stage, bivalents can be connected by a chiasma in one arm only giving rise to a rod-like shape (**Figure 7D** blue asterisks) or have both arms bound by chiasmata resulting in a ring-like configuration (**Figure 7D** yellow asterisks); univalents are chromosomes without any chiasma (**Figure 7D** pink asterisks).

In wild-type male meiocytes, five bivalents were observed with an average minimum number of COs of 8.5 (**Figure 7E**). In contrast, in *comet* male meiocytes, univalents were observed in 29 out of 71 cells and the average minimum number of COs was significantly reduced to 6.3 ( $p < 0.001$ ) (**Figure 7E**).

In the wildtype, meiosis progresses with the segregation of homologs after metaphase I, giving rise to two pools of five chromosomes separated by an organellar band, and subsequently with the segregation of sister chromatids leading to the formation of four haploid nuclei at the end of the second meiotic division (**Figure 7A**). In *comet* meiocytes, we observed defects in segregation, i.e., the formation of unbalanced pools of chromosomes at the end of the first meiotic division (27 cells out of 135) and the second meiotic division (23 cells out of 54) as expected for mutants with defective CO formation (**Figure 7B and 7F**). This unbalanced segregation presumably leads to the formation of aneuploid pollen grains and is hence likely the reason for the observed dead pollen as described above and occasionally to aborted seeds if a mutant pollen grain survives.

The results of our chromosome spread analysis are consistent with previous work in rice that has implicated P31<sup>comet</sup> in homolog pairing and synapsis [42]. Notably, in *p31<sup>comet</sup>* mutants in rice, no DSBs are formed and *p31<sup>comet</sup>* mutants suppress the fragmentation defects seen in mutants of *RAD51C*, which encodes for a recombinase that binds to DSB sites and is needed for DSB repair. To test whether this is also the case in Arabidopsis, we performed immuno-localization studies of RAD51, an interactor of *RAD51C*, involved in DSB repair, that localizes

to DSB sites. In contrast to rice, we found that the localization pattern of RAD51 is indistinguishable from that of the wildtype suggesting that DSB formation is not compromised in *comet* mutants ( $108 \pm 19.2$  RAD51-positive foci,  $n=8$  *comet* meiocytes analyzed versus  $112.4 \pm 11$  RAD51-positive foci,  $n=7$  wild-type meiocytes;  $p=0.62$ ) (**Figure 9A and 9B**).

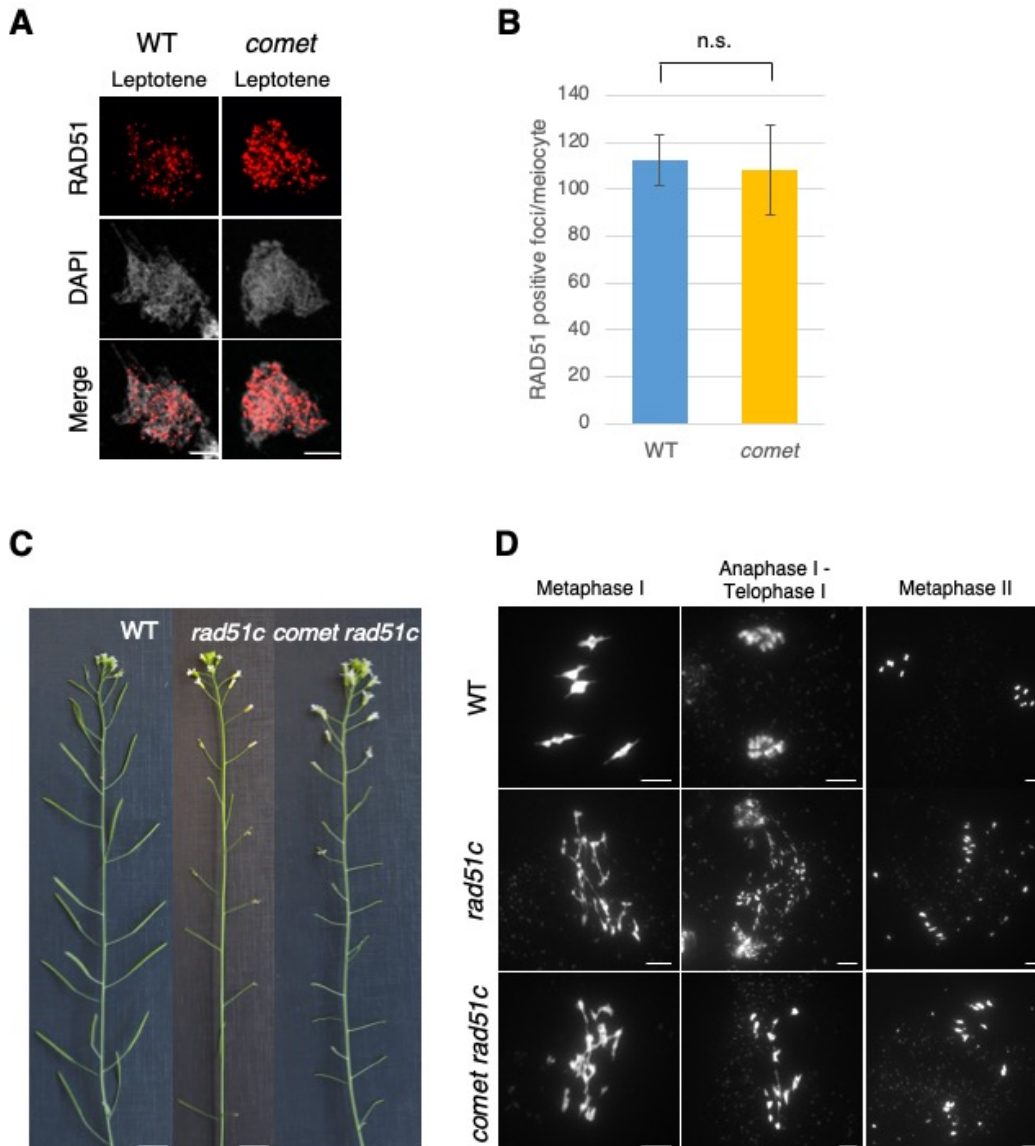


**Figure 9: DSB formation is not compromised in *comet***

Immunolocalization of RAD51 in wild-type and *comet* meiocytes at leptotene stage (A). Quantification of RAD51-positive foci in wild-type ( $n=7$ ) and *comet* ( $n=8$ ) meiocytes; data are represented as the mean value  $\pm$  standard deviation (SD) (B). Main inflorescence of wildtype, *rad51c* and *comet rad51c* double mutant. Bars 1 cm (C). Meiotic chromosome behaviors of pollen mother cells (PMCs) in wildtype, *rad51c* and *comet rad51c* double mutant at metaphase I, anaphase I and metaphase II. Bars: 5  $\mu$ m. Level of significance is

determined by Student's t-test; n.s. depicts no significant difference. The figures 9A and 9B are made with the data kindly provided by Dr. Chao Yang.

To further test DSB formation in *comet*, we constructed a *comet rad51c* double mutant, which was highly sterile resembling the fertility defect of *rad51c* single mutants (**Figure 9C**) [47]. Next, we analyzed the meiotic chromosome behavior of the *comet rad51c* double mutant in comparison to the wildtype and *rad51c* by chromosome spreads (**Figure 9D**). While in wild-type meiosis, five bivalents are visible at metaphase I and thereafter homologs segregate at anaphase I (see also above), *rad51c* is characterized by the presence of numerous chromosome fragments due to unrepaired DSBs (**Figure 9D**). Matching the sterility of the double mutant, *comet rad51c* plants exhibit chromosome fragmentation to a similar extent as *rad51c*.

Taken together, loss of *COMET* cannot suppress the defects of chromosome fragmentation in *rad51c* mutants. The difference in the mutant phenotype of *comet* between rice and Arabidopsis suggests that *COMET* plays different roles in different species and/or that the function of *COMET* is not completely understood yet.

### **2.3 Chromosome axis remodeling is affected in *comet***

To unravel what causes the defective synapsis and reduced chiasma frequency in *comet* mutants, we analyzed the formation of the chromosome axis, which plays pivotal roles in homolog interactions [48, 49]. To assess axis formation, we introduced the previously generated functional reporter constructs for different components of the chromosome axis, i.e., *PRO<sub>REC8</sub>:REC8:GFP*, as a member of the cohesin complex, *PRO<sub>ASY3</sub>:ASY3:RFP*, as an axis core protein and *PRO<sub>ASY1</sub>:ASY1:GFP*, as a meiotic HORMA domain protein, into *comet* mutants [21, 46, 50].

Whereas *REC8* and *ASY3* showed a localization pattern that was indistinguishable from the wildtype (**Figure 10A and 10B; Figure 10C and 10D**, respectively), several deviations from the wildtype were observed with respect to the accumulation of *ASY1* in *comet* (**Figure 11**).

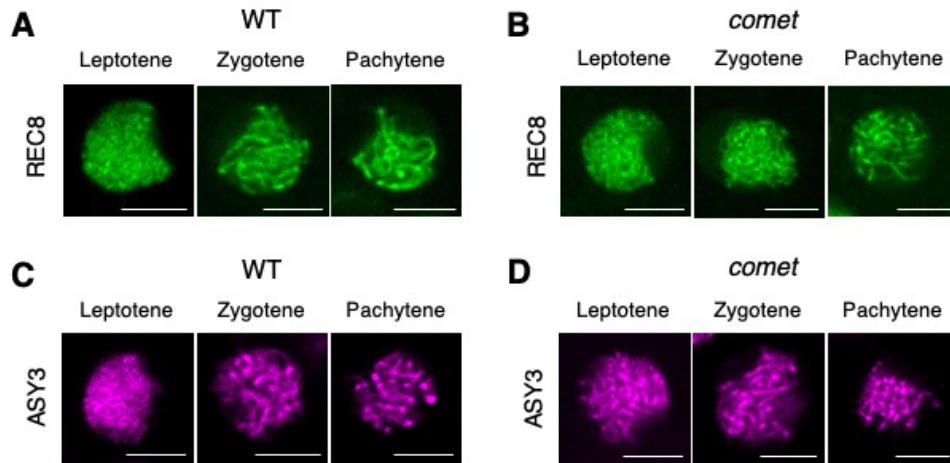


**Figure 10: The localization of the chromosome axis components REC8 and ASY3 is not affected in *comet***

Confocal laser scanning micrographs of REC8 in wild-type (A) and *comet* (B) meiotic cells at leptotene, zygotene and pachytene stages. Confocal laser scanning micrographs of ASY3 in wild-type (C) and *comet* (D) meiotic cells at leptotene, zygotene and pachytene stages. Bars: 5  $\mu$ m.

First, while ASY1 in the wildtype strictly accumulates in nuclei and decorates all chromosomes of male meiotic cells from leptotene to pachytene (**Figure 11A**), ASY1 was present in both the cytoplasm and on chromosomes in *comet* mutants (**Figure 11B**), revealing a role of COMET in regulating the nuclear targeting of ASY1.

Second, we also found differences in ASY1 localization with respect to its chromosome association. In the wildtype, ASY1 is targeted to the nucleus at early prophase I and is then progressively removed from the synapsed axes (**Figure 11A**, white arrowheads), starting at zygotene and with the removal process being completed by pachytene, as revealed by the accumulation of a nucleoplasmic diffused signal indicative of the removal of ASY1 from the chromosome axis. In contrast, although a partial nuclear targeting of ASY1 could be observed in *comet* mutants, its dynamic localization pattern, i.e., the late removal from chromosomes, was clearly affected (**Figure 11B**). This was confirmed by co-immunolocalization experiments using antibodies against ASY1 and ZYP1 (**Figure 11C and 11D**, please note that the ASY1 signal is now depicted in magenta while the ZYP1 signal is shown in green).



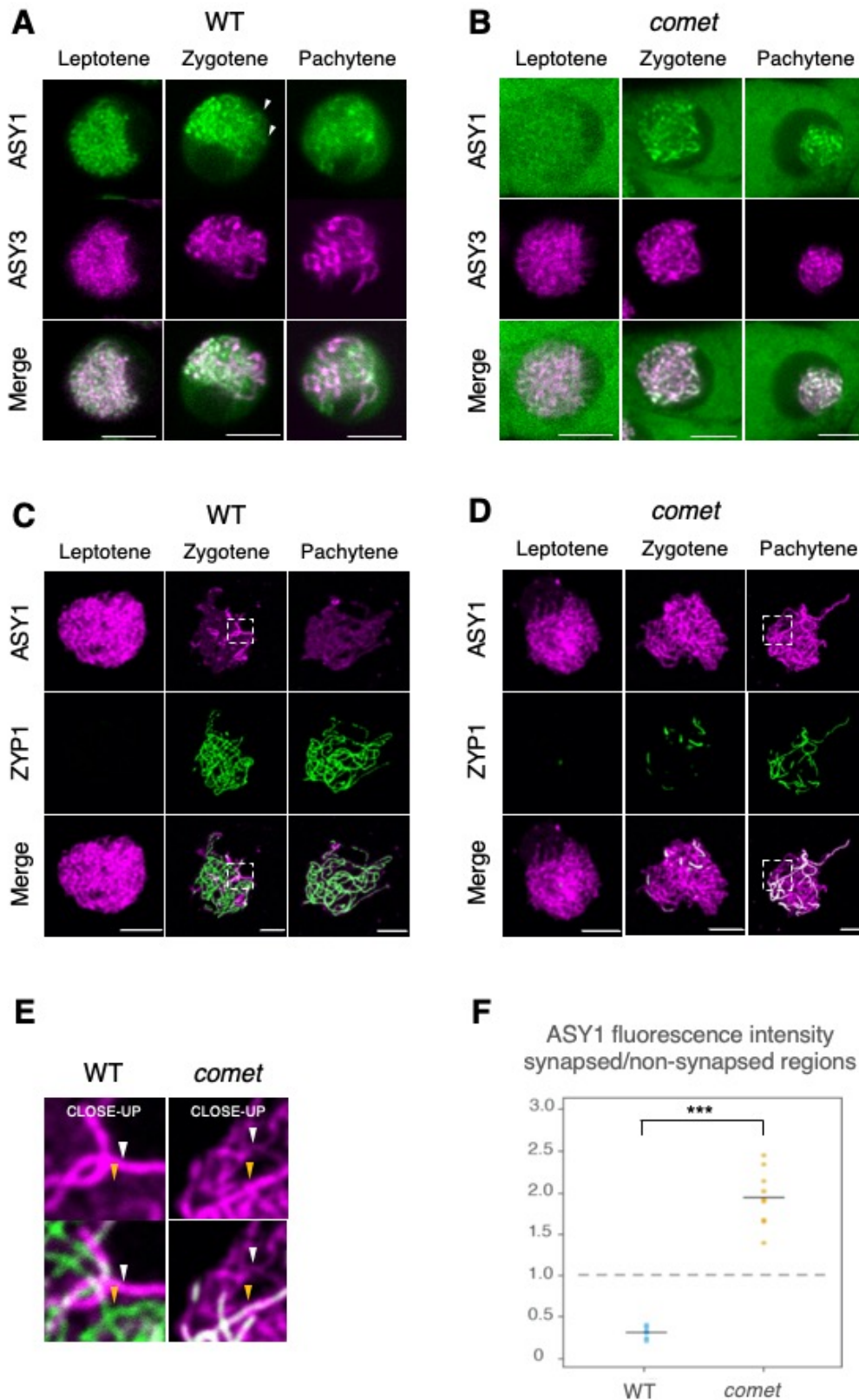


**Figure 11: Chromosome axis remodeling is affected in *comet***

Confocal laser scanning micrographs of co-localization of ASY1 and ASY3 in wild-type (A) and *comet* (B) meocytes at leptotene, zygotene and pachytene stages. White arrowheads indicate chromosome axis region depleted of ASY1. Co-immunolocalization of ASY1 and



ZYP1 in wild-type (C) and *comet* (D) meiocytes at leptotene, zygotene and pachytene stages. Close-up of regions highlighted in the dashed white boxes shown in (C) and (D) for the wildtype and *comet*; white and yellow arrowheads indicate the non-synapsed and synapsed chromosome axes, respectively (E). Quantification of ASY1 fluorescence intensity on synapsed and non-synapsed regions; data are represented as the ratio between ASY1 fluorescence intensity on synapsed and non-synapsed regions in wild-type (n=9) and *comet* (n=9) meiocytes (H). Level of significance is determined by Student's t-test (\*\*\*)  $p < 0.001$ ). Bars: 5  $\mu\text{m}$ . The figures 11C, 11D and 11E are made with the data kindly provided by Dr. Chao Yang.

In the wildtype, the removal of ASY1 from the synapsed chromosome regions leads to a large difference in ASY1 signal intensities between the synapsed and the non-synapsed regions (**Figure 11C and 11E**, yellow and white arrowheads respectively). In contrast, the ASY1 signal appeared not reduced on the synapsed regions compared to the non-synapsed domains at pachytene-like stage in *comet* meiocytes (**Figure 11D and 11E**, yellow and white arrowheads respectively).

To further investigate this aspect, we quantified the ASY1 fluorescence intensity at synapsed and non-synapsed regions and calculated the relative ratio, in wild-type (n=9) and *comet* meiocytes (n=9). While the ASY1 signal intensity on synapsed regions was lower than at the non-synapsed regions in wild-type meiocytes, the signal intensity at synapsed chromosomes appeared even stronger than at non-synapsed regions in *comet* meiocytes (**Figure 11F**). This suggests that COMET is required for ASY1 removal from the chromosome axis.

The alterations in the localization dynamics of ASY1 observed in *comet* mutants plus the defective synapsis and chiasma formation are reminiscent of the meiotic phenotypes induced by the loss of *PCH2* [20], giving rise to the hypothesis that COMET functions in the same pathway as *PCH2*. To explore this possibility, we first determined the subcellular localization of COMET during meiosis. To this end, the functional *PRO<sub>COMET</sub>:COMET:GFP* reporter line was combined with plants containing the chromosome axis marker *PRO<sub>ASY3</sub>:ASY3:RFP* that is expressed during prophase I and can be used for staging of meiosis. Observing these two reporters simultaneously by confocal microscopy, we found that COMET accumulated in both the cytoplasm and nucleus of male meiocytes, supporting the finding that COMET regulates ASY1 in both cell compartments (**Figure 12A**).

Specifically, in nuclei of male meiocytes, COMET formed numerous dot-like signals at leptotene that co-localized with the ASY3 thread-like signal, suggesting that COMET was recruited onto the axes at early meiosis. As meiosis progressed, the COMET signal increased and became more linear along with the ASY3 axial signal at zygotene. At pachytene, the COMET signal fully overlapped with the thicker thread-like ASY3 signal highlighting the paired axes.

This localization pattern largely resembled the distribution of PCH2 as revealed here (**Figure 12B**) and reported previously [21], i.e., both COMET and PCH2 accumulate in the cytoplasm and in the nucleus and at late stages of prophase I both are present on the synapsed chromosomes.

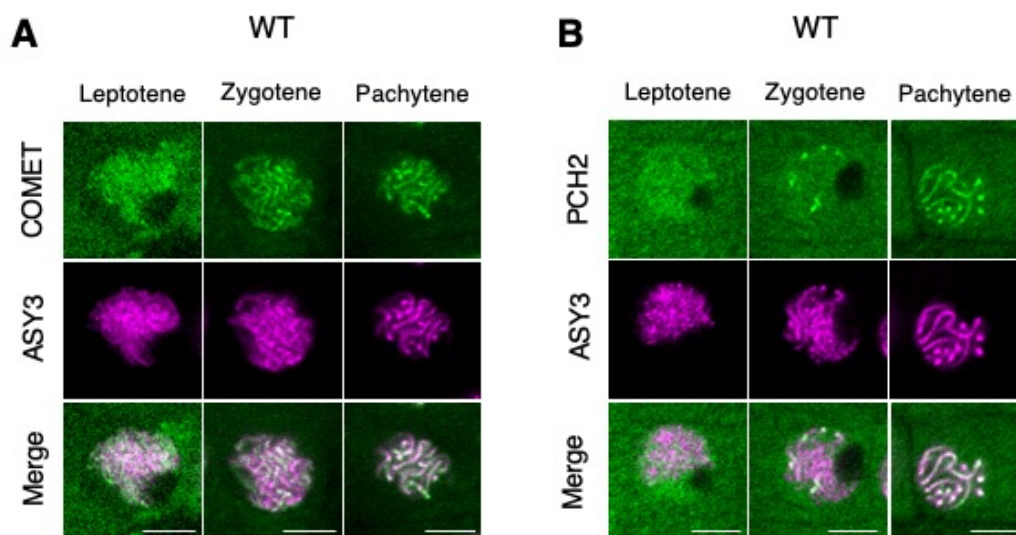


**Figure 12: COMET and PCH2 accumulate in the cytoplasm and in the nucleus during prophase I**

Confocal laser scanning micrographs of COMET and ASY3 (A) and PCH2 and ASY3 (B) in wild-type meiocytes at leptotene, zygotene and pachytene stages. Bars: 5  $\mu\text{m}$ .

The similarities between COMET and PCH2 were further supported by the analysis of the localization of a mutant of ASY1 protein in which two presumptive CDK phosphorylation sites are mutated into non-phosphorylatable amino acids (ASY1<sup>T142V;T184V</sup>:GFP). These mutations result in a reduced affinity of ASY1 to ASY3 and hence resulted in a failure of ASY1 to localize on the axes in wild-type meiocytes (**Figure 13A**) [21]. We previously found that the chromosome

association of ASY1<sup>T142V;T184V</sup>:GFP was largely restored in the absence of *PCH2* (**Figure 13C**) [21]. Remarkably, its chromosome association was also recovered in *comet* mutants supporting that COMET also plays a role in regulating the chromosomal assembly of ASY1 at early prophase I (**Figure 13B**).

Finally, we constructed the double mutant *comet pch2* and found that ASY1 dynamics in male meiocytes was indistinguishable between the double mutant (**Figure 13E**) and both single mutants (**Figure 11B and 13D**). Taken together, these data suggest that COMET and PCH2 function in the same pathway with regard to the regulation of ASY1 dynamics.

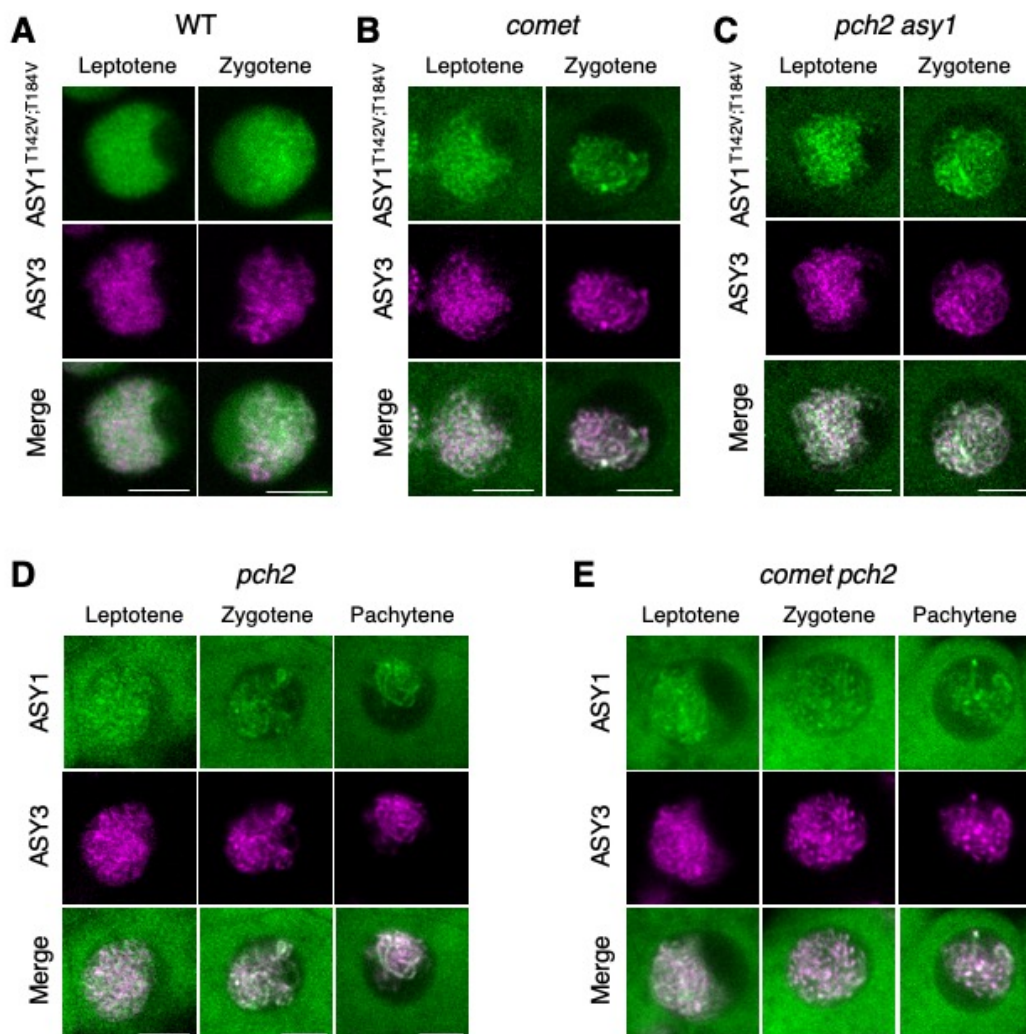


**Figure 13: COMET regulates ASY1 chromosome association together with PCH2**

Confocal laser scanning micrographs of the non-phosphorylatable ASY1<sup>T142V;T184V</sup> and ASY3 in wild-type (A), *comet* (B), and *pch2 asy1* (C) meiocytes at leptotene and zygotene stages. Confocal laser scanning micrographs of co-localization of ASY1 and ASY3 in *pch2* (D) and

*comet pch2* double mutants (E) meiocytes at leptotene, zygotene and pachytene stages. Bars: 5  $\mu$ m.

## 2.4 COMET functions as a cofactor for the action of PCH2

Given the function of p31<sup>comet</sup> in SAC signaling and the results described in the previous section, we next asked whether COMET could mediate the interaction between PCH2 and ASY1. To address this, we tested their interaction in a Yeast-2-Hybrid (Y2H) assay (**Figure 14**).

Consistent with previous reports, we could not detect any interaction between PCH2<sup>FL</sup> and ASY1<sup>FL</sup> as well as its N- and C-terminal domains (ASY1<sup>1-300</sup> or ASY1<sup>301-593</sup>) (**Figure 14A**). However, when we tested for interaction between COMET and ASY1 and COMET and PCH2, we found that COMET<sup>FL</sup> strongly interacts with PCH2<sup>FL</sup> and ASY1<sup>FL</sup> (**Figure 14B**). We next asked which domain of ASY1 is involved in the interaction with COMET. COMET<sup>FL</sup> interacts with ASY1<sup>1-300</sup>, which contains the HORMA domain, but not with ASY1<sup>301-593</sup> in which the HORMA domain is missing (**Figure 14C**). Since we found that yeast cells harboring COMET<sup>FL</sup> and ASY1<sup>1-200</sup> or ASY1<sup>1-100</sup> did not grow as a sign of lacking interaction, we conclude that the entire N-terminal HORMA domain of ASY1 is necessary for the interaction with COMET (**Figure 14C**).

Conversely, we asked whether there is a specific domain in COMET responsible for HORMA recognition. However, since we did not find evidence for an interaction between COMET<sup>1-150</sup> or COMET<sup>151-265</sup> with ASY1<sup>1-300</sup> in our Y2H assay, we conclude that the entire or at least large parts of the COMET protein are needed for the interaction with ASY1 consistent with the predication that COMET is a single-domain protein (**Figure 14C**).

Next, we dissected the COMET-PCH2 interaction and found that COMET<sup>FL</sup> only interacted with PCH2<sup>1-130</sup> and not with PCH2<sup>131-467</sup>. Interestingly, both the N- and the C-terminal part of COMET, COMET<sup>1-150</sup> and COMET<sup>151-265</sup>, interacted with PCH2<sup>1-130</sup>, possibly arguing for two interaction interfaces between these two proteins (**Figure 14D**).

The interaction of COMET with ASY1 and PCH2 was further investigated by Ni<sup>2+</sup> pull-down assay using recombinant proteins purified from *E. coli* (**Figure 14**). To this end, we used a GST fusion to COMET, a His-MBP fusion to ASY1 and two

independent fusions of PCH2, one to a His-tag and one to a His-MBP tag, revealing that COMET can directly interact with ASY1 and PCH2.

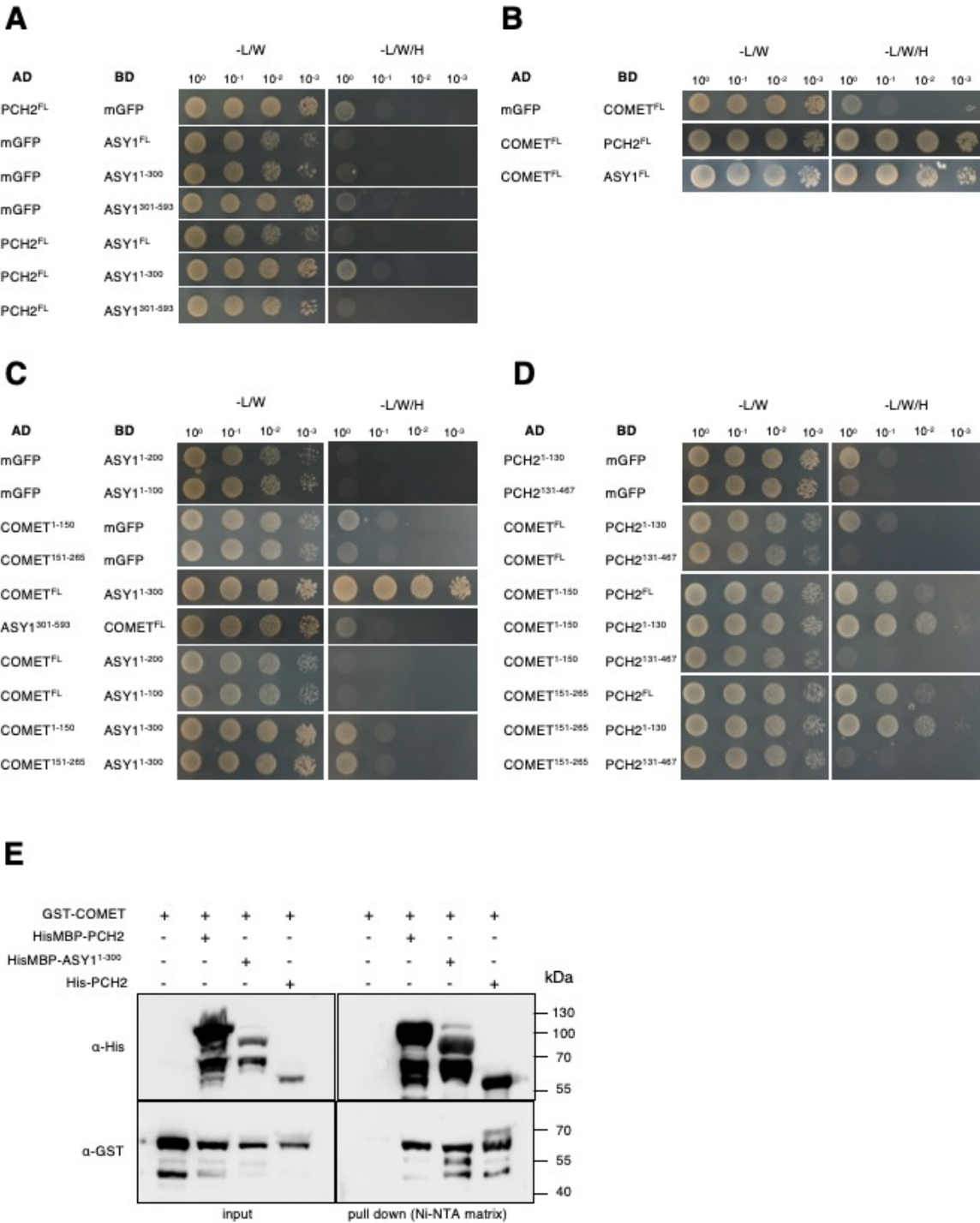


**Figure 14: COMET interacts with both PCH2 and ASY1**

Yeast Two-Hybrid interaction assay between PCH2 and ASY1 (A), COMET, PCH2 and ASY1 (B), COMET and ASY1 (C), COMET and PCH2 (D). Full length (FL) and truncated versions of the relevant proteins were used for the assay. Monomeric GFP (mGFP) was used as a

negative control. Yeasts were spotted on SD plates without leucine and tryptophan (L/W) as growth control and on plates without leucine, tryptophan, and histidine (L/W/H) for interaction evaluation. Ni<sup>2+</sup> pull down assay of COMET with PCH2 and ASY1 (E). The input and pull-down fractions were analyzed by immuno-blotting with the anti-GST (COMET), anti-His (PCH2 and ASY1) and anti-MBP (PCH2) antibodies. The results shown are representative of two independent experiments. The figure 14 is made with the data kindly provided by Dr. Chao Yang.

Finally, to explore the functional relevance of these interactions *in planta*, we investigated the localization pattern of COMET in *pch2* and PCH2 in *comet* as well as the accumulation pattern of both proteins in *asy1* mutants (**Figure 15**). To this end, we used the functional reporter for COMET described here and a previously generated functional reporter for PCH2 [21] and combined them with ASY3:RFP for staging. In early prophase I of the wildtype, PCH2 starts to accumulate in the cytoplasm and in the nucleus, where it associates with the chromosome axis on the synapsed areas from zygotene stage onwards (**Figure 12B**). When we analyzed the localization of COMET and PCH2 in *asy1* mutants, we found that the association of both proteins with the chromosome axis, labeled by ASY3:RFP, is abolished in this mutant (**Figure 15B and 15D**).

Next, we asked whether COMET localization would be affected in *pch2* mutants and *vice versa*. COMET properly localized and associated with the chromosome axis in *pch2* mutants indistinguishably from the wildtype, as shown by the co-localization of ASY3, which labels the chromosome axis (**Figure 15A**; please note the localization of COMET and ASY3 in wild-type meiocytes in **Figure 12A**). Strikingly, PCH2 localization was severely affected in *comet* mutants, and only short stretches of the chromosome axis were decorated by PCH2 in pachytene (**Figure 15C**).

These results are consistent with the idea that COMET serves as an adaptor protein that mediates PCH2 and ASY1 interaction during prophase I. Moreover, these localization patterns suggested a hierarchical organization, i.e., COMET first binds to ASY1 and then PCH2 is recruited to the axis via interaction with COMET.



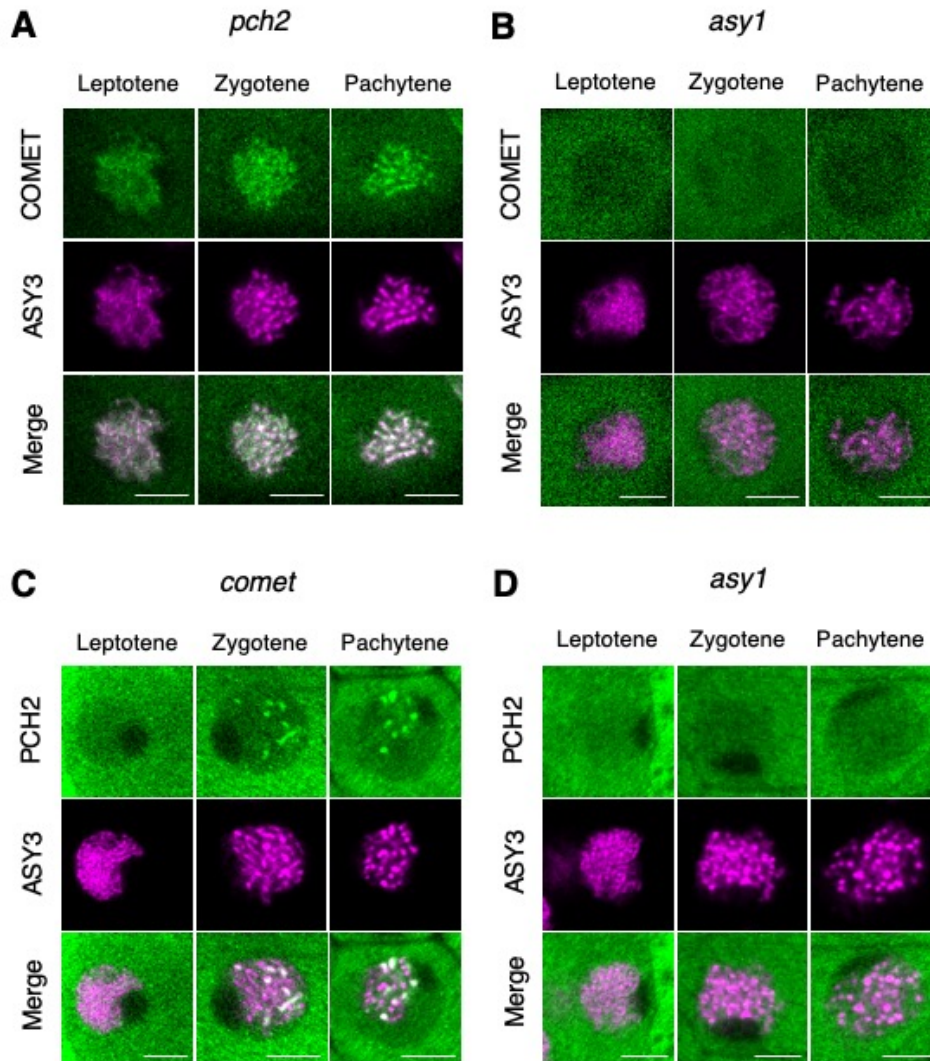


**Figure 15: Mutual dependency of COMET, PCH2 and ASY1 localization**

Confocal laser scanning micrographs of COMET and ASY3 in *pch2* (A) and *asy1* (B) meocytes at leptotene, zygotene and pachytene stages. Confocal laser scanning micrographs of PCH2 and ASY3 in *comet* (C) and *asy1* (D) meocytes at leptotene, zygotene and pachytene stages. (Please note the localization of COMET and ASY3 and PCH2 and ASY3 in wild-type meocytes in Figure 12). Bars: 5  $\mu$ m.

### 3 Discussion

During cell division, many macromolecular complexes are assembled, change in their composition and are subsequently disassembled, with the chromosome axis in meiosis being a paradigm for this dynamic behavior. Specific domain folds seem to be particularly useful to facilitate protein-protein or protein-DNA interactions. For example, the constitution of several functionally unrelated complexes relies on HORMA domain proteins, such as Mad2 in the spindle assembly checkpoint and Rev7 as part of the translesion DNA polymerase  $\zeta$  [14]. Likewise, the HORMA domain protein Hop1 in yeast and its homologs, such as ASY1 in Arabidopsis, show dynamic association with the chromosome axis and are of key importance for meiotic recombination [14]. How the dynamics of these multi-protein complexes is brought about is often poorly understood. Here, we have demonstrated that the Arabidopsis homolog of p31<sup>comet</sup>, called COMET, acts as an adaptor for the AAA+ ATPase PCH2 to first mediate nuclear targeting of ASY1 and later to promote the release of ASY1 from the chromosome axes to allow full synapsis. Interestingly, this resembles the role of p31<sup>comet</sup> and PCH2 in regulating Mad2 in the context of the SAC in mammals [5, 7, 24, 40, 51]. Thus, the regulation of HORMA domain proteins by the p31<sup>comet</sup>-PCH2 pair represents a regulatory module that is used in diverse biological processes.

#### 3.1 Multiple roles of COMET-PCH2

One of the best-studied HORMA domain proteins is Mad2, which functions in the SAC. Mad2 can adopt two distinct, stably folded conformations, referred to as 'open' (O-Mad2) and 'closed' (C-Mad2). O-Mad2 is converted into C-Mad2 at kinetochores to which spindle fibers have not yet been attached, and is subsequently incorporated in the MCC complex that inhibits the APC/C [14]. To shut down the SAC action after all kinetochores are correctly attached to spindle fibers, the MCC is disassembled by the action of p31<sup>comet</sup> and PCH2. It was observed that O-MAD2 spontaneously converts to C-MAD2 at physiological temperatures [7]. The joint action of p31<sup>comet</sup> and PCH2 counteracts this spontaneous conversion [7, 39, 51, 52]. Therefore, the p31<sup>comet</sup>-PCH2 pair has two roles in the SAC, early in ensuring a sufficient supply of O-MAD2 for kinetochore recruitment and late in shutting down the SAC.



Previous work has shown that the meiotic HORMA domain proteins also adopt a stable closed conformation by interacting with the 'closure motifs' in partner proteins and wrapping their C-terminal 'safety belt' region entirely around this motif [14, 34, 37]. A recent study in *Arabidopsis* has suggested that the meiotic HORMAD ASY1 intrinsically tends to fold into a stable self-closed state with its HORMA domain being bound by ASY1's own closure motif. Furthermore, PCH2 was found to promote the conversion to an, albeit transient, open state of ASY1, thus allowing its binding to the axis protein ASY3 [38].

We show here that COMET together with PCH2 is needed to release ASY1 from the chromosome axis. Thus, it is tempting to speculate that COMET, by mediating the interaction between PCH2 and ASY1, promotes the conversion of the closed state of ASY1 into the transient open state, which eventually leads to the removal from the chromosome axis.

In addition, we found that ASY1 accumulates not only in the nucleus, but also in the cytoplasm in *comet* mutants, similar to the situation in *pch2* mutants, indicating that the import of ASY1 to the nucleus is also affected by the loss of COMET function. Hence, it seems likely that at early prophase the COMET-PCH2 pair counteracts the spontaneous self-closing of ASY1 in the cytoplasm, which would preclude its nuclear import. Thus, the combination of a p31<sup>comet</sup>-type protein with PCH2 appears to function in regulating early and late phases of SAC signaling as well as early and late events of meiotic chromosome axis formation.

Moreover, as we have shown here, COMET also counteracts a less stable association of ASY1 with the chromosome axis as documented by the observation that an ASY1 phospho-mutant, which is not strongly associated with the chromosome axis, regains its chromosome localization in *comet* mutants. Thus, COMET and PCH2 appear to have at least three roles in meiosis (**Figure 16**). In analogy, it is tempting to speculate that p31<sup>comet</sup>-PCH2 could also have a third role in the SAC by assuring that the formed MCC is really in a stable and biologically active conformation.

## COMET controls chromosome axis remodeling

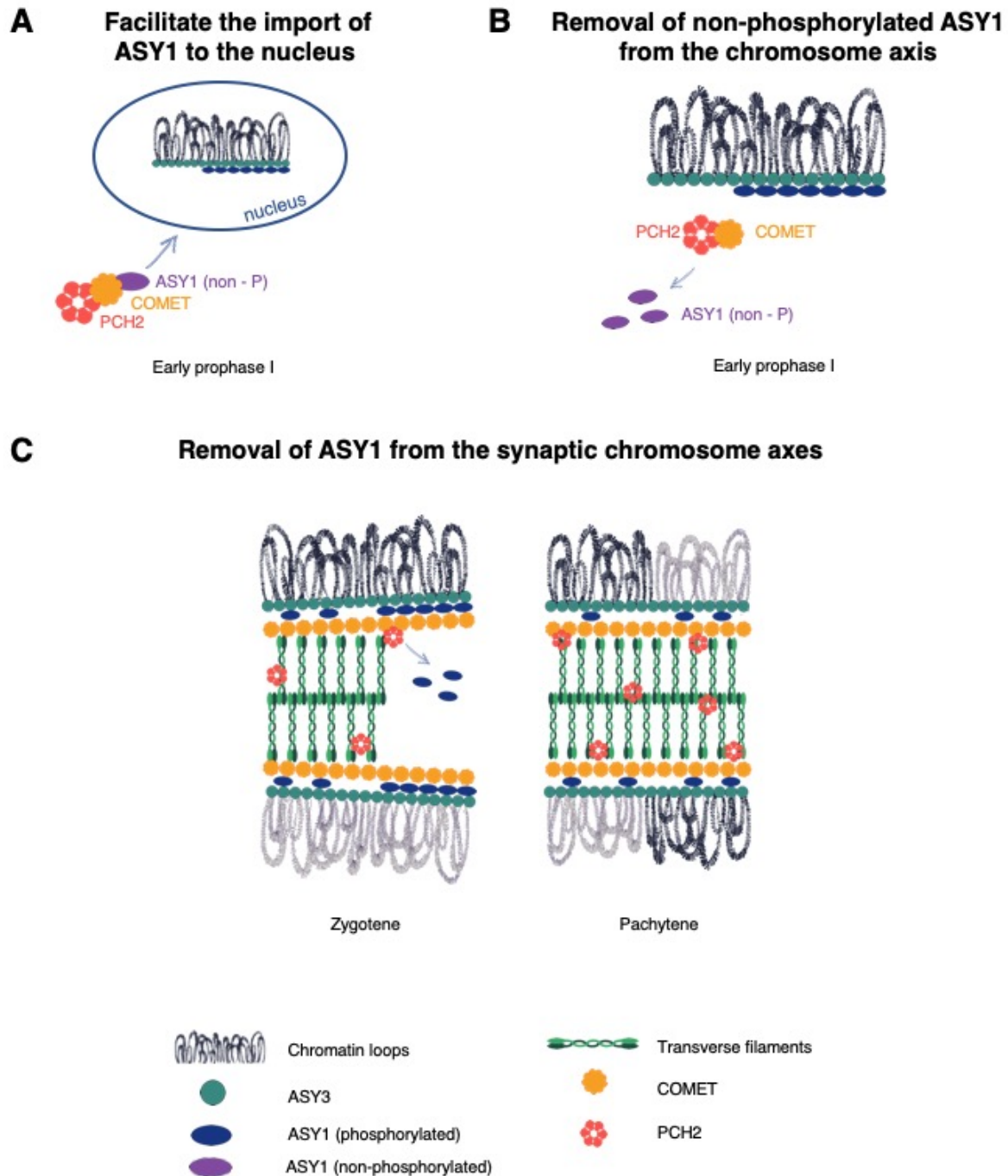


**Figure 16: A model of COMET's role in controlling chromosome axis remodeling during meiosis**

At early prophase, COMET together with PCH2 facilitates the nuclear import of ASY1 (A). In the nucleus, the joint action of COMET and PCH2 at early prophase promotes the removal of non-phosphorylated ASY1 (purple) from the chromosome axis (B), while a phosphorylated ASY1 (blue) is assembled onto the axis. During zygotene, COMET and PCH2 promote the removal of phosphorylated ASY1 from the synaptic chromosome axis to allow

the deposition of the transverse filament and the completion of the SC by the end of pachytene (C).

It is interesting to understand how the early and late functions of COMET-PCH2 become separated in both systems. In other words, how are an early release of ASY1 from the axis and the premature disassembly of the MCC prevented? One out of possibly more mechanisms appears to be the phosphorylation of ASY1 by CDKA<sub>1</sub>, the Arabidopsis Cdk1 and Cdk2 homolog. Previous work indicated that phosphorylated ASY1 has a higher affinity towards ASY3 than non-phosphorylated ASY1 [21]. Notably, the respective phosphorylation sites are conserved in human HORMADs but not in yeast (see below). However, a phosphorylation-mimic version of ASY1 could still be removed from the axis in late prophase with no apparent differences to the wild-type version, indicating that additional factors and/or posttranslational mechanisms might work to activate the ASY1-releasing forces of COMET-PCH2 at late prophase in Arabidopsis [21]. Interestingly, it was recently shown that phosphorylation of human p31<sup>comet</sup> decreases its affinity for Mad2 [53]. Whether COMET is also regulated by phosphorylation in plants, is not clear at the moment and further work is required to explore the regulation of COMET-PCH2 activity.

It is also not clear whether COMET functions in the SAC in Arabidopsis. Arabidopsis has a Mad2 homolog and likely a mobile MCC is formed as in other organisms [45, 54]. Here, we have shown that *comet* mutants are not hypersensitive to oryzalin as the roots of *comet* mutants grow as much as the wildtype when treated with this microtubule-destabilizing drug. Since p31<sup>comet</sup> has both positive and negative effects on the SAC, it is also not easy to formulate a clear hypothesis how *comet* mutants, if COMET were to regulate the SAC in Arabidopsis, would affect the growth of roots under activated checkpoint conditions. On the one hand, the checkpoint could be less active due to the absence of COMET since presumably fewer MCC complexes are formed resulting possibly in enhanced root growth. On the other hand, active MCC might be more slowly dissolved, slowing down root growth. It seems even possible that both effects could compensate for each other resulting in no net growth changes. Recent data indicated that the SAC in Arabidopsis is *per se* not very strong and even under severe microtubule destabilizing conditions, the SAC was only active for about 1.5

hours [45]. Thus, the MCC might be anyway less stable in plants in comparison to other species and/or the APC/C might be activated irrespective of an MCC being formed. With several reporter lines being recently generated [45, 55] it might be possible now to carefully monitor SAC activity and MCC composition in *comet* and *pch2* mutants.

### 3.2 COMET in meiosis outside of Arabidopsis

A role of P31<sup>comet</sup> in meiosis was first described in rice. Mutant plants were completely sterile and P31<sup>comet</sup> was found to be required for homolog pairing, synapsis and DSB formation [42]. This is partly in contrast to what we have described here for Arabidopsis since we did not find any alterations in DSB number as judged by the amount of RAD51-positive foci and the fact that *comet rad51c* were completely sterile as a consequence of the severe chromosome fragmentation, similarly to *rad51c*. Moreover, *comet* mutants in Arabidopsis are only partially sterile resembling the reduction in fertility observed in *pch2* mutants [20]. Thus, COMET may play a different role in meiosis in different species.

However, we favor a model in which COMET has the same function in Arabidopsis and rice. A first hint for this comes from the fact that in both species synapsis fails and P31<sup>comet</sup> in rice and COMET in Arabidopsis both localize to synapsed regions. Moreover, *p31<sup>comet</sup>* mutants also resemble mutants in *CRC1*, the homolog of *PCH2* in rice [56], including the requirement for DSB formation, being consistent with the assumption that P31<sup>comet</sup> and *CRC1* likely act in one pathway. Whether the association of *PAIR2*, the ortholog of *ASY1* in rice, with the axis is affected and whether *PAIR2* is present in a prolonged manner in *p31<sup>comet</sup>* mutants, as we reported here for *ASY1* in *comet*, is not clear at the moment but will be instrumental to judge functional conservation.

The difference in the mutant phenotypes between Arabidopsis and rice could possibly be explained by a difference in the timing/dependency of DSB formation with respect to *ASY1* loading onto the axis, i.e., in Arabidopsis DSB formation would precede *ASY1* loading or would be largely independent of it while in rice, DSB formation would depend on the presence of *PAIR2*, the *ASY1* homolog in rice, on the axis. Evidence for this comes from the observation that *ASY1* is not required for DSBs in Arabidopsis [57]. In contrast, *PAIR2* appears to be required for DSB formation in rice since *RAD51C* and *DMC1*, both involved in recombination repair, fail to localize to chromatin in *pair2* mutants [58-60]. At the same time, *pair2*

mutants do not have fragmented chromatin typically seen in mutants with compromised recombination repair activity indicating the absence of DSBs in *pair2* [61]. Consequently, anything that affects the dynamics of PAIR2 in rice will likely compromise DSB formation.

A discrepancy in terms of DSB formation between Arabidopsis and rice has also been found in the function of the meiotic cyclin SOLO DANCERS (SDS). In Arabidopsis, SDS is required for homolog pairing and synapsis, but not for DSB formation [62]. In contrast, the rice SDS homolog has been described to be required for DSB formation, too [63]. Interestingly, SDS, in complex with CDKA;1, was found to phosphorylate, at least *in vitro*, ASY1 in Arabidopsis resulting in an increased affinity towards ASY3 [21]. If a similar CDK-phosphorylation-dependent mechanism were at work in rice and required for PAIR2 association with the axis, this could explain the difference in the mutant phenotypes for *sds* in both species along the lines that PAIR2 loading would be required for DSB formation in rice.

PCH2-type proteins often function together with adaptor proteins which target them to specific substrates, an example being Xrs2, a member of the MRX complex, whose interaction with PCH2 at DSB sites regulates interhomolog bias and the meiotic recombination checkpoint in budding yeast [64]; or Orc1 which together with PCH2 plays a role in controlling meiotic DSBs formation within repetitive ribosomal DNA (rDNA) in budding yeast [65].

Notably, no p31<sup>comet</sup> homolog has been identified up to now in budding yeast. However, a direct interaction between Hop1 and Pch2 has been found in yeast in contrast to all other organisms studied so far [22]. Thus, yeast Pch2 might have circumvented the requirement of an adaptor protein for regulating Hop1 dynamics. It will now be interesting to see whether mammals and other metazoan use COMET-like proteins to target PCH2-type proteins to the meiotic HORMADs or whether they follow other mechanisms as likely present in yeast.

## 4 Material and methods

### 4.1 Plant material

*Arabidopsis thaliana* accession Col-0 was used as wild-type reference in this study and for the generation of transgenic lines. *comet-1* mutant line was generated by CRISPR/Cas9 (Clustered Regularly Interspaced Short Palindromic Repeats CRISPR-Associated Proteins 9) [66] with Cas9 from *Streptococcus pyogenes*; *comet-2*, *comet-3*, *comet-4* and *comet-5* were generated by CRISPR/Cas9 with Cas9 from *Staphylococcus aureus*. The T-DNA insertion lines SALK\_046272 (*asy1-4*) [67], SALK\_031449 (*pch2-2*) [20], SALK\_02196 (*rad51c*) [47] and SAIL\_191G06 (*mad2*) [68] were obtained from the T-DNA mutant collection at the Salk Institute Genomics Analysis Laboratory (SIGnAL, <http://signal.salk.edu/cgi-bin/tdnaexpress>) via NASC (<http://arabidopsis.info/>). ASY3:RFP and ZYP1B:GFP reporters [46], ASY1:GFP, ASY1<sup>T142V;T184V</sup>:GFP and PCH2:GFP reporters [21] and REC8:GFP reporter [50] were previously described. All genotypes were determined by PCR, using the primer pairs listed in **Table 1** and the PCR conditions listed in **Table 2** and **3**.

### 4.2 Plant growth conditions

All seeds were surface-sterilized with chloride gas, sown on 1% agar plates (½ Murashige and Skoog (MS), see **Table 4**) and stored 3 days at 4°C in the dark for stratification. Antibiotics were added for seed selection when required. For seed germination, plates were transferred to long-day conditions (16 h day/8 h night regime at 21°C/18°C). After germination, plants were transferred to soil and grown under long-day conditions until seed production.

For the crosses, flowers of the female parent were emasculated 1 day before anthesis under a dissecting microscope and hand-pollinated 1 to 2 days later.

### 4.3 Plasmid construction

To generate the *COMET* reporter, a 5.2 Kb genomic fragment of the *COMET* gene (*At1g03180*) was amplified by PCR and cloned into pENTR2B vector by SLiCE reaction [69]. A *SmaI* restriction site was introduced between the 154-155 aa of *COMET* by PCR. The construct was linearized by *SmaI* digestion and ligated with the GFP fragment also restricted by *SmaI*. The resulting entry construct was

integrated into the destination vector *pGWB501* via LR gateway reaction. *COMET* reporter was established by floral dipping transformation of *comet* homozygous plants. Primers used for plasmid construction are shown in **Table 1**; PCR conditions are shown in **Table 2** and **3**.

#### **4.4 Plant transformation**

The floral dip method was used for the transformation of *Arabidopsis thaliana* [70]. Plants were grown under long day conditions until bolting. Before transformation, siliques and opened flowers were cut off. *Agrobacterium tumefaciens* carrying the construct of interested was cultured overnight at 28 °C in 3 ml of LB (see **Table 4**) supplemented with 30 mg/L gentamycin and 100 mg/L spectinomycin. The bacterial suspension was centrifuged at 4000 rpm for 3 min, the supernatant was removed and the pellet was dissolved in 3 ml of transformation medium (see **Table 4**). Closed flowers were coated with *Agrobacterium* suspension by using a pipette. Transformed plants were covered in plastic bags and incubated for 2 days in the dark. Finally, plants were grown under long-day conditions until seed production. T1 plants were selected on ½ MS agar plates supplemented with 25 mg/L Hygromycin. T2 seeds from individual T1 plants were germinated on ½ MS agar plates supplemented with 25 mg/L Hygromycin.

#### **4.5 CRISPR/Cas9 genome editing**

Mutant in *COMET* were generated by CRISPR/Cas9, *comet-1* with cas9 from *Streptococcus pyogenes* and *comet-2*, *comet-3*, *comet-4* and *comet-5* with cas9 from *Staphylococcus aureus* [66]. Oligo DNAs the for *comet-1* target site were annealed and inserted into the entry vector *pEn-Chimera*. Oligo DNAs for *comet-2*, *comet-3*, *comet-4* and *comet-5* target sites were annealed and inserted into the entry vector *pEn-Sa-Chimera*. All entry clones were then introduced into the destination vector *pDe-CAS9* and *pDe-Sa-CAS9*, respectively, by LR gateway reaction. Constructs were subsequently transformed into *Arabidopsis thaliana* by floral dipping. T1 plants transformed with *pDe-CAS9* were selected on ½ MS agar plates supplemented with 10 mg/L Basta and T1 plants transformed with *pDe-Sa-CAS9* were selected on ½ MS agar plates supplemented with 30 mg/L Kanamycin. To check the CRISPR edits, the genomic DNA of T1 plants encompassing the targeting regions was amplified by PCR and then subjected to sequencing. T2

plants devoid of the CRISPR/Cas9 constructs were confirmed again for the mutations via sequencing, and the T3 stable mutant lines were used for the experimental analyses. Primer pairs used are described in **Table 1**; PCR conditions are shown in **Table 2** and **3**.

#### **4.6 Genotyping**

A small leaf of Arabidopsis plants at rosette stage was collected and placed into a well of a 96 deep-well polypropylene block, beforehand prepared with one metal bead and 250 µl of magic buffer (see **Table 4**) in each necessary well. The block was shaken for three minutes (MM300, Retsch, Haan) and then centrifuged at 2500 rpm for 1 minute. 100 µl of DNA in magic buffer were aliquoted and stored at -20°C. 1 µl of the extracted DNA was used as template for PCR amplification with the primers and PCR conditions indicated in **Table 1, 2 and 3**, respectively.

#### **4.7 Phenotype evaluation**

Pollen viability was determined by Peterson staining [71]. A mature flower bud containing dehiscent anthers was dipped in 15 µl of Peterson staining solution (see **Table 4**) for 10 s on a microscopy slide that was then covered by a cover-slip. Slides were heated at 80°C for 10 min prior to light microscope observation. Three different mature flower buds per plant were analyzed. Seed sets were determined by quantifying plump and aborted seeds of mature siliques; 5 siliques per plant were analyzed.

#### **4.8 Root growth assay and oryzalin treatment**

A stock solution of oryzalin in dimethyl sulfoxide (DMSO) was prepared and kept at -20°C. ½ MS plates were prepared by adding the oryzalin to the final concentration of 100, 150, and 200 nM. The final concentration of DMSO in the medium was 0.05% and the plates containing only DMSO were used as the non-treatment control. For quantification of root growth, five-day-old seedlings grown on plates with and without oryzalin were photographed and the primary root lengths were measured by the ImageJ software.



## 4.9 Chromosome spread analysis

Meiotic progression at a cytological level was analyzed via cell spreads as previously described [72]. In brief, fresh flower buds were fixed in 3:1 Ethanol:Acetic Acid (fixative solution) for at least 48h at 4°C, washed twice with fresh fixative solution and stored for further use in 70% ethanol at 4°C. Prior to chromosome spreading, the entire flower buds were digested in 10mM citrate buffer (see **Table 4**) for 3h at 37°C. Single flower buds were transferred onto a glass slide and squashed with a bended needle for 1min in 12 µl of 45% acetic acid. Spreading was performed on a 46°C hot plate for 1 min. Afterwards the slide was washed with the fixative solution and mounted in Vectashield with DAPI (Vector Laboratories).

## 4.10 Confocal microscopy

Young anthers harboring the reporters of interest were dissected and immediately imaged using a Leica TCS SP8 inverted confocal microscope and a Zeiss LSM 880 confocal microscope. The meiotic stages of male meiocytes were determined by the cell shape of meiocytes, the position of the nucleolus and the chromosome morphology [21, 50].

To quantify ASY1 fluorescence intensity, a region of interest (ROI) of the same size was defined on synapsed and non-synapsed region. The fluorescence intensity was calculated and the background was subtracted to obtain the corrected fluorescence intensity (CFI). Thereafter, the ratio between the CFI of the synapsed and non-synapsed regions was calculated.

## 4.11 Yeast two-hybrid assay

The *ASY1-FL*, *ASY1<sup>1-300</sup>* and *ASY1<sup>301-596</sup>* constructs were generated previously [21]. To generate the full-length constructs of *PCH2* and *COMET*, their coding sequences were amplified by PCR with primers flanked by attB recombination sites and subcloned into *pDONR223* vector by gateway BP reactions creating the entry clones. To generate the truncated versions of *PCH2*, *COMET*, *ASY1<sup>1-100</sup>* and *ASY1<sup>1-200</sup>*, the PCR-based deletion was first performed using either *PCH2-FL/pDONR223*, *COMET-FL/pDONR223* or *ASY1<sup>1-300</sup>/pDONR223* as templates, and subsequently the PCR fragments were re-ligated, producing the entry clones of the truncated constructs. The resulting entry constructs were subsequently integrated into the

*pGADT7-GW* or *pGBKT7-GW* vectors by gateway LR reactions. Primers used for generating all constructs mentioned above are shown in **Table 1**. Yeast two-hybrid assays were performed according to the Matchmaker Gold Yeast two-hybrid system manual (Clontech). Different combinations of constructs were co-transformed into yeast strain AH109 using the polyethylene glycol/lithium acetate method as described in the manual of Clontech. Yeast cells harboring the relevant constructs were grown on the SD/-Leu-Trp and SD/-Leu-Trp-His plates to test protein-protein interactions.

#### **4.12 Protein expression and purification**

To generate the GST-COMET, HisMBP-PCH2 and His-PCH2 constructs, the corresponding coding sequences were amplified by PCR using primers with attB1/2 flanking sequences and subcloned into pDONR223 vector by gateway BP reactions. The resulting constructs were integrated by gateway LR reactions into pGGWK (for GST-COMET), pHMGWA (for HisMBP-PCH2) and pHGWA (for His-PCH2) vectors. HisMBP-ASY1<sup>1-300</sup> construct was previously generated [21]. For heterologous expression, the constructs were transformed into the *E. coli* BL21(DE3) pLysS cells, which were first grown at 37°C until the OD<sub>600</sub> of 0.6 and then incubated at 16°C after adding the IPTG to the final concentration of 0.2 mM for overnight growth. All proteins were purified under native conditions according to the manufactures' manuals by using the Ni-NTA (Qiagen) and GST-binding resin (Novagen).

#### **4.13 Pull down assay**

For the Ni<sup>2+</sup> pull down assay, 10 µg of the bait proteins (HisMBP-PCH2, His-PCH2 and HisMBP-ASY1<sup>1-300</sup>) plus 20 µg of prey protein (GST-COMET) were incubated at 4°C for 90 mins in the 200 µl binding buffer (see **Table 4**). Subsequently, 15 µl Ni-NTA beads pre-incubated with 10% BSA for reducing unspecific binding, were mixed with the samples and further incubated for 30 mins. The beads were washed three times using the binding buffer and eluted with 50 µl 2X SDS-PAGE sample buffer by boiling. The eluate was subjected to SDS-PAGE followed by western blot analysis using antibodies against His (Qiagen) and GST (Santa Cruz). Two independent pull down experiments were performed showing the same result.

#### **4.14 Immunolocalization**

Freshly harvested young flower buds were sorted by size and the intact anthers were macerated in 10  $\mu$ l enzyme mix (see **Table 4**) for 5 min in a moisture chamber at 37 °C followed by squashing. Subsequently, 10  $\mu$ l enzyme mix was added onto the Poly-Prep slides (Sigma) that were incubated for further 7 min in a moisture chamber. Afterwards, a fine smashing of the anthers was performed in 20  $\mu$ l 1% Lipsol for 2 min. Cell fixation was then performed by incubating 35  $\mu$ l 4% (w/v) paraformaldehyde for 2–3 h until dry. After three times washing with PBST buffer (PBS with 1% Triton X-100), slides were then blocked in PBS buffer with 1% BSA (PBSA) for 30 min at 37°C in a moisture chamber followed by an incubation with anti-ASY1 (1:400 dilution), anti-ZYP1 (1:500 dilution) or anti-RAD51 (1:500 dilution) antibodies (see key resources table) at 4 °C for 48 h. After three times of washing (10 min each) in PBST, fluorescein-conjugated secondary antibodies were added onto the slides followed by 24 h incubation at 4 °C in a moisture chamber. After three times washing in PBST, the chromosomes were counterstained with anti-fade DAPI solution (Vector Laboratories). The images were captured using the Leica SP8 laser scanning microscope.

#### **4.15 Quantification and statistical analysis**

Student's t-test (two-tailed) was used to evaluate the significance of the difference between two groups. The significance of differences between more than two groups was calculated using the ANOVA one-way, followed by Turkey's test. \* denotes  $p < 0.05$ , \*\* denotes  $p < 0.01$  and \*\*\*  $p < 0.001$ . The numbers of samples are indicated in the figure legends.

**Table 1: Primer used in the research**

Purpose	Primer name	Sequence
COMET:GFP reporter	gCOMET-F	AATATGTGGTACGTACAACGGCCACATG
	gCOMET-R	CTTCTTCCTCCTACCTAGAAATCGAAAATTG
	pENTR2B-COMET-F	TCGATTTCTAGGTAGGAGGAAGAAGGCGGC CGCACTCGAGATATCTAG
	pENTR2B-COMET-R	GTGGCCGTTGTACGTACCACATATTGGATCC AGTCGACTGAATTGGTTC
	COMET-SmaI-F	GGGGGCTACGAAGGTGACTTTTGCTAAATC
	COMET-SmaI-R	GGGTAGAACATGGTCTCTGCGTTGTGTG
Oligos for CRISPR editing	COMET-oligoCRISPR-F	ATTGGCACTGATCTCGACGGGTGC
	COMET-oligoCRISPR-R	AAACGCACCCGTCGAGATCAGTGC
	COMET-oligoCRISPR-Sa-F	ATTGTCTGCTGGTGCATATAGAGG
	COMET-oligoCRISPR-Sa-R	AAACCCTCTATATGCACCAGCAGA
Genotyping of <i>comet-1</i>	COMET-CRISPR-check-F	AGTAGAAAGAGAGAGGTGAAGAATGAG
	COMET-CRISPR-check-R	GAACCAATATGAAGAGCCTCATTGGAC
Genotyping of <i>comet-2</i> ; <i>comet-3</i> ; <i>comet-4</i> ; <i>comet-5</i> ;	COMET-CRISPR-Sa-check-F	GTTGGGTGATTTTCTTCTCTGG
	COMET-CRISPR-Sa-check-R	CACTAATCCATCCAGAATCC
Genotyping for CAS9 ( <i>S. aureus</i> )	CAS9-aureus-F	ACATCCTCGGACTCGATATC
	CAS9-aureus-R	TAAGCCTTCTGCACCTTGAG
Genotyping of <i>asy1</i>	N546272L	AGGTGGCTCGTAATCTGGTGGCTGC
	N546272U	TCTATGTTTGTTACGCGTTAATCAG
	SALK LBb1.3	ATTTTGCCGATTTGCGAAC
Genotyping of <i>pch2</i>	Salk_031449 LP	CAATCCGGTGCAACTCCAGGTC
	Salk_031449 RP	CCATCTTCTCCACCATCTCTTGG
	SALK LBb1.3	ATTTTGCCGATTTGCGAAC
Yeast two-hybrid and protein expression	PCH2-attB1-F	GGGGACAAGTTTGTACAAAAAAGCAGGCTT CATGGTGGAGGACCCGATTCCTCTTC
	PCH2-attB2-R	GGGGACCACTTTGTACAAGAAAGCTGGGTT TCATTCAGGTTGTTTCAGACTTCTCT
	PCH2-130aa-R	GTGCACAACCTGGCTTCACTTGCCAGAACAAG
	PCH2-131aa-F	ACCTTTCAGCTCATTGAAGAAGGACCATGTG
	COMET-attB1-F	GGGGACAAGTTTGTACAAAAAAGCAGGCTT CATGGAAATGGCGGAAGGGGAA
	COMET-attB2-R	GGGGACCACTTTGTACAAGAAAGCTGGGTT TTATTCTTCACTGGTTGATGGA
	COMET-150aa-R	TCTGCGTTGTGTGAATAACAACCTCATAAGC
	COMET-151aa-F	GACCATGTTCTAGGCTACGAAGGTGACTTTG
	ASY1 100aa-R	CGGACCATCAACAGTTTCACATATG
	ASY1 200aa-R	TTCGTCTTCTGTACAGCCTCTGAAG
	attL1-R2	GAAGCCTGCTTTTTTGTACAAAGTTGG
	TGA-attL2-F	TGAAACCCAGCTTCTTGTACAAAGT

**Table 2: PCR reaction mix used in the research**

Purpose	PCR reaction mix	Volume/reaction
Plasmid construction	PrimeSTAR Max Premix	25 $\mu$ l
	Primer F	1.5 $\mu$ l
	Primer R	1.5 $\mu$ l
	Nuclease Free Water	21 $\mu$ l
Genotyping	DreamTaq Green PCR mastermix	7.5 $\mu$ l
	Primer F	0.5 $\mu$ l
	Primer R	0.5 $\mu$ l
	Nuclease Free Water	5.5 $\mu$ l

**Table 3: PCR conditions used in the research**

Purpose	PCR conditions	Temperature	Time
Plasmid construction	Initial denaturation	94 °C	30 s
	Denaturation	98 °C	10 s
	Annealing	55 °C	5 s
	Elongation	72 °C	5 s/Kb
	Final elongation	72 °C	2 min
	Hold	16 °C	$\infty$
Genotyping	Initial denaturation	95 °C	5 min
	Denaturation	95 °C	30 s
	Annealing	55 °C	30 s
	Elongation	72 °C	1 min/Kb
	Final elongation	72 °C	5 min
	Hold	16 °C	$\infty$

**Table 4: Resources table**

<b>REAGENT or RESOURCE</b>	<b>SOURCE</b>
<b>Antibodies</b>	
Rat polyclonal anti-ASY1	[73]
Rabbit polyclonal anti-ZYP1	[74]
Rat polyclonal anti-RAD51	[75]
Mouse monoclonal anti-GST	Santa Cruz; Cat# sc-138, RRID: AB_627677
Mouse monoclonal anti-His	Qiagen; Cat# 34660, RRID: AB_2619735
<b>Bacterial and Virus Strains</b>	
<i>E. coli</i> Top10	Thermo Fisher Scientific; C404010
<i>Agrobacterium tumefaciens</i> strain GV3101	N/A
<i>S. cerevisiae</i> AH109	Clontech; Cat# K1612-1
<i>E. coli</i> BL21 (DE3) pLysS	Thermo Fisher Scientific; Cat#C606003
<b>Buffers and media</b>	
Binding buffer (pull down assay)	50 mM NaH <sub>2</sub> PO <sub>4</sub> 100 mM NaCl 10% glycerol 25 mM imidazole 1 mM DTT 0.1% Triton X-100 pH 8.0
Citrate buffer (chromosome spreads)	1.5% cellulose 1.5% pectolyase 1.5% cytohelicase
Enzyme mix (immunolocalization)	0.4% cytohelicase 1% polyvinylpyrrolidone
LB	1% Tryptone 0.5% Yeast Extract 0.5% NaCl 0.8% agar (for solid medium)
Magic Buffer	50 mM Tris-HCl (pH 7.5) 300 mM NaCl 300 mM sucrose
Murashige and Skoog (½ MS)	0.2% MS basal powder 1% sucrose 1% agar pH 5.8

Peterson staining	10% ethanol 0.01% malachite green 25% glycerol 0.05% acid fuchsin 0.005% orange G 4% glacial acetic acid
Transformation medium	5% sucrose 0.05% silwet-77
<b>Commercial Assays</b>	
Gateway BP Clonase II Enzyme mix	Thermo Fisher Scientific; Cat# 11789020
Gateway LR Clonase II Enzyme mix	Thermo Fisher Scientific; Cat# 11791020
Presto™ Mini Plasmid Kit	Geneaid; Cat#PDH300
NucleoSpin® Gel and PCRClean-up	MACHEREY-NAGEL; Cat# 740609.250
PrimeSTAR® Max DNA Polymerase	TAKARA BIO INC®;Cat# R045A
DreamTaq Green PCR Master Mix (2X)	Thermo Scientific™; Cat# K1081
Ligation mix	TAKARA BIO INC®; Cat# 6023
<b>Experimental Models: Organisms/Strains</b>	
<i>Arabidopsis thaliana: asy1-4</i>	SALK_046272; [67]
<i>Arabidopsis thaliana: pch2-2</i>	SALK_031449; [20]
<i>Arabidopsis thaliana: comet-1</i>	This study
<i>Arabidopsis thaliana: comet-2</i>	This study
<i>Arabidopsis thaliana: comet-3</i>	This study
<i>Arabidopsis thaliana: comet-4</i>	This study
<i>Arabidopsis thaliana: comet-5</i>	This study
<i>Arabidopsis thaliana: rad51c</i>	SALK_021960; [47]
<i>Arabidopsis thaliana: comet rad51c</i>	This study
<i>Arabidopsis thaliana: mad2</i>	SAIL_191G06; [68]
<i>Arabidopsis thaliana: PROCOMET: COMET:GFP #1</i> in comet	This study
<i>Arabidopsis thaliana: PROCOMET: COMET:GFP #2</i> in comet	This study
<i>Arabidopsis thaliana: PROCOMET: COMET:GFP #3</i> in comet	This study
<i>Arabidopsis thaliana: PROCOMET: COMET:GFP +</i> <i>PROASY3: ASY3:RFP</i> in Col-0	This study
<i>Arabidopsis thaliana: PROCOMET: COMET:GFP +</i> <i>PROASY3: ASY3:RFP</i> in pch2-2	This study
<i>Arabidopsis thaliana: PROCOMET: COMET:GFP +</i> <i>PROASY3: ASY3:RFP</i> in asy1-4	This study
<i>Arabidopsis thaliana: PROPCH2: PCH2:GFP +</i> <i>PROASY3: ASY3:RFP</i> in Col-0	This study

<i>Arabidopsis thaliana</i> : <i>PROPCH2: PCH2:GFP</i> + <i>PROASY3: ASY3:RFP</i> in comet	This study
<i>Arabidopsis thaliana</i> : <i>PROPCH2: PCH2:GFP</i> + <i>PROASY3: ASY3:RFP</i> in <i>asy1-4</i>	This study
<i>Arabidopsis thaliana</i> : <i>PROASY1: ASY1:GFP</i> + <i>PROASY3: ASY3:RFP</i> in Col-0	[21]
<i>Arabidopsis thaliana</i> : <i>PROASY1: ASY1:GFP</i> + <i>PROASY3: ASY3:RFP</i> in comet	This study
<i>Arabidopsis thaliana</i> : <i>PROASY1: ASY1:GFP</i> + <i>PROASY3: ASY3:RFP</i> in <i>pch2-2</i>	This study
<i>Arabidopsis thaliana</i> : <i>PROASY1: ASY1:GFP</i> + <i>PROASY3: ASY3:RFP</i> in comet <i>pch2-2</i>	This study
<i>Arabidopsis thaliana</i> : <i>PROASY1: ASY1<sup>T142V</sup></i> <i>T184V:GFP</i> + <i>PROASY3: ASY3:RFP</i> in Col-0	[21]
<i>Arabidopsis thaliana</i> : <i>PROASY1: ASY1<sup>T142V</sup></i> <i>T184V:GFP</i> + <i>PROASY3: ASY3:RFP</i> in comet	This study
<i>Arabidopsis thaliana</i> : <i>PROASY1: ASY1<sup>T142V</sup></i> <i>T184V:GFP</i> + <i>PROASY3: ASY3:RFP</i> in <i>pch2-2-</i> <i>asy1-4</i>	This study
<i>Arabidopsis thaliana</i> : <i>PROASY3: ASY3:RFP</i> + <i>PROZYP1B: ZYP1B:GFP</i> in Col-0	[46]
<i>Arabidopsis thaliana</i> : <i>PROASY3: ASY3:RFP</i> + <i>PROZYP1B: ZYP1B:GFP</i> in comet	This study
<i>Arabidopsis thaliana</i> : <i>PROASY3: ASY3:RFP</i> in Col-0	[46]
<i>Arabidopsis thaliana</i> : <i>PROASY3: ASY3:RFP</i> in comet	This study
<i>Arabidopsis thaliana</i> : <i>PROREC8: REC8:GFP</i> + <i>PROASY3: ASY3:RFP</i> in Col-0	This study
<i>Arabidopsis thaliana</i> : <i>PROREC8: REC8:GFP</i> + <i>PROASY3: ASY3:RFP</i> in comet	This study
Yeast: pGADT7/ASY1-FL in AH109	[21]
Yeast: pGADT7/ASY1 <sup>301-596</sup> in AH109	[21]
Yeast: pGBKT7/ASY1-FL in AH109	[21]
Yeast: pGBKT7/ASY1 <sup>301-596</sup> in AH109	[21]
Yeast: pGBKT7/ASY1 <sup>1-300</sup> in AH109	[21]
Yeast: pGBKT7/ASY1 <sup>1-100</sup> in AH109	This study
Yeast: pGBKT7/ASY1 <sup>1-200</sup> in AH109	This study
Yeast: pGADT7/PCH2-FL in AH109	This study
Yeast: pGBKT7/PCH2-FL in AH109	This study
Yeast: pGBKT7/PCH2 <sup>1-130</sup> in AH109	This study
Yeast: pGBKT7/PCH2 <sup>131-467</sup> in AH109	This study
Yeast: pGADT7/COMET-FL in AH109	This study
Yeast: pGADT7/COMET <sup>1-150</sup> in AH109	This study
Yeast: pGADT7/COMET <sup>151-265</sup> in AH109	This study



<b>Recombinant DNA</b>	
PROASY1: ASY1:GFP	[21]
PROASY1: ASY1 <sup>T142V T184V</sup> :GFP	[21]
PROASY3: ASY3:RFP	[46]
PROPCH2: PCH2:GFP	[21]
PRO <sub>ZYP1B</sub> : ZYP1B:GFP	[46]
PROCOMET: COMET:GFP	This study
PROREC8: REC8:GFP	[50]
pGADT7/ASY1-FL	[21]
pGADT7/ASY1 <sup>301-596</sup>	[21]
pGBKT7/ASY1-FL	[21]
pGBKT7/ASY1 <sup>301-596</sup>	[21]
pGBKT7/ASY1 <sup>1-300</sup>	[21]
pGBKT7/ASY1 <sup>1-100</sup>	This study
pGBKT7/ASY1 <sup>1-200</sup>	This study
pGADT7/PCH2-FL	This study
pGBKT7/PCH2-FL	This study
pGBKT7/PCH2 <sup>1-130</sup>	This study
pGBKT7/PCH2 <sup>131-467</sup>	This study
pGADT7/COMET-FL	This study
pGADT7/COMET <sup>1-150</sup>	This study
pGADT7/COMET <sup>151-265</sup>	This study
pHMGWA/HisMBP-ASY1 <sup>1-300</sup>	[21]
pHMGWA/HisMBP-PCH2	This study
pHGWA/His-PCH2	This study
pGGWK/COMET	This study
<b>Software and Algorithms</b>	
Fiji	<a href="https://imagej.net/Fiji/">https://imagej.net/Fiji/</a> ; [76]

## References

1. Aravind, L., and Koonin, E. V. (1998). The HORMA domain: a common structural denominator in mitotic checkpoints, chromosome synapsis and DNA repair. *Trends in biochemical sciences* *23*, 284-286.
2. Xia, G., Luo, X., Habu, T., Rizo, J., Matsumoto, T., and Yu, H. (2004). Conformation-specific binding of p31comet antagonizes the function of Mad2 in the spindle checkpoint. *The EMBO journal* *23*, 3133-3143.
3. Yang, M., Li, B., Tomchick, D. R., Machius, M., Rizo, J., Yu, H., and Luo, X. (2007). p31comet blocks Mad2 activation through structural mimicry. *Cell* *131*, 744-755.
4. Tipton, A. R., Wang, K., Oladimeji, P., Sufi, S., Gu, Z., and Liu, S.-T. (2012). Identification of novel mitosis regulators through data mining with human centromere/kinetochore proteins as group queries. *BMC Cell Biol* *13*, 15.
5. Eytan, E., Wang, K., Miniowitz-Shemtov, S., Sitry-Shevah, D., Kaisari, S., Yen, T. J., Liu, S.-T., and Hershko, A. (2014). Disassembly of mitotic checkpoint complexes by the joint action of the AAA-ATPase TRIP13 and p31comet. *Proceedings of the National Academy of Sciences* *111*, 12019-12024.
6. Habu, T., Kim, S. H., Weinstein, J., and Matsumoto, T. (2002). Identification of a MAD2-binding protein, CMT2, and its role in mitosis. *The EMBO journal* *21*, 6419-6428.
7. Ye, Q., Rosenberg, S. C., Moeller, A., Speir, J. A., Su, T. Y., and Corbett, K. D. (2015). TRIP13 is a protein-remodeling AAA+ ATPase that catalyzes MAD2 conformation switching. *eLife* *4*, e07367.
8. Jao, C. C., Ragusa, M. J., Stanley, R. E., and Hurley, J. H. (2013). A HORMA domain in Atg13 mediates PI 3-kinase recruitment in autophagy. *Proceedings of the National Academy of Sciences* *110*, 5486-5491.
9. Hegedűs, K., Nagy, P., Gáspári, Z., and Juhász, G. (2014). The putative HORMA domain protein Atg101 dimerizes and is required for starvation-induced and selective autophagy in *Drosophila*. *BioMed research international* *2014*.
10. Suzuki, H., Kaizuka, T., Mizushima, N., and Noda, N. N. (2015). Structure of the Atg101-Atg13 complex reveals essential roles of Atg101 in autophagy initiation. *Nat Struct Mol Biol* *22*, 572.
11. Musacchio, A., and Salmon, E. D. (2007). The spindle-assembly checkpoint in space and time. *Nature reviews Molecular cell biology* *8*, 379-393.
12. Luo, X., and Yu, H. (2008). Protein Metamorphosis: The Two-State Behavior of Mad2. *Structure* *16*, 1616-1625.
13. Mapelli, M., Massimiliano, L., Santaguida, S., and Musacchio, A. (2007). The Mad2 Conformational Dimer: Structure and Implications for the Spindle Assembly Checkpoint. *Cell* *131*, 730-743.
14. Rosenberg, S. C., and Corbett, K. D. (2015). The multifaceted roles of the HORMA domain in cellular signaling. *Journal of Cell Biology* *211*, 745-755.

15. Lara-Gonzalez, P., Westhorpe, Frederick G., and Taylor, Stephen S. (2012). The Spindle Assembly Checkpoint. *Current Biology* 22, R966-R980.
16. Musacchio, A. (2015). The Molecular Biology of Spindle Assembly Checkpoint Signaling Dynamics. *Current Biology* 25, R1002-R1018.
17. Sudakin, V., Ganoth, D., Dahan, A., Heller, H., Hershko, J., Luca, F. C., Ruderman, J. V., and Hershko, A. (1995). The cyclosome, a large complex containing cyclin-selective ubiquitin ligase activity, targets cyclins for destruction at the end of mitosis. *Mol Biol Cell* 6, 185-197.
18. King, R. W., Peters, J.-M., Tugendreich, S., Rolfe, M., Hieter, P., and Kirschner, M. W. (1995). A 20S complex containing CDC27 and CDC16 catalyzes the mitosis-specific conjugation of ubiquitin to cyclin B. *Cell* 81, 279-288.
19. Wojtasz, L., Daniel, K., Roig, I., Bolcun-Filas, E., Xu, H., Boonsanay, V., Eckmann, C. R., Cooke, H. J., Jasin, M., and Keeney, S. (2009). Mouse *HORMAD1* and *HORMAD2*, two conserved meiotic chromosomal proteins, are depleted from synapsed chromosome axes with the help of *TRIP13* AAA-ATPase. *PLoS genetics* 5.
20. Lambing, C., Osman, K., Nuntasontorn, K., West, A., Higgins, J. D., Copenhaver, G. P., Yang, J., Armstrong, S. J., Mechtler, K., Roitinger, E., et al. (2015). *Arabidopsis* *PCH2* Mediates Meiotic Chromosome Remodeling and Maturation of Crossovers. *PLOS Genetics* 11, e1005372.
21. Yang, C., Sofroni, K., Wijnker, E., Hamamura, Y., Carstens, L., Harashima, H., Stolze, S. C., Vezon, D., Chelysheva, L., Orban-Nemeth, Z., et al. (2020). The *Arabidopsis* *Cdk1/Cdk2* homolog *CDKA;1* controls chromosome axis assembly during plant meiosis. *The EMBO journal* 39, e101625.
22. Chen, C., Jomaa, A., Ortega, J., and Alani, E. E. (2014). *Pch2* is a hexameric ring ATPase that remodels the chromosome axis protein *Hop1*. *Proceedings of the National Academy of Sciences* 111, E44-E53.
23. Hanson, P. I., and Whiteheart, S. W. (2005). AAA+ proteins: have engine, will work. *Nature reviews Molecular cell biology* 6, 519-529.
24. Miniowitz-Shemtov, S., Eytan, E., Kaisari, S., Sitry-Shevah, D., and Hershko, A. (2015). Mode of interaction of *TRIP13* AAA-ATPase with the *Mad2*-binding protein *p31comet* and with mitotic checkpoint complexes. *Proceedings of the National Academy of Sciences* 112, 11536-11540.
25. Brulotte, M. L., Jeong, B.-C., Li, F., Li, B., Eric, B. Y., Wu, Q., Brautigam, C. A., Yu, H., and Luo, X. (2017). Mechanistic insight into *TRIP13*-catalyzed *Mad2* structural transition and spindle checkpoint silencing. *Nature communications* 8, 1-14.
26. Alfieri, C., Chang, L., and Barford, D. (2018). Mechanism for remodelling of the cell cycle checkpoint protein *MAD2* by the ATPase *TRIP13*. *Nature* 559, 274-278.
27. Hollingsworth, N. M., Goetsch, L., and Byers, B. (1990). The *HOP1* gene encodes a meiosis-specific component of yeast chromosomes. *Cell* 61, 73-84.
28. Couteau, F., and Zetka, M. (2005). *HTP-1* coordinates synaptonemal complex assembly with homolog alignment during meiosis in *C. elegans*. *Genes Dev* 19, 2744-2756.

29. Goodyer, W., Kaitna, S., Couteau, F., Ward, J. D., Boulton, S. J., and Zetka, M. (2008). HTP-3 links DSB formation with homolog pairing and crossing over during *C. elegans* meiosis. *Developmental cell* *14*, 263-274.
30. Hodgkin, J., Horvitz, H. R., and Brenner, S. (1979). Nondisjunction mutants of the nematode *Caenorhabditis elegans*. *Genetics* *91*, 67-94.
31. Nonomura, K.-I., Nakano, M., Murata, K., Miyoshi, K., Eiguchi, M., Miyao, A., Hirochika, H., and Kurata, N. (2004). An insertional mutation in the rice PAIR2 gene, the ortholog of Arabidopsis ASY1, results in a defect in homologous chromosome pairing during meiosis. *Mol Genet Genomics* *271*, 121-129.
32. Caryl, A. P., Armstrong, S. J., Jones, G. H., and Franklin, F. C. H. (2000). A homologue of the yeast HOP1 gene is inactivated in the Arabidopsis meiotic mutant *asy1*. *Chromosoma* *109*, 62-71.
33. Severson, A. F., Ling, L., van Zuylen, V., and Meyer, B. J. (2009). The axial element protein HTP-3 promotes cohesin loading and meiotic axis assembly in *C. elegans* to implement the meiotic program of chromosome segregation. *Genes Dev* *23*, 1763-1778.
34. Kim, Y., Rosenberg, S. C., Kugel, C. L., Kostow, N., Rog, O., Davydov, V., Su, T. Y., Dernburg, A. F., and Corbett, K. D. (2014). The chromosome axis controls meiotic events through a hierarchical assembly of HORMA domain proteins. *Developmental cell* *31*, 487-502.
35. Niu, H., Wan, L., Baumgartner, B., Schaefer, D., Loidl, J., and Hollingsworth, N. M. (2005). Partner choice during meiosis is regulated by Hop1-promoted dimerization of Mek1. *Mol Biol Cell* *16*, 5804-5818.
36. Friedman, D. B., Hollingsworth, N. M., and Byers, B. (1994). Insertional mutations in the yeast HOP1 gene: evidence for multimeric assembly in meiosis. *Genetics* *136*, 449-464.
37. West, A. M., Komives, E. A., and Corbett, K. D. (2018). Conformational dynamics of the Hop1 HORMA domain reveal a common mechanism with the spindle checkpoint protein Mad2. *Nucleic acids research* *46*, 279-292.
38. Yang, C., Hu, B., Portheine, S. M., Chuenban, P., and Schnittger, A. (2020). State changes of the HORMA protein ASY1 are mediated by an interplay between its closure motif and PCH2. *Nucleic Acids Research*.
39. Ma, H. T., and Poon, R. Y. (2018). TRIP13 functions in the establishment of the spindle assembly checkpoint by replenishing O-MAD2. *Cell reports* *22*, 1439-1450.
40. Wang, K., Sturt-Gillespie, B., Hittle, J. C., Macdonald, D., Chan, G. K., Yen, T. J., and Liu, S.-T. (2014). Thyroid hormone receptor interacting protein 13 (TRIP13) AAA-ATPase is a novel mitotic checkpoint-silencing protein. *Journal of Biological Chemistry* *289*, 23928-23937.
41. Corbett, K. D. (2017). Molecular Mechanisms of Spindle Assembly Checkpoint Activation and Silencing. In *Centromeres and Kinetochores: Discovering the Molecular Mechanisms Underlying Chromosome Inheritance*, B. E. Black, ed. (Cham: Springer International Publishing), pp. 429-455.
42. Ji, J., Tang, D., Shen, Y., Xue, Z., Wang, H., Shi, W., Zhang, C., Du, G., Li, Y., and Cheng, Z. (2016). P31comet, a member of the synaptonemal complex, participates

- in meiotic DSB formation in rice. *Proceedings of the National Academy of Sciences of the United States of America* *113*, 10577-10582.
43. Madeira, F., Park, Y. M., Lee, J., Buso, N., Gur, T., Madhusoodanan, N., Basutkar, P., Tivey, A. R. N., Potter, S. C., Finn, R. D., et al. (2019). The EMBL-EBI search and sequence analysis tools APIs in 2019. *Nucleic acids research* *47*, W636-W641.
  44. Kelley, L. A., Mezulis, S., Yates, C. M., Wass, M. N., and Sternberg, M. J. E. (2015). The Phyre2 web portal for protein modeling, prediction and analysis. *Nature Protocols* *10*, 845-858.
  45. Komaki, S., and Schnittger, A. (2017). The spindle assembly checkpoint in Arabidopsis is rapidly shut off during severe stress. *Developmental cell* *43*, 172-185. e175.
  46. Yang, C., Hamamura, Y., Sofroni, K., Böwer, F., Stolze, S. C., Nakagami, H., and Schnittger, A. (2019). SWITCH 1/DYAD is a WINGS APART-LIKE antagonist that maintains sister chromatid cohesion in meiosis. *Nature Communications* *10*, 1755.
  47. Li, W., Yang, X., Lin, Z., Timofejeva, L., Xiao, R., Makaroff, C. A., and Ma, H. (2005). The AtRAD51C gene is required for normal meiotic chromosome synapsis and double-stranded break repair in Arabidopsis. *Plant Physiol* *138*, 965-976.
  48. Zickler, D., and Kleckner, N. (1999). Meiotic Chromosomes: Integrating Structure and Function. *Annual Review of Genetics* *33*, 603-754.
  49. Zickler, D., and Kleckner, N. (2015). Recombination, pairing, and synapsis of homologs during meiosis. *Cold Spring Harbor perspectives in biology* *7*, a016626.
  50. Prusicki, M. A., Keizer, E. M., van Rosmalen, R. P., Komaki, S., Seifert, F., Muller, K., Wijnker, E., Fleck, C., and Schnittger, A. (2019). Live cell imaging of meiosis in Arabidopsis thaliana. *Elife* *8*.
  51. Ma, H. T., and Poon, R. Y. C. (2016). TRIP13 regulates both the activation and inactivation of the spindle-assembly checkpoint. *Cell reports* *14*, 1086-1099.
  52. Kim, D. H., Han, J. S., Ly, P., Ye, Q., McMahon, M. A., Myung, K., Corbett, K. D., and Cleveland, D. W. (2018). TRIP13 and APC15 drive mitotic exit by turnover of interphase- and unattached kinetochore-produced MCC. *Nature Communications* *9*, 4354.
  53. Date, D. A., Burrows, A. C., and Summers, M. K. (2014). Phosphorylation regulates the p31Comet-mitotic arrest-deficient 2 (Mad2) interaction to promote spindle assembly checkpoint (SAC) activity. *Journal of Biological Chemistry* *289*, 11367-11373.
  54. Komaki, S., and Schnittger, A. (2016). The spindle checkpoint in plants—a green variation over a conserved theme? *Current opinion in plant biology* *34*, 84-91.
  55. Komaki, S., Takeuchi, H., Hamamura, Y., Heese, M., Hashimoto, T., and Schnittger, A. (2020). Functional analysis of the plant chromosomal passenger complex. *Plant Physiol*, pp.00344.02020.
  56. Miao, C., Tang, D., Zhang, H., Wang, M., Li, Y., Tang, S., Yu, H., Gu, M., and Cheng, Z. (2013). CENTRAL REGION COMPONENT1, a Novel Synaptonemal Complex Component, Is Essential for Meiotic Recombination Initiation in Rice. *The Plant Cell* *25*, 2998-3009.

57. Sanchez-Moran, E., Santos, J.-L., Jones, G. H., and Franklin, F. C. H. (2007). ASY1 mediates AtDMC1-dependent interhomolog recombination during meiosis in Arabidopsis. *Genes Dev* 21, 2220-2233.
58. Wang, H., Hu, Q., Tang, D., Liu, X., Du, G., Shen, Y., Li, Y., and Cheng, Z. (2016). OsDMC1 Is Not Required for Homologous Pairing in Rice Meiosis. *Plant Physiol* 171, 230-241.
59. Tang, D., Miao, C., Li, Y., Wang, H., Liu, X., Yu, H., and Cheng, Z. (2014). OsRAD51C is essential for double-strand break repair in rice meiosis. *Frontiers in Plant Science* 5.
60. Xue, Z., Liu, C., Shi, W., Miao, Y., Shen, Y., Tang, D., Li, Y., You, A., Xu, Y., Chong, K., et al. (2019). OsMTOPVIB is required for meiotic bipolar spindle assembly. *Proceedings of the National Academy of Sciences* 116, 15967-15972.
61. Wang, K., Wang, M., Tang, D., Shen, Y., Qin, B., Li, M., and Cheng, Z. (2011). PAIR3, an axis-associated protein, is essential for the recruitment of recombination elements onto meiotic chromosomes in rice. *Mol Biol Cell* 22, 12-19.
62. De Muyt, A., Pereira, L., Vezon, D., Chelysheva, L., Gendrot, G., Chambon, A., Laine-Choinard, S., Pelletier, G., Mercier, R., and Nogue, F. (2009). A high throughput genetic screen identifies new early meiotic recombination functions in Arabidopsis thaliana. *PLoS genetics* 5.
63. Wu, Z., Ji, J., Tang, D., Wang, H., Shen, Y., Shi, W., Li, Y., Tan, X., Cheng, Z., and Luo, Q. (2015). OsSDS is essential for DSB formation in rice meiosis. *Frontiers in plant science* 6, 21.
64. Ho, H.-C., and Burgess, S. M. (2011). Pch2 acts through Xrs2 and Tel1/ATM to modulate interhomolog bias and checkpoint function during meiosis. *PLoS genetics* 7.
65. Vader, G., Blitzblau, H. G., Tame, M. A., Falk, J. E., Curtin, L., and Hochwagen, A. (2011). Protection of repetitive DNA borders from self-induced meiotic instability. *Nature* 477, 115-119.
66. Fauser, F., Schiml, S., and Puchta, H. (2014). Both CRISPR/C as-based nucleases and nickases can be used efficiently for genome engineering in Arabidopsis thaliana. *The Plant Journal* 79, 348-359.
67. Crismani, W., and Mercier, R. (2013). Identifying meiotic mutants in Arabidopsis thaliana. In *Plant Meiosis*. (Springer), pp. 227-234.
68. Ding, D., Muthuswamy, S., and Meier, I. (2012). Functional interaction between the Arabidopsis orthologs of spindle assembly checkpoint proteins MAD1 and MAD2 and the nucleoporin NUA. *Plant Molecular Biology* 79, 203-216.
69. Zhang, Y., Werling, U., and Edlmann, W. (2012). SLiCE: a novel bacterial cell extract-based DNA cloning method. *Nucleic acids research* 40, e55-e55.
70. Clough, S. J., and Bent, A. F. (1998). Floral dip: a simplified method for Agrobacterium-mediated transformation of Arabidopsis thaliana. *The plant journal* 16, 735-743.

71. Peterson, R., Slovin, J. P., and Chen, C. (2010). A simplified method for differential staining of aborted and non-aborted pollen grains. *International Journal of Plant Biology* *1*, e13-e13.
72. Ross, K., Fransz, P., and Jones, G. (1996). A light microscopic atlas of meiosis in *Arabidopsis thaliana*. *Chromosome research* *4*, 507-516.
73. Armstrong, S. J., Caryl, A. P., Jones, G. H., and Franklin, F. C. H. (2002). Asy1, a protein required for meiotic chromosome synapsis, localizes to axis-associated chromatin in *Arabidopsis* and *Brassica*. *Journal of cell science* *115*, 3645-3655.
74. Higgins, J. D., Sanchez-Moran, E., Armstrong, S. J., Jones, G. H., and Franklin, F. C. H. (2005). The *Arabidopsis* synaptonemal complex protein ZYP1 is required for chromosome synapsis and normal fidelity of crossing over. *Genes Dev* *19*, 2488-2500.
75. Kerzendorfer, C., Vignard, J., Pedrosa-Harand, A., Siwiec, T., Akimcheva, S., Jolivet, S., Sablowski, R., Armstrong, S., Schweizer, D., Mercier, R., et al. (2006). The *Arabidopsis thaliana* *MND1* homologue plays a key role in meiotic homologous pairing, synapsis and recombination. *Journal of Cell Science* *119*, 2486-2496.
76. Schindelin, J., Arganda-Carreras, I., Frise, E., Kaynig, V., Longair, M., Pietzsch, T., Preibisch, S., Rueden, C., Saalfeld, S., and Schmid, B. (2012). Fiji: an open-source platform for biological-image analysis. *Nat Methods* *9*, 676-682.

## **Chapter 2**

**Towards live cell imaging of meiosis in *Zea mays***



# 1 Introduction

## 1.1 Maize as a crop model system

Maize (*Zea mays*) is a large grain plant that evolved from its wild-grass ancestors by the direct intervention of human agriculture. Since then maize became one of the most important crops in the world: it is an excellent source of food, feed and fuel; moreover, its by-products are used in the production of various commercial materials, such as biodegradable foams, plastics and adhesives.

In addition to its economic value, maize has been a keystone model organism for biological research for over 100 years. Many scientific discoveries have first been made in maize, such as the identification of transposable elements by Barbara McClintock [1], the correlation between cytological and genetic crossing over [2] and the discovery of epigenetic phenomena [3].

Several scientific advantages of the maize plant, including a vast collection of mutant stocks, its large chromosomes and a sequenced genome, have positioned it as a centrepiece for studies in crop plant genetics, cytogenetics, genomics, physiology and development. Other characteristics that make maize an attractive system include the ease to culture it on any scale, from a few plants in pots to many acres, the fact that it is quite hardy and can be grown outdoors under a range of conditions, from tropical to temperate climates [4] or that it can be successfully grown all year round in greenhouses. In addition, maize plants produce separate male and female inflorescences, which facilitates experimentally controlled crosses; moreover the vast amount of pollen produced by a single plant ( $10^7$  pollen grains) [5] allows many crosses to be performed with one pollen donor.

Despite the ease of growing and crossing maize, there are some drawbacks when working with this model system. Maize has a relatively long life-cycle (13 weeks) compared to the model system *Arabidopsis thaliana* (8 weeks), i.e., it can be crossed only 60 days after planting and requires another 30–45 days post-pollination for seed maturation.

Maize has a large genome that is 2.5 Gb in total and it is organized into 10 chromosomes ( $2N = 20$ ); a full maize genome sequence of the B73 inbred line was assembled by a BAC-by-BAC Sanger-based method in 2009 [6] and is publicly available.

The ability to produce maize transgenics and the development of new genome editing technologies advanced maize research in both fundamental studies and breeding. The primary method nowadays used for maize transformation is the *Agrobacterium*-mediated transformation. Key factors for a successful transformation include the selection of suitable plant material for infection (in maize, the preferred tissue is immature embryos) , choice of vectors, choice of strains of *A. tumefaciens* and optimization of tissue culture techniques [7]. However, despite all optimization attempts only a limited number of genotypes have been so far efficiently transformed, i.e., A188.

A new transformation approach involving overexpression of the maize *Baby boom* (*Bbm*) and maize *Wuschel2* (*Wus2*) genes was recently presented [8]. The overexpression of *Bbm* and *Wus2* after transformation of immature embryos resulted in a growth stimulation of embryogenic tissue [8]; although there are still wide margins for improvement in this protocol, it successfully led to high transformation frequencies in numerous previously non-transformable maize inbred lines. Furthermore, the system has also been tested on other target tissues, such as mature seed-derived embryo axes or leaf segments without an intervening callus or meristem culture step, avoiding the need of intensive labor and greenhouse space required to supply sufficient immature embryos [8].

Alternatively, the biolistic method can be used for stable transformation [9]. This technique relies on the use of fine particles coated with DNA in various forms – i.e., plasmids, linear molecules, PCR products – to directly deliver transgenes into immature embryos. Multiple transgenes can be introduced at once by biolistic transformation and the size of the constructs is not a major limiting factor. However, this method is not as heavily used as T-DNA transformation because it yields high incidences of multiple transgene insertions per genome, frequent structural rearrangements of the transgene and it can result in unstable transgene expression [10].

## **1.2 Meiosis in maize**

Maize is one of the first model organisms used for studying meiosis because of its large, well defined chromosomes and the ease in which meiotic stages can be identified cytologically and in combination with genetic, molecular and biochemical techniques [11].

The male and female reproductive organs in maize are accessible and separable (**Figure 1**). Microsporogenesis in maize occurs within the anthers of male flowers on the tassel, the terminal inflorescence. From one tassel, it is possible to harvest large amounts of anthers (i.e., hundreds of anthers) in near-synchronous sub-stages of meiosis. The female germ cells are located in the ears, which grow from the base of leaves in the midsection of the plant. An ear generally contains several hundred egg cells that develop into kernels after fertilization. Both male and female meiocytes are visually distinctive because of their larger size and position in the anther or ovary. The ease to access large amounts of meiocytes makes genomics-scale experiments and proteomic studies possible.

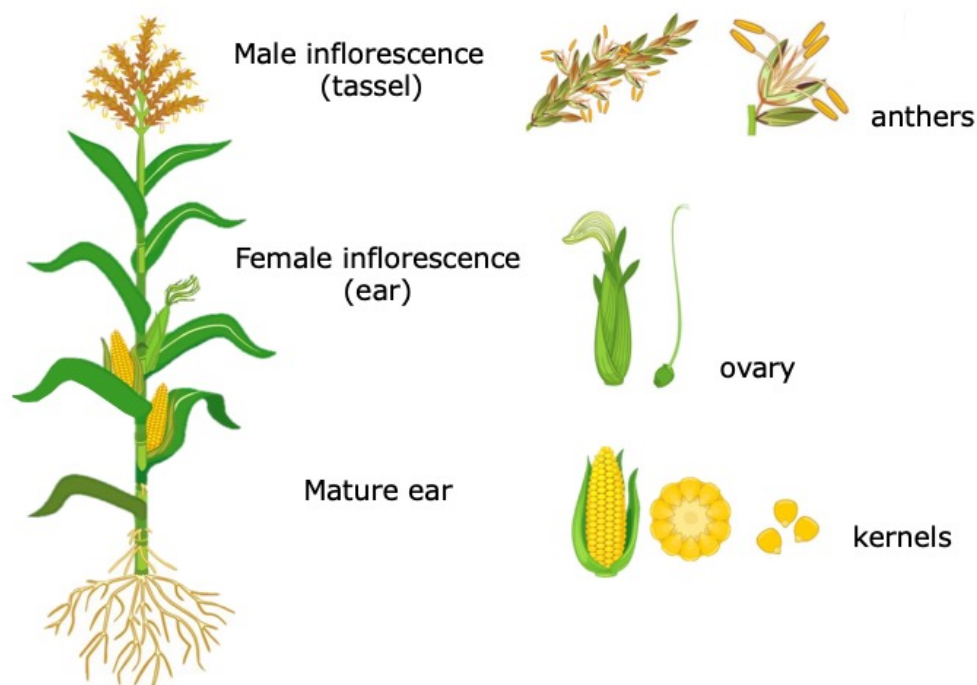


**Figure 1: Maize plant morphology**

Schematic representation of a maize plant (adapted from [12]). At the reproductive stage the male and female inflorescences, the tassel and the ears respectively, develop on a maize plant. Microsporogenesis occurs within the anthers of the tassel, while megasporogenesis in the ovules, within the ovary. After fertilization, a mature ear harbours several kernels.

In maize, the analysis of meiosis at the cytological level has been very successful for more than 70 years. Over 50 meiotic mutants, which were found in forward

genetic screens for male sterility, are now available and for some the defective gene has been identified [11]. Maize meiotic mutants have been grouped based on their phenotypes: meiotic commitment mutants (including differentiation of meiocytes and the switch to the meiotic cell cycle), desynaptic mutants (one or more prophase I events are affected, e.g., telomere bouquet, homologous synapsis, homology search, recombination), sister chromatid cohesion and chromosome segregation mutants (including monopolar centromere attachment, meiotic cytoskeleton/spindle, sister chromatid cohesion and condensation mutants) and meiotic exit mutants [11]. Several maize mutants have phenotypes not yet found in any other organism, such as *am1-pra1*, which is arrested at the leptotene to zygotene transition [13] and therefore might be pivotal for our general understanding of meiosis.

While much has been learnt in the recent years, some questions remain still unanswered, especially concerning the temporal aspect of meiosis, including the dynamics of meiotic proteins. In fact, studies of meiosis in plants have been traditionally conducted using genetic and cytological approaches, which rely on the analysis of fixed material. Although these reconstructions provide information on the general patterns of chromosome behaviour, microscopic images collected from fixed cells have clear shortcomings in accurately portraying the dynamics of meiotic processes, as the temporal and spatial aspects remain vastly understudied.

Interestingly, the cellular events that occur in meiosis are evolutionarily conserved as are many of the proteins associated with meiosis, but the duration of meiosis itself is one of the most variable aspects of this developmental process, ranging from less than 6 hours in yeast to more than 40 years in the human female [14].

With regards to maize, studies investigating this aspect date back to 1988 [15]. 30 different corn strains have been analysed; the spikelets were sampled at or near the onset of meiosis until anther dehiscence and analysed by acetocarmine staining. The time of each meiotic step was calculated as an estimation of the distribution of the meiotic stages over the samples, after a certain interval of times. This led to the estimation of the relative duration of the different stages during microsporogenesis, suggesting that meiosis in maize takes several days (**Figure 2**). In particular, from leptotene onset to tetrad formation the time estimated was of almost 5 days, followed by 36 hours for tetrad maturation till the production of

microspores and eventually by the maturation of microspores into trinucleate pollen grains (roughly 16 days).

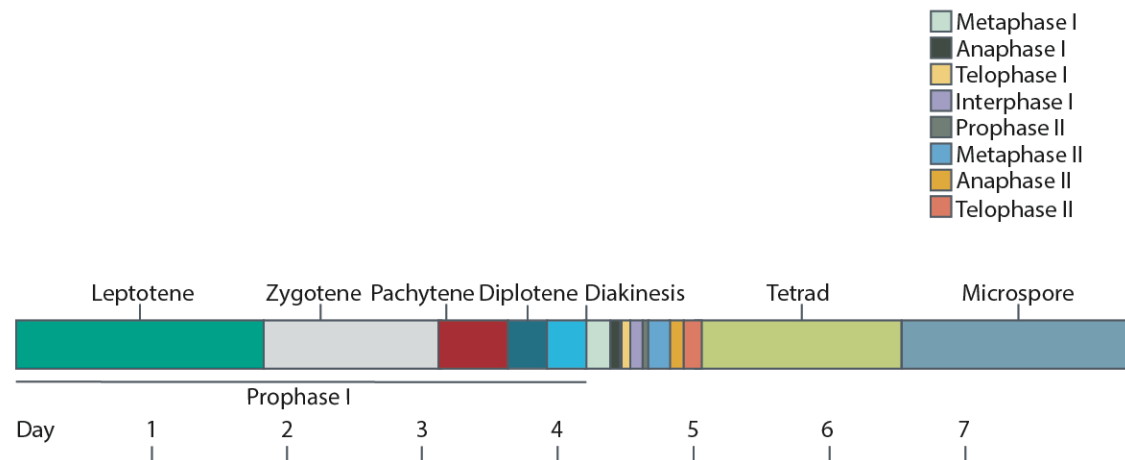


**Figure 2: Time course of male meiosis in maize**

Each stage is represented by a different colour, from leptotene onset till microspores formation. The duration is indicated in number of days (based on [15]).

A common feature that emerged from the description of the temporal aspects of meiosis in different plants species is that prophase I is always the most extended phase compared to the other meiotic stages [14]. During early stages of meiotic prophase chromosomes undergo dramatic changes in behaviour and morphology, resulting in a major spatial reorganization in the nucleus. In most eukaryotes, this chromosome repositioning includes clustering of telomeres at the nuclear envelope during zygotene while centromeres generally point into the other direction, an assembly known as the telomere bouquet [16, 17]. A first step to better understand such intricate chromosome movements in maize would be a more precise temporal and spatial description, which could be achieved by a live cell imaging approach.

### 1.3 Studying meiosis: a live cell imaging approach

Live cell imaging represents a unique tool to investigate the dynamics of developmental cellular processes and responses to environmental and genetic perturbations. Moreover, live cell imaging allows the observation of these processes on the scale of individual cells over time.

Plants are sensitive to changes in light, temperature, osmolality and humidity amongst other variables [18]; hence, when performing a live cell imaging experiment, it is crucial to keep proper environmental conditions to maintain tissue viability without altering the speed of growth and its development. With respect to meiosis, some attempts of live cell imaging have already been conducted, using different kinds of microscopes, different cellular markers and a variety of sample types, i.e., isolated cells (e.g., meiocytes), cultured reproductive organs (e.g., anthers) or whole flower buds.

### **1.3.1 Previous experimental set-ups for live cell imaging of meiosis**

The adaptation of methods used to culture lily and rye meiocytes to a genetically amenable system such as maize was an important advance for research in meiosis. Living maize meiocytes were successfully cultured and could be kept viable from pachytene to telophase II, so that chromosome segregation could be successfully monitored using epifluorescence microscopy [19]. Two environmental factors were described as crucial for culturing maize meiocytes: the osmotic strength of the medium, in particular the sucrose concentration (0.28 M to 0.34 M) [19] and the temperature - maize meiocytes cannot be cultured at temperatures lower than 25°C without showing abnormal chromosome segregation [20].

Further experiments on isolated meiocytes have been conducted only in maize and culturing of meiocytes was based on the same White's solution [21], with few adjustments. Meiocytes extruded into this medium were viable for 9 hours and were followed undergoing meiosis II [20]. The same medium was used to support growth of maize male meiocytes while imaging live-cell division during meiosis I and meiosis II by using fluorescence microscopy [22, 23]. The cells are cultured in liquid medium, thus they can be easily treated with dyes, such as Syto12, to label the chromosomes, while other cellular components such as microtubules can be visualized by making use of stable fluorescent reporter lines. While this set-up is easily applicable, it can only be used to study short meiotic phases, failing to provide information on the extended meiotic prophase. Nonetheless, the applications of this technique gave important contribution in understanding the regulation of meiotic spindles, which could not be revealed by fixed specimen [22, 23].

A different approach relies on the use of multiphoton microscopy; exploiting its great focus depth of roughly 200 µm allows observing meiocytes inside intact

living anthers. This set-up has been successfully applied in maize [24]; fresh anthers were cultured in a microscope chamber slide containing Artificial Pond Water (APW) medium, a minimal medium which allows to maintain tissue viability without inducing major alterations to the size or morphology of the anthers [25]. This set-up ensured a viability for over 30 hours and allowed examining chromosome dynamics in meiotic prophase I, revealing that maize chromosomes are extremely dynamic and that different movement patterns characterize zygotene and pachytene [24]. This approach counts only few attempts to date. On the one hand, imagining the anthers in their integrity have the advantage of keeping the developmental context as close as possible to the native environment, thus limiting the impact of *in vitro* culturing on meiocytes. On the other hand, it requires the availability of advanced microscope technology, such as multiphoton excitation microscopy, with the potential to reach and resolve meiotic cells which are located at a depth of more than 100  $\mu\text{m}$  from the anther surface [24, 25].

Finally, a different strategy relies on the imaging of the whole flower organ. This has been performed, to date, only in Arabidopsis. In the first attempts dissected apices were used, harbouring young flower primordia, devoid of sepals (removed either by laser ablation or manually) and embedded in a medium, e.g., apex growth medium [26]. This allowed imaging the development of emerging floral buds with an upright or an inverted microscope for five days [26]. In another attempt, addressing methylation changes during Arabidopsis sporogenesis and gametogenesis, the inflorescences were embedded in a solid *in vitro* culture medium (Nitsch medium), dissected with a vibratome and observed by multiphoton microscopy [27]. However, as the aim was to follow the complete sexual development of the plant, meiosis was considered a single unit, without the distinction of the different sub-phases. Additionally, an approach using light sheet fluorescence microscopy has been developed for live imaging of the germ cell lineage, both male and female, embedded within the floral organs. Flower buds in the stage of interest were detached from inflorescences and the dissected buds were put into capillaries containing medium with 1% low melting point agarose [28]. Exploiting the fast image acquisition, low phototoxicity and little photobleaching of light sheet fluorescence microscopy allowed long term imaging, up to several days, but with less subcellular resolution compared to confocal microscopy.

Recently, a protocol for live cell imaging of Arabidopsis flower buds to follow the whole duration of meiosis using confocal microscopy was established [29] and allowed the observation of meiotic sub-phases with high temporal resolution as well as the description of new aspects of a known meiotic mutant [30]. The inflorescences were harvested and all but one young flower primordium, containing meiotic stages, were removed. Whereas the petals are shorter than the anthers when the flower buds undergo meiosis and therefore do not cover the tissue of interest, it was necessary to remove the upper sepal to gain access to two of the six anthers. Finally, the remaining bud along with the pedicel and few millimetres of the stem was embedded in Arabidopsis Apex Culture Medium (ACM), stabilized with a drop of agarose, submerged in water and imaged with an up-right confocal laser scanning microscope, equipped with a water immersion objective [30]. Importantly, with this method samples were kept alive for up to several days allowing the analysis of meiosis in its entirety [30].

Hence, in this study, I focused on establishing a robust live cell imaging technique for studying meiosis in a crop model system such as maize, translating the knowledge and the technique from Arabidopsis. My work included the determination of the correct developmental stage for sample harvesting, the generation of reporter lines highlighting hallmarks of meiosis and the identification of suitable culturing and imaging conditions for maize anthers by confocal microscopy.



## 2 Results

### 2.1 Determination of the developmental stage for sample harvesting

Maize has defined stages of growth leading to its eventual maturity. The growth stages comprise the vegetative and the reproductive stages. Maize is a monoecious plant that produces male flowers on a terminal tassel (**Figure 1 and Figure 3A**) and female flowers on lateral ears (**Figure 1 and Figure 3B**). Male flowers have been used throughout this study because the developmental timing of male meiocytes is synchronized within anthers and it is less variable than on the female side. Moreover, there are more male meiocytes than female meiocytes on a plant and, finally, the dissection of male flowers has less potential to damage the meiocytes.

In maize, immature flowers that contain cells undergoing meiosis are not visible without dissection as, at the time of meiosis, the immature tassel is still inside the stalk. The presence of the immature tassel can be felt by gentle squeezing the leaf whorl below the top node of the plant. To reach the immature tassel, a small incision is made with a razor blade cutting a window (**Figure 3C**) into the leaves surrounding the immature tassel (**Figure 3D**). The individual reproductive units on the tassel are spikelets (**Figure 3E**), which occur in pairs: one pedicellate and the other sessile (**Figure 3F**, depicted by "p" and "s", respectively). There are two florets in each spikelet, enclosed within palea and lemma, and each floret contains three large anthers (**Figure 3G**), which develop synchronously and contain cells undergoing meiosis, the meiocytes (**Figure 3H**).

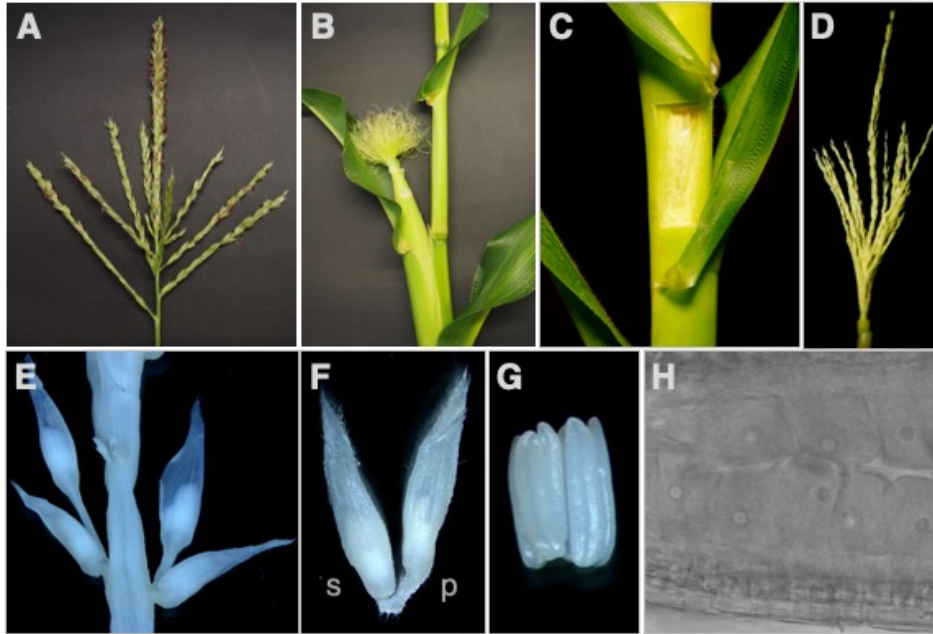


**Figure 3: Maize inflorescences architecture**

A maize plant produces two inflorescences, a tassel at the apex of the plant (a mature tassel, with dehiscent anthers releasing pollen grains is shown in (A)) and the ear in the axil of a leaf (B). The immature tassel containing cells undergoing meiosis is still enclosed within the stalk; an incision is made into the stalk (C) to collect samples from the immature tassel (D). The individual reproductive units on the tassel are spikelets, which occur in pairs (E): one pedicellate and the other sessile (F, depicted by "p" and "s", respectively). There are two florets in each spikelet and each floret harbours 3 anthers (G) which contain cells undergoing meiosis, the meiocytes (H).

A simple and effective way to check meiotic progression along the tassel is to perform acetocarmine staining. Spikelets are progressively collected, dissected in order to isolate the anthers which are then placed on a microscope slide with acetocarmine stain (**Figure 4**). Meiosis progresses gradually, from the top of the tassel towards the bottom, so spikelets at different locations on the tassel harbour anthers with meiocytes at different stages.

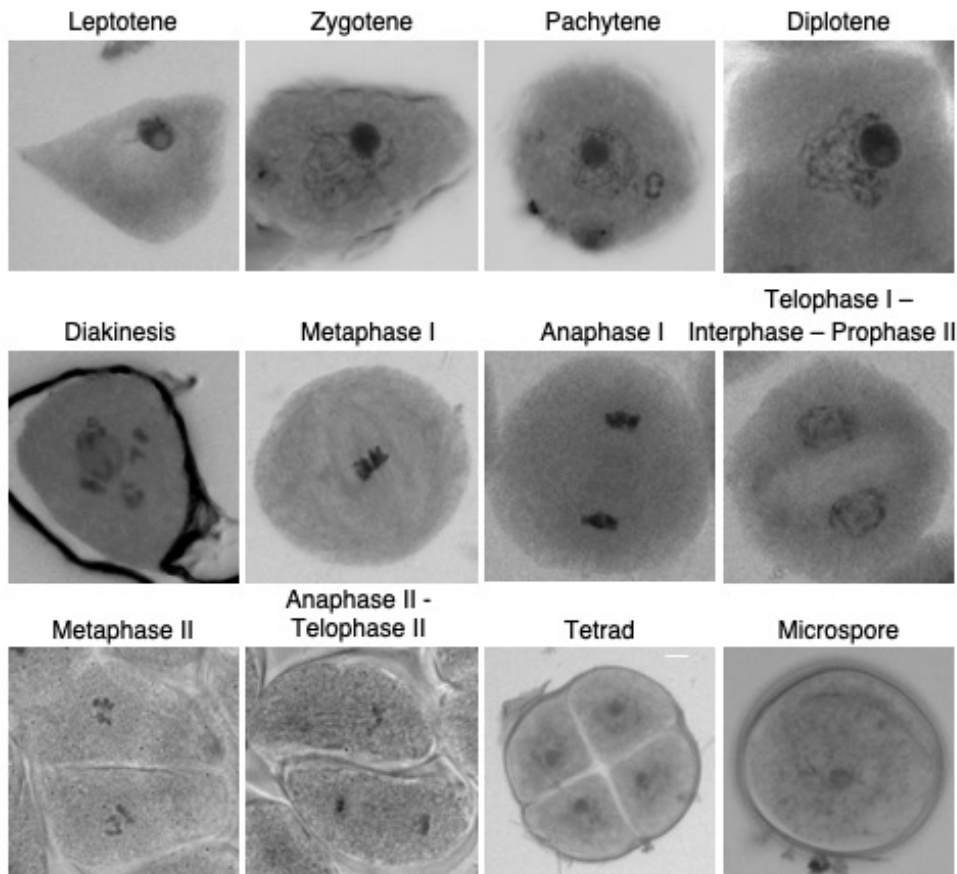


**Figure 4: Acetocarmine staining of male meiocytes**  
Chromosome behaviour of wild-type meiocytes during meiosis.

With this method, it was possible to define 6-8 weeks after germination as the correct time point at which, with the current greenhouse growing conditions, the immature tassel can be found in the stalk of A188 maize plants, used in this study as wild-type reference and for the generation of transgenic lines.

## 2.2 Identification of candidate genes

Identifying the complete set of meiotic genes is an on-going process. In the well-studied model dicot plant, *Arabidopsis thaliana*, around 70 genes involved in meiosis have been characterized [31-35]. With regards to crops some attempts have been made in maize, rice, wheat and barley to generate a comprehensive atlas of meiotic genes corresponding to well-characterized homologs from other organisms [36, 37].

In this study, the isolation of candidate genes to further use as live cell imaging markers for maize meiosis has been performed on the basis of sequence homology to Arabidopsis genes, on the basis of transcriptome studies e.g., from isolated meiocytes at early stages of prophase I [38] as well as on previously published work on mutants.

To identify the maize homolog of each gene of interest, different online databases have been used: NCBI [39], maizeGDB [40], Phytozome (Phytozome v12) [41] and Gramene (<http://www.gramene.org> release52 – November2016) [42].

I employed the BLASTp tool using the respective Arabidopsis protein as the initial query to search the proteome of *Zea mays* B73 based on the current reference genome annotations (assembly B73 RefGen\_v3 – aka B73 RefGen\_v3, AGPv3 – and Zm-B73-REFERENCE-GRAMENE-4.0 – aka B73 RefGen\_v4, AGPv4). The results obtained from the different database searches for each gene of interested were analysed and compared, e.g., for the gene sequence, the gene organization and the accuracy in the annotation. I further examined the putative maize homologs regarding their expression levels in reproductive tissues according to the maize RNA-seq expression atlas on maizeGDB. Moreover, the recently generated transcriptome data of isolated meiocytes [38] was used as a source of important information. In fact, a group of genes has been designated as “meiocyte genes” based on their expression level in isolated meiocytes compared to other tissues, i.e., whole anthers and seedlings. This dataset supported the selection of the best candidates for a role in meiosis when more than one gene was identified in the initial homology research, possibly as a consequence of a duplication event.

Finally, at a protein level, I investigated the presence of a conserved secondary structure and of similar domains between the putative maize protein and the homologs in other species, e.g., Arabidopsis and the more closely related rice.

Different databases use different IDs for the same gene and protein, thus the corresponding information for each gene of interest is shown in **Table 1**. The selected genes of interest fall into different categories: chromosome markers, synapsis marker, meiotic entry and progression markers, early meiotic recombination markers and cytoskeleton markers.

The details for each gene of interest are presented in its respective paragraph below.

**Table 1: Maize candidate genes**

Marker	Gene	Gene name	Reference
<b>Chromosomes</b>	<i>DESYNAPTIC2</i> ( <b>DSY2</b> )	<i>GRMZM2G148758</i>	[43]
		<i>AC210848.3_FG004</i>	
		<i>Zm00001d015469</i>	
<b>Chromosomes</b>	<i>ABSENCE OF FIRST DIVISION 1</i> ( <b>AFD1</b> )	<i>GRMZM2G059037</i>	[44]
		<i>LOC732730</i>	
		<i>Zm00001d039132</i>	
<b>Chromosomes</b>	<i>Centromeric histone H3</i> ( <b>CENH3</b> )	<i>GRMZM2G158526</i>	[45]
		<i>LOC542500</i>	
<b>Synapsis</b>	<i>ZYPPER1</i> ( <b>ZYP1</b> )	<i>GRMZM2G143590</i>	[46]
		<i>LOC100500741</i>	
		<i>Zm00001d025575</i>	
<b>Meiotic entry and progression</b>	<i>AMEIOTIC1</i> ( <b>AM1</b> )	<i>GRMZM5G883855</i>	[13, 47, 48]
		<i>LOC100271891</i>	
		<i>Zm00001d013659</i>	
<b>Meiotic entry and progression</b>	<i>SOLO DANCERS</i> ( <b>SDS</b> )	<i>GRMZM2G093157</i>	
		<i>LOC100283361</i>	
		<i>Zm00001d048026</i>	
<b>Meiotic recombination</b>	<i>Meiotic recombination protein 11 homolog B</i> ( <b>Mre11B</b> )	<i>GRMZM2G309109</i>	[49]
		<i>LOC100125648</i>	
		<i>Zm00001d049471</i>	
<b>Meiotic recombination</b>	<i>Completion of meiotic recombination1</i> ( <b>COM1</b> )	<i>GRMZM2G076617</i>	[50]
		<i>LOC100278695</i>	
		<i>Zm00001d046761</i>	
<b>Cytoskeleton</b>	<i>Tubulin-<math>\alpha</math>-4</i> ( <b>TUA4</b> )	<i>GRMZM2G152466</i>	
		<i>LOC100381303</i>	
		<i>Zm00001d013367</i>	
<b>Cytoskeleton</b>	<i>Tubulin-<math>\beta</math>-2</i> ( <b>TUB2</b> )	<i>GRMZM2G334899</i>	
		<i>LOC542380</i>	
		<i>Zm00001d010275</i>	

### 2.3 Generation of reporter lines

In an attempt to copy the native expression level and the native expression domain of each gene of interest, its genomic sequence has been used to generate the live cell imaging markers. The full genomic sequence of each gene of interest plus the flanking regulatory regions have been subcloned into a gateway entry vector [51]. The regulatory regions were chosen as  $\approx 3$  Kb upstream and  $\approx 1$  Kb downstream of the coding region (**Figure 5A**). As the maize genome is large and transposable elements (TEs) are often nested between genes, I carefully checked

on maizeGDB the regulatory regions of each gene of interest to avoid including a flanking TE or a flanking gene. Genomic regions of up to 16 Kb could be successfully sub-cloned.

The sub-cloning of each gene of interest into an entry vector (pDONOR221 or pENTR2B) (**Figure 5B**) was followed by the insertion of a fluorescent tag (see below) (**Figure 5C and 5D**) and eventually with the recombination into the plant transformation vector. The choice of the destination vector was dependent on the choice of the *Agrobacterium* strain coupled to the maize genotype used for transformation. The current protocol relies on the use of the *Agrobacterium* strain LBA4404 for the infection of immature embryos of the maize line A188.

A LBA4404/A188 compatible destination vector is p7oM-LH, which harbours a *bar* gene under the control of the 35S promoter as a plant selection marker, but lacks the GATEWAY elements. In order to facilitate cloning by the use of the GATEWAY system, a GATEWAY cassette containing *attR* recombination sites (*attR1* and *attR2*), has been transferred from the destination vector pTF101 into the Multiple Cloning Site (MCS) of p7oM-LH. The now GATEWAY compatible destination vector is referred to as p7oM-LH-GW (**Figure 5E**).

*Agrobacterium* mediated transformation of immature maize embryos was performed at the University of Hamburg (this work was kindly done by Dr. Reinhold Brettschneider, Dagmar Stang and Katja Müller) and at Crop Genetic Systems (Hamburg). This protocol relies on several steps of *in vitro* tissue culture, e.g., selection of transformed calli, growth and regeneration of transformed plants (see details in material and methods).

The putative transgenic plants from tissue culture (T0) were first acclimatize to the greenhouse condition and thereafter screened for Basta resistance, in order to ensured that all regenerated plants taken to seed were expressing the introduced *bar* transgene, thus the construct of interest. Regenerated plants were obtained from different transformation events for each gene of interest.

Basta resistant plants were grown in the greenhouse till maturity. When the plants reached the anthesis stage, the pollen was collected to pollinate A188 plants and, concurrently, ears were pollinated with A188 pollen. Upon maturation, seeds were collected. T1 young plantlets were screened for *bar*-gene expression by spraying with Basta and T1 resistant plants were analysed for expression of the reporter construct.

### 2.3.1 Fluorescent proteins

Different colour variants and codon optimized fluorescent proteins (FPs) for maize have been recently developed [52, 53]. In this study, Citrine FP, a YFP variant which is brighter and more resistant to photobleaching than EYFP, and the red FP mRFP1 have been selected. This choice allows combining two different live cell imaging markers because of the different excitation and emission spectra of YFP and mRFP1.

The FP insert is flanked by linker peptides to minimize folding interference between the FP and tagged protein. The FPs are either fused as N-terminal, C-terminal or internal tags, respecting the location and ensuring the integrity of known functional domains.

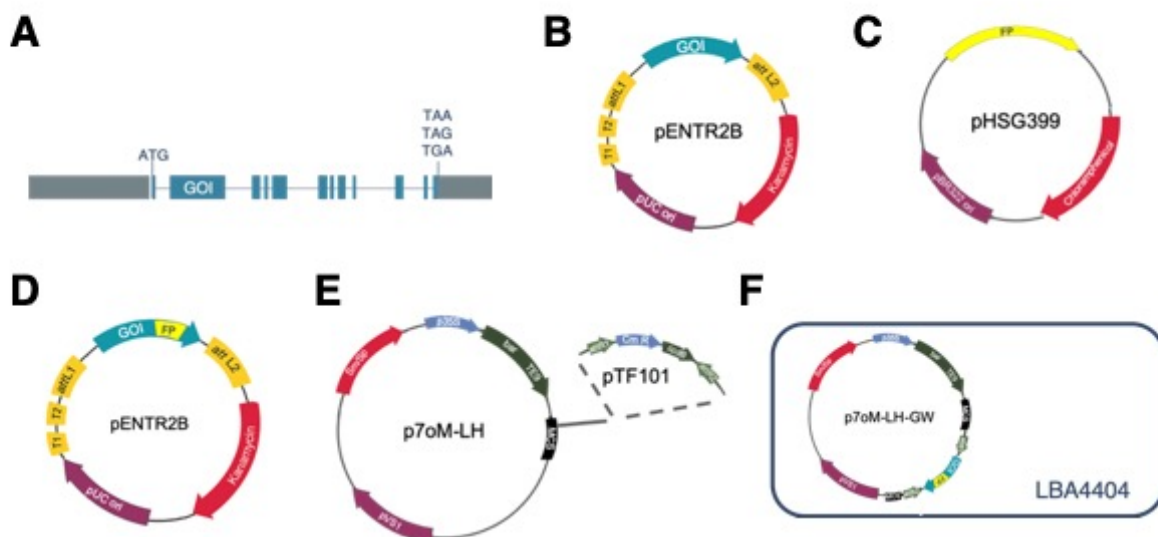


**Figure 5: Overview of the cloning steps**

Schematic representation of the genomic region of a gene of interest (GOI), blue boxes corresponds to exons, bars to introns, grey boxes represent the regulatory region subcloned upstream the start codon (ATG) and downstream the stop codon (TAA, TAG or TGA) (A). The GOI is subcloned into an entry vector (B), pENTR2B is shown as the representative entry vector; the fluorescent tag, subcloned in the entry vector pHSG399 (C), is amplified and integrated into the entry vector with the GOI (D). Integration of the gateway cassette into the destination vector p7oM-LH (E). p7oM-LH-GW carrying the GOI is transformed into *Agrobacterium* strain LBA4404 for plant transformation (F).

### 2.3.2 Chromosome markers

One of my first goals in the set-up of the live cell imaging technique was to be able to clearly visualize and follow chromosomes during meiosis.

Previously, a transgenic maize line expressing a fluorescent histone fusion protein, H2B-mCherry, was characterized [54]. As the nucleosome constitutes a fundamental structural unit of chromatin (**Figure 6A**), histone proteins can be good candidates for visualizing chromatin structure. However, when analysing this H2B-mCherry transgenic line, I observed a low germination rate and the plants harboured smaller and shorter tassels when compared to the wild-type plants. Due to these phenotypic defects, I decided to not make use of this line as a live cell imaging marker.

A second line harbouring a Histone-marker was identified via the MAIZE CELLGENOMICS database (<http://maize.jcvi.org/cellgenomics>), i.e., histone H1B (GRMZM2G164020) fused to YFP. When analysed by confocal microscopy a bright staining of nuclei, with some detectable chromatin structure and no signal in the cytoplasm was observed in root tissue (**Figure 6B**). Young leaves were also analysed and, similarly to what observed in root cells, the signal was exclusively localized in the nucleus (**Figure 6C**). Seedlings with confirmed H1B-YFP signal in the roots and leaves were also checked for H1B-YFP expression in anthers. While the signal of H1B-YFP was present in the outer layer (**Figure 6D**), no signal was detected from nuclei of meiocytes (**Figure 6E**, as representative picture of different lines analysed).



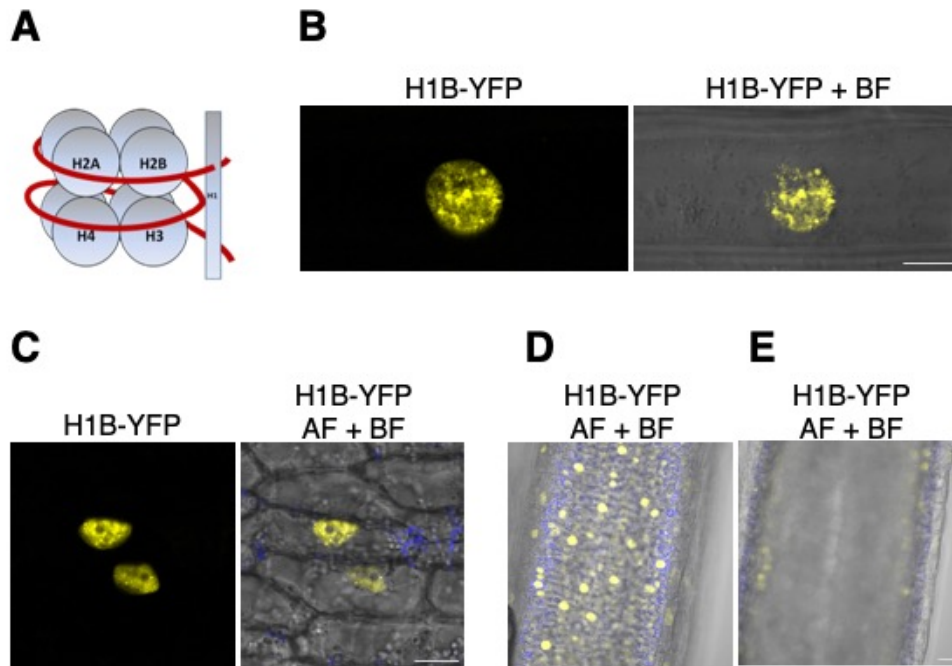


### Figure 6: Histone H1B localization

Schematic representation of the organization of histone proteins (A). Histone H1B-YFP localization in root (B), leaf (C), anther (D) and meicytes (E) in combination with autofluorescence (AF, in blue) and the bright field (BF). Bars 10  $\mu$ m.

Considering these results, I proceeded with the identification of alternative genes which could be used as chromosome markers in meiosis in order to generate stable genomic reporter lines.

#### 2.3.2.1 DSY2

The first candidate protein which I selected as putative chromosome marker was DSY2, a meiosis specific coiled-coil protein of the chromosome axis (**Figure 7A**). The gene (*AC210848.3\_FG004* in B73) is located on chromosome 5 and consists of 12 exons and 11 introns, spanning a genomic region of 5,3 Kb [43]. In order to generate a genomic reporter line, the presumptive regulatory regions of 2,3 Kb upstream ATG and 950 bp after the stop codon were included (**Figure 7B**). *AttB* sites were added by PCR using the BAC AC210848 as template and the resulting fragment was integrated by BP reaction into the entry vector pDONOR221. Then, a unique restriction site (*SmaI*) was inserted by PCR directly in front of the stop codon, to later insert the fluorescent tag. Since DSY2 shares similarity with

*Arabidopsis* ASY3, for which a functional C-terminally tagged genomic reporter line has already been generated [55], the same FP insertion site was chosen for the maize DSY2. YFP and mRFP1 were selected as fluorescent tags (**Figure 7B**).

Young spikelets of BASTA resistant T1 plants were collected from the immature tassel, the anthers were dissected and mounted on a microscope slide for analysis with the confocal microscope.

In order to collect spikelets at the correct developmental stage for DSY2 observation, spikelets located close to the bottom of the tassel were collected first and then sampling proceeded towards the top of the tassel following the developmental gradient of meiosis. In very young and small anthers, no signal was observed – presumably, because meiocytes in these anthers are in a pre-meiotic stage (**Figure 7C, panel I**). The first signal was discovered in slightly older anthers exclusively in the nucleus and as discontinuous stretches (**Figure 7C, panel II and III**), which became more linear and continuous in later samples (**Figure 7C, panel IV**), highlighting the formation of the chromosome axes. Thereafter, the signal became more intense and thicker, likely reflecting changes in chromosomes morphology, e.g., condensation and synapsis (**Figure 7C, panel V and VI**) and chromosome shapes could be discerned. In samples of even older anthers, the DSY2 signal decreased and was no longer visible as chromosome threads (**Figure 7C, panel VII**), likely reflecting the disassembly of the synaptonemal complex. DSY2 signal is not detectable anymore when cells have undergone cytokinesis (**Figure 7C, panel VIII**).

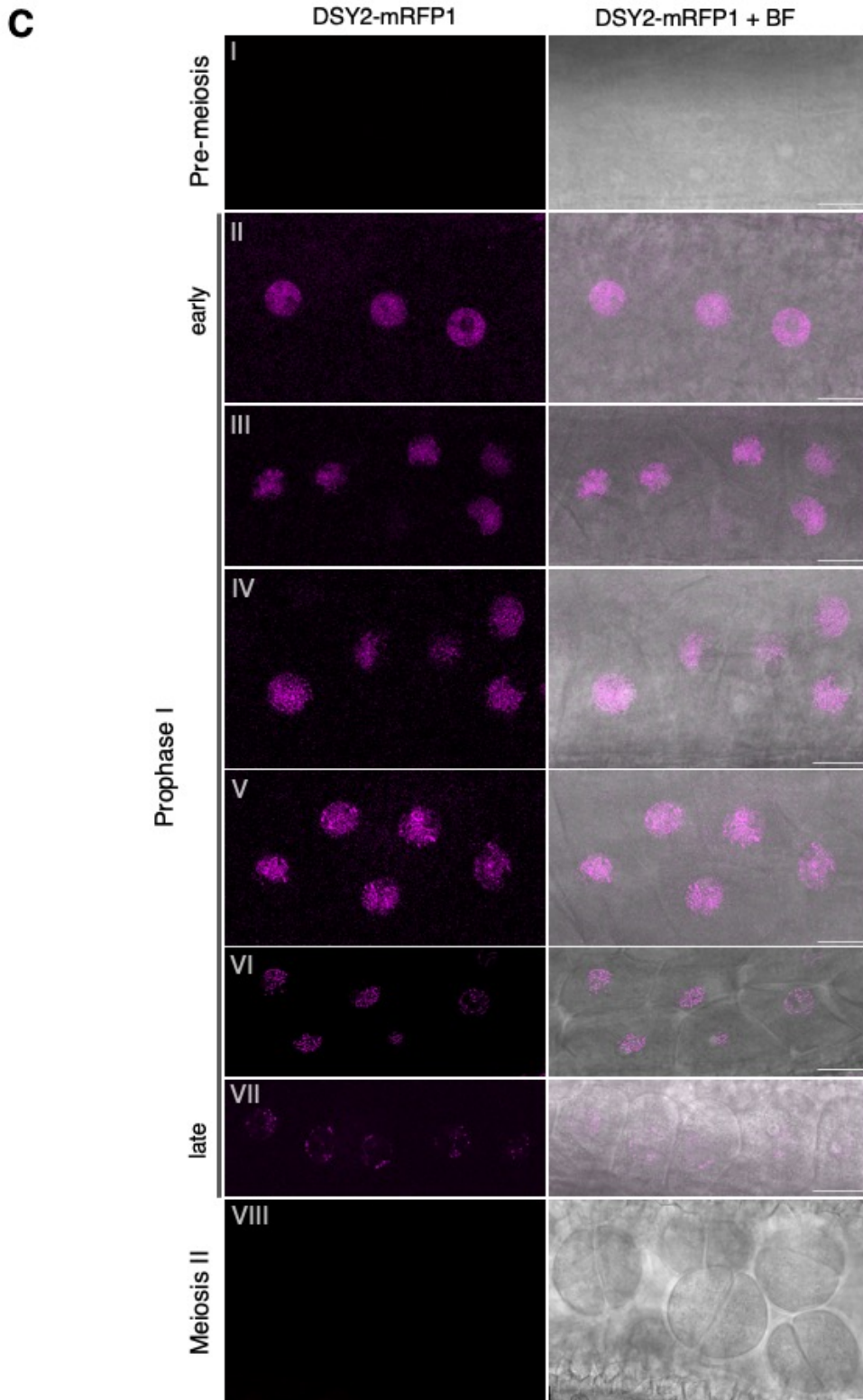


### Figure 7: DSY2, a maize axis core component

Schematic representation of the chromosome axis organization (A). Illustration of the *DSY2* locus, blue boxes corresponds to exons, bars to introns; grey boxes represent the regulatory region subcloned upstream the start codon and downstream the stop codon. The position of the fluorescent tag (mRFP1 or YFP) is indicated. Localization pattern of the reporter line *DSY2*-mRFP1 in maize meiocytes (C) at pre-meiotic stage (panel I), early (panel II and III), mid- (panel IV, V and VI) and late (panel VII) prophase I, and during meiosis II (panel VIII). Bar 10  $\mu$ m.

The localization pattern observed was consistent with previous observations of *DSY2* localization in maize meiocytes, based on fixed material, i.e., immunolocalization studies [43], as well as with the observation of a genomic reporter line for the *Arabidopsis* ortholog *ASY3* [55]. However, further work is required to validate the functionality of the *DSY2* reporter.

In addition to the change in *DSY2* localization, I could observe morphological changes, i.e., changes in the shape of the meiocytes, during the progression of prophase I. Young and small anthers harbour square, small meiocytes, in close proximity to each other. With the progression of meiosis, the cell shape changes from squared to trapezoidal, thereafter becoming oval and eventually round, right before cytokinesis (**Figure 8**).

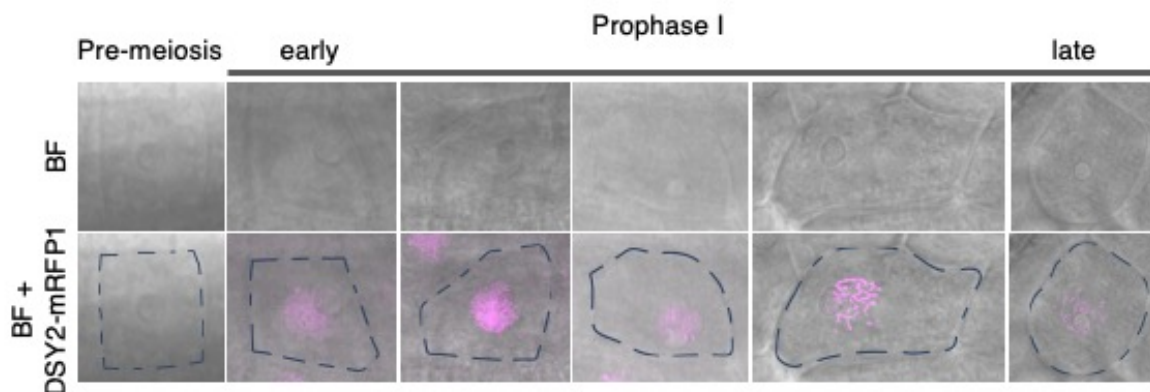


**Figure 8: The cell shape of meiocytes changes with the progression of prophase** Localization pattern of *DSY2*-mRFP1 in combination with the bright field (BF) during pre-meiosis and prophase I. A single representative cell for each stage is depicted, cell shape is highlighted with a dashed blue line.

Interestingly, changes in cell morphology have also been previously observed in Arabidopsis; in particular, specific cell features such as the cell shape, the nucleus and the nucleolus position contributed to a reliable landmark system to determine the meiotic stage and temporally dissect meiotic phases [30]. Additional experiments and a profound statistical analysis are needed to corroborate these first observations in maize. However, it will be interesting to define, similarly to Arabidopsis, specific cell features of maize meiocytes and possibly use them to set up a landmark system subdividing maize meiosis.

### 2.3.2.2 AFD1

AFD1 (absence of first division1) was identified as the meiotic  $\alpha$ -kleisin cohesion protein in maize [44] (**Figure 9A**), required for meiotic chromosome formation and sister chromatid cohesion (SCC). The role of  $\alpha$ -kleisin subunits in cohesion, e.g., REC8 in yeast and Arabidopsis, is conserved across kingdoms [56-58]. AFD1 localization in meiosis has been previously revealed by immunolocalization studies. The AFD1 signal was detected along the chromosome axis at leptotene, zygotene and pachytene [44] corresponding to what observed in Arabidopsis for REC8, which serves as an excellent chromosome marker during prophase I [30].

The *AFD1* gene (*GRMZM2G059037*) is located on chromosome 6, spanning a genomic region of 31,8 Kb in the B73 reference genome; it contains 20 exons and 19 introns and it encodes a predicted protein of 602 amino acids. A genomic size of 31,8 Kb goes beyond the limit imposed to ensure good cloning efficiency, therefore I excluded the genomic region in correspondence of the annotated transposable elements located in the introns 6 and 10 of *AFD1*. Two different versions have been constructed, which differ in the length of the region excluded from intron 10. This allowed reducing the genomic size of the constructs to 10,5 Kb and 14,2 Kb (referred to as AFD1-I and AFD1-II, respectively) both including 2,4 Kb upstream the start codon and 1,5 Kb downstream the stop codon as potential regulatory regions (**Figure 9B**, AFD1-II is shown as representative illustration). Based on a functional genomic reporter line for Arabidopsis which carries a C terminal tag [30], I chose the same site for the YFP insertion for both versions of the maize AFD1. The YFP was inserted by SLiCE reaction. Different T0 plants were obtained for both versions of the reporter and crossed to and by A188 plants. Meiocytes of Basta resistant T1 plants need to be analysed by confocal microscopy.

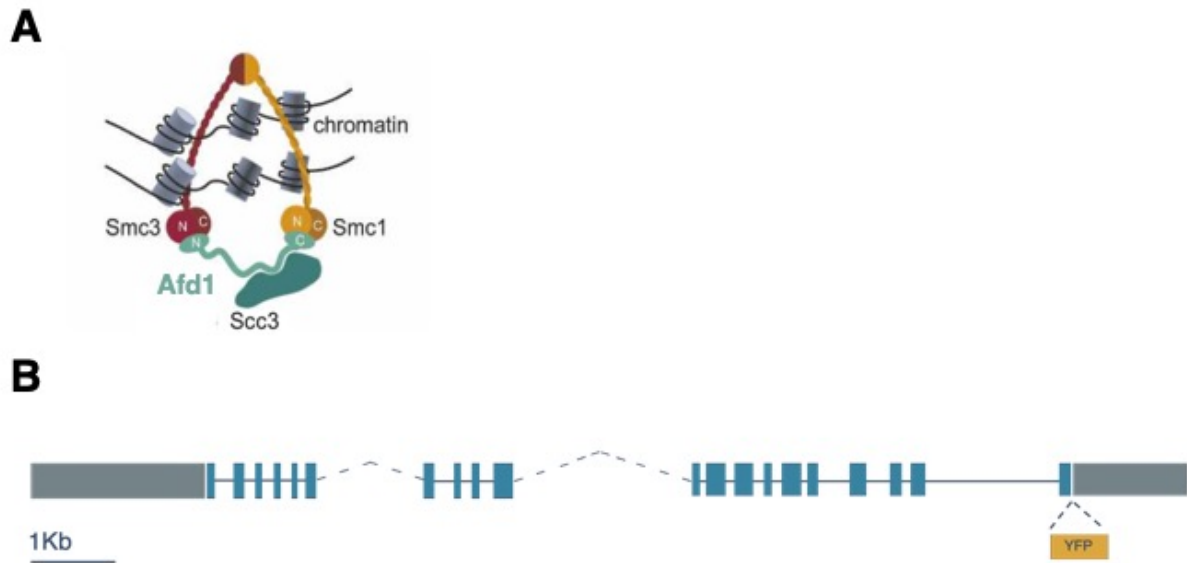


**Figure 9: AFD1, the meiotic  $\alpha$ -kleisin in maize**

Schematic representation of the cohesin complex on chromatin (A), adapted from [59]. Illustration of the *AFD1* locus, blue boxes corresponds to exons, bars to introns, dashed bars to genomic regions in intron 6 and 10 which have been included in generating AFD1-II reporter line; grey boxes represent the upstream and downstream regulatory region used. The position of the fluorescent tag (YFP) is indicated.

### 2.3.2.3 CENH3

The centromeric histone H3 (CENH3) substitutes histone H3 within the nucleosomes of active centromeres in all eukaryotes (**Figure 10A**). CENH3 deposition at centromeres is needed to assemble the kinetochore, a complex of conserved proteins responsible for correct chromosome movement and segregation. In addition, not only telomeres but also centromere interactions play a key role in facilitating the initiation of homologous chromosome pairing [60, 61]. Thus, CENH3 appears to be an interesting candidate to explore the dynamics of chromosome pairing and synapsis.

The maize gene encoding for CENH3 (GRMZM2G158526) is located on chromosome 6, it consists of 7 exons and 6 introns, and it encodes for a protein of 157 amino acids. In order to generate a genomic reporter line comprising the native regulatory elements, 2 Kb upstream of the start codon and 680 bp after the stop codon have been subcloned along with the CENH3 locus (**Figure 10B**). The fragment was amplified from BAC AC209457\_3, adding *attB* sites by PCR and

integrated by BP reaction into the entry vector pDONOR221. In a second PCR a unique restriction site (*NaeI*) was inserted after the start codon, to later insert the fluorescent tag.

CENH3 proteins share a common histone H3 core sequence and display a highly variable N-terminal and C-terminal part [45, 62]. In Arabidopsis the C-terminal portion was found to be responsible to direct CENH3 to centromere [63], hence a tag position at the N terminal region of the protein was chosen for maize.

As CENH3 was expected to be expressed in both somatic and meiotic cells, at first the root tip of Basta resistant T1 young plantlets was collected and imaged by confocal microscopy. Several dots were detected exclusively in the nuclei of the root cells (**Figure 10C**), as expected from a centromere marker line. When meiocytes from plants with confirmed mRFP1-CENH3 signal in roots were analysed by confocal microscopy, a distinct CENH3 signal was clearly visible in the nuclei (**Figure 10D and 10E**).



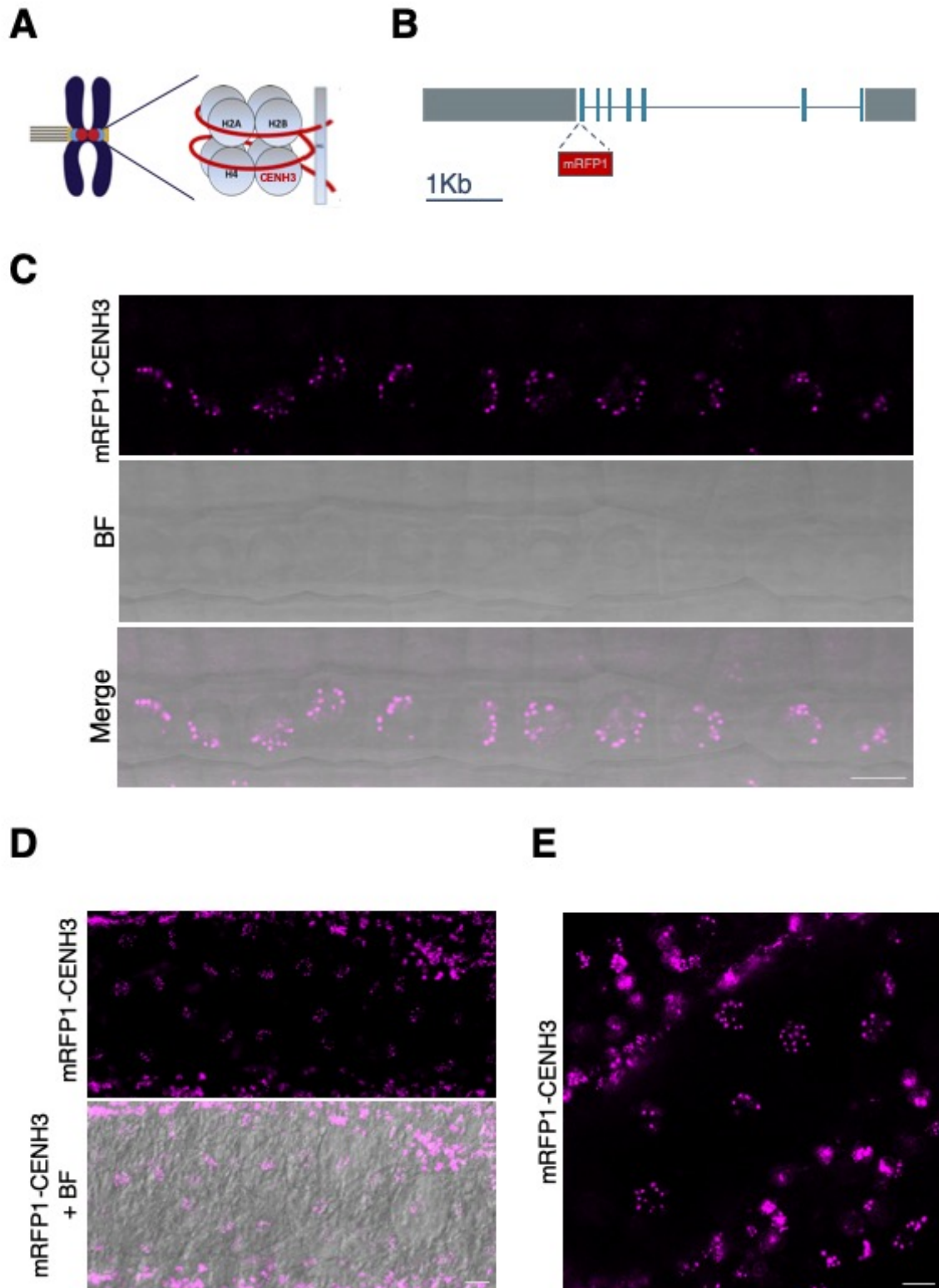


**Figure 10: CENH3, the centromeric Histone H3**

Schematic representation of the nucleosome at the centromeres (A). Illustration of the *CENH3* locus, blue boxes corresponds to exons, bars to introns; grey boxes represent the upstream and downstream regulatory region used. The position of the fluorescent tag



(mRFP1) is indicated. CENH3 localization in root cells (C) and in meiocytes (D). Maximum intensity projection image of CENH3 localization in maize anther (E). Bars 10  $\mu$ m.

### **2.3.3 Marker for synapsis**

Synapsis is an extensive and stable interaction between chromosomes that involves the formation of a complex tripartite proteinaceous structure called the synaptonemal complex (SC). The establishment of the SC is characterized by the appearance of transverse filaments (TFs) which span the gap between the chromosome axes and constitute the central region of the SC.

#### **2.3.3.1 ZYP1**

ZYP1 was identified as the transverse filament protein of the SC in maize [46] and thus it has been selected as candidate for a live cell imaging marker to follow synapsis. Previous studies based on different techniques, such as TEM of silver-stained chromosome spreads and immunolocalization studies in maize [46, 64], revealed the localization of ZYP1 between the chromosome axes, highlighting the synapsed regions.

The maize gene encoding for ZYP1 (GRMZM2G143590) is located on chromosome 10 and encodes for a protein of 867 amino acids. The full genomic region of 10 Kb along with 2,2 Kb upstream the start codon and 500 bp after the stop codon have been subcloned into the entry vector pENTR2B by SLiCE (**Figure 11B**). The fragments covering the genomic region have been obtained by PCR amplification using the BAC AC204395.5 as template. When choosing the insertion site for the fluorescent tag, a few considerations were made. First, the TF proteins of the SC share similar structural properties that account for the high degree of conservation of the SC ultrastructure among eukaryotes [64]. In fact, a central domain – mainly comprised of coiled-coil structure – is flanked at the N and C termini by globular domains [65, 66]; TFs form parallel homodimers that are oriented such that their C termini align along the lateral elements while the N termini of opposing dimers overlap in the central region of the SC, giving rise to the central element [64] (**Figure 11A**).

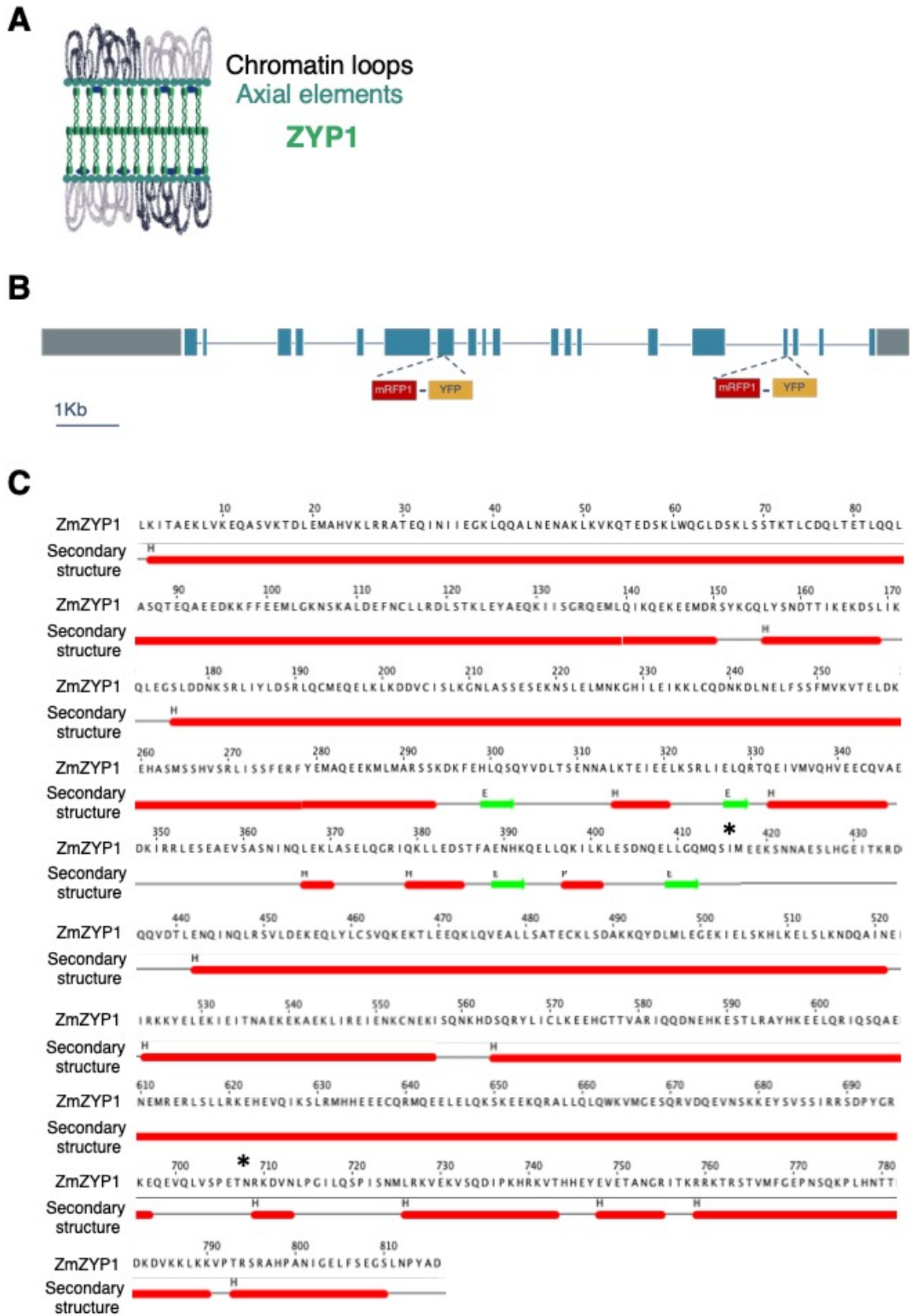


**Figure 11: ZYP1, a transverse filament protein of the synaptonemal complex**

Schematic representation of the transverse filament protein ZYP1, spanning the gap between the chromosome axes (A). Illustration of the *ZYP1* locus, blue boxes corresponds

to exons, bars to introns; grey boxes represent the upstream and downstream regulatory region used. The position of the fluorescent tag (mRFP1 or YFP) is indicated. Secondary structure prediction of ZYP1 protein (46-861 amino acids) using the Phyre2 server (C);  $\alpha$ -helixes are displayed in red,  $\beta$ -strand in green. The asterisks depict the insertion sites for the internal tag.

Since previously, a functional reporter line for Arabidopsis has been generated [55], which carries the fluorescent tag internally, an alignment between the amino acid sequences of the two Arabidopsis proteins ZYP1A and ZYP1B, along with the rice ZEP1 and the maize ZYP1 was made. The amino acids alignment revealed that Arabidopsis, maize and rice proteins are conserved to a high extent (**Figure 12**). In addition, I used the Phyre2 algorithm to investigate the predicted secondary structure of maize ZYP1 protein (PDB: c6yvub; 99.7% confidence and 94% coverage) and this revealed the presence of numerous  $\alpha$  helixes (**Figure 11C**) covering most of the maize protein sequence.

Two different internal insertion sites have been previously tested in Arabidopsis – depicted by asterisks in **Figure 12**. Looking at the same sites within the maize sequence, revealed that, according to the secondary structure prediction, they are likely located in a loop region rather than in an ordered secondary structure (**Figure 11C**, the corresponding insertion sites are depicted by asterisks). Hence, both positions have been selected to generate two different reporter lines with the internal insertion site, referred to in follow as ZYP1-IntI and ZYP1-IntII; for both, mRFP1 and YFP have been used as alternative fluorescent tags. Several regenerated plants (T0) were obtained for both versions of ZYP1-IntI and ZYP1-IntII (mRFP1 and YFP).

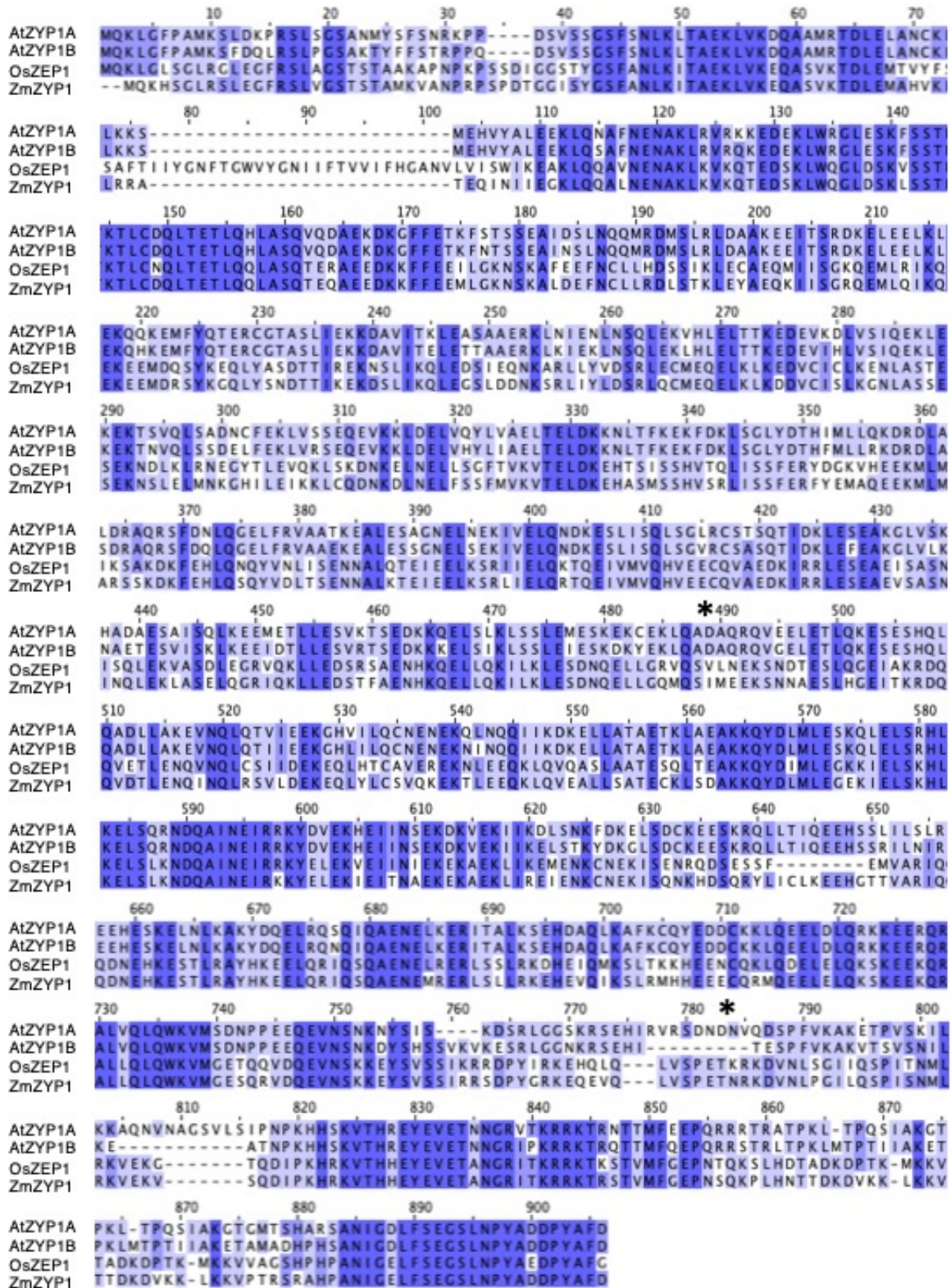


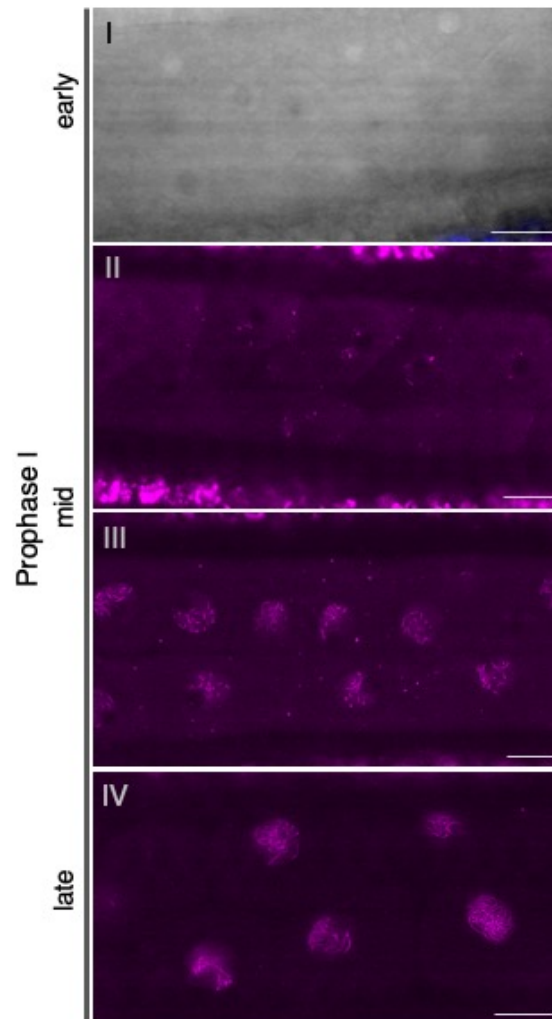
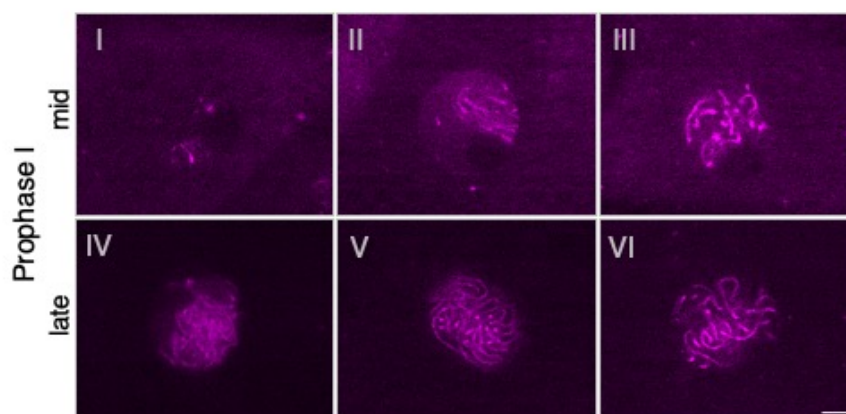
**Figure 12: Alignment of the TF protein sequence of the SC**

Alignment of full-length protein sequence of ZYP1A and ZYP1B (*Arabidopsis thaliana*), ZEP1 (*Oryza sativa*) and ZYP1 (*Zea mays*). The alignment was done with Clustal Omega [67]; conserved residues are highlighted. Asterisks depict the insertion sites for the internal tag.

With respect to the reporter line ZYP1-IntI-mRFP1, meiocytes of several Basta resistant T1 plants have already been screened for expression. In very young and small anthers, no signal for ZYP1 was observed (**Figure 13A, panel I**), this is likely because the meiocytes are before synapsis. When proceeding with sampling towards later stages, the ZYP1 signal first appeared as small and bright foci in the nuclei of meiocytes – at the same time a diffuse signal was also detected both in the cytoplasm and in the nucleus (**Figure 13A, panel II**). The foci developed into stretches (**Figure 13A, panel III**) that progressively formed a more linear signal. At later stages the signal became more extended, presumably labelling the entire length of the synapsed chromosomes (**Figure 13A, panel IV**). A single representative cell is depicted in **Figure 13B**, at different stages of mid- and late prophase I (**Figure 13B, panel I-III and IV-VI**, respectively), following the development of the ZYP1 signal.

The localization pattern of ZYP1-IntI-mRFP1 resembled what was previously observed via immunolocalization experiments [46]. Now, further experiments are required to confirm the functionality of the here-generated reporter, i.e., the introgression into the *zyp1* mutant. Moreover, further screening of T1 plants for ZYP1-IntI-YFP, ZYP1-IntII-mRFP1 and ZYP1-IntII-YFP needs to be performed. Additionally, for a more thorough investigation of the dynamics of synapsis, the ZYP1 reporter will be combined with other markers, e.g., the axis component DSY2.



**A****B****Figure 13: Overview of ZYP1 localization**

Localization pattern of ZYP1-IntI-mRFP1 in meiotic cells at early (panel I), mid- (panel II and III) and late (panel IV) prophase I (A). ZYP1-IntI-mRFP1 localization in a single representative meiotic cell at mid- (panel I-II) and late (panel IV-VI) prophase I (B). Bar 10  $\mu\text{m}$ .

### 2.3.4 Meiosis initiation and progression

In maize, the product of *AM1* gene is important for the irreversible commitment of cells to meiosis and for marking the passage from premeiotic interphase into prophase I (**Figure 14A**). It is the earliest acting meiotic gene identified so far and all initial meiotic processes require *AM1*, including expression of meiosis-specific genes, establishment of the meiotic chromosome structure, meiosis-specific telomere behaviour, meiotic recombination, pairing, synapsis, and installation of the meiosis-specific cytoskeleton [11, 13, 47]. Additionally, unlike the genes involved in initiating meiosis in yeast and mouse, *AM1* also has a second downstream function as it regulates the transition from leptotene to zygotene.

With respect to meiotic progression, numerous studies have been conducted to understand the molecular control of it, e.g., cyclins and cyclin dependent kinases have been identified and play central roles in regulating the meiotic cell cycle [68, 69]. In this study, the putative maize SDS ortholog has been selected as a candidate to monitor meiotic progression and to unravel its relation to homolog interactions, such as pairing and synapsis in maize meiosis.

#### 2.3.4.1 *AM1*

The maize *AMEIOTIC1* gene (*AM1*; *GRMZM5G883855*) is located on chromosome 5 and encodes a plant-specific protein of 780 amino acids with yet unknown biochemical function. The whole genomic sequence along with 2,7 Kb upstream the start codon and 900 bp downstream the stop codon has been subcloned in the entry vector pENTR2B by SLiCE (**Figure 14B**). The two fragments covering the genomic region were obtained by PCR amplification using the B73 genome as template.

The *AM1* protein does not exhibit significant similarity to any protein with a known biochemical function [47] and no information on where the best insertion site for the fluorescent tag is could be extracted from structure predictions or experiments done in other organisms. Thus, two different insertion sites were chosen, one with the fluorescent tag at the N terminal position and one at the C terminus. Both mRFP1 and YFP have been used as fluorescent tag for each position. Basta resistant T1 plants need to be screened for the expression of each construct in meiocytes. Furthermore, the functionality of the reporter lines will be assessed by their introgression in the mutant background (5 different mutants are available for the *AM1* locus [11]). If the constructs are expressed and functional, it will now be

possible to explore the dynamics of AM1 localization and especially elucidate the relation with other meiotic processes, i.e., the formation of the chromosome axis and of the synaptonemal complex to ensure proper synapsis.

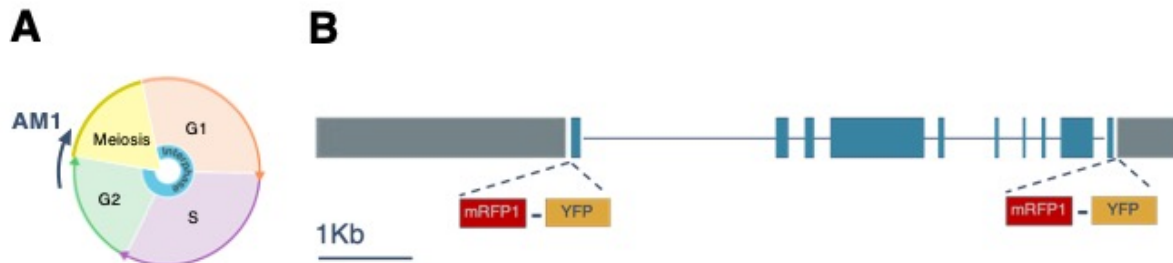


**Figure 14: AM1 in maize**

Schematic representation of the putative time frame of AM1 activity with respect to the cell cycle (A). Illustration of the *AM1* locus, blue boxes corresponds to exons, bars to introns; grey boxes represent the upstream and downstream regulatory regions used. The position of the fluorescent tag (mRFP1 or YFP) is indicated (B).

#### 2.3.4.2 SDS

The *SOLO DANCERS* (*SDS*) gene encodes for a cyclin like protein that is important for male meiosis, as shown in Arabidopsis as well as in the monocot rice [70-72]. BLASTP searches using the amino acid sequences of the Arabidopsis and rice SDS proteins as queries identified two putative maize homologs (GRMZM2G093157 and GRMZM2G344416), suggesting that in maize there could be two putative SDS cyclin-like proteins. The maize proteins share the highest sequence similarity to Arabidopsis and rice SDS in the C-terminal portion, which corresponds to the cyclin domain (**Figure 15**, the maize proteins GRMZM2G093157 and GRMZM2G344416 are referred to as ZmSDS57 and ZmSDS16, respectively; blue boxes highlight the sequence corresponding to the predicted cyclin domain).



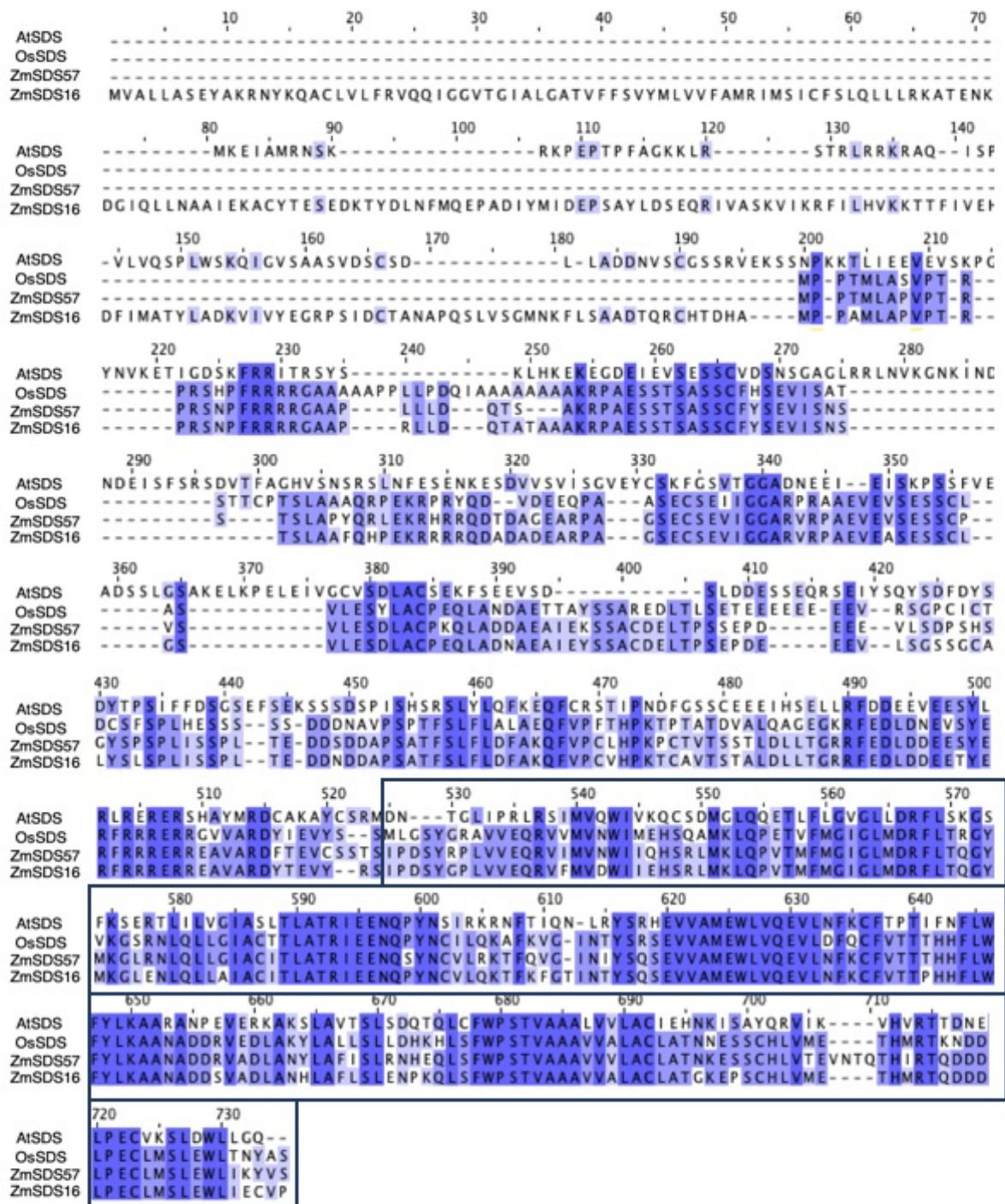


**Figure 15: SDS proteins alignment**

Alignment of full-length protein sequence of AtSDS (*Arabidopsis thaliana*), OsSDS (*Oryza sativa*) and the two putative maize (*Zea mays*) SDS proteins (GRMZM2G093157 and GRMZM2G344416 are referred to as ZmSDS57 and ZmSDS16). The alignment was done with Clustal Omega [67]; conserved residues are highlighted, blue boxes enclose the predicted cyclin domain.

When the maize RNA-seq expression data on MaizeGDB was consulted for both candidates, higher expression levels were seen for *GRMZM2G093157* than for *GRMZM2G344416* in the meiotic tassel and within the anther. Likewise, the recently generated transcriptomic data on isolated meiocytes [38] indicated that the expression level of *GRMZM2G093157* is more than three times higher than the one of *GRMZM2G344416*. Hence, *GRMZM2G093157* was selected as the first SDS candidate gene in maize and it is referred to in following as SDS. It is located on chromosome 9 and comprises 7 exons and 6 introns (**Figure 16B**). For the SDS reporter construct the whole genomic sequence along with the native regulatory elements (2 Kb upstream the start codon and 550 bp after the stop codon) was amplified by PCR using the BAC AC205249.4 as template and integrated into the entry vector pENTR2B by SLiCE. A unique restriction site (*SmaI*) was inserted by PCR directly before the stop codon to add mRFP1 or YFP as fluorescent tag. Different T0 plants were obtained for both versions of the reporter and crossed to and by A188 plants. Meiocytes of Basta resistant T1 plants harbouring the SDS-mRFP1 construct have already been analysed by confocal microscopy.

In very young and small anthers, no signal was observed – presumably, as meiocytes are still in a pre-meiotic stage (**Figure 16C, panel I**). The SDS signal starts to be detected when meiocytes still have a squared shape, hence likely at an early stage of prophase I (**Figure 16C, panel II**). The SDS signal is confined exclusively to the nucleus, diffused with some detectable bright foci. This kind of signal was detected also in meiocytes at mid- prophase (**Figure 16C, panel III, IV and V**). At later stages, the signal decreased in its intensity and disappeared by the end of prophase I (**Figure 16C, panel VI**). In later stages, no signal could be detected (**Figure 16C, panel VII**). This suggests that SDS localization is confined to early-mid- prophase I, hence SDS might be exclusively active during this time frame in maize meiosis (**Figure 16A**). In future, it will be interesting to investigate whether the distinct foci of the maize SDS reporter are located on chromosomes; further, if they associate with recombination sites, which would be consistent with the *sds* mutant phenotype in Arabidopsis where defective recombination has been observed [73].

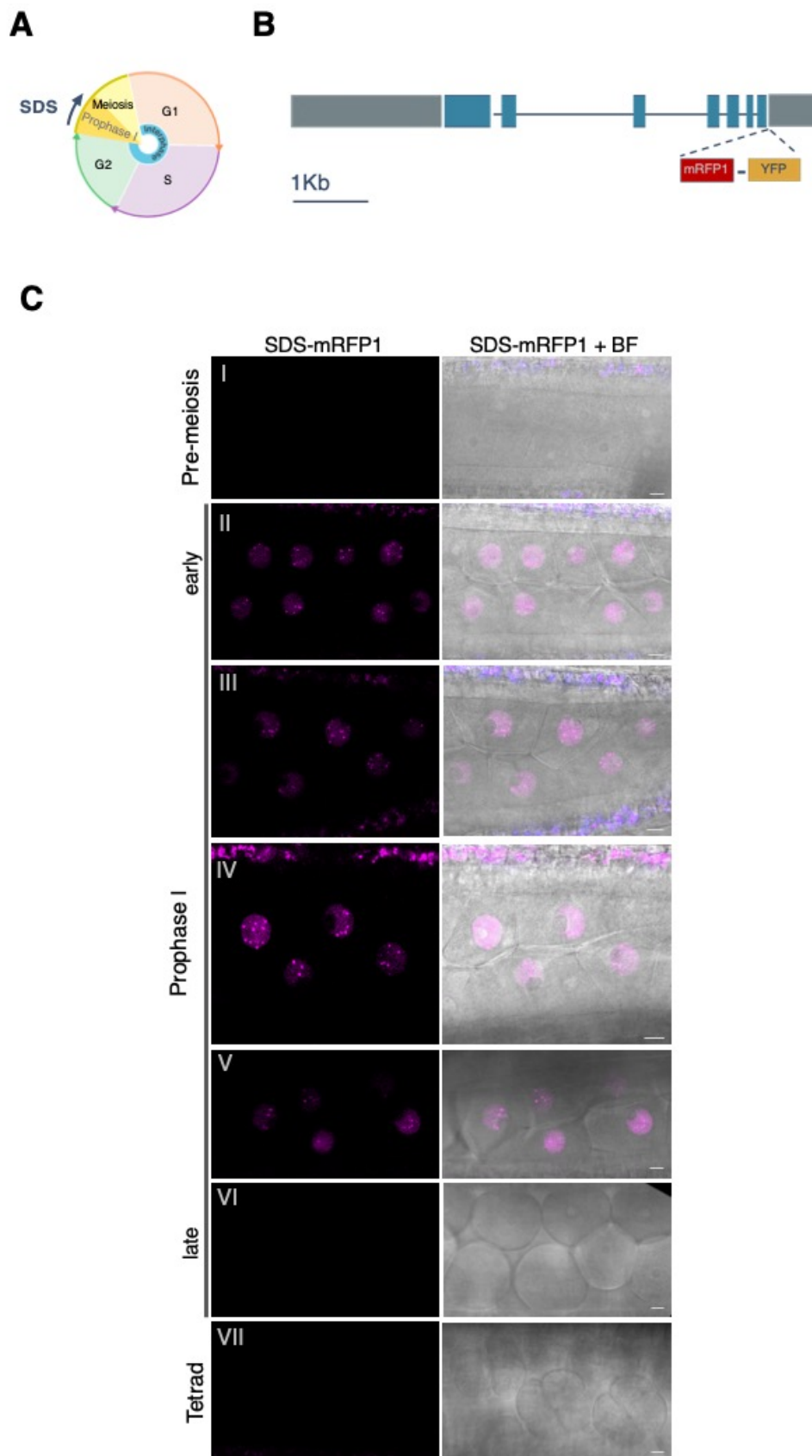


**Figure 16: SDS in maize**

Schematic representation of the putative time frame of SDS activity with respect to the cell cycle (A). Illustration of the *SDS* locus, blue boxes corresponds to exons, bars to

introns; grey boxes represent the upstream and downstream regulatory regions used. The position of the fluorescent tag (mRFP1 or YFP) is indicated (B). SDS localization in meiocytes (C) at pre-meiotic stage (panel I), early (panel II), mid- (panel III, IV and V) and late (panel VI) prophase I, and at tetrad stage (panel VII). Bar 10  $\mu$ m.

### 2.3.5 Marker for meiotic recombination

Meiotic recombination is initiated by the formation of programmed DNA double-strand breaks (DSBs) by Spo11 [74]; thereafter, Spo11 remains covalently attached to the 5'-ends of the DNA, until the MRN complex (Mre11–Rad50–Nbs) and Com1 (**Figure 17A**) promote its endonucleolytic cleavage, removal and eventually DSB processing [75], a prerequisite to the generation of COs. Hence, MRE11 and COM1 were selected as markers for the early steps of the recombination pathway (see paragraph 1.5 of introduction, for details on the recombination pathway).

#### 2.3.5.1 MRE11

On the MAIZE CELLGENOMICS database (<http://maize.jcvi.org/cellgenomics>), a reporter line for MRE11b fused to YFP was available. When the anthers of this reporter line were analysed by confocal microscopy, the signal was detected in the outside layer of the anther (**Figure 17B**), exclusively in the nucleus. However, no signal was visible in meiocytes at any stage of prophase I (**Figure 17C**).

An explanation for this could be the fact that maize genome encodes for two distinct *MRE11* genes, *MRE11a* (*GRMZM2G106056*) and *MRE11b* (*GRMZM2G309109*) respectively. The MRN complex is known to be involved in many aspects of chromosome metabolism in both somatic and meiotic cells [76]. Hence, in maize MRE11A and MRE11B could be differentially involved in these processes. This is not only supported by the fact that MRE11B was detected in somatic cells and not in meiocytes, but also by the RNA-seq expression data available on MaizeGDB (**Figure 17D**). MRE11A and MRE11B show very different expression pattern and strength in the tissues analysed, with MRE11A having a generally higher expression, also in the flowers (**Figure 17D**, in orange). Finally, based on transcriptomic data generated on isolated meiocytes, only *MRE11A* is listed as meiotic candidate gene, with the highest number of reads in meiocytes

compared to anthers and seedlings [38]. Thus, in future a reporter construct for MRE11A should be generated.

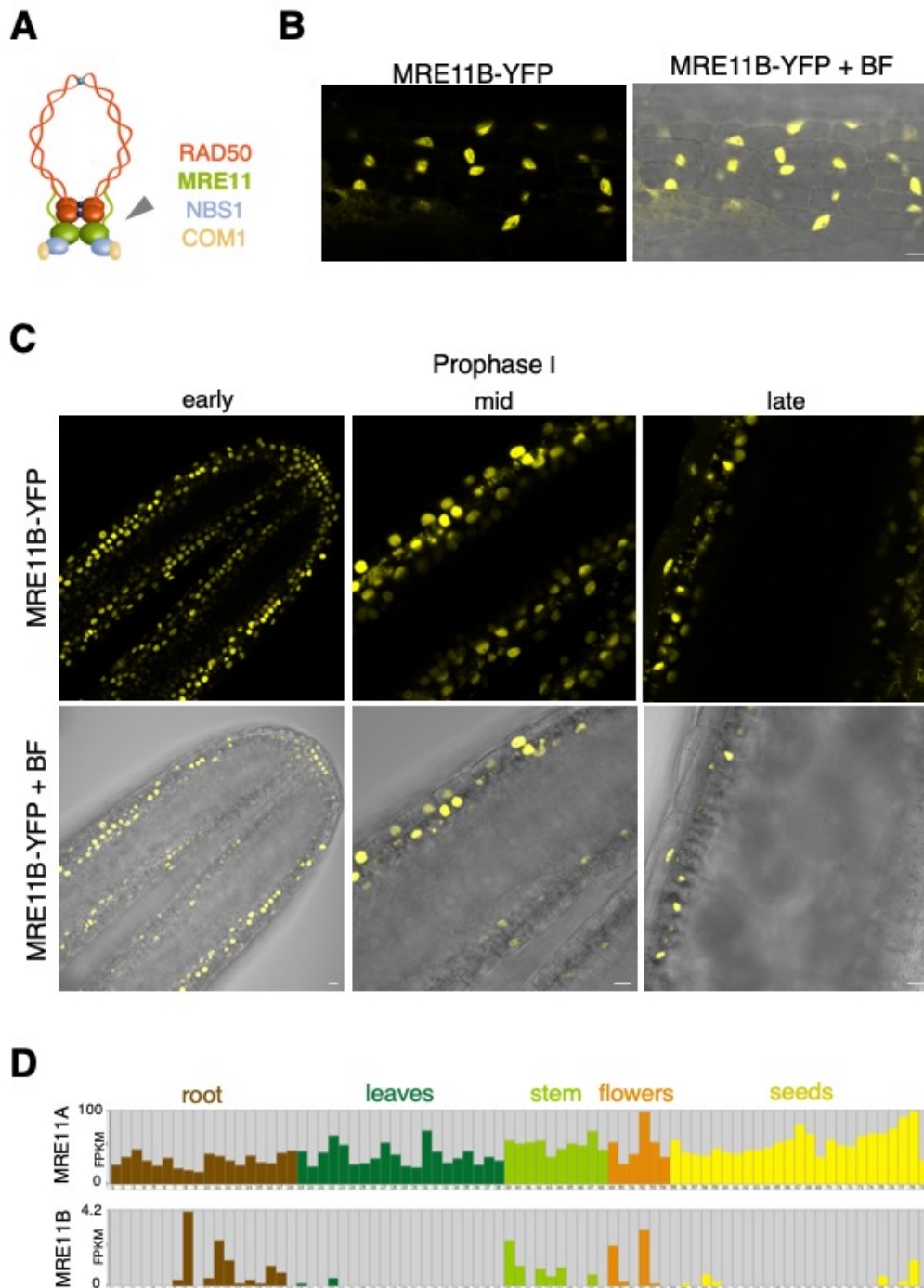


**Figure 17: MRE11 in maize**

Schematic representation of the MRN complex (adapted from [77]), grey arrowhead indicates MRE11 (in green) (A). MRE11B-YFP localization in somatic (B) and meiotic cells at early, mid- and late prophase I (C). Bars 10  $\mu$ m. RNA seq expression data available on MaizeGDB for *MRE11A* and *MRE11B* in root, leaves, stem, flowers and seeds. FPKM

(fragments per kilobase of exon model per million reads mapped) is the normalized estimation of gene expression based on RNA-seq data; the x axis represents different samples analysed for each tissue (D).

### 2.3.5.2 COM1

COM1/SAE2 is a highly conserved protein from yeast to higher eukaryotes, known to cooperate with the MRN complex and required for DNA double-strand break repair through homologous recombination (**Figure 18A**).

BLASTp searches using the amino acid sequence of the previously characterized rice and Arabidopsis COM1 proteins, resulted in the identification of a putative COM1 homolog in maize (*GRMZM2G076617*), which was subsequently confirmed as the maize ortholog by a recent publication [50].

The gene *GRMZM2G076617* is located on chromosome 9 and consists of two exons and one intron (**Figure 18B**); it encodes for a protein of 555 amino acids, which shares 35% identity and 48% similarity with the Arabidopsis COM1 and 62% identity and 72% similarity with the rice COM1. In order to generate a reporter line, the genomic sequence of COM1, including 3.2 Kb upstream the start codon and 900 bp downstream the stop codon, was subcloned into the entry vector pENTR2B by SLiCE (**Figure 18B**) using the B73 gDNA as template. A unique restriction site (*SmaI*) was inserted by PCR either directly after the start codon to generate a N terminal tagged version of COM1 or right before the stop codon for a C-terminal fusion. In both positions, mRFP1 and YFP have been used as fluorescent tag, resulting in four different constructs which have been transformed into maize.

As yet, only the reporter construct for COM1 with a C-terminal YFP tag has been checked in meiocytes. In a preliminary screening, COM1 signal was detected in the nuclei of meiocytes at early, mid- and late prophase I (**Figure 18C**). The signal was located in the nucleus and did not show a completely homogenous pattern, as occasionally some brighter dots and short stretches could be observed (**Figure 18C**, white arrowheads). Further experiments are needed to see if the brighter dots and stretches represent chromosomes, to observe their dynamic evolution and to analyse if there is an association with other meiotic players. Additionally, a screening of the N-terminal tagged COM1 lines need to be performed to see, if a more distinct localization pattern can be obtained. Moreover,



as two independent *Mutator* transposon insertion lines are now available, the introgression of the N-terminally and C-terminally tagged constructs into this mutant background will be instrumental to judge their functionality.

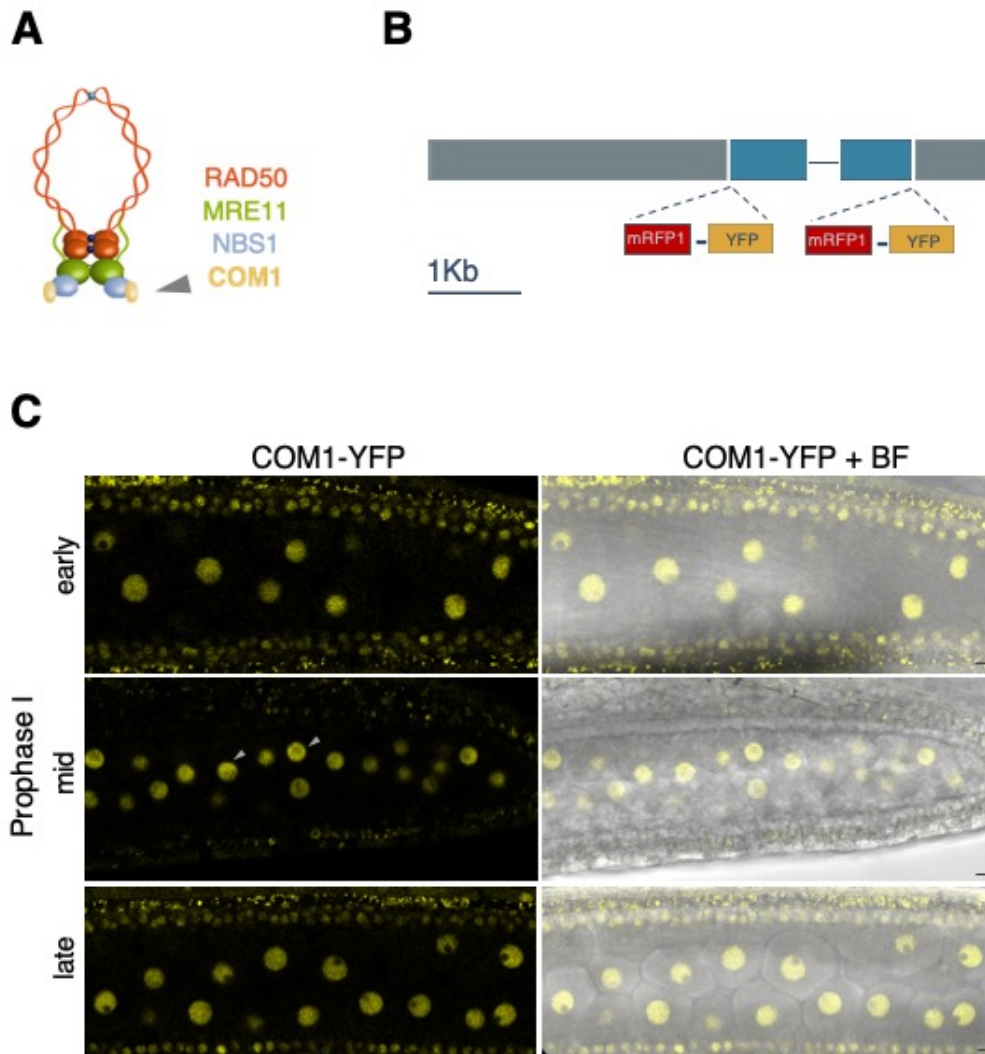


### Figure 18: COM1 in maize

Schematic representation of COM1 in association with the MRN complex (adapted from [77]), grey arrowhead indicates COM1 (in yellow) (A). Illustration of the *COM1* locus, blue boxes corresponds to exons, bars to introns; grey boxes represent the upstream and downstream regulatory region used. The positions of the fluorescent tag (mRFP1 or YFP) are indicated (B). COM1-YFP localization in meiocytes at early, mid- and late prophase I; grey arrowheads depict brighter dots and short stretches (C). Bars 10  $\mu$ m.

### 2.3.6 Cytoskeleton marker

Plant cells possess highly dynamic cytoskeletal networks of microtubules and actin microfilaments, which constantly undergo remodelling to fulfil their roles in supporting several cellular events, such as cell division. Hence, fluorescent reporters of cytoskeletal elements are of key importance to study meiotic progression in living cells.

Via the MAIZE CELLGENOMICS database (<http://maize.jcvi.org/cellgenomics>), several reporter lines for tubulin were available, i.e., YFP-Tubulin- $\alpha$  (tua1; GRMZM2G153292), CFP-Tubulin- $\beta$  and RFP-Tubulin- $\beta$  (tub1; GRMZM2G164696). Hence, I tested if those already available reporter lines could be used as markers in meiosis. Since the expression of these reporters is not restricted to meiocytes, root cells of young plantlets were analysed in a first screening to identify good expressing plants from a segregating population.

The YFP-tubulin- $\alpha$  signal was detected in root cells, labelling the cortical microtubules and the mitotic spindle (**Figure 19A and 19B**). The spindle dynamics could be followed in living root cells and a time laps experiment (**Figure 19C**) revealed the formation of the spindle (**Figure 19C, panel I, II and III**), the anaphase onset (**Figure 19C, panel IV**) and, after completion of anaphase (**Figure 19C, anaphase progression and completion, panel V-IX**) the development of the phragmoplast (**Figure 19C, panel X, XI and XII**).

Concomitantly, I proceeded with the screening of the tubulin- $\beta$  reporters in root cells. Although some CFP-tubulin- $\beta$  signal could be detected, microtubule structures were not well recognizable, whereas the observation of the RFP-tagged version distinctly labelled cortical microtubules (**Figure 19D**) and marked the spindle (**Figure 19E**) as well as the formation of the phragmoplast (**Figure 19F**) in root cells.

However, no signal could be detected in meiocytes for any of the lines analysed, neither for the tubulin- $\alpha$  nor the tubulin- $\beta$  constructs (**Figure 19G** as representative picture).



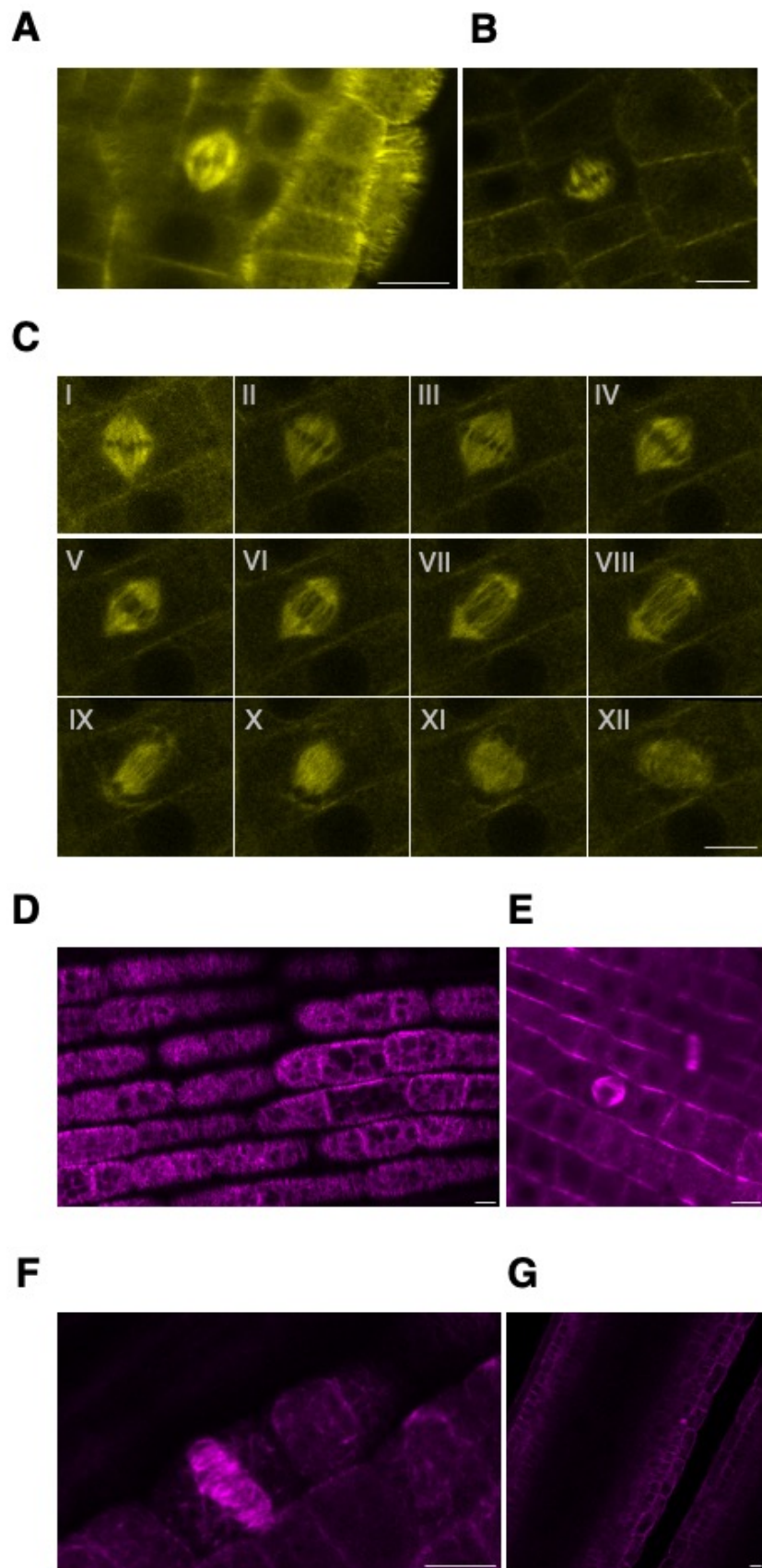


**Figure 19: Tubulin- $\alpha$  and a tubulin- $\beta$  localization in somatic and meiotic cells**

Localization pattern of YFP-Tubulin- $\alpha$  reporter line in root cells (A and B). Pictures from time-lapse imaging of microtubule dynamics in root cells (C). Localization pattern of RFP-

Tubulin- $\beta$  in root cells labelling cortical microtubules (D), the mitotic spindle (E), the phragmoplast (F) and in the anther (G). Bars 10  $\mu\text{m}$ .

The annotated B73 maize genome encodes for six tubulin- $\alpha$ , eight tubulin- $\beta$  and three tubulin- $\gamma$  genes. The information regarding their relative RNA-seq expression data was integrated with the transcriptomic data on seedlings, anthers and isolated meiocytes [38] and guided the choice of new candidate genes. First, *GRMZM2G152466* was selected; it encodes for a tubulin- $\alpha$  protein (tubulin4; *tua4*) and it was found to be strongly expressed in all tissues. Second, *GRMZM2G334899* which instead encodes for a tubulin- $\beta$  protein (tubulin2; *tub2*) and, interestingly, was defined as a meiocyte gene [38], hence being a promising candidate as cytoskeleton marker in meiotic cells.

The genomic sequence of *TUA4*, including 2.9 Kb upstream the start codon and 1 Kb downstream the stop codon, was subcloned into the entry vector pENTR2B by SLiCE. mRFP1 was used as fluorescent tag and added at the N-terminal position by SLiCE (**Figure 20A**). For *TUB2*, the genomic sequence spanning from 2.2 Kb upstream the start codon to 1 Kb downstream the stop codon, was subcloned in pENTR2B by SLiCE. A unique restriction site (*SmaI*) was inserted by PCR directly after the start codon for the insertion of mRFP1 (**Figure 20B**). Basta resistant T1 plants need to be screened for their expression in meiocytes.

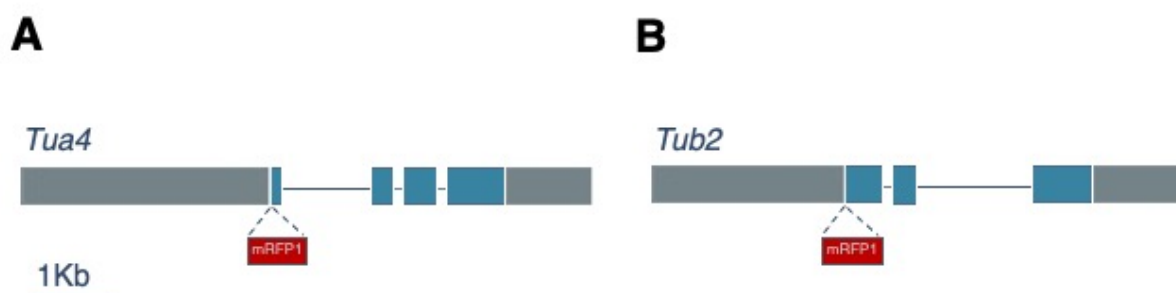


**Figure 20: *Tua4* and *Tub2* as new microtubule reporter constructs**

Illustration of the *Tua4* (A) and *Tub2* (B) locus, blue boxes corresponds to exons, bars to introns; grey boxes represent the upstream and downstream regulatory region used. The positions of the fluorescent tag (mRFP1) is indicated.

## 2.4 Overview of the generated and analysed reporter lines

In this study, I generated 21 genomic constructs for different genes of interest which highlight hallmarks of meiosis, as reported in **Table 2**, and which have been successfully transformed into maize.

**Table 2: Reporter lines generated in this study**

<b>Marker</b>	<b>Reporter line</b>
<b>Chromosomes</b>	PRODSY2: DSY2:mRFP1
	PRODSY2: DSY2:YFP
	PROAFD1: AFD1-I:YFP
	PROAFD1: AFD1-II:YFP
	PROCENH3: mRFP1:CENH3
<b>Synapsis</b>	PROZYP1 ZYP1-IntI:mRFP1
	PROZYP1 ZYP1-IntI:YFP
	PROZYP1 ZYP1-IntII:mRFP1
	PROZYP1 ZYP1-IntII:YFP
<b>Meiotic entry and progression</b>	PROAM1: YFP:AM1
	PROAM1: mRFP1:AM1
	PROAM1: AM1:YFP
	PROAM1: AM1:mRFP1
	PROSDS: SDS:mRFP1
<b>Meiotic recombination</b>	PROSDS: SDS:YFP
	PROCOM1: YFP:COM1
	PROCOM1: mRFP1:COM1
	PROCOM1: COM1:YFP
<b>Cytoskeleton</b>	PROCOM1: COM1:mRFP1
	PROTubulin- $\alpha$ 4: mRFP1-Tubulin- $\alpha$ 4
	PROTubulin- $\beta$ 2: mRFP1-Tubulin- $\beta$ 2

The result of the screening performed up to now for the expression in meiocytes of the here-generated reporter constructs along with already available reporter lines is summarized in **Table 3**. Each generated construct and especially the combination of two different reporter lines will allow investigating the dynamics of key meiotic events by live cell imaging and studying maize meiosis from a spatio-temporal perspective.

**Table 3: Analysed reporter lines**

Reporter line	Expression in meiocytes	Source
PROH1B: H1B:YFP	no	<a href="http://maize.jcvi.org/cellgenomics">http://maize.jcvi.org/cellgenomics</a>
PRODSY2: DSY2:mRFP1	yes	This study
PROCENH3: CENH3:mRFP1	yes	This study
PROZYP1 ZYP1-IntI:mRFP1	yes	This study
PROSDS: SDS:mRFP1	yes	This study
PROMRE11B: MRE11B:YFP	no	<a href="http://maize.jcvi.org/cellgenomics">http://maize.jcvi.org/cellgenomics</a>
PROCOM1: COM1:YFP	yes	This study
PROTubulin- $\alpha$ : YFP-Tubulin- $\alpha$	no	<a href="http://maize.jcvi.org/cellgenomics">http://maize.jcvi.org/cellgenomics</a>
PROTubulin- $\beta$ : CFP-Tubulin- $\beta$	no	<a href="http://maize.jcvi.org/cellgenomics">http://maize.jcvi.org/cellgenomics</a>
PROTubulin- $\beta$ : RFP-Tubulin- $\beta$	no	<a href="http://maize.jcvi.org/cellgenomics">http://maize.jcvi.org/cellgenomics</a>

## 2.5 Experimental set-up for maize live cell imaging

The method established in this study is based on a previously published protocol for live cell imaging of Arabidopsis flower buds [30]. The technique relies on confocal laser scanning microscope equipped with water dipping objectives and it has been adapted to support the culturing and imaging of maize anthers.

### 2.5.1 Sample isolation and mounting

Plants harbouring the construct of interest were grown in the greenhouse; 6-week-old plants were checked for the presence of the immature tassel by cutting a small window into the leaves of the last internode. If the tassel was not yet sufficiently developed, the incision was taped over with surgical tape and the plants were checked again one day or two later. If the immature tassel was visible, young spikelets were collected and positioned into a petri dish containing 1% agarose dissolved in MilliQ water under a stereo dissecting microscope.

Since maize meiocytes develop in the centre of the anthers, which during prophase I lies roughly 70  $\mu\text{m}$  below the anther surface, spikelets needed to be carefully dissected to isolate the three primary anthers. Hence, spikelets were opened and the secondary florets removed, as were lemma and palea of the main floret, to expose the anthers. The three anthers along with the short pedicel have been positioned on a petri dish containing 0.8% agarose dissolved in the culturing medium APW (Artificial Pond Water) and were eventually stabilized by a drop of 2% agarose dissolved in MilliQ water. APW (Artificial Pond Water) medium was

selected as culturing medium, since it has been previously reported to support the growth of maize anthers in liquid medium for over 30 hours [78]. I also tested half strength MS and full MS medium, but anthers were viable for a shorter time than when cultured on APW medium with 0.8% agarose. Several anthers collected from different spikelets can be positioned in the same petri dish, allowing the concomitant observation of several specimens.

### **2.5.2 Microscope set-up**

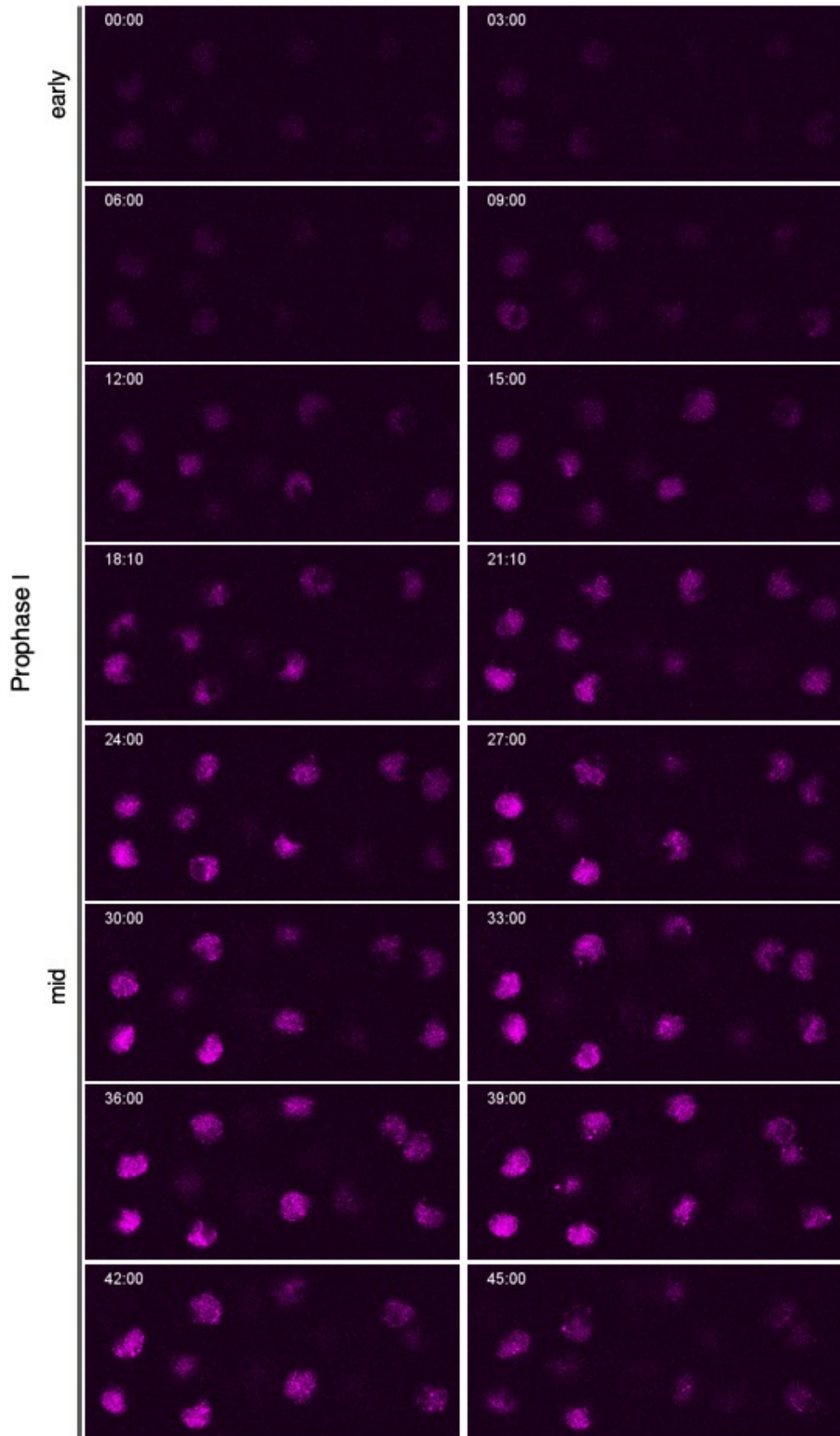
The upright confocal microscope used in this study was equipped with water dipping objectives, which are particularly suitable for live cell imaging experiments as they can be submerged into water, bypassing the use of a cover glass. Therefore, the specimen had been mounted on solid medium in a small petri dish as described, which was then filled with autoclaved water. Such set-up allows sample growth without constraints in the vertical direction, but at the same time offers an anchoring system to avoid flotation.

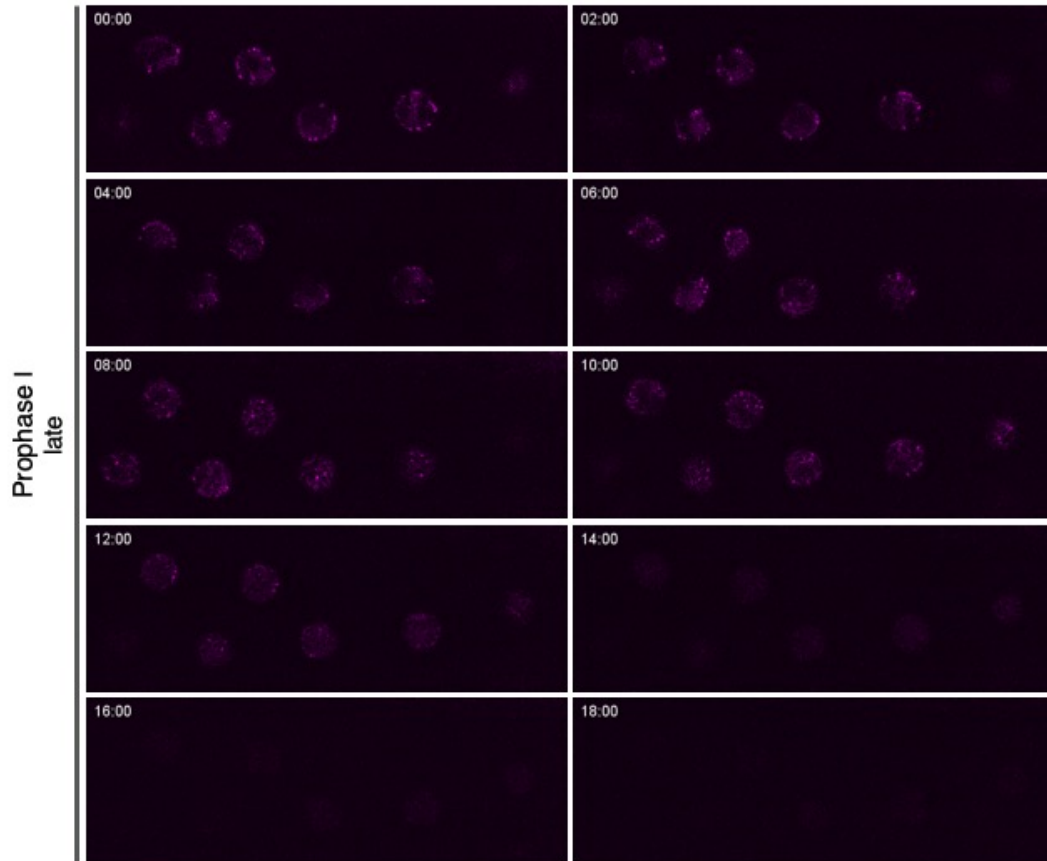
## **2.6 Live cell imaging of DSY2 in maize anthers**

Different attempts have been performed in order to identify the most suitable imaging conditions for maize meiosis, using the DSY2-mRFP1 reporter line as a test case. Images were acquired as a series of 9 z-stack, with 80  $\mu\text{m}$  distance; this allowed the buffering of small vertical movement of the sample, assuring that the same meiocytes would be followed during the whole data acquisition. The interval time between the acquisition of different z-stacks was set as 20 minutes.

The observation of the first set of time-lapses revealed a few interesting aspects. First, the accumulation pattern of DSY2 is dynamic. At early stages, a faint signal was detectable in the nucleus in the form of short stretches (**Figure 21A**). Thereafter the signal became more continuous and longer stretches appeared, concomitantly with an increase in the signal intensity. Finally, the chromosomes could be seen as bright threads (**Figure 21A**), which in later samples decreased in signal intensity (**Figure 21B**). The gradual disappearance of the DSY2 signal from the chromosomes (**Figure 21C**), likely reflects changes in chromosome morphology, such as the disassembly of the synaptonemal complex, hence highlighting a late stage of prophase I.

**A**



**B****C**

**Figure 21: DSY2 localization in living maize meiocytes**

DSY2 localization pictures from a time-lapse experiment showing the progression through early-mid- (A), mid-late (B) and late (C) prophase I; the interval time (hh:mm) from the beginning of the acquisition is indicated in the top left corner.

Furthermore, also the chromosomes themselves were highly dynamic. This is consistent with a previous maize study which showed that chromosome mobility was especially prominent during prophase I and thought to drive the search of homologs [24].

Although preliminary, these observations revealed that keeping meiocytes in their native environment inside the intact anther allows imaging over an extended period of time. In fact, with this approach, it was possible to follow the dynamics of meiotic chromosomes for a period of up to 50 hours, which is longer than achieved in any previous studies on maize meiosis.



## 3 Discussion

Understanding the spatial and temporal complexity of biological pathways requires knowledge on the dynamics of the proteins involved. The use of live cell imaging has revolutionized the analysis of the spatial and temporal organization of plant cells and has been widely developed in the model plant *Arabidopsis thaliana*, while studies in maize have not advanced so rapidly.

As maize is one of the most important food crops worldwide, the establishment of such technique represents a unique opportunity to more precisely study meiosis in a crop model system and ultimately could provide guiding information for crop improvement. Hence, my work aims to expand and improve our knowledge of meiosis in crops.

Here I discuss, first, the key aspects of establishing a technique to perform live cell imaging of meiosis in maize - i.e., how to visualize meiotic players in living cells, the choice of the specimen as well as the culturing medium along with the imaging conditions. Second, I describe which aspects of chromosome dynamics in meiosis could be explored with the here-generated material and the developed method.

### 3.1 Live cell imaging: technique development

The here-presented live cell imaging set-up relies on the use of reporter lines highlighting hallmarks of meiosis combined with a suitable culturing system for living maize anthers in order to monitor the dynamics of proteins in living meiocytes embedded in their native environment. This method allows fulfilling the main requirements of a live cell imaging experiment, i.e., the visualization of cellular components, such as chromosomes and microtubules, and the maintenance of sample viability for an extended period of time, i.e., days.

#### 3.1.1 How to visualize meiotic players in living cells

A typical set-up for live cell imaging of meiosis relies on the visualization of chromosomes. Early attempts made use of different stains, e.g., the vital chromatin stain SYTO [19, 20, 22] and 4',6-diamidino-2-phenylindole (DAPI) [78]. These are fast methods, as directly after a short incubation time, the specimen can be observed and the whole chromosomes visualized at the microscope.

However, ideal vital chromatin stains need to effectively penetrate the tissue, produce an adequate staining, while neither altering chromosome dynamics nor affecting the viability of meiocytes, and should be resistant to photobleaching. SYTOs staining were suitable for isolated meiocytes, but could not adequately penetrate maize anthers, hence the use of DAPI [78]. DAPI is usually applied to fixed material, but at higher concentrations it can be used to stain living cells, as it can pass through membranes.

Outside of maize, the visualization of chromosomes in live cell imaging experiments has largely relied on the use of fluorescent reporter constructs, especially in *Arabidopsis* [28, 30, 55, 79], which could be successfully visualized for an extended period of time, i.e., days. The use of such a fluorescent protein approach gives the possibility to visualize, at least theoretically, any kind of proteins in meiosis, allowing a more detailed analysis compared to the staining of the whole chromosomal DNA with dyes. As the capacity for and quality of maize transformation has recently improved, it has become possible to make use of fluorescent tagged lines also in maize.

Previously, a comprehensive set of maize marker lines, which highlights different cellular components, has been developed (<http://maize.jcvi.org/cellgenomics>), including a line for Histone H1 and several tubulin reporter lines. However, no signal could be detected in meiocytes for any of the lines tested. Therefore, I started with the generation of new genomic reporter lines for 9 meiotic genes of interest.

The generation of a genomic reporter construct relies on the cloning of significant upstream ( $\cong 3$  Kb) and downstream ( $\cong 1$  Kb) sequences – sizes previously reported to be sufficient for correct expression of a gene of interest [52] - along with the genomic region of the gene of interest, namely exons and introns. On the one hand this implies the cloning of large genomic fragments, challenging the size limit for good cloning efficiency, in contrast to a reporter construct based on only the coding sequence (CDS) of a gene. On the other hand, a genomic construct is meant to include all native regulatory regions to ensure a faithful representation of the native expression pattern of the protein of interest. Thus, all the reporter lines generated in this study are based on the genomic locus, along with some surrounding sequence to include associated native regulatory regions.

Moreover, careful considerations were made with respect to the choice of the fluorescent tag and its insertion site. For this purpose, I searched for fluorescent

tags suitable for maize. Several fluorescent protein variants have been previously tested to ensure proper expression in maize cells, and some have been maize codon optimized [52]. The first choice was Citrine YFP, a YFP variant which is brighter and more resistant to photobleaching, acidic pH, and other environmental effects than EYFP [80]. With the aim to observe two different reporters concomitantly in living anthers, mRFP1 was selected as a second fluorescent tag. In fact, the separated excitation and emission spectra of the two fluorochromes allows the reliable and concomitant detection of two differently tagged proteins and permits to maximize the information gained in a live cell imaging experiment. Additionally, to prevent the fluorescent tag from disrupting the native protein folding and function, the tags are flanked by linker peptides. Also, the insertion site (N terminal, C terminal or internal) has been selected based on functional domain analysis and sequence conservation, trying to keep domains and highly conserved regions undisrupted.

### **3.1.2 Sample mounting and imaging**

Live cell imaging of isolated meiocytes requires laborious handling of the sample; as previously reported, damages inflicted during the steps of extraction severely affect the survival of the cells *in vitro* [20, 81] and in addition, isolated meiocytes could be so far cultured for a maximum of 9 hours, i.e., could only be used to study short phases of meiosis, such as metaphase I and anaphase I and have been failing to provide information on the extended meiotic prophase I [22]. Instead, imaging the anthers in their integrity limits the impact of *in vitro* culturing on meiocytes and has the advantage of keeping the developmental context as close as possible to the native environment, which allows longer image acquisition [24].

The method applied in this study, with respect to sample mounting and imaging, is based on a protocol for live cell imaging of Arabidopsis flower buds, previously established in the lab [30]. Nonetheless, several changes were made to adapt it to maize since meiosis in maize takes longer than in Arabidopsis (5 days from leptotene onset to telophase II [15] vs 26 hours from late leptotene to telophase II in Arabidopsis [30]) and maize anthers require a different medium to be kept alive. Revisiting the culturing conditions previously described for maize anthers [78], I decided to test the same culturing medium and to use APW as the main component of the solid medium supporting sample growth and development during imaging. Such set up allowed imaging maize anthers for a period of 50

hours, which is, so far, longer than any previous live cell imaging experiment in maize meiosis. However, considering that meiosis lasts for a few days in maize, this technique requires further improvements to extend the time window for which maize anthers can be cultivated *in vitro*.

Such improvements could be achieved by changing the composition of the current medium. The APW medium is a minimal medium and as such it lacks a carbon source. On the one hand such medium is less likely to be contaminated over the course of an experiment – which was considered to be an important aspect regarding the final goal of a long-term imaging. On the other hand, a source of sugar, e.g., sucrose, was previously reported to support meiocytes and spikelet growth, but only in a very narrow concentration range (0.28 M to 0.34 M) [19, 82]. Nonetheless, addition of sucrose within this concentration range to the APW medium could be tested also for isolated anthers. Other studies also aimed to culture the whole maize male inflorescence, the tassel [82], or only the spikelets [83] from an immature stage till pollen production. Even though this was not done for imaging purposes, it could be interesting to explore the culturing conditions used. For example, a component which appeared to be relevant for proper tassel growth was the presence of kinetin [82]. Hence, the supplement of kinetin or other cytokinins to the medium could be tested. Also the optimal pH value for the medium needs to be tested, in order to keep the value similar to the anther locule, which is approximately 7 [83].

An environmental aspect to further take into consideration is the temperature. Maize plants are grown in the greenhouse at 25°C, hence such a temperature might also be best during culturing and imaging. This is supported by the fact that culturing maize meiocytes at temperatures lower than 25°C was previously reported to cause abnormal chromosome segregation [20]. As all the previous studies were performed on different maize varieties, it will be important to test if the same holds true for A188, which has been used here.

Finally, another observation was that when culturing plant explants, either isolated meiocytes [20, 81], the entire spikelet [19, 81] or isolated anthers as done in this study, the rate of success depended on the initial developmental stage of the explant with younger samples being harder to cultivate. It will be necessary to test whether this is the consequence of physical damage incurred during the preparation of the sample and, if so, to which extent this could be prevented or

whether this is due to a lack of nutrients which are needed to support the growth of maize sample at earlier stages, such as pre-meiosis or early prophase I.

To validate each culturing condition, it will be instrumental to compare the temporal progression of development between cultured anthers and anthers collected from greenhouse-grown plants at regular intervals, e.g., by performing acetocarmine staining.

Finding the optimal culturing condition will be necessary to perform long term imaging, e.g., for following the cellular events that characterize prophase I, where many important processes take place, such as pairing, synapsis and recombination.

### **3.2 Future experiments**

The localization pattern of my reporter constructs was by and large consistent with what was observed in previous experiments, such as immunolocalization studies, and with results on homologous proteins in Arabidopsis. This suggests, but does not determine the functionality of the generated reporter constructs. A next experiment could be a phenotypic analysis of all meiotic stages by acetocarmine staining to evaluate the presence of any dominant negative effect due to the introgression of the fluorescently tagged gene.

Moreover, for some genes mutant lines are available, e.g., for *DSY2* (*dsy2-1* and *dsy2-2*), *ZYP1* (*zyp1*), *AM1* (*am1-1*, *am1-2*, *am1-485*, *am1-489* and *am1-praI*) and *AFD1* (*afd1-1*, *afd1-2*, *afd1-3*, *afd1-4*). Thus, it will be mandatory to introgress each reporter in the respective mutant background and analyze if the mutant phenotype can be rescued, which would prove full functionality of the fusion protein. Additionally, one could screen a recently established collection of maize mutants obtained by insertional mutagenesis, BonnMu, or generate CRISPR/Cas mutants for those genes, where no mutant has been described yet, e.g., *SDS*, and then perform the respective complementation studies.

With the generated reporter lines, it will be possible to directly monitor the progression of meiosis by live cell imaging within the same cell and not estimate the duration of different stages from a mean of all cells prepared at a certain time point. This will provide a more precise estimation of the meiotic time-course compared to previous studies based on fixed material [15]. A first indication comes from a recent live cell imaging study analyzing chromosome segregation during meiosis I and II in maize [22]. This study revealed a significantly shorter duration

for both anaphase I and II than previously reported in studies on fixed material (roughly 15 min for each vs 1.6 and 2.1 hours, respectively).

Using an optimized imaging procedure and the material generated in this study, a first goal would be a precise time-course of prophase I. A combination of different markers and their concomitant observation along with transmitting light images to evaluate changes in cell morphology could be used. This will provide the identification of specific cell features which will define a landmark system for maize meiosis, similarly to what previously described for Arabidopsis with such approach [30].

A first combination of markers which could be instrumental to temporally dissect prophase I consists of the reporter line for the axis protein DSY2 along with ZYP1. DSY2 appears in the form of numerous foci already at late interphase, as previously detected by immunolocalizations studies [43] and subsequently it begins to form discontinuous stretches at leptotene stage, as also reported here (see paragraph 2.3.2.1 and 2.6 of results). Hence, this first change in the distribution of DSY2 could be used as a first reference point to determine the onset of leptotene. Subsequently, in zygotene, the homologous chromosomes start to synapse. As the establishment of the SC is characterized by the appearance of transverse filament proteins, such as ZYP1, the observation of the ZYP1 reporter would be informative with respect to synapsis. Hence, the detection of the first foci coming from the ZYP1 reporter would mark the zygotene stage. The concomitant observation of DSY2 and ZYP1 allows the visualization of the chromosome axes in its integrity and of the synapsed regions. Therefore, it will be possible to judge when synapsis is completed and pachytene is reached. By then, the signal coming from ZYP1 should entirely span the gap between the chromosome axes, labeled by DSY2. Similarly, the disassembly of the SC could be monitored by the progressive reduction of ZYP1 and DSY2 signal along the axes defining diplotene.

Alternatively, the plant specific protein AM1 could be used to monitor early stages of meiosis and especially meiosis onset. Previous immunolocalization studies revealed that AM1 is diffuse in the nucleus during premeiotic interphase and after meiotic entry it binds to chromatin during leptotene and zygotene [47]. The combination with the ZYP1 marker, which starts accumulating from zygotene on, could additionally provide important information in the time dissection of the substages of prophase I.

Furthermore, the visualization of a marker which covers the complete division and with a distinct accumulation pattern, such as a cytoskeleton marker, e.g., tubulin- $\alpha$  and a tubulin- $\beta$  reporter lines generated in this study, will allow to resolve meiosis in its integrity. This marker could be combined with a chromosome marker, such as DSY2 to maximize the information gained, at least during prophase I, and would also allow comparing the length of meiotic phases in maize with the previous time course experiment [22].

In addition, the introgression of reporter constructs in a mutant background could promote the understanding of the mutant phenotype and thus meiotic progression in general. For example, such approach could be helpful to precisely re-analyze maize mutants which show a phenotype not found yet in any other organism, such as *am1-pra1*, which is arrested at the leptotene to zygotene transition, but also to characterize new meiotic mutants found in forward genetic screens for male sterility or in the BonnMu collection, which provides insertion mutants for nearly 50% of all maize genes.

Other applications of the live cell imaging technique with the here-generated material could be addressed to investigate different aspects of meiosis, such as the formation of the chromosome axis.

How chromosomes are organized with respect to axial element organization is not yet completely known in maize. This is an important question to answer since appropriate chromosome architecture is required for homologous pairing, recombination and synapsis.

Live cell imaging using the AFD1 and DSY2 reporters can be used to look at changes in axial element establishment and organization and will allow following them in individual cells throughout prophase I. Changes could be further investigated in relation with the establishment of the synaptonemal complex, when the chromosome axes of both homologs are integrated into the synaptonemal complex (SC) as lateral elements. The availability of a reporter line for the transverse filament protein ZYP1 will allow to monitor synapsis.

Furthermore, it will also be interesting to investigate the relation between AM1, which upon meiotic entry localizes to chromatin, and the chromosome axis. AM1 was found to be required for the transition to meiosis and progression through the early stages of prophase I [47], i.e., essentially all meiotic processes, including the establishment of the meiotic chromosome structure, require AM1.

Finally, a better understanding of chromosome architecture could also give new insight into how the loading of the recombination machinery is controlled, namely how chromosome architecture creates a favorable environment for the recombination machinery. For this, additional reporter constructs, such as RAD51 and MLH1 will have to be created and combined with the here-generated set. Understanding the frequency and placement of recombination events in maize could help developing new breeding strategies and eventually contribute to crop improvement.



## 4 Material and methods

### 4.1 Plant material and growth conditions

The maize inbred line A188 was used as wild-type reference in this study and for the generation of transgenic lines. Plants were grown in the greenhouse at 25°C, with 16 h day/8 h night regime and 50% humidity. Seeds were initially planted ~3 cm deep in soil in small pots (8 cm diameter).

To screen for transgenic plants carrying the construct of interest, plantlets (10-14 days after germination) were sprayed with Basta (final concentration of 250 mg/L), as the transgenes carry the Basta resistance gene (*bar*) as selectable marker. After 4 days, sensitive plants have discoloured, wilted and/or leaves died, while resistant plants (with the transgene) are healthy and with green leaves.

14-20 days after germination, plantlets are transferred to larger pots (7.5 L, 24.5 cm diameter) containing soil supplemented with fertilizer (10 gr Plantosan Compact per pot).

Controlled crosses are made by placing a bag over the tassel and shaking gently to collect the pollen, which is then sprinkled onto silks. The ears are covered before silks emerge to prevent contamination.

### 4.2 Generation of reporter lines

The genomic sequence of *AFD1*, *AM1*, *COM1*, *Tubulin  $\alpha$*  and *Tubulin  $\beta$*  have been obtained by PCR amplification using the gDNA from B73 as template. The genomic sequence of *DSY2*, *CENH3*, *SDS* and *ZYP1* was obtained by PCR amplification using the corresponding BAC as template, respectively BAC AC210848 for *DSY2*, BAC AC209457\_3 for *CENH3*, BAC AC205249.4 for *SDS* and AC204395.5 for *ZYP1*. The primer pairs used for PCR amplification are listed in **Table 4**; PCR conditions used in **Table 5 and 6**. The PCR fragment spanning the genomic region of *DSY2* and *CENH3* has been integrated by BP reaction into the entry vector pDONOR221. *AFD1*, *AM1*, *COM1*, *Tubulin  $\alpha$*  and  *$\beta$* , *SDS* and *ZYP1* have been cloned into pENTR2B by SLiCE [84]. A *SmaI* restriction site was introduced by PCR after the start codon of *Tubulin  $\alpha$*  and  *$\beta$* , in front of the stop codon of *DSY2* and *SDS*, and after the start codon and before the stop codon of *COM1*. A *NaeI* insertion site was introduced by PCR after the start codon of *CENH3*. The constructs were linearized by *SmaI* or *NaeI* restriction and ligated to YFP or mRFP1 fragments. The YFP and/or mRFP1

fragments were integrated by SLiCE into the entry vector carrying the gene of interest as follow: after the start codon and before the stop codon of *AM1*, before the stop codon of *AFD1*, internally in *ZYP1*, between the 460-461 and 752-753 amino acids with respect to ZYP1 protein. Each entry clone with the fluorescent tag was fully confirmed by sequencing and then integrated into the destination vector p7oM-LH-GW by LR reaction. All constructs were transformed into *Agrobacterium* strain LBA4404 and positive *Agrobacterium* clones were selected for plant transformation (see below). All constructs generated are listed in **Table 7**.

### 4.3 Plant transformation

*Agrobacterium tumefaciens* strain LBA4404 containing the destination vector (p7oM-LH-GW) with each gene of interest was cultivated on YEB medium containing 100 mg/L Spectinomycin (for p7oM-LH-GW selection) and 10 mg/L Tetracycline (for LBA4404 selection). Bacterial cultures are initiated from stock plates. One full loop of bacteria culture is scraped from the three-day old plate and suspended in 5 mL of liquid infection medium (see **Table 7**) supplemented with acetosyringone in a 50 mL centrifuge tube. The tube is fixed horizontally to a bench-top shake and shaken at 100 rpm at RT for 1-4 hours.

Immature embryos in the size of 1.8 - 2.1 mm of the maize A188 genotype are dissected from greenhouse-grown ears harvested 10 days after self-pollination. Ears are stored up to three days at 4°C before dissection. For dissection, each ear is divided in two halves and sterilized in a beaker with 3% NaOCl + 0.1% Labosol solution for 25 min; thereafter, rinsed with approx. 1.5 l of sterile water. Embryos are dissected and collected into a tube with 2 ml infection medium supplemented with acetosyringone. Afterwards the embryos are washed twice with fresh infection medium. The final wash is removed and 1 ml of *Agrobacterium* suspension (OD600 = 0.4) is added to the embryos. Embryo infection is accomplished by gently inverting the tube 20 times before resting it upright with embryos submerged for five minutes at room temperature. Embryos are transferred to the surface of co-cultivation medium (scutellum side up) and excess *Agrobacterium* suspension is pipetted off the medium surface (see **Table 7**).

Plates are incubated for 3 days at 22°C in the dark. Afterwards, embryos are transferred to as follow: resting medium (7 days at 28°C, in the dark), selection medium I (14 days at 28°C, in the dark), selection medium II (14 days

at 28°C, in the dark), selection medium III (14 days at 28°C, in the dark), regeneration medium I (21 days at 26°C, in the dark), regeneration medium II (21 days at 26°C, in the light) (see **Table 7** for all media composition). Regenerated plantlets are transferred to magenta boxes with regeneration medium II for one week and thereafter transferred to the greenhouse.

This work was kindly performed at the University of Hamburg by Dr. Reinhold Brettschneider, Dagmar Stang and Katja Müller and at Crop Genetic Systems (Hamburg).

#### **4.4 Chromosome spreads (acetocarmine staining)**

Fresh spikelets were collected and fixed in 3:1 Ethanol:Acetic Acid (fixative solution) for at least 24h at 4°C, washed twice with fresh fixative solution and stored in 70% ethanol at 4°C. The spikelets are dissected under a stereo dissecting microscope; the anthers are positioned on a microscope slide, squashed and stained with acetocarmine (see **Table 7**). After adding a coverslip, slides are heated until the colour of the stain turns from deep red to purple. The stage of meiosis is determined under a wide-field light microscope.

#### **4.5 Confocal microscopy**

##### **4.5.1 Localization analysis**

Young anthers harbouring the reporters of interest were dissected under a stereo dissecting microscope, transferred into a drop of tap water on a microscope slide, covered with a cover slide and immediately imaged using a Leica TCS SP8 inverted confocal microscope or a Zeiss LSM 880 confocal microscope. Pictures were captured with a 40X water immersion objective. YFP was excited at  $\lambda$  488 nm or at  $\lambda$  514 nm and detected at  $\lambda$  between 510 and 560; mRFP1 was excited at  $\lambda$  561 nm and detected at  $\lambda$  between 578-650 nm. Autofluorescence from chloroplasts was highlighted in blue using excitation at  $\lambda$  488 and detection at  $\lambda$  between 680-750 nm.

##### **4.5.2 Live cell imaging**

Time-lapses were acquired using a Zeiss LSM 880 confocal microscope. Spikelets were dissected and isolated anthers positioned on the petri dish with APW solid

medium (see **Table 7**). During image acquisition the petri dish was filled with autoclaved water and placed under a W-plan-Apochromat 40X/1.0 DIC objective. mRFP1 was excited at  $\lambda$  561 nm and detected at  $\lambda$  between 578-650 nm. Time lapses were acquired as series of Z-stacks (9 planes, 80  $\mu$ m distance) with an interval time of 20 minutes between the acquisitions.

#### **4.5.3 Live cell imaging data processing**

Time lapses obtained in the .czi format were converted into sequential images by ImageJ [85] and opened with MetaMorph software (Version 7.8.0.0; Molecular devices LLC., San Jose, CA, USA). One focal plane was selected from the all Z-stacks acquired for each time point using the function "Review Multi-Dimensional Data" and the file was exported as .tiff stack file. Image drift on XY plane was corrected using the "Stack Reg" plugin (Rigid Body option) of ImageJ, with "Solid Body" as transformation parameter. Brightness and contrast were adjusted and the file was converted into an RGB file in ImageJ.

**Table 4: Primer used in the research**

Reporter	Primer name	Sequence
DSY2	gDSY2-F	CAAAAAAGCAGGCTGCGTGTACTGCTGCTG CGTTTGTTTGC
	gDSY2-R	CGTTTGCAAAAAGCGACGGTTGAAGTGCG
	DSY2-SmaI-F	GGGTGACTGATCGAAGTTGCTTCAC
	DSY2-SmaI-R	GGGATCAACAGTCTCTGTGATAAGC
AFD1	gAFD1-F1	GACTGGATCCCCGAGGCCAGCCATGATGAG TAAGTAGC
	gAFD1-R1	ATGCCACATCTATCACCGTTCATATCCACT CCATGC
	gAFD1-F2	ACCGGTGATAGATGTGGCATGCTTATCTGAC AGCCG
	gAFD1-R2-I	ATATATCAGGAATCACCTAAGCCTACTCCTC ATCT
	gAFD1-R2-II	ATATATCAGGTCACGCGCTCCGAAGGGGT CAATACCG
	gAFD1-F3	GAGCGCGTGACCTGATATATTACAACTGGC TGC
	gAFD1-R3	GTGCGGCCGCGTGACCAGATGAAGCACACG CTAG
	pENTR2B-AFD1-F	GTTTCATCTGGTCACGCGGCCGCACTCGAG ATATCTAG
	pENTR2B-AFD1-R	CATGGCTGGCCTCGGGATCCAGTCGACTG AATTGGTTC
	AFD1-YFP-F1	GCGGCCGCTGGGGCCTGACTTGGTGATGTT GGAAACAATT
AFD1-YFP-R1	CTCCAGGCCGCCCATCATCTTTAATCCTCT GGAGATCAAG	
CENH3	gCENH3-F	TTTGTACAAAAAAGCAGGCTTGGAGGAGCAT AATGGCCTGATC
	gCENH3-R	ACTTTGTACAAGAAAGCTGGGTTCCAACCTT GAATATATGGGTAC
	NaeI-CENH3-F	GGCATGGCTCGAACCAAGCACCAGGC
	NaeI-CENH3-R	GGCCGCGGTGGGCGCCTCGCACTGCTCTC
ZYP1	gZYP1-F1	GACTGGATCCCGTGCCTACGTTGTACGTAC ATAGG
	gZYP1-R1	GTTGCAGAAAGCAATGCTTCGACCTGGGC
	gZYP1-F2	CATAAGTCCATAACAGTCTTTTGAATCC
	gZYP1-R2	GTGCGGCCGCGTTCCAGAATTCGTATCGT GCTTGC
	pENTR2B-ZYP1-F	GACGAATTCTGGAACGCGGCCGCACTCGAG ATATCTAGAC
	pENTR2B-ZYP1-R	CGTACAACGTACGCACGGGATCCAGTCGAC TGAATTGGTTC
	ZYP1-intI-F	GCGGCCGCTGGGGCCCCTATGGAAGAGAAA TCAAATAATG
	ZYP1-intI-R	TCCAGGCCGGCCATCCTAATGGACTGCATT TGTCCTAGG
	ZYP1-intII-F	GCGGCCGCTGGGGCCCCTAATCGGAAGGTA AGATGCC
	ZYP1-intII-R	TCCAGGCCGGCCATCCTGGTCTCCGGACT TACCAACTGG
AM1	gAM1-F1	GACTGGATCCGAGTGTTACTGTGTCAGGTG CATGTGC
	gAM1-R1	CTGCTATGACTACTGCTCGTCTTC
	gAM1-F2	GCCACAGGTGAAGAAGTACTACTTC
	gAM1-R2	GTGCGGCCGCCCCTGCTGACTCTATGCAA TCAGGATTGG

	pENTR2B-AM1-F	TAGAGTGCAGACCGGGCGGCCGCACTCGAG ATATCTAGAC
	pENTR2B-AM1-R	GACACAGTAACACTCGGATCCAGTCGACTGA ATTGGTTCC
SDS	gSDS-F1	CGCTTGACTGTCTCGCTTTCTAC
	gSDS-R1	AGATTCCCCGGATAGAGACTGCT
	pENTR2B-SDS-F	AAAGCAGTCTCTATCCGGGGAATCTGCGGC CGCACTCGAGATATCTAG
	pENTR2B-SDS-R	TTGTAGAAAGCGAGACAGTCAAGCGGGATC CAGTCGACTGAATTGGTTC
	SDS-SmaI-F	GGGTGATACCCAGAGCTCCCAGGTG
	SDS-SmaI-R	GGGCGAGACGTACTTGATCAGCCACTC
COM1	gCOM1-F1	TTGCCAAAACCTGCATCACA
	gCOM1-R1	CCTCCCTCCTCCCATTTAGC
	gCOM1-F2	GCTAAATGGGAGGAGGGAGG
	gCOM1-R2	TCAATCAAGTCCCTCCGCTT
	gCOM1-F3	AAGCGGAGGGACTTGATTGA
	gCOM1-R3	TCGCCTACCCCTAAATCGAC
	pENTR2B-COM1-F	GTCGATTTAGGGGTAGGCGAGCGGCCGCAC TCGAGATATCTAG
	pENTR2B-COM1-R	TGTGATGCAGGTTTTGGCAAGGATCCAGTC GACTGAATTGGTTC
	SmaI-COM1-F	GGGATGGAGGGGAAGGCGGTAGCCG
	SmaI-COM1-R	GGGCTATACATTAAGAACAGAATCGC
	COM1-SmaI-F	GGGTAGCACTACATCAAGTAGCAGG
	COM1-SmaI-R	GGGCATTTCTGATTTCGAAACCAATG
Tubulin- $\alpha$ 4	gTUA4-F	GACTGGATCCCCCGGCTTTGATTTGAGAAGA GAAGCTC
	gTUA4-R	GCGGCCGCCCTTTTATCGTTTTGTTTCCTA AT
	pENTR2B-TUA4-F	CAAAACGATAAAAAGGGGCGGCCGCACTCGA GATATCTAG
	pENTR2B-TUA4-R	CAAATCAAAGCCGGGGGATCCAGTCGACTG AATTGGTTC
	TUA4-mRFP1-F	CGCTGGGGCCATGAGGGAGTGCATCTCGAT CCACA
	TUA4-mRFP1-R	CGGCCCATGGTGTGTTGTTGAACGGGGGGAGC GGC
Tubulin- $\beta$ 2	gTUB2-F	GACTGGATCCCCAAGCATATGGTCAACATTA AGTC
	g TUB2-R	GTGCGGCCGCCTCAAGCTTTTCTTCTGCTAC ATTG
	pENTR2B-TUB2-F	GAAGAAAAGCTTGAGGCGGCCGCACTCGAG ATATCTAG
	pENTR2B- TUB2-R	GTTGACCATATGCTTGGGGATCCAGTCGACT GAATTGGTTC
	SmaI-TUB2-F	GGGATGAGGGAGATCCTGCATATCC
	SmaI-TUB2-R	GGGCTTACTCTCACCTGTAACACC

**Table 5: PCR reaction mix used in the research**

Purpose	PCR reaction mix	Volume/reaction
Plasmid construction (I)	PrimeSTAR Max Premix	25 $\mu$ l
	Primer F	1.5 $\mu$ l
	Primer R	1.5 $\mu$ l
	Nuclease Free Water	21 $\mu$ l
Plasmid construction (II)	5x Phusion GC buffer	16 $\mu$ l
	Phusion DNA Polymerase	1 $\mu$ l
	dNTPs (10 mM)	1.6 $\mu$ l
	DMSO	2.4 $\mu$ l
	Primer F	4 $\mu$ l
	Primer R	4 $\mu$ l
	Nuclease Free Water	Up to 80 $\mu$ l
Colony PCR	DreamTaq Green PCR mastermix	7.5 $\mu$ l
	Primer F	0.5 $\mu$ l
	Primer R	0.5 $\mu$ l
	Nuclease Free Water	5.5 $\mu$ l

**Table 6: PCR conditions used in the research**

Purpose	PCR conditions	Temperature	Time
Plasmid construction (I)	Initial denaturation	94 °C	30 s
	Denaturation	98 °C	10 s
	Annealing	55 °C	5 s
	Elongation	72 °C	5 s/Kb
	Final elongation	72 °C	2 min
	Hold	16 °C	$\infty$
Plasmid construction (II)	Initial denaturation	98 °C	30 s
	Denaturation	98 °C	10 s
	Annealing	*	30 s
	Elongation	72 °C	30 sec/Kb
	Final elongation	72 °C	10 min
Colony PCR	Initial denaturation	95 °C	5 min
	Denaturation	95 °C	30 s
	Annealing	55 °C	30 s
	Elongation	72 °C	1 min/Kb
	Final elongation	72 °C	5 min
	Hold	16 °C	$\infty$

Calculated with <http://tmcalculator.neb.com/#!/main>

**Table 7: Resources table**

<b>REAGENT or RESOURCE</b>	<b>SOURCE</b>
<b>Bacterial and Virus Strains</b>	
<i>E. coli</i> Top10	Thermo Fisher Scientific; C404010
<i>Agrobacterium tumefaciens</i> strain LBA4404	N/A
<b>Buffers and media</b>	
LB	1% Tryptone 0.5% Yeast Extract 0.5% NaCl 0.8% agar (for solid medium)
YEB	1% Peptone 0.5% Yeast Extract 0.5% NaCl 0.8% agar (for solid medium) pH 6.8
Infection-Medium (1X)	For 1L 100 mL N <sub>6</sub> -Macro-Salts 1 ml N <sub>6</sub> -Micro-Salts 1 ml N <sub>6</sub> -Vitamine 2 ml NaFe-EDTA 0,7 g Proline 1,5 ml 2,4-D (1mg/ml) 68.4 g Sucrose 36 g Glucose pH 5.2 acetosyringone (100 µM) is added prior to use
Co-cultivation medium (2X)	For 1L 8.6 MS basal powder 2 ml MS Vitaminstock (1000X; 100 ml with 200 mg glycine, 50 mg Thiamin HCL, 50 mg Pyridoxin, 5 mg Nicotinic acid) 60 g Sucrose 4 ml myo-Inositol (50 mg/ml) 200 mg cas-Aminoacids 1.4 g Proline 1 ml Dicamba (30 mM dissolved in 50% EtOH) pH 5.8 + Silvernitate (50 mM) + L-Cysteine (15mg7ml) + Acetosyringone (100 mM)



Resting and Selection medium (2X)	For 2L 17.2 MS basal powder 4 ml MS Vitaminstock (see above) 2 ml Dicamba (30 mM) 120 g Sucrose 2 g MES 400 mg myo-Inositol (50 mg/ml) 400 mg cas-Aminoacids 2.8 g Proline pH 5.8 + Silvernitate (50 mM) + Carbenicillin (250 mg/ml) + Basta (20 mg/ml) 37,5 µl for Selection I; 75 µl for Selection II; 125 for Selection III
Regeneration medium I (2X)	For 2L 17.2 MS basal powder 4 ml MS Vitaminstock (see above) 240 g Sucrose 8 ml myo-Inositol (50 mg/ml) pH 5.8 + Cefotaxim (250 mg/ml) + Basta (20 mg/ml)
Regeneration medium II	For 500 ml 250 ml 2XMS 250 ml Phytigel (1.5 g/250 ml) 1 ml myo-Inositol (50 mg/ml) + Basta
Murashige and Skoog (½ MS)	0.2% MS basal powder 1% sucrose 1% agar pH 5.8
Artificial Pond Water (APW)	0.1 M NaCl 0.1 M CaCl <sub>2</sub> 0.1 M KCl 0.8% agar (for solid medium)
Acetocarmine staining	0.5 g carmine in 45% acetic acid
<b>Commercial Assays</b>	
Gateway BP Clonase II Enzyme mix	Thermo Fisher Scientific; Cat# 11789020
Gateway LR Clonase II Enzyme mix	Thermo Fisher Scientific; Cat# 11791020
Presto™ Mini Plasmid Kit	Geneaid; Cat#PDH300
NucleoSpin® Gel and PCRClean-up	MACHEREY-NAGEL; Cat# 740609.250
PrimeSTAR® Max DNA Polymerase	TAKARA BIO INC®; Cat# R045A
DreamTaq Green PCR Master Mix (2X)	Thermo Scientific™; Cat# K1081

Phusion® High-Fidelity DNA Polymerase	Thermo Fisher Scientific; Cat# F-530XL
Ligation mix	TAKARA BIO INC®; Cat# 6023
<b>Experimental Models: Organisms/Strains</b>	
<i>Zea mays</i> : PROH1B: H1B:YFP	<a href="http://maize.jcvi.org/cellgenomics">http://maize.jcvi.org/cellgenomics</a>
<i>Zea mays</i> : PRODSY2: DSY2:mRFP1	This study
<i>Zea mays</i> : PROCENH3: CENH3:mRFP1	This study
<i>Zea mays</i> : PROZYP1 ZYP1-IntI:mRFP1	This study
<i>Zea mays</i> : PROSDS: SDS:mRFP1	This study
<i>Zea mays</i> : PROMRE11B: MRE11B:YFP	<a href="http://maize.jcvi.org/cellgenomics">http://maize.jcvi.org/cellgenomics</a>
<i>Zea mays</i> : PROCOM1: COM1:YFP	This study
<i>Zea mays</i> : PROTubulin- $\alpha$ : YFP-Tubulin- $\alpha$	<a href="http://maize.jcvi.org/cellgenomics">http://maize.jcvi.org/cellgenomics</a>
<i>Zea mays</i> : PROTubulin- $\beta$ : CFP-Tubulin- $\beta$	<a href="http://maize.jcvi.org/cellgenomics">http://maize.jcvi.org/cellgenomics</a>
<i>Zea mays</i> : PROTubulin- $\beta$ : RFP-Tubulin- $\beta$	<a href="http://maize.jcvi.org/cellgenomics">http://maize.jcvi.org/cellgenomics</a>
<b>Recombinant DNA</b>	
PRODSY2: DSY2:mRFP1	This study
PRODSY2: DSY2:YFP	This study
PROAFD1: AFD1-I:YFP	This study
PROAFD1: AFD1-II:YFP	This study
PROCENH3: mRFP1:CENH3	This study
PROZYP1 ZYP1-IntI:mRFP1	This study
PROZYP1 ZYP1-IntI:YFP	This study
PROZYP1 ZYP1-IntII:mRFP1	This study
PROZYP1 ZYP1-IntII:YFP	This study
PROAM1: YFP:AM1	This study
PROAM1: mRFP1:AM1	This study
PROAM1: AM1:YFP	This study
PROAM1: AM1:mRFP1	This study
PROSDS: SDS:mRFP1	This study
PROSDS: SDS:YFP	This study
PROCOM1: YFP:COM1	This study
PROCOM1: mRFP1:COM1	This study
PROCOM1: COM1:YFP	This study
PROCOM1: COM1:mRFP1	This study
PROTubulin- $\alpha$ 4: mRFP1-Tubulin- $\alpha$ 4	This study
PROTubulin- $\beta$ 2: mRFP1-Tubulin- $\beta$ 2	This study
<b>Software and Algorithms</b>	
Fiji	<a href="https://imagej.net/Fiji">https://imagej.net/Fiji</a> ; [85]

## References

1. McClintock, B. (1950). The origin and behavior of mutable loci in maize. *Proceedings of the National Academy of Sciences* 36, 344-355.
2. Creighton, H. B., and McClintock, B. (1931). A correlation of cytological and genetical crossing-over in *Zea mays*. *Proceedings of the National Academy of Sciences of the United States of America* 17, 492.
3. Coe Jr, E. (1966). The properties, origin, and mechanism of conversion-type inheritance at the B locus in maize. *Genetics* 53, 1035.
4. Sprague, G., and Dudley, J. W. (1988). *Corn and corn improvement*, (American Society of Agronomy).
5. Coe Jr, E., Neuffer, M., and Hoisington, D. (1988). The genetics of corn. *Corn and corn improvement* 18, 81-258.
6. Schnable, P. S., Ware, D., Fulton, R. S., Stein, J. C., Wei, F., Pasternak, S., Liang, C., Zhang, J., Fulton, L., and Graves, T. A. (2009). The B73 maize genome: complexity, diversity, and dynamics. *Science* 326, 1112-1115.
7. Ishida, Y., Hiei, Y., and Komari, T. (2007). *Agrobacterium*-mediated transformation of maize. *Nature protocols* 2, 1614.
8. Lowe, K., Wu, E., Wang, N., Hoerster, G., Hastings, C., Cho, M.-J., Scelonge, C., Lenderts, B., Chamberlin, M., and Cushatt, J. (2016). Morphogenic regulators Baby boom and Wuschel improve monocot transformation. *The Plant Cell* 28, 1998-2015.
9. Gordon-Kamm, W. J., Spencer, T. M., Mangano, M. L., Adams, T. R., Daines, R. J., Start, W. G., O'Brien, J. V., Chambers, S. A., Adams, W. R., Willetts, N. G., et al. (1990). Transformation of Maize Cells and Regeneration of Fertile Transgenic Plants. *The Plant Cell* 2, 603-618.
10. Pawlowski, W. P., and Somers, D. A. (1996). Transgene inheritance in plants genetically engineered by microprojectile bombardment. *Mol Biotechnol* 6, 17-30.
11. Cande, W. Z., Golubovskaya, I., Wang, C. R., and Harper, L. (2009). Meiotic genes and meiosis in maize. In *Handbook of Maize*. (Springer), pp. 353-375.
12. <https://depositphotos.com/266178658/stock-illustration-parts-plant-morphology-corn-maize.html> (December 2020).
13. Golubovskaya, I., Grebennikova, Z. K., Avalkina, N. A., and Sheridan, W. (1993). The role of the *ameiotic1* gene in the initiation of meiosis and in subsequent meiotic events in maize. *Genetics* 135, 1151-1166.
14. Bennett, M. D. (1977). The time and duration of meiosis. *Philosophical Transactions of the Royal Society of London. B, Biological Sciences* 277, 201-226.
15. Hsu, S.-Y., Huang, Y.-C., and Peterson, P. A. (1988). Development pattern of microspores in *Zea mays* L. The maturation of upper and lower florets of spikelets among an assortment of genotypes. *Maydica* 33, 77-98.
16. Harper, L., Golubovskaya, I., and Cande, W. Z. (2004). A bouquet of chromosomes. *Journal of Cell Science* 117, 4025-4032.

17. Scherthan, H. (2007). Telomere attachment and clustering during meiosis. *Cell Mol Life Sci* 64.
18. Buchanan, B. B., Gruissem, W., and Jones, R. L. (2015). *Biochemistry and molecular biology of plants*, (John Wiley & Sons).
19. Chan, A., and Cande, W. Z. (2000). Maize meiocytes in culture. *Plant cell, tissue and organ culture* 60, 187.
20. Yu, H.-G., Hiatt, E. N., Chan, A., Sweeney, M., and Dawe, R. K. (1997). Neocentromere-mediated chromosome movement in maize. *The Journal of cell biology* 139, 831-840.
21. White, P. R. (1964). The cultivation of animal and plant cells. *Soil Sci* 97, 74.
22. Nannas, N. J., Higgins, D. M., and Dawe, R. K. (2016). Anaphase asymmetry and dynamic repositioning of the division plane during maize meiosis. *Journal of cell science* 129, 4014-4024.
23. Higgins, D. M., Nannas, N. J., and Dawe, R. K. (2016). The Maize Divergent spindle-1 (dv1) Gene Encodes a Kinesin-14A Motor Protein Required for Meiotic Spindle Pole Organization. *Frontiers in Plant Science* 7.
24. Sheehan, M. J., and Pawlowski, W. P. (2009). Live imaging of rapid chromosome movements in meiotic prophase I in maize. *Proceedings of the National Academy of Sciences* 106, 20989-20994.
25. Feijó, J. A., and Cox, G. (2001). Visualization of meiotic events in intact living anthers by means of two-photon microscopy. *Micron* 32, 679-684.
26. Prunet, N., Jack, T. P., and Meyerowitz, E. M. (2016). Live confocal imaging of Arabidopsis flower buds. *Dev Biol* 419, 114-120.
27. Ingouff, M., Selles, B., Michaud, C., Vu, T. M., Berger, F., Schorn, A. J., Autran, D., Van Durme, M., Nowack, M. K., and Martienssen, R. A. (2017). Live-cell analysis of DNA methylation during sexual reproduction in Arabidopsis reveals context and sex-specific dynamics controlled by noncanonical RdDM. *Genes Dev* 31, 72-83.
28. Valuchova, S., Mikulkova, P., Pecinkova, J., Klimova, J., Krumnikl, M., Bainer, P., Heckmann, S., Tomancak, P., and Riha, K. (2020). Imaging plant germline differentiation within Arabidopsis flowers by light sheet microscopy. *Elife* 9, e52546.
29. Prusicki, M. A., Hamamura, Y., and Schnittger, A. (2020). A Practical Guide to Live-Cell Imaging of Meiosis in Arabidopsis. In *Plant Meiosis*. (Springer), pp. 3-12.
30. Prusicki, M. A., Keizer, E. M., van Rosmalen, R. P., Komaki, S., Seifert, F., Muller, K., Wijnker, E., Fleck, C., and Schnittger, A. (2019). Live cell imaging of meiosis in Arabidopsis thaliana. *Elife* 8.
31. Ma, H. (2006). A Molecular Portrait of Arabidopsis Meiosis.
32. Osman, K., Higgins, J. D., Sanchez-Moran, E., Armstrong, S. J., and Franklin, F. C. H. (2011). Pathways to meiotic recombination in Arabidopsis thaliana. *New Phytologist* 190, 523-544.
33. Hamant, O., Ma, H., and Cande, W. Z. (2006). Genetics of meiotic prophase I in plants. *Annu Rev Plant Biol* 57, 267-302.

34. Mercier, R., Mézard, C., Jenczewski, E., Macaisne, N., and Grelon, M. (2015). The molecular biology of meiosis in plants. *Annual review of plant biology* 66, 297-327.
35. Chen, C., Farmer, A. D., Langley, R. J., Mudge, J., Crow, J. A., May, G. D., Huntley, J., Smith, A. G., and Retzel, E. F. (2010). Meiosis-specific gene discovery in plants: RNA-Seq applied to isolated *Arabidopsis* male meiocytes. *BMC Plant Biol* 10, 280.
36. Bovill, W. D., Deveshwar, P., Kapoor, S., and Able, J. A. (2009). Whole genome approaches to identify early meiotic gene candidates in cereals. *Functional & integrative genomics* 9, 219-229.
37. Tang, X., Zhang, Z.-Y., Zhang, W.-J., Zhao, X.-M., Li, X., Zhang, D., Liu, Q.-Q., and Tang, W.-H. (2010). Global gene profiling of laser-captured pollen mother cells indicates molecular pathways and gene subfamilies involved in rice meiosis. *Plant Physiol* 154, 1855-1870.
38. Dukowic-Schulze, S., Sundararajan, A., Mudge, J., Ramaraj, T., Farmer, A. D., Wang, M., Sun, Q., Pillardy, J., Kianian, S., and Retzel, E. F. (2014). The transcriptome landscape of early maize meiosis. *BMC Plant Biol* 14, 118.
39. Sayers, E. W., Barrett, T., Benson, D. A., Bolton, E., Bryant, S. H., Canese, K., Chetvernin, V., Church, D. M., DiCuccio, M., and Federhen, S. (2010). Database resources of the national center for biotechnology information. *Nucleic acids research* 39, D38-D51.
40. Portwood, J. L., II, Woodhouse, M. R., Cannon, E. K., Gardiner, J. M., Harper, L. C., Schaeffer, M. L., Walsh, J. R., Sen, T. Z., Cho, K. T., Schott, D. A., et al. (2018). MaizeGDB 2018: the maize multi-genome genetics and genomics database. *Nucleic Acids Research* 47, D1146-D1154.
41. Goodstein, D. M., Shu, S., Howson, R., Neupane, R., Hayes, R. D., Fazo, J., Mitros, T., Dirks, W., Hellsten, U., Putnam, N., et al. (2011). Phytozome: a comparative platform for green plant genomics. *Nucleic Acids Research* 40, D1178-D1186.
42. Gupta, P., Naithani, S., Tello-Ruiz, M. K., Chougule, K., D'Eustachio, P., Fabregat, A., Jiao, Y., Keays, M., Lee, Y. K., and Kumari, S. (2016). Gramene database: navigating plant comparative genomics resources. *Current plant biology* 7, 10-15.
43. Lee, D. H., Kao, Y.-H., Ku, J.-C., Lin, C.-Y., Meeley, R., Jan, Y.-S., and Wang, C.-J. R. (2015). The axial element protein DESYNAPTIC2 mediates meiotic double-strand break formation and synaptonemal complex assembly in maize. *The Plant Cell* 27, 2516-2529.
44. Golubovskaya, I. N., Hamant, O., Timofejeva, L., Wang, C.-J. R., Braun, D., Meeley, R., and Cande, W. Z. (2006). Alleles of *afd1* dissect REC8 functions during meiotic prophase I. *Journal of cell science* 119, 3306-3315.
45. Zhong, C. X., Marshall, J. B., Topp, C., Mroczek, R., Kato, A., Nagaki, K., Birchler, J. A., Jiang, J., and Dawe, R. K. (2002). Centromeric retroelements and satellites interact with maize kinetochore protein CENH3. *The Plant Cell* 14, 2825-2836.
46. Golubovskaya, I. N., Wang, C. R., Timofejeva, L., and Cande, W. Z. (2011). Maize meiotic mutants with improper or non-homologous synapsis due to problems in pairing or synaptonemal complex formation. *Journal of experimental botany* 62, 1533-1544.

47. Pawlowski, W. P., Wang, C.-J. R., Golubovskaya, I. N., Szymaniak, J. M., Shi, L., Hamant, O., Zhu, T., Harper, L., Sheridan, W. F., and Cande, W. Z. (2009). Maize AME10TIC1 is essential for multiple early meiotic processes and likely required for the initiation of meiosis. *Proceedings of the National Academy of Sciences* *106*, 3603-3608.
48. Nan, G.-L., Ronceret, A., Wang, R. C., Fernandes, J. F., Cande, W. Z., and Walbot, V. (2011). Global transcriptome analysis of two ameiotic1alleles in maize anthers: defining steps in meiotic entry and progression through prophase I. *BMC Plant Biol* *11*, 120.
49. Waterworth, W. M., Altun, C., Armstrong, S. J., Roberts, N., Dean, P. J., Young, K., Weil, C. F., Bray, C. M., and West, C. E. (2007). NBS1 is involved in DNA repair and plays a synergistic role with ATM in mediating meiotic homologous recombination in plants. *The Plant Journal* *52*, 41-52.
50. Wang, Y., Jiang, L., Zhang, T., Jing, J., and He, Y. (2018). ZmCom1 is required for both mitotic and meiotic recombination in maize. *Frontiers in plant science* *9*, 1005.
51. Reece-Hoyes, J. S., and Walhout, A. J. M. (2018). Gateway Recombinational Cloning. *Cold Spring Harbor protocols* *2018*, pdb.top094912-pdb.top094912.
52. Wu, Q., Luo, A., Zadrozny, T., Sylvester, A., and Jackson, D. (2013). Fluorescent protein marker lines in maize: generation and applications. *Int J Dev Biol* *57*, 535-543.
53. Mohanty, A., Luo, A., DeBlasio, S., Ling, X., Yang, Y., Tuthill, D. E., Williams, K. E., Hill, D., Zadrozny, T., and Chan, A. (2009). Advancing cell biology and functional genomics in maize using fluorescent protein-tagged lines. *Plant Physiol* *149*, 601-605.
54. Howe, E. S., Clemente, T. E., and Bass, H. W. (2012). Maize histone H2B-mCherry: a new fluorescent chromatin marker for somatic and meiotic chromosome research. *DNA and cell biology* *31*, 925-938.
55. Yang, C., Hamamura, Y., Sofroni, K., Böwer, F., Stolze, S. C., Nakagami, H., and Schnittger, A. (2019). SWITCH 1/DYAD is a WINGS APART-LIKE antagonist that maintains sister chromatid cohesion in meiosis. *Nature Communications* *10*, 1755.
56. Uhlmann, F. (2003). Chromosome cohesion and separation: from men and molecules. *Current Biology* *13*, R104-R114.
57. Watanabe, Y. (2012). Geometry and force behind kinetochore orientation: lessons from meiosis. *Nature reviews Molecular cell biology* *13*, 370-382.
58. Kitajima, T. S., Miyazaki, Y., Yamamoto, M., and Watanabe, Y. (2003). Rec8 cleavage by separase is required for meiotic nuclear divisions in fission yeast. *The EMBO Journal* *22*, 5643-5653.
59. Peters, J.-M., Tedeschi, A., and Schmitz, J. (2008). The cohesin complex and its roles in chromosome biology. *Genes Dev* *22*, 3089-3114.
60. Zhang, J., Feng, C., Su, H., Liu, Y., Liu, Y., and Han, F. (2020). The Cohesin Complex Subunit ZmSMC3 Participates in Meiotic Centromere Pairing in Maize. *The Plant Cell* *32*, 1323-1336.

61. Zhang, J., Pawlowski, W. P., and Han, F. (2013). Centromere pairing in early meiotic prophase requires active centromeres and precedes installation of the synaptonemal complex in maize. *The Plant cell* *25*, 3900-3909.
62. Yu, H.-G., Dawe, R. K., and Hiatt, E. N. (2000). The plant kinetochore. *Trends Plant Sci* *5*, 543-547.
63. Lermontova, I., Schubert, V., Fuchs, J., Klatte, S., Macas, J., and Schubert, I. (2006). Loading of *Arabidopsis* centromeric histone CENH3 occurs mainly during G2 and requires the presence of the histone fold domain. *The Plant Cell* *18*, 2443-2451.
64. Higgins, J. D., Sanchez-Moran, E., Armstrong, S. J., Jones, G. H., and Franklin, F. C. H. (2005). The *Arabidopsis* synaptonemal complex protein ZYP1 is required for chromosome synapsis and normal fidelity of crossing over. *Genes Dev* *19*, 2488-2500.
65. Heyting, C. (1996). Synaptonemal complexes: structure and function. *Curr Opin Cell Biol* *8*, 389-396.
66. Page, S. L., and Hawley, R. S. (2001). *c(3)G* encodes a *Drosophila* synaptonemal complex protein. *Genes Dev* *15*, 3130-3143.
67. Madeira, F., Park, Y. M., Lee, J., Buso, N., Gur, T., Madhusoodanan, N., Basutkar, P., Tivey, A. R. N., Potter, S. C., Finn, R. D., et al. (2019). The EMBL-EBI search and sequence analysis tools APIs in 2019. *Nucleic acids research* *47*, W636-W641.
68. Murray, A. W. (1994). Cyclin-dependent kinases: regulators of the cell cycle and more. *Chem Biol* *1*, 191-195.
69. Wijnker, E., and Schnittger, A. (2013). Control of the meiotic cell division program in plants. *Plant reproduction* *26*, 143-158.
70. Azumi, Y., Liu, D., Zhao, D., Li, W., Wang, G., Hu, Y., and Ma, H. (2002). Homolog interaction during meiotic prophase I in *Arabidopsis* requires the SOLO DANCERS gene encoding a novel cyclin-like protein. *The EMBO journal* *21*, 3081-3095.
71. Chang, L., Ma, H., and Xue, H.-W. (2009). Functional conservation of the meiotic genes SDS and RCK in male meiosis in the monocot rice. *Cell Res* *19*, 768-782.
72. Wu, Z., Ji, J., Tang, D., Wang, H., Shen, Y., Shi, W., Li, Y., Tan, X., Cheng, Z., and Luo, Q. (2015). OsSDS is essential for DSB formation in rice meiosis. *Frontiers in plant science* *6*, 21.
73. De Muyt, A., Pereira, L., Vezon, D., Chelysheva, L., Gendrot, G., Chambon, A., Laine-Choinard, S., Pelletier, G., Mercier, R., and Nogue, F. (2009). A high throughput genetic screen identifies new early meiotic recombination functions in *Arabidopsis thaliana*. *PLoS genetics* *5*.
74. Keeney, S., Giroux, C. N., and Kleckner, N. (1997). Meiosis-specific DNA double-strand breaks are catalyzed by Spo11, a member of a widely conserved protein family. *Cell* *88*, 375-384.
75. Wang, Y., and Copenhaver, G. P. (2018). Meiotic recombination: mixing it up in plants. *Annual review of plant biology* *69*, 577-609.

76. D'amours, D., and Jackson, S. P. (2002). The Mre11 complex: at the crossroads of DNA repair and checkpoint signalling. *Nature reviews Molecular cell biology* 3, 317-327.
77. Casari, E., Rinaldi, C., Marsella, A., Gnugnoli, M., Colombo, C. V., Bonetti, D., and Longhese, M. P. (2019). Processing of DNA Double-Strand Breaks by the MRX Complex in a Chromatin Context. *Frontiers in Molecular Biosciences* 6.
78. Sheehan, M. J., and Pawlowski, W. P. (2012). Imaging chromosome dynamics in meiosis in plants. In *Methods in enzymology*, Volume 505. (Elsevier), pp. 125-143.
79. Sofroni, K., Takatsuka, H., Yang, C., Dissmeyer, N., Komaki, S., Hamamura, Y., Böttger, L., Umeda, M., and Schnittger, A. (2020). CDKD-dependent activation of CDKA;1 controls microtubule dynamics and cytokinesis during meiosis. *Journal of Cell Biology* 219.
80. Griesbeck, O., Baird, G. S., Campbell, R. E., Zacharias, D. A., and Tsien, R. Y. (2001). Reducing the environmental sensitivity of yellow fluorescent protein mechanism and applications. *Journal of biological chemistry* 276, 29188-29194.
81. Ito, M., and Stern, H. (1967). Studies of meiosis in vitro: I. In vitro culture of meiotic cells. *Dev Biol* 16, 36-53.
82. Paredy, D., and Greyson, R. (1985). In vitro culture of immature tassels of an inbred field variety of *Zea mays*, cv. Oh43. *Plant cell, tissue and organ culture* 5, 119-128.
83. Stapleton, A. E., and Bedinger, P. A. (1992). Immature maize spikelets develop and produce pollen in culture. *Plant Cell Rep* 11, 248-252.
84. Zhang, Y., Werling, U., and Edelmann, W. (2012). SLiCE: a novel bacterial cell extract-based DNA cloning method. *Nucleic acids research* 40, e55-e55.
85. Schindelin, J., Arganda-Carreras, I., Frise, E., Kaynig, V., Longair, M., Pietzsch, T., Preibisch, S., Rueden, C., Saalfeld, S., and Schmid, B. (2012). Fiji: an open-source platform for biological-image analysis. *Nat Methods* 9, 676-682.





# Publications and presentations

## Publication

- COMET Functions as a PCH2 Cofactor in Regulating the HORMA Domain Protein ASY1  
**Balboni M**, Yang C, Komaki S, Brun J, Schnittger A  
**Current Biology** 30, 1–15, November 2, 2020

## Oral presentations

- 12th International PhD School in Plant Development, 2-4 October 2019, Retzbach, Germany  
Presentation title: "ASY1 recruitment to and release from the meiotic chromosome axis is controlled by P31<sup>COMET</sup>"
- Trends in Microscopy: Bridging the Worlds, 12-14 March 2018, Düsseldorf, Germany  
Presentation title: "Towards Live Imaging of Meiosis in Maize"

## Poster presentations

- 12th International PhD School in Plant Development, October 2-4, 2019, Retzbach, Germany
- EMBO Workshop on Meiosis, August 25-29, 2019, La Rochelle, France
- 3rd Edition European Maize Meeting, May 15-17, 2019, Montpellier, France
- The 2<sup>nd</sup> Biology Conference of Doctoral Candidates, May 4, 2018, Hamburg, Germany
- 60th Annual Maize Genetics Conference, March 22-25, 2018, Saint-Malo, France
- The 1<sup>st</sup> Biology Conference of Doctoral Candidates, June 9, 2017, Hamburg, Germany
- European Molecular Maize Symposium, May 3-5, 2017, Ghent, Belgium
- 59th Annual Maize Genetics Conference, 9-12 March 2017, St. Louis, USA

## **Eidesstattliche Versicherung/Declaration On Oath**

**Hiermit erkläre ich an Eides statt, dass ich die vorliegende  
Dissertationsschrift selbst verfasst und keine anderen als die  
angegebenen Quellen und Hilfsmittel benutzt habe.**

I hereby declare, on oath, that I have written the present dissertation by  
my own and have not used other than the acknowledged resources and  
aids.

Hamburg, den

Unterschrift

## Declaration of contributions

I hereby declare that all results shown in this thesis are obtained by my own, except from the ones indicated in the respective figure legends. Here, I summarize the contributions from the collaborators.

### In **Chapter 1**:

- The figures 3E and 3F are made with the root growth assay data kindly provided by Dr. Shinichiro Komaki
- The figures 5D, 5E and 5F are made with the data kindly provided by Jordan Brun
- The figures 8C and 8D, 9A and 9B, 11C-E are made with the immunolocalization data kindly provided by Dr. Chao Yang
- The figure 14 is made with the Yeast-2-Hybrid data and the Ni<sup>2+</sup> pull down assay kindly performed by Dr. Chao Yang

### In **Chapter 2**:

- The maize transformation of all the reporter constructs generated in this study was kindly performed by Dr. Reinhold Brettschneider, Dagmar Stang, Katja Müller and at Crop Genetic System (Hamburg).

# Confirmation of correct English

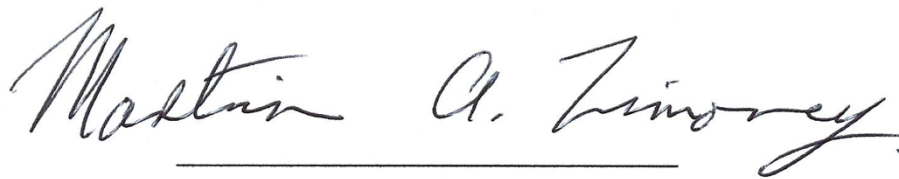
*Bóthar an Chorainn,*  
Cloonagh,  
Keash,  
Ballymote,  
Co. Sligo.  
Ireland  
F56 AE72

14 January 2021

To whom it may concern,

I am writing to confirm that the thesis submitted by Martina Balboni has been written in correct English throughout the entire text.

Kind regards,



**Martin A. Timoney**

*Author of over 250 archaeological articles, Editor of two books of essays (2002; 2013) and of six volumes of a Journal (2015-2020).*

Martin A. Timoney, BA, HDEd., FRSAI, MIAI,  
*Research Archaeologist,*  
*TASKS,*  
[martin.timoney06@gmail.com](mailto:martin.timoney06@gmail.com)  
Tel: +353 71-91 83293  
Mob: +353 87-2863301

## Acknowledgments

My first acknowledgments are for Prof. Dr. Arp Schnittger for giving me the opportunity to join the lab, for the guidance during my PhD, for the trust and for the enthusiasm for science, which has always inspired me during these years.

I would like to thank Prof. Dr. Sigrun Reumann for kindly accepting to be my second supervisor, for examining my thesis and for the time dedicated to me.

A special thank goes to Reinhold, Dagmar and Katja for supporting my work by performing the maize transformation experiments and, also, for always being there to reply to all my questions during this time.

Thanks to Maren H for the critical reading of my thesis.

Thanks to all the present and former lab members, who provided me scientific advices, constructive discussion and, also, emotional support during these years. In particular, I would like to thank Joke, Meri, Shini, Chao, Yuki, Jordan, Kost, Viola, Poyu, Reinhold, Dagmar, Katja, Seijiro, Misato, Maren H and Maren R. It has been a pleasure working with you!

Thanks to Joke, Meri, Chris, Yuki, Shini, Poyu, Kost and Kim for the everyday life support and for all the dinners, games evenings, discoveries of delicious restaurants, interminable walks throughout Hamburg, badminton games, coffee and talks together, laughs and nice trips. Each of this moment enriched my life in Hamburg during these years and made it so special...Thank you!!

It has been an unforgettable journey!

A big thanks goes to my family, who always believed in me, encouraged me and supported me! Finally, I would like to dedicate this entire thesis to my grandma, who has been and will always be by my side.